182
55

3.0 SYNTHESIS AND CHARACTERIZATION OF OPTICALLY ACTIVE AND RACEMIC POLY(LACTIC ACIDS)

3.1.0 INTRODUCTION

Over the past 15 years, research interest in the synthesis and characterization of poly(lactic acids) has been fostered by their industrial applications in medicine and surgery (1). Biomedical applications cover a broad range of end uses including sutures (2), burn wound covering (3), drug release systems (4), and resorbable prosthesis in orthopedic surgery (5). Although lactic acids can undergo a condensation polymerization (6,7), the molecular weight of the product is too low to be suitable for biomedical applications. Presumably, this low molecular weight is due to the standard problems associated with condensation polymerizations. These problems include the necessity for effective removal of water from the polymerization, exact stoichiometry, high temperatures, and long reaction cycles (8). However, diastereoisomeric lactides, derived from the L- and D- lactic acid enantiomers have been shown to undergo a ring-opening polymerization both in solution and the bulk

phase to yield molecular weights which are considerably higher and of industrial importance (9,10). This ring-opening polymerization is shown schematically in Fig. 3.1. Lactide is a member of a class of cyclic esters known as glycolides, that are, in general, cyclic dimer esters of α-hydroxy-acids. As such, lactide is considered to be a modified lactone whose polymerization behavior is reported to be similar to conventional six membered lactones, like δ-valerolactone (11).

Within the context of some general aspects of lactone polymerization chemistry discussed below, the purpose of this study was to investigate the polymerization of both optically active L-lactide and racemic D,L-lactide. Control of molecular weight in a polymerization scheme with stannous octoate as the catalyst/initiator system was the primary objective. Previous attempts at determining the relationship between melt polymerization conditions and the molecular weight for D,L-lactide initiated with tetraphenyl tin were unsuccessful (12). The observed irreproducibility of product molecular weight was considered to be related to contaminants stemming from the hydrolysis products of lactide (12). The following work will deal with the effects of stannous octoate concentration, lactic acid concentration, and polymerization temperature on molecular weight and molecular weight distribution. In addition, reaction profiles (kinetics) were monitored in terms of monomer conversion and molecular weight

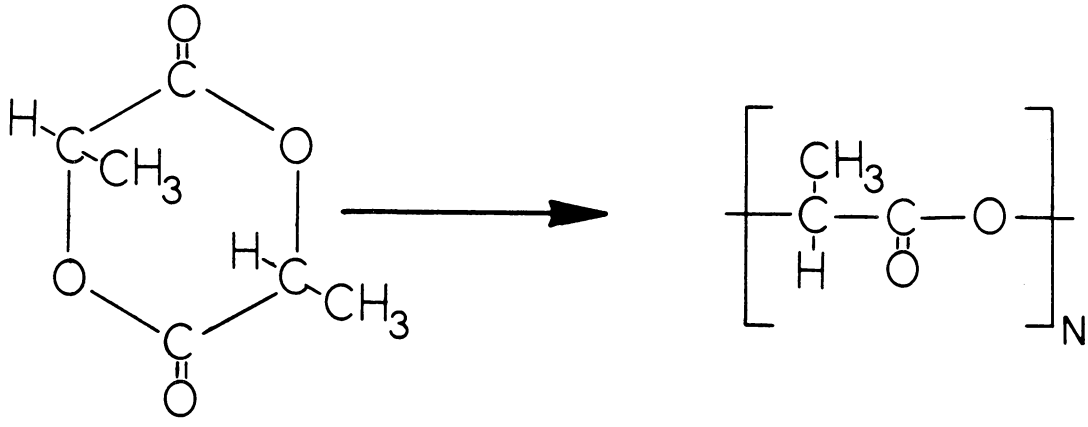

Figure 3.1. Schematic of ring-opening polymerization of poly(lactic acids).

distribution. Finally, some configurational structures of lactic acid stereopolymers were determined by ^{13}C NMR techniques.

As a precursor to the aforementioned study, some general aspects of lactone polymerization will be discussed. Lactone ring-opening thermodynamics and mechanism will be addressed as well as some of the specifics on the stereochemistry and thermal stability of poly(lactic acids).

3.1.1 SOME GENERAL THERMODYNAMICS OF RING-OPENING POLYMERIZATION

In contrast to condensation polymerization, the ring-opening polymerization of lactones can lead to an extremely high molecular weight polyester in comparatively short reaction times and lower reaction temperatures (13). Depending on the catalyst/initiator system employed, the number of reacting sites does not change during polymerization with a stepwise addition of monomer to the growing chain and consequent regeneration of propagating species. This can also lead to the exact control of end groups which can be critical in the final applications for the polyester (14).

Although there is no generation of a by-product in ring-opening polymerization, and this is generally considered to be an advantage, it must be emphasized that lactone polymerizations are equilibrium processes which are normally biased toward the product polymer side (13). Formal thermodynamics predicts this equilibrium in terms of a ceiling temperature. From a practical point of view, the ceiling temperature can be considered as the highest temperature at which an acceptable amount of monomer exists in equilibrium with the polymer. Assuming a suitable mechanism is available through which the reaction may proceed, high molecular weight products are achieved only if

a negative Gibbs free energy change for the propagation reaction is realized. At equilibrium, the propagation step in the polymerization of any ring-opening system may be generalized as:

$$\sim P_N^* + M \underset{K_d}{\overset{K_p}{\rightleftharpoons}} \sim P_{N+1}^* \qquad (3.1)$$

where K_p and K_d are the propagation and depropagation rate constants respectively. At equilibrium, the overall free energy change for the reaction is identically zero:

$$\Delta G = \Delta G^\circ + RT \ln K = 0 \qquad (3.2)$$

where ΔG° is the free energy of polymerization at appropriate standard states and K is the equilibrium constant for the overall reaction and can be expressed as:

$$K = \frac{[P_{N+1}^*]}{[P_N^*][M]} \approx \frac{1}{[M]} \qquad (3.3)$$

for $[P_{N+1}^*] \approx [P_N^*]$. Substitution of Eq. 3.3 into Eq. 3.2 yields:

$$\ln[M] = \frac{\Delta H^\circ}{R T_c} - \frac{\Delta S^\circ}{R} \qquad (3.4)$$

with T_c defined as the ceiling temperature. This relationship shows that the equilibrium concentration of

monomer is clearly a reciprocal function of reaction temperature (ceiling temperature). In the case of lactones of five, six, or seven membered rings, the temperatures at which substantial amounts of monomer are present may be quite low (15). For example, poly- δ -valerolactone under conditions of polymerization where the temperature is in excess of 150 C, a substantial amount of monomer is present in the reaction mixture at equilibrium (16). Conversely, if the polymeric valerolactone reaction product, once isolated from residual monomer, is reheated to temperatures in excess of 150 C, monomeric lactone again can be regenerated to the point of equilibrium.

The overall driving force for the polymerization and the resulting reversibility of reaction with a ring-opening type of polymerization is, in general, thought to arise from strain within the ring structure. This discussion would naturally begin with the classic work of Dainton and co-workers (17,18) in which the thermodynamics of the hypothetical polymerizations of liquid cycloparaffins to liquid polymers at 25 C were theoretically calculated. The Gibbs free energy change associated with the hypothetical reactions as a function of ring size show a maximum positive (non-favorable) value for a six membered ring. The values become progressively more negative (favorable) with both increasing and decreasing ring size. Thus, the most favorable polymerization reactions within the series of 3 to

8 membered rings are for cyclopropane and cyclooctane. Further calculations indicated that pendent alkane substitution along the ring tended to stabilize the ring structure with respect to the linear polymeric product and, thus, increase the Gibbs free energy of polymerization. Subsequent calculations by Small (19) predicted the influence of an ether oxygen hetero atom substitution in alkane rings on the free energy for polymerization. Again, these results indicated a maximum in the Gibbs free energy for six membered rings preventing the polymerization of tetrahydropyran and 1,4 dioxane (13). Insertion of an ester group in the cyclic ring system significantly alters the polymerization habits of the lactone cyclic series. Hall and Schneider (20) have investigated the polymerization of ring systems containing carbonyl groups including lactones. Although the maximum free energy for lactam rings still occurs for six membered rings, the lactone maximum was shifted to γ-butyrolactone allowing facile polymerization of δ-valerolactone a six membered ring (19). Consistent with the predictions of Dainton et al. (17,18), recent work on the copolymerization of glycolide and lactide has shown a significantly enhanced reactivity of glycolide as compared with lactide which has pendant methyl groups on each of two α carbons (21).

Early conclusions by Hall et al. (22) indicated that the polymerizability of lactones was dependent on internal ring strain. Brown (23) described the internal ring strain as

arising from bond angle distortion, and van der Waals radii compression. Thus, in small three or four membered rings, bond angle distortion was considered as the principal source of strain. In intermediately sized rings, only bond opposition forces prevailed. The largest rings were considered to be susceptible to both van der Waals compression forces as well as bond opposition forces. Later authors (24) reviewed the correlation between ring strain and polymerizability of lactones and have found some fault with the correlation. However, as reviewed by Lundberg and Cox (15), some general conclusions are still valid:

1) The polymerizability of five and six membered carbonyl cyclic monomers depends on the class of the compound. Valerolactone (6 membered) shows facile reactivity while butyrolactone is at best extremely difficult to polymerize (25).

2) Four, seven, and eight membered ring polymerize in all cases.

3) Alkyl or aryl pendant substituents on lactone rings always decrease reactivity.

3.1.2 LACTONE POLYMERIZATION MECHANISMS

Polymerizations of lactones, especially β -propiolactone and ϵ -caprolactone, have been extensively studied. A great number of organometallic compounds, metals, metal hydrides, Lewis acids, protonic acids, amines, and alcohols have been examined as catalysts and/or initiators for lactone polymerization. The term catalyst as applied in the ensuing discussion may appear technically incorrect since occasionally the named catalyst may become attached to the polymer molecule. Catalyst and initiator are used interchangeably in the literature. Most of the species, which when combined with lactones result in polymerization, will be termed catalysts. The term initiator will be used exclusively with those species which have active hydrogens and are designed to become a part of the polymer. A number of excellent reviews (14,15) have compiled a list of catalysts and initiators used in the ring-opening polymerization of lactones and the reader is referred to these for specific details.

Brode and Koleske (14) categorize all initiators and catalysts for lactone polymerization into one of three systems summarized below:

1) Active Hydrogen Initiated Polymerizations without Catalyst

Conventional active hydrogen initiators such as

carboxylic acids, alcohols, and amines are restricted to the synthesis of relatively low molecular weight polyesters (16). This reaction scheme is also characterized by relatively slow reaction kinetics as exemplified by the polymerization of δ-valerolactone initiated with ethylene glycol or ethanolamine (16). Although rapid rates were reported for the initial reaction between the monomer and amino group (ethanolamine), the initiation step is followed by a slow propagation step as monomer is added to the terminal hydroxyl group. In general, when a lactone is heated in the presence of an active hydrogen initiator, both initiation and propagation are very slow (26).

2) Nonactive Hydrogen Initiated Polymerizations

Anionic and cationic, as well as coordination, initiators have been used to prepare high molecular weight polyesters from lactones. Although these initiators have been often referred to as catalysts, a clear distinction needs to be made between the two terms. Catalysts influence only reaction rates while initiators are incorporated into the polymer product. On occasion, initiators may also act as catalysts, however, in general they can be distinguished from catalysts by their influence on molecular weight. Both ϵ-caprolactone and δ-valerolactone have been polymerized to high molecular weights with the use of such organometallic catalysts as stannous diacylate (27), stannic tetracylate (27), dimethyl cadmium (28), methyl magnesium bromide (28),

and dibutyl zinc (28). The absence of active hydrogen initiators, often used in conjunction with these nonactive hydrogen initiators, generally results in poor control of molecular weight and end groups. More recently, an exception to this generality has been found in the polymerization of lactones with aluminum alkoxides (29) and bimetallic μ-oxoalkoxides (30).

3) Active Hydrogen Initiated Polymerizations with Catalyst

The use of an active hydrogen initiator in conjunction with a catalyst (organometallic initiator) has resulted in good molecular weight and end group control. Carboxylic acids and polyols, as well as polyamines, have been used with catalyst systems such as zinc or lead salts (31), alkyl titanates (31), stannous esters (32), stannic esters (32), and phosphines (32).

Ring-opening polymerization mechanisms of lactones are thought to be a function of the catalyst and/or initiator employed and are subdivided into anionic, cationic, and coordination type mechanisms (13). Note that the anionic and cationic mechanisms referenced above can be considered to be limiting cases with the coordination mechanism as the intermediate case between the other two modes (33). In actual practice, the identification of a particular catalyst that functions as an anionic or cationic catalyst is somewhat subjective for lactone systems (15). Based on the early work of Cherdron and Ohse (34,35) with the polymerization of δ-

valerolactone with acetyl perchlorate, there appears little doubt that all three mechanisms involve the cleavage of the acyl-oxygen bond. Exceptions to the acyl-oxygen bond cleavage may be found in highly strained lactones such as in the anionic polymerization of α , α disubstituted-propiolactones (36) and the cationic polymerization of β , β dimethyl propiolactone wherein ring-opening is thought to occur via alkyl-oxygen cleavage (37). Figure 3.2 shows the acyl-oxygen and alkyl-oxygen bonds in lactide. Presumably, the "configurational retaining" characteristics of some of the known catalysts for lactides such as tetraphenyl tin (12), stannic chloride (38), zinc (39), and stannous octoate (40,41) preclude the cleavage of the alkyl-oxygen bond since this could potentially cause racemization of the optically active carbon. Recently, alkali metal carbonates were shown to be reactive initiators for L-lactide polymerization yet were shown to cause considerable racemization even at low reaction temperatures (42,43). Since racemization increases with basicity of the catalyst, it was suggested that deprotonation of the monomer at the carbon is the main source of racemization. Thus, the proposed mechanism of ring-opening through acyl-oxygen cleavage is assumed to be operative even for alkali metal carbonates.

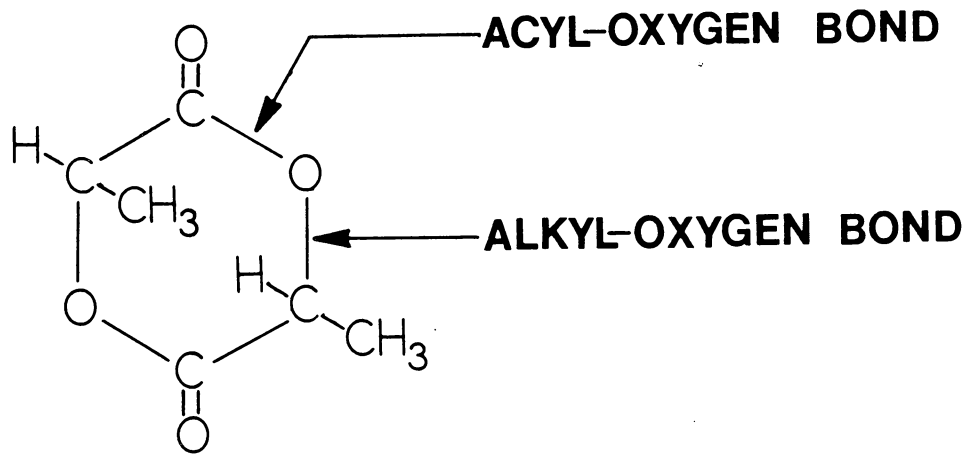

Figure 3.2. Potential for bond cleavage in ring-opening of lactide.

3.1.2.1 ANIONIC POLYMERIZATION OF LACTONES

Some of the most effective anionic catalysts for the polymerization of lactones appear to be metal alkyls and metal alkoxides (35). The nature of the actual initiating species for most anionic/lactone polymerization systems is somewhat obscure (44,35). Combination of certain modifying agents with metal alkyls has led to enhanced activity of the catalytic species. These modifying agents include water, oxygen, and alcohol (44). In contradiction, several patents dealing with organometallic catalysts for the homopolymerization of lactones have cited the necessity of the absence of water and other impurities (45,46). Despite the apparent confusion, Cherdron et al. (34) have proposed that the mechanism for anionic polymerization involves the acyl-oxygen cleavage of the lactone rings as shown in Fig. 3.3. The attack of the base upon the carbonyl group is the characteristic feature of the initiation process. The anion produced upon the opening of the ring is the propagating intermediate. Addition of subsequent monomers continues until termination or equilibrium monomer concentration is reached.

It has been speculated that, excluding any termination or side reactions, these anionic systems should lead to "living polymers", and the molecular weight should be inversely proportional to the concentration of the "catalyst"

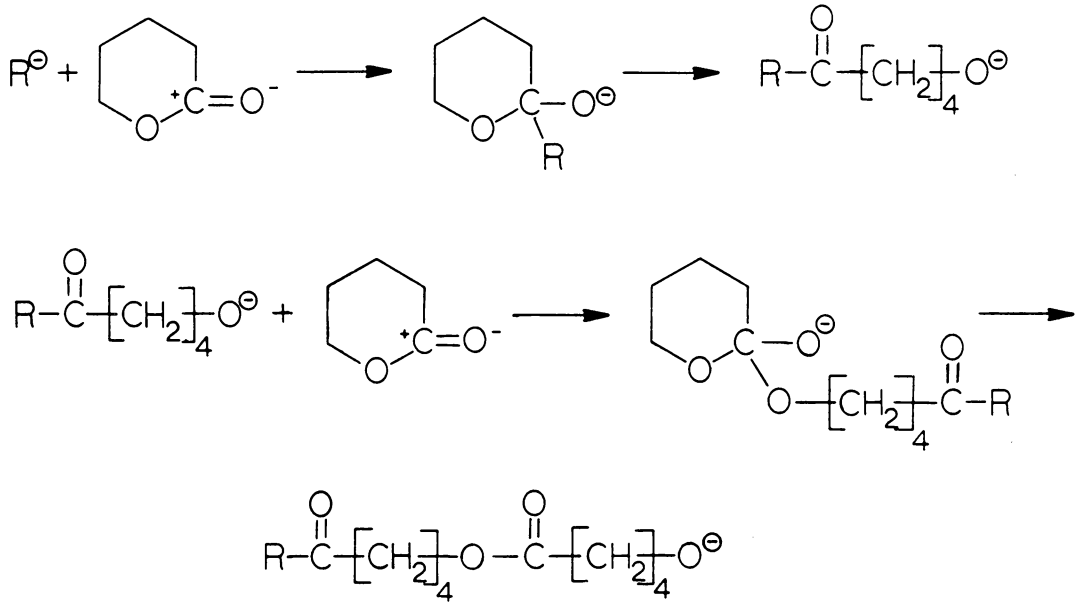

Figure 3.3. Reaction mechanism proposed for anionic polymerization of valerolactone (34).

species. For example, the polymerization of ϵ-caprolactone and α,α dimethyl- β -isopropylidene β lactones when catalyzed with dibutyl zinc, shows reaction profiles indicative of a "living polymer" system (47,36), although molecular weight distribution data to support this premise were unavailable.

3.1.2.2 CATIONIC POLYMERIZATION OF LACTONES

Most reported polymerizations employing only acid catalysts, Lewis or protonic, describe only the preparation of low molecular weight polyesters (34,37). Cationic catalysts, in the absence of active hydrogen initiators, have been suggested to involve propagation through either an oxonium ion or the carbonium ion derived by the ring-opening of the oxonium ion (37). For the case of ring-opening ethers, it has been argued that since the trialkyloxonium ion is the more stable of these, the oxonium ion is the predominant species in the propagation (37). Generally, the accepted scheme for propagation, as shown in Fig. 3.4, involves both the oxonium and carbonium ion in equilibrium. Through the work of Cherdron et al. (34) and Yamashita et al. (37), it has been shown that both the basicity and free energy of polymerization participate in determining the kinetic and thermodynamic characteristics (respectively) of the cationic (non-active hydrogen) polymerization of lactones.

In the presence of an active hydrogen compound, where a carbonium/oxonium ion intermediate would not be possible, cationic catalysts are postulated to aid in the acyl-oxygen cleavage (16). Specific intermediate structures have not been proposed (37).

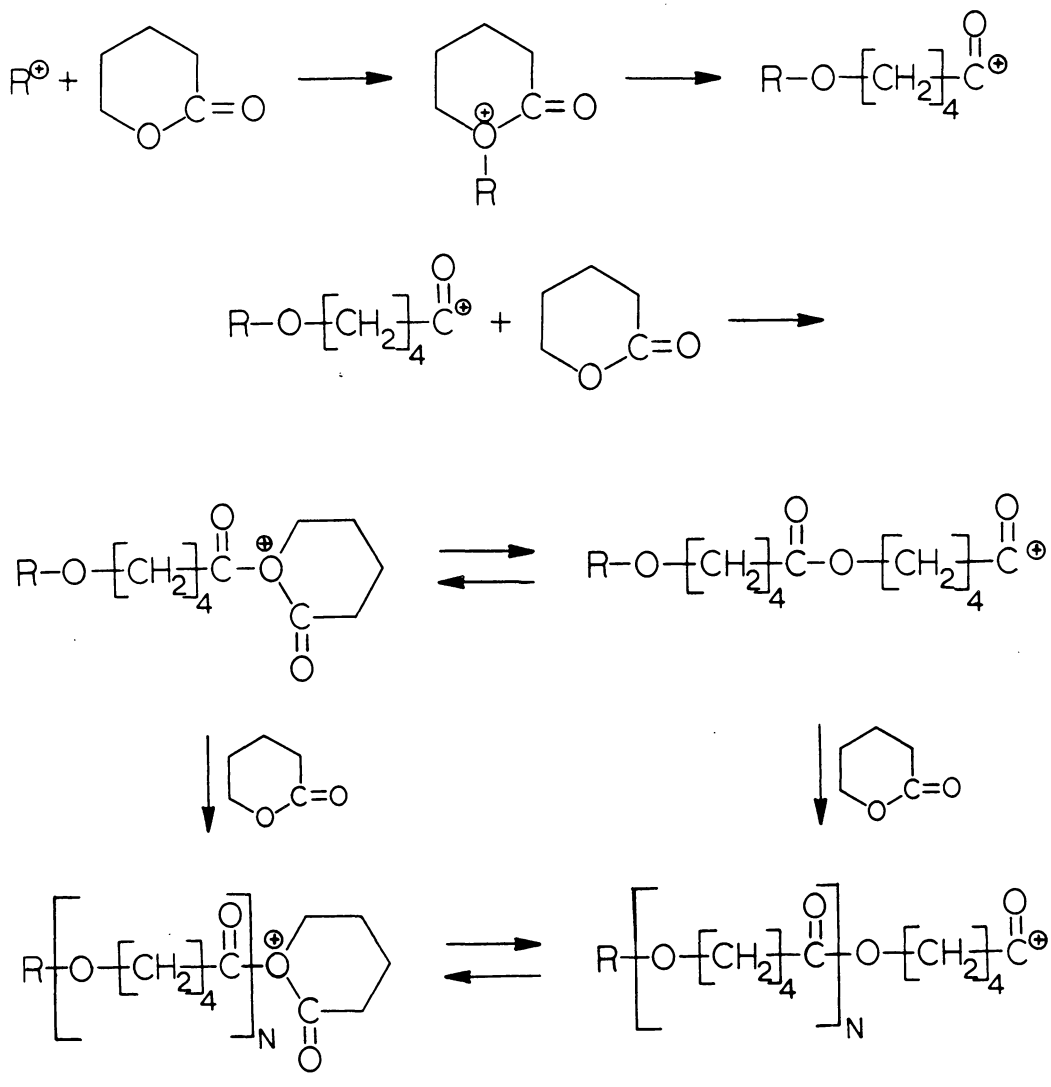

Figure 3.4. Reaction mechanism proposed for cationic polymerization of valerolactone (37).

3.1.2.3 POLYMERIZATION OF LACTONES INITIATED BY ACTIVE HYDROGEN SPECIES

Various alcohols, amines, and carboxylic acids have been shown to react with lactones to form a variety of adducts (48). By reducing the reaction concentration of active hydrogen species, the molecular weights of the product polyesters were demonstrated to increase, suggesting a stepwise addition of lactone monomer. The polymerization of δ-valerolactone with an alcohol and amine has generally led to low absolute molecular weight, suggesting a substantial amount of unreacted monomer in equilibrium with the polymer (16). A kinetic study indicated that in the initial stages of the reaction, a rapid reaction between the active hydrogen species and δ-valerolactone occurred followed by very slow propagation. The mechanism postulated for active hydrogen polymerization of lactones is given in Fig. 3.5. Presumably the propagating species in lactone polymerizations so initiated is the terminal hydroxyl group. Generally, these polymerizations require temperatures of 100 to 200 C and long reaction times.

The accelerating effects of various catalysts mentioned previously on the active hydrogen initiated polymerizations are considered to be related to the use of these catalysts in promoting transesterification (31,32,42,43).

Kohn et al. (49) have proposed a mechanism for the

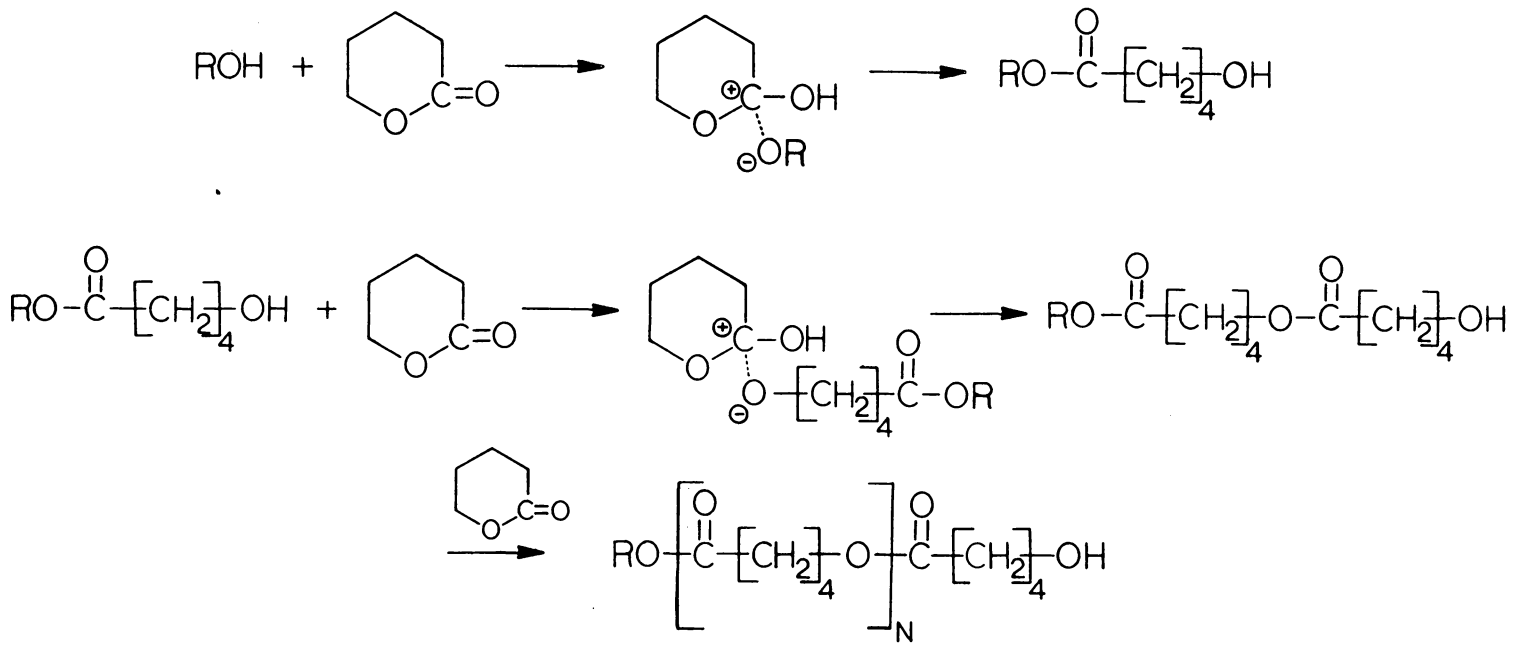

Figure 3.5. Reaction mechanism proposed for active hydrogen polymerization of valerolactone (48).

polymerization of glycolides in the presence of active hydrogen species based on a transesterification reaction. Figure 3.6 shows the detail of the steps involved. In general, it was postulated that attempts at polymerizing glycolides with strong Lewis acids (cationic catalysts) under anhydrous conditions failed because trace amounts of water were necessary to form protonic acids from the hydrolysis of Lewis acids. The resulting protonation of one of the two carboxyl oxygens on glycolides will promote a transesterification type of addition of glycolide followed by a proton shift. Polymerization proceeds through the repeat of this process. If, in fact, this is the mechanism, it would aid in the explanation of the use of known transesterification catalysts in promoting active hydrogen initiated polymerizations of lactones.

It might be expected that the conditions for a "living polymerization" would be fulfilled under some of these mechanisms. However, the possibility of ester interchange, both intra- and inter- molecular, is a strong possibility and would tend to broaden the molecular weight distribution to that of a most-probable distribution.

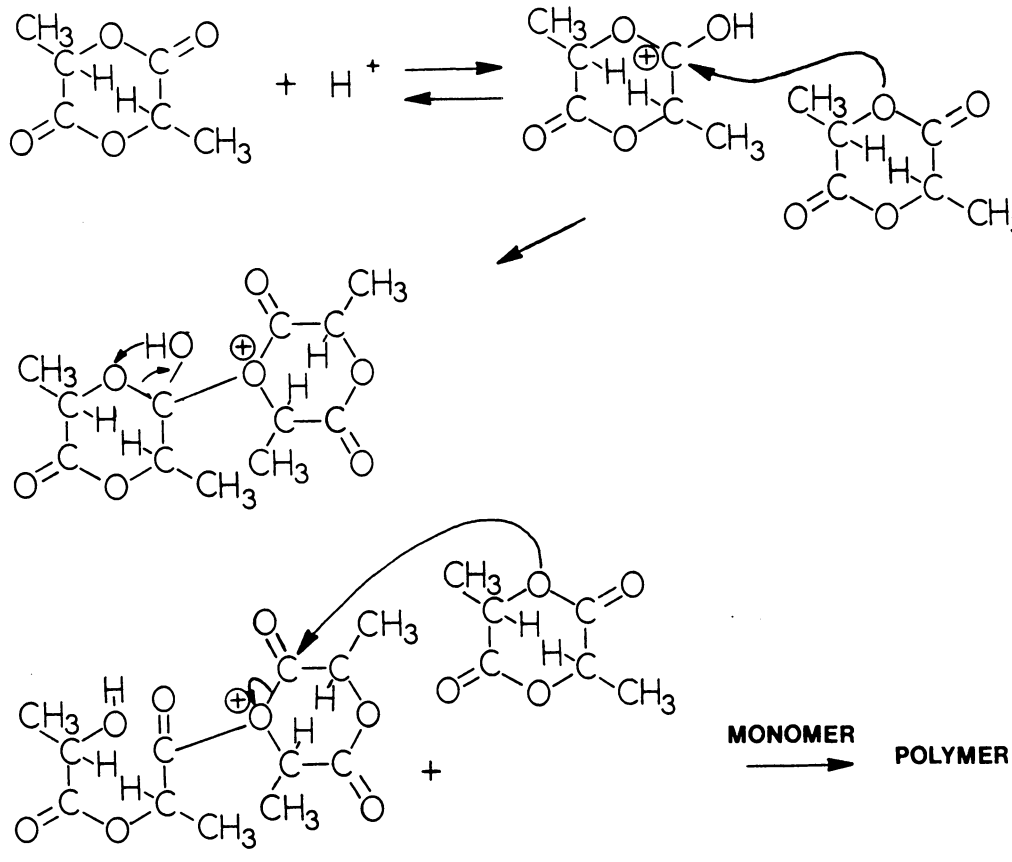

Figure 3.6. Transesterification (S_N2 type) polymerization mechanism for lactide (49).

3.1.2.4 POLYMERIZATION OF LACTONES CATALYZED BY COORDINATION TYPE MECHANISMS

A number of publications document the insertion reaction of lactone monomers into the metal hetero-atom of chosen organometallic compounds and indicate that catalyst incorporation into the polymer backbone may take place (14). The coordination catalyzed polymerization involves a concerted insertion with concurrent cleavage of covalent bonds in catalyst and monomer (33). The scheme is shown in Fig. 3.7, again, showing the anticipated acyl-oxygen fission. However, the occurrences of alkyl-oxygen cleavage in this mode of "catalysis" is clearly more prevalent as reviewed by Brode and Koleske (14). It may serve to reiterate that the anionic and cationic mechanism previously discussed may be considered as limiting cases. Depending on experimental conditions, a given compound may be observed to behave anywhere within the spectrum whose limits are defined as anionic and cationic.

Triisobutylaluminum has been claimed as an anionic catalyst for the polymerization of some optically active lactones derived as substituted caprolactones (15). As testimony to the subjectivity of the classification of catalyst systems into cationic, anionic, or coordination types, more recent authors claim that triisobutylaluminum functions as a coordination type catalyst in the

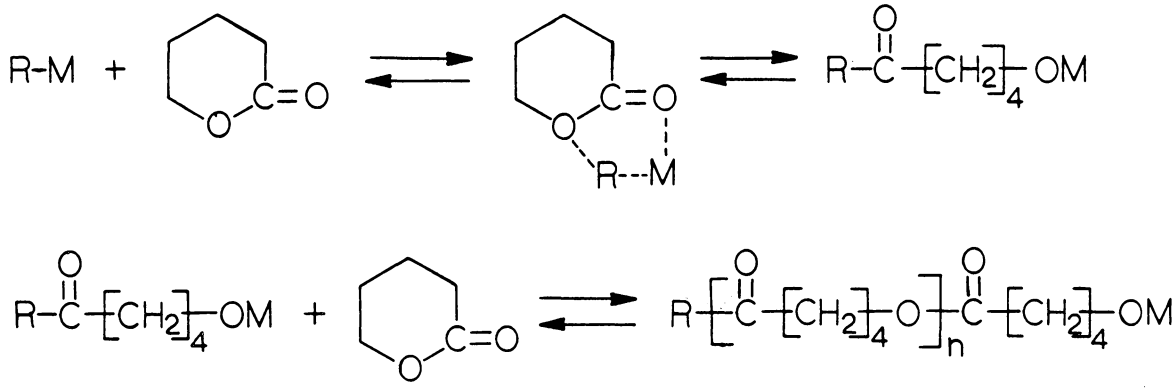

Figure 3.7. Coordination mechanism for polymerization of valerolactone (33).

polymerization of glycolide and lactide (49).

3.1.2.5 MOLECULAR WEIGHT DISTRIBUTIONS

A number of authors have suggested that ring-opening polymerization of lactones should, under ideal conditions, proceed via a "living" mechanism (15,30,47). This would, in fact, yield polymers with very narrow molecular weight distributions referred to as a Poisson distribution (8). Flory (8) states that the following conditions must be met in order to achieve narrow molecular weight distributions:

1) The growth of each polymer molecule proceeds by consecutive addition of monomer units to an active chain terminal group, the number of which is proportional to the initiator concentration.

2) All active terminal centers (one per molecule) must at all times during the course of the reaction be equally reactive.

3) The active centers for monomer addition must all be introduced at the onset of polymerization.

4) There must be no chain transfer, termination, ester interchange, or depolymerization steps during the course of the reaction.

In general, most ring-opening reactions (50), including lactone polymerizations (33), result in broader distributions. The ideal conditions above are only known to exist for lactone polymerizations for some limited solution polymerization conditions (29). In fact, prediction and/or

control of molecular weight based on catalyst concentration for the melt polymerization of lactide (21,41,51,52), as well as six membered lactone rings in general (14,15,53-58), cannot be made based on the literature data available. Kinetic data on the polymerization of caprolactone in the melt do not fit Flory's "living" mechanism. This has led to the conclusions that, in addition to initiation and propagation steps, side reactions involving co-initiators, chain transfer phenomena, transesterification reactions, and the formation of cyclics in depolymerization reactions are involved (33).

3.1.3 STEREOCHEMICAL SEQUENCE CONSIDERATION IN POLY(LACTIC ACIDS)

Different configurational structures in poly(lactic acid) are obtainable depending on the diastereoisomeric composition of the lactide feed (10). In particular, the six membered cyclic diester, with two chiral centers per molecule, can exist as four different compounds. Both the L,L and D,D antipoles are known to exist as L- and D-lactides, respectively. The equimolar solid racemic combination of L- and D- lactides, and finally the D,L diastereoisomer or meso-lactide have also been isolated. As discussed previously, many of the known initiators for the ring-opening polymerization are configurational respecting. Thus, the pair addition mechanism of lactide ring-opening polymerization provides a means of synthesizing some controlled tacticities (39). For example, the L-lactide will polymerize to a crystallizable isotactic polymer with a melting point of 180 C and a glass transition temperature of 60 C (59). Polymerization of racemic lactide will yield a tacticity dominated by random sequences of meso dyads as dictated by the D,D and L,L dimer repeat units. Racemic poly(lactic acid) is an amorphous polymer with a slightly lower glass transition temperature at 53 C (41). Poly(L-lactic acid) and racemic poly(lactic acid) are the two systems synthesized in this study. However, two additional

possibilities exist and should be mentioned for completeness. Meso-lactide polymerizes to a predominantly syndiotactic configuration since racemic dyads are favored, while a completely atactic poly(lactic acid) is also possible via a condensation route from a racemic lactic acid feed stock (60). Figure 3.8, originally constructed by previous authors (60), shows the theoretical configurational structures of the four simplest lactic acid stereocopolymers discussed above.

Sporadic work over the last twenty years has demonstrated the configurational dependence of physical and biological properties of lactic acid copolymers (61-64). In the most recent work, a systematic introduction of D units into predominantly poly(L-lactic acid) affected the control of the tensile strength and biodegradability of the stereocopolymers. It has been suggested that the occurrence of transesterification reactions in the polymerization reaction or in subsequent thermal processing could affect stereosequence distributions although the overall enantiomeric purity of the copolymers is unaffected since chiral bonds are not broken in transesterification (65). Thus, transesterification has the potential of destroying intended sequence distributions in poly(lactic acids) copolymers (random and/or block) and thus, in turn, affect biomedical end use performance.

Lillie and Schulz (38) were the first to attempt quantitative NMR techniques in order to characterize

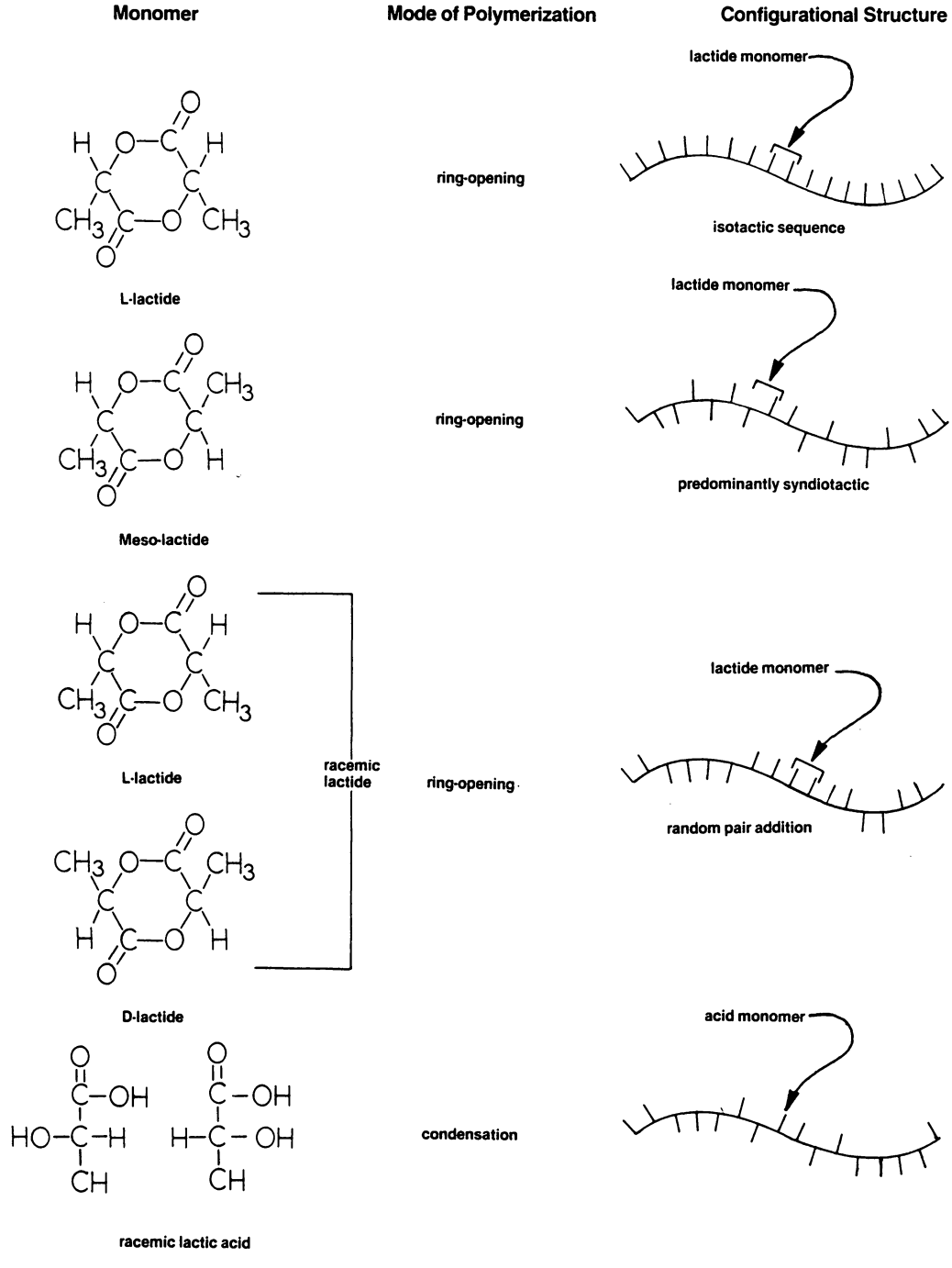

Figure 3.8. Configurational structures of lactic acid stereocopolymers (60).

stereosequence distributions in poly(lactic acid) stereocopolymers. Recognizing the potential for transesterification, two models for the microstructure of the polymer were formulated. Assuming no transesterification, the polymer sequence distributions were calculated based on the retention of the stereochemical grouping of the monomer. Bernoullian statistics were used to simulate paired addition of chiral centers in a random propagation step. In the other extreme, wherein transesterification would tend to randomize the aforementioned structure, Bernoullian statistics were used to simulate single addition of D or L units in chain propagation step. Neither model was conclusively eliminated since it was deemed that the spectra resolutions in both ^{1}H and ^{13}C NMR were not sufficient to allow distinction between the models.

Schindler and Harper (66), with a similar analysis of only proton NMR of racemic poly(lactic acid), generally found agreement between peak assignments and Bernoullian statistics for pair addition. For a 60-MHz spectrum, the methine region showed two quartets whose intensity ratios agreed with the Bernoullian pair addition statistics prediction of 3/1 for a dyad assignment. The methyl spectrum at 100 MHz showed 3 doublets whose ratios agreed with the calculated ratios for triad assignment. The methine spectrum at 100 MHz was postulated to show tetrad sensitivity, however, the resolution of the twenty peaks anticipated from 5 quartets

was cumbersome and only two of the five tetrads could be unambiguously assigned. The generally close adherence to Bernoullian statistics for pair addition caused the authors to conclude that the frequency of transesterification reactions during polymerization, if they occurred at all, were too infrequent to generate stereosequences detectable by NMR. Polymerization conditions were summarized as a bulk phase synthesis at 130 C with 50 ppm stannous octoate for 260 hours.

More recently, Chabot et al. (60) published a fairly detailed ^{13}C NMR study of a series of stereocopolymers of poly(lactic acids). The copolymers were synthesized from various lactide monomer mixtures of L-lactide and racemic lactide. In addition, a polymer synthesized from meso-lactide and a condensation polymer synthesized from racemic lactic acid were used in the study. The resolution of the fine structure in each of the three ^{13}C NMR peaks seen in poly(lactic acid) deteriorate in the order carboxyl, methine, and methyl. The focus of this study was directed towards the assignment of the peaks in the carboxyl region.

Racemic poly(lactic acid), whose fine structure was seen to improve by increasing the frequency of measurement from 22.51 MHz to 62.86 MHz, was determined to be consistent with the pair addition of monomer. The carboxyl spectrum, although obviously very complex, was simplified into three distinct areas. Previous authors (38) tentatively assigned

the three regions to random triads corresponding to isotactic, heterotactic, and syndiotactic sequences. However, if pair addition of monomer dyads was the sole mechanism determining the sequence distribution, the formation of syndiotactic triad sequences would not be possible without inversion of an asymmetric carbon during polymerization or the presence of meso-dilactide. In consideration of this, Chabot et al. show that the best fit is apparently obtained for pentad stereosensitivity assuming pair addition statistics. The anticipated number of peaks for pentad sensitivity in a pair addition mechanism is seven. Thus, the analysis was done by assuming that the lowest field peak in the carboxyl spectrum was the isotactic peak while the highest field peak was a lone heterotactic peak. All other heterotactic peak areas were assumed to be grouped under the third and largest peak at intermediate field strength. This grouping of peaks is, in part, supported by the observation that the unique peak observed for poly(L-lactic acid) occurs at the same chemical shift as the low field peak in racemic poly(lactic acid).

Auxiliary proof that the racemic spectrum represents pair addition statistics is gleaned from a comparison with the spectra of the condensation product of racemic lactic acid. This latter polymer, by the nature of the polymerization technique, was known to have single addition statistics and as such showed 16 individual peaks in the NMR

spectra, the precise number required by pentad single addition statistics.

Fine structure of the racemic poly(lactic acid) NMR spectra indicates the possible presence of peaks numbering greater than seven. This hints at the presence of some of the forbidden pentads denied by pair addition. Thus, Chabot et al. (60) conjecture that some transesterification may take place during polymerization. A 50%/50% mixture of poly(L-lactic acid) and racemic poly(lactic acid) was formed to test the transesterification hypothesis. The NMR spectra before and after heating the blend for 72 hours at 140 C were compared. Before heating, the spectrum was an obvious superposition of the blend components while after heating, there was a severe modification of the spectrum. The dominant trend being the growth of the heterotactic intensity at the expense of the isotactic intensity. Thus, rearrangement of stereochemical sequence, ostensibly through transesterification, would seem likely especially since the resulting polymer was soluble in acetone which is a known non-solvent for stereochemically pure poly(L-lactic acid). However, these observations do not seem consistent with the published polymerization conditions. Many of the stereocopolymers were exposed to a reaction temperature of 140 C for times in excess of 700 hours without significant deviation from pair addition statistics. An additional oversight may be mentioned here, in that it is well known

that the melting point of poly(L-lactic acid) is approximately 180 C. Thus, annealing a blend containing this crystallizable material at 140 C would necessarily cause phase separation. Thus, the poly(L-lactic acid) would be removed from participating in the transesterification reaction by crystallization. Finally, Chabot et al. (60) comment that the redistributions of the D and L units through transesterification seem to be somewhat limited since they were unable to randomize the stereosequence completely.

In summary, it would seem that there is limited data concerning the transesterification reactions in poly(lactic acids) and more importantly, even less data regarding its effect on stereochemical sequence distributions. In light of the increasing importance of poly(lactic acids) stereocopolymers in biomedical applications (1-5), and the sensitivity of the end use properties to configurational structure, it would seem worthwhile to improve on NMR techniques for the characterization of sequence distributions in poly(lactic acids). Also, additional effort is necessary if transesterification mechanisms and their effects on the reorganization of stereochemical sequences in poly(lactic acids) are to be understood.

3.1.4 THERMAL DEGRADATION BEHAVIOR IN LACTONE POLYMERS

In early studies in the polymerization of lactones Carothers (67) noted that both poly(glycolic acid) and poly(lactic acid), in common with other polymers formed by ring-opening valerolactone derivatives, regenerate the original cyclic monomer on thermal degradation. Based on these observations, it was argued that the polymerization was a reversible process (67). Subsequently, detailed investigations of the degradation products and mechanisms of breakdown of these glycolide based polymers have been limited to principally two groups (68-73). An understanding of the thermal degradation behavior is important because of the temperatures required in processing the polymers. Thermal sensitivity and/or hydrolytic degradation have been the major obstacles to the extensive commercialization of poly(lactic acid). A brief overview of thermal degradation in lactone polymers is discussed, culminating in a summary of the conclusions regarding the previous work on the thermal degradation of glycolide based polymers, principally poly(glycolic acid), poly(isopropylidene carboxylate), and poly(lactic acid).

Based on the previous investigations of the pyrolitic decomposition of simple non polymeric, esters, it appears that β -elimination is the preferred mechanism if a hydrogen atom occupies a position beta to the ether oxygen in

the ester linkage (74). Figure 3.9 depicts the β - elimination mechanism.

The behavior of polyesters in thermal decomposition seems to be somewhat more complex and can be closely linked to the type of end group and/or the nature and extent of catalyst/initiator system present. For example, the depolymerization of lactone macromolecules, whether through an ester interchange process (67) or a back biting mechanism (16), has been shown to be a function of the nature of the end group. Saotome et al. (16) has shown that poly δ - valerolactone begins to depolymerize at temperatures as low as 180 C unless the hydroxyl end groups have been acetylated, in which case, excellent stability is extended to an upper limit of 200 C. More recently, this method has been adopted in the stabilization of poly(lactic acid) (75). Although hydroxyl-terminated poly ϵ -caprolactone reportedly does not begin to depolymerize to monomer up to temperatures of 270 C, addition of tetrabutyl titanate, metal chlorides, and other catalysts to the polymer caused the depolymerization to a variety of cyclic compounds at temperatures as low as 250 C (48,76).

The detrimental effect of carboxylic acid end groups on thermal stability of polyesters is well documented (77). Assuming an acid catalyzed hydrolysis, regeneration of acid would have an autocatalytic effect with a precipitous drop in molecular weight. Even at ambient conditions, carboxylic

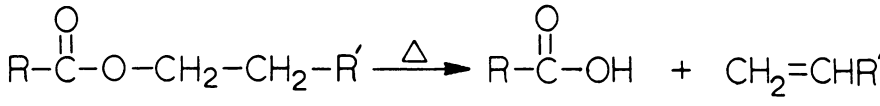

Figure 3.9. β-elimination mechanism in simple esters (74).

acid groups have been shown to decrease polymer molecular weight over prolonged periods of time (14).

Hydrolytic and thermal stability are particularly low for some lactone polymer systems initiated via coordination types of catalysts. These reactions can lead to the incorporation of catalyst residues into the main chain as polymer end groups. Such linkages have been shown to result in severe loss of molecular weight even for low temperature exposures. For example, poly ϵ-caprolactone prepared with dibutyl zinc catalyst exhibits a rapid decrease in molecular weight when exposed to 120 C for short periods of time (14). Similar instability results are realized for the ring-opening of lactones with ethylzincdiphenylamine (78).

Brode and Koleske (14) report an interesting case wherein just the presence of tin based catalysts such as stannous octoate and trimethyltinacetate can result in thermal instability. Extensive work investigating the possibility of lactone insertion into the tin catalyst using equivalent molar quantities of lactone and tin ester functionality failed to show any trace of insertion. However, small amounts of polylactone were recovered, suggesting to the workers that stannous octoate behaves as an initiator as well as a catalyst. Brode and Koleske (14) also point out that catalyst incorporation as a polymer end group could also result from the reaction of the stannous octoate with the active hydrogen end group. In any event, the

mechanism supporting either the enhanced thermal degradation of polylactones in the presence of stannous octoate or the suggested initiation activity of this catalyst was not disclosed.

In general, thermal stability may be expected from lactone based polyesters if catalyst insertion has not occurred, polymer terminal end groups are of a stable variety, and the free energy of polymerization is such that depolymerization to monomer is not favored.

Sutton et al. (68-71) have taken a very systematic approach in analyzing the degradation mechanism of polylactones based on the glycolide family of monomers. From the start, they listed all anticipated thermal decomposition mechanisms of polyesters as follows:

1) random homolytic or heterolytic chain scission possibly followed by chain depolymerization from the point of chain scission,

2) inter or intramolecular ester interchange,

3) chain depolymerization from chain ends,

4) molecular decarboxylation or decarbonylation possibly accompanied by chain recoupling.

From an analysis of kinetic and analytical results that characterize the thermal degradation of three polyglycolides, poly(isopropylidene carboxylate), poly(glycolic acid), and poly(lactic acid), most of the possibilities can be eliminated.

A brief summary of experimental observations from the series of publications by Sulton et al. (68-71) is discussed as they pertain to both the elimination of the possibilities described above and the support of the accepted mechanism of degradation.

Over a wide range of temperatures, the observed degradation products of poly(tetramethylglycolic acid) were cyclic monomer, and to a progressively lesser extent, acetone, carbon monoxide and methacrylic acid. Similarly, the degradation of poly(lactic acid) has led to lactide, acetaldehyde, and carbon monoxide (72,73). In either case, the production of cyclic monomer is considered the rate determining step with subsequent decomposition of the monomer to the more volatile components.

First order kinetics were observed for the degradation behavior of all these polymers, both in standard thermogravimetry results and in gas evolution analysis, wherein the degradation products were allowed to stay in proximity to the polymer. In the later stages of the gas evolution experiment, deviations from first order kinetics were observed and ascribed to an autocatalytic effect.

Molecular weight change during degradation was estimated with solution viscometry techniques. Although very slow decrease in molecular weights was demonstrated in thermogravimetry experiments, the autocatalytic effects in the gas evolution experiments caused the molecular weight to

fall at substantially steeper rates. This was confirmed by allowing poly(glycolic acid) to degrade in a stagnant atmosphere in the presence of benzoic acid and recording the enhanced weight loss kinetics.

The effect of initial polymer molecular weight on the kinetics of degradation was seen to be a progressive deviation from first order behavior only for species with number average molecular weights below 10,000 with little or no sensitivity to molecular weight above this threshold value.

Temperature effects on the rate of decomposition processes were found only to change the value of the first order rate constant which led to the calculation of an activation energy of 27.2 kcal/mole, a frequency factor of 4.1×10^7 sec^{-1}, and an entropy of activation of -29 cal/deg. mole for the degradation of poly(isopropylidene carboxylate).

Decarboxylation and/or decarbonylation were discounted because these mechanisms were not consistent with the production of the major degradation product, the cyclic monomer. In addition, intermolecular ester interchange, as well as decarboxylation and/or decarbonylation, is inconsistent with the first order kinetics observed. Generally, Sutton et al. (69) suggest that radical reactions resulting from homolytic scission are of little importance below 400 C although there was some sensitivity of rate constants to the presence of oxygen. More recent work has

shown that the poly(lactic acid) chain is susceptible to radical attack at temperatures as low as 230 C (73). An ionic heterolytic scission process is energetically improbable at temperatures in and around the anticipated processing conditions although a dipolar process might be acceptable. The molecular weight dependence on the overall degradation kinetics would indicate that there are relatively small contributions from mechanisms involving chain ends. One such mechanism is shown in Fig. 3.10 which involves the β-hydrogen elimination ester decomposition mechanism followed elimination of methacrylic acid fragments for the poly(isopropylidene carboxylate) chain end. Another such mechanism, shown in Fig. 3.11, shows a backbiting phenomenon that results in cyclic monomer formation. Although both of these mechanisms show first order kinetics with respect to residual polymer, they are important only for high chain end concentrations (low molecular weights). Thus, in order to be consistent with the first order kinetics and the slow decrease in molecular weight observed in thermogravimetric experiments, a mechanism based on intramolecular transesterification and a reduction in chain length by one repeat unit for every step in the degradation process was proposed. This contrasts with the drastic molecular weight reduction which results from random chain scission mechanisms. For example, the autocatalytic reduction in molecular weight in the gas evolution experiments of Sutton

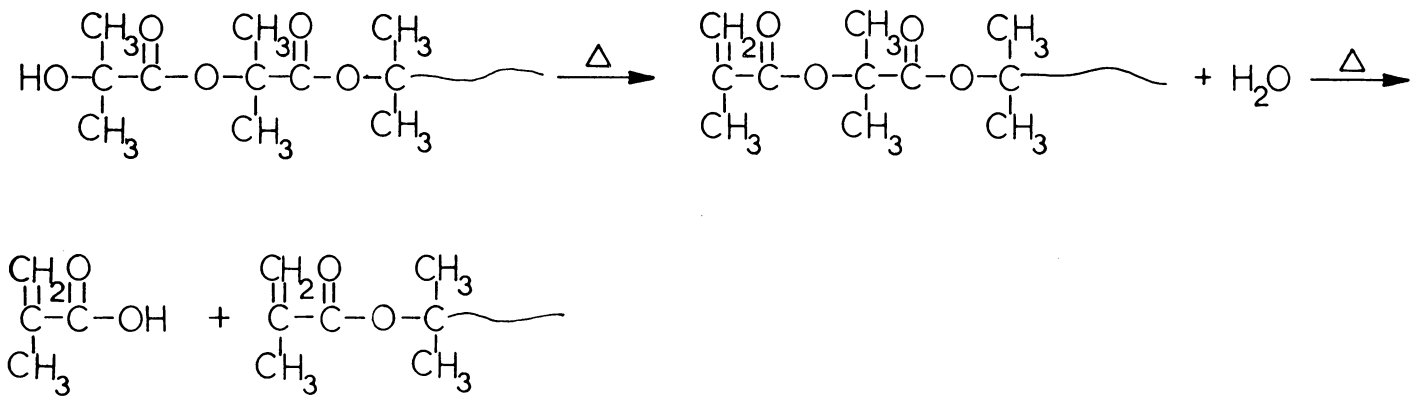

Figure 3.10. β -elimination mechanism for thermal degradation of poly(isopropylidene) (70).

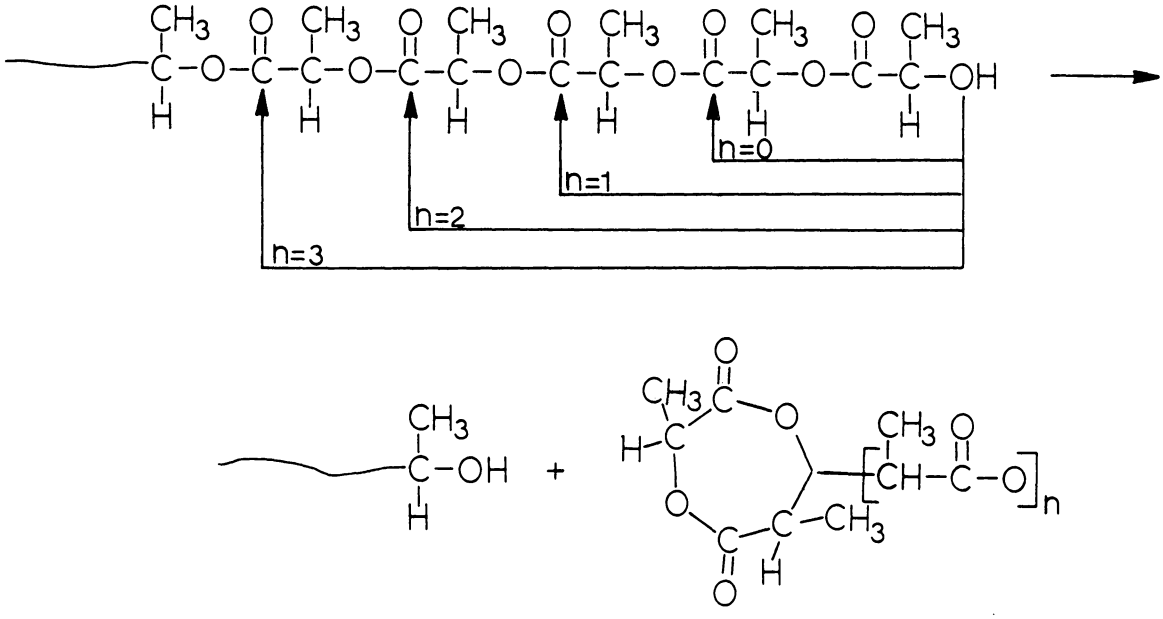

Figure 3.11. Back biting mechanism for the formation of cyclics (72).

et al. (69) are thought to be the acid catalyzed hydrolysis of the polyester.

Stannett and Szwarc (79) were the first to consider the now accepted mechanism for the thermal degradation of polyglycolides, which is shown in Fig. 3.12 as an intramolecular transesterification process in poly(lactic acid). The special configurations are such that the process may take place with little or no movement of the carbon centers. This high degree of steric order, along with the highly ordered and highly polar transition state, is quite consistent with the relatively low energetics of reaction summarized previously. The mechanism correlates well with the kinetic behavior and explains the formation of cyclic monomer with the minimal effect on molecular weight.

The primary mechanism for the thermal degradation of polyesters based on glycolide monomers (dimers of hydroxy-acids) is intramolecular transesterification leading to the formation of cyclic monomers. This has relatively subtle influences on molecular weight and molecular weight distributions. Other mechanisms which lead to more severe molecular weight loss and potentially less severe weight losses involve hydrolysis (potentially autocatalytic), homolytic chain cleavage, and backbiting mechanisms for the formation of cyclics and/or the depolymerization of the polyester. Other mechanisms have also been discussed above, however, these latter three mechanisms are generally judged

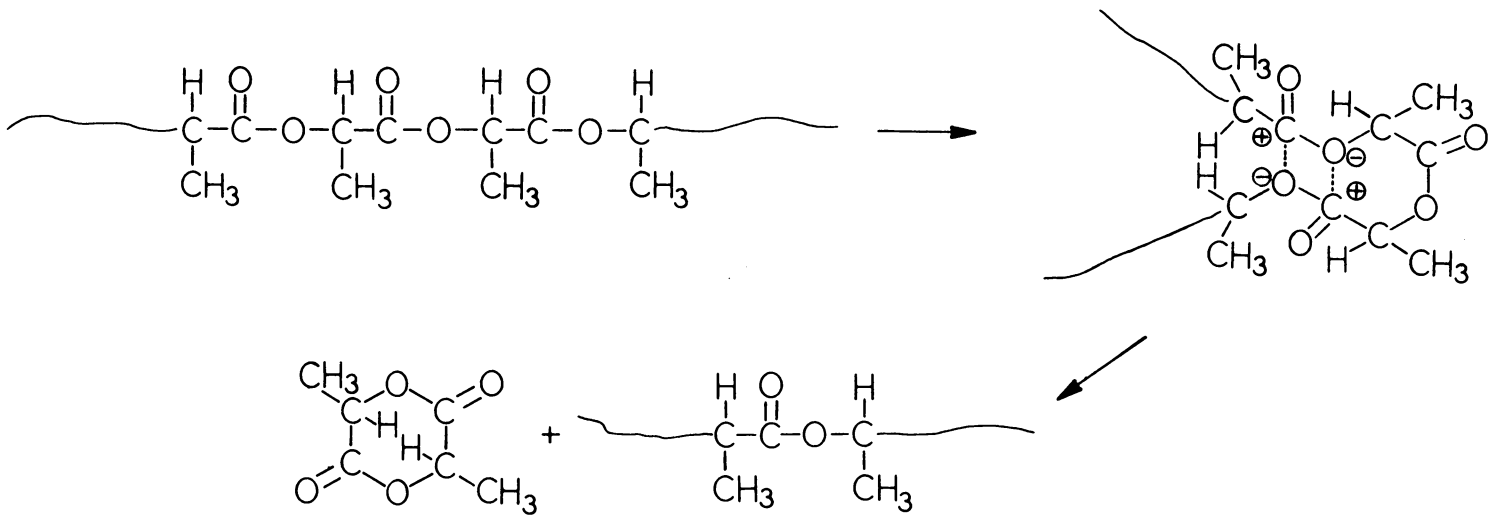

Figure 3.12. Intramolecular transesterification process in poly(lactic acid) (69).

to be the most likely competitors to the primary weight loss mechanism of intramolecular transesterification (70,72).

3.2.0 EXPERIMENTAL

3.2.1 MATERIALS

Both the optically pure L-lactide as well as the racemic D,L-lactide were obtained in polymerization purity from Boehringer through the importers Henley and Co. Based on previous attempts to polymerize these monomers (12), it was deemed necessary to further purify the lactides by recrystallizing twice from ethyl acetate. The ethyl acetate was previously dried over molecular sieves. Best results were obtained if the second recrystallization was done from solutions with very low supercoolings over a long time scale, approximately one to three days, to yield large crystals on the order of 5 mm in dimension. Exposure to ambient moisture was minimized by always handling the monomer under a dry nitrogen atmosphere. After recovery from the mother liquor, the lactide crystals were stored in a vacuum desiccator over phosphorous pentoxide.

Stannous octoate (2-ethyl hexanoate), obtained from Polysciences Inc., was used as the initiator/catalyst for the polymerization without further purification.

D,L-lactic acid in concentrated aqueous solution (88% purity) was used as a potential active hydrogen initiator and was also obtained from Polysciences, Inc.

The polymerizations of the purified lactides were

carried out via the ring-opening polymerizations in the melt based on the procedures originally developed by Kulkarni et al. (61) and Sinclair and Gynn (40). All details regarding the synthesis procedures will be applicable to the ring-opening of either L-lactide or the D,L-lactide with the following exception. The melting point of the optically pure monomer (98 C) is almost 30 C less than that of the racemic lactide (126 C). This allows the melt phase polymerization of the poly(L-lactic acid) to be carried out at considerably milder conditions.

Just prior to use, the lactide crystals were washed with cold ethyl ether freshly distilled from calcium hydride. This was thought to remove any residual lactic acid excluded from the bulk monomer by recrystallization but still residing on the crystal surface due to exposure to the mother liquor. Exposure to moisture was minimized by performing this procedure under dry nitrogen.

The polymerizations were carried out on two different scales. The first small scale synthesis on 1 gram batches was designed to investigate the effects of stannous octoate concentration, reaction temperature, lactic acid concentration, and reaction coordinate on molecular weight. Once a better understanding of the polymerization chemistry was in hand, the scheme was scaled up to a 300 gram scale. Larger batches of material were paramount to the subsequent study of the strain induced crystallization of blends of

poly(lactic acids) in biaxial deformation.

3.2.2 SMALL SCALE SYNTHESIS

The glass polymerization tube assembly shown schematically in Fig. 3.13 was washed in an aqueous base solution, rinsed in distilled water, and dried at 150 C overnight. Approximately one gram of lactide was charged to the bottom of the tube through the designated charge port under a dry nitrogen atmosphere. A serum cap was placed over the open port and the reactor was attached to a vacuum line at the seal.

Once a vacuum was established above the seal, the magnetic stir bar was used to break the seal and evacuate the reactor to a pressure below one millitorr. The monomer was then sublimed from the bottom of the reactor to the tube walls at the top. A heating bath was used to supply the heat of sublimation and a cooling jacket was used to localize the condensation. Heating bath temperatures were themostated to approximately 3 to 5 degrees centigrade below the melting point of the monomer. Ice water was the cooling medium in the condensation jacket. This final step in monomer purification was crucial in removing any residual water or other contaminating solvents which would lead to lower yields and reduced molecular weights. After sublimation was complete and the heating bath and the cooling jacket removed, the reactor chamber was put under a slightly positive pressure of dry argon. The serum cap was removed allowing a

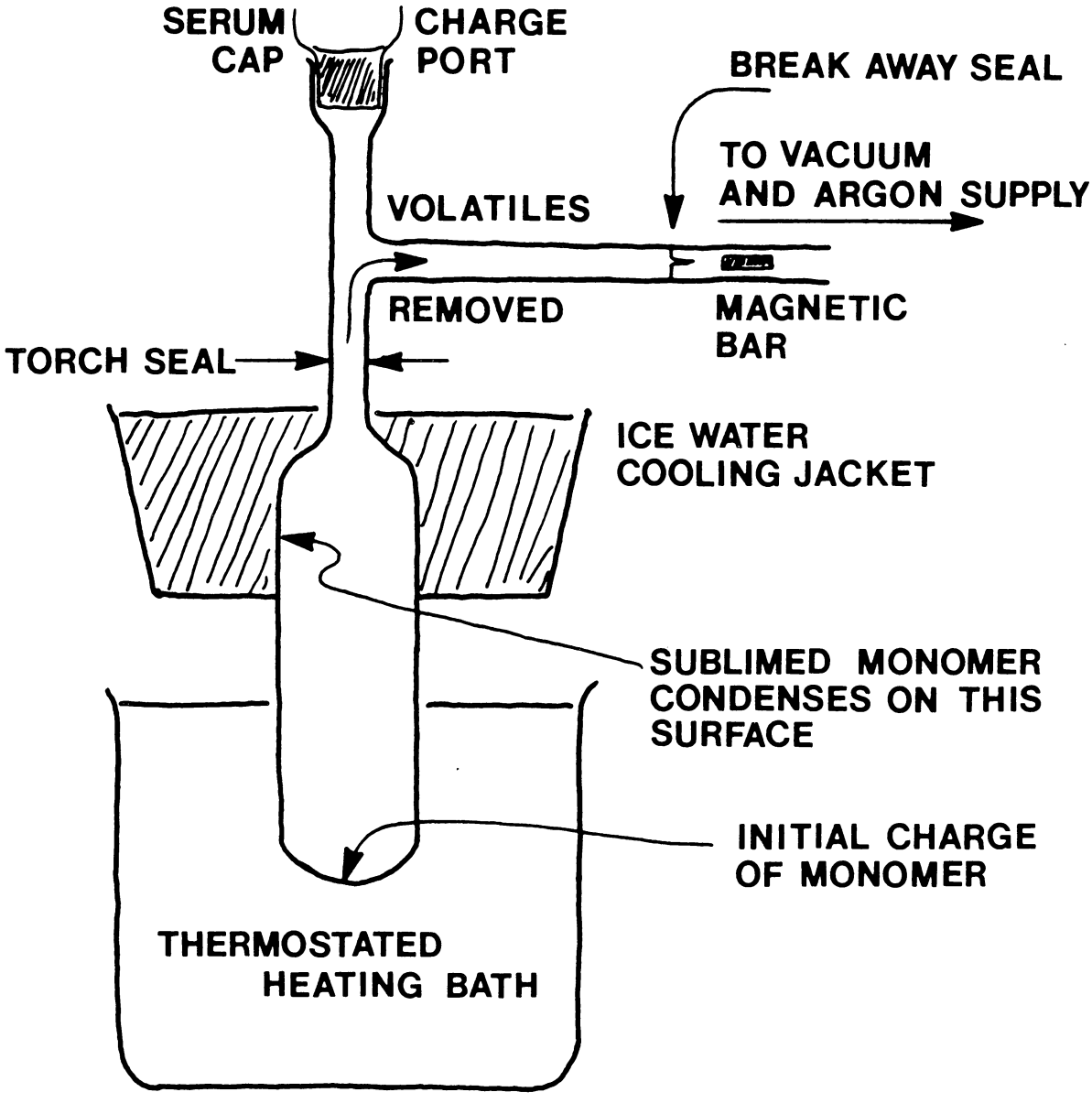

Figure 3.13. Small scale polymerization reactor.

positive flow of argon and the stannous octoate was added to the bottom of the reactor in a dilute dry pentane solution via a syringe. Stannous octoate was diluted in pentane to concentrations appropriate to a 0.5 ml. charge. The range of stannous octoate to lactide molar ratios investigated ranged from $1x10^{-3}$ to $1x10^{-5}$ mole/mole. As will be subsequently discussed, lactic acid was often added to the reaction scheme. Typically, the acid was added in an ethyl ether solution (also 0.5 ml per charge) via a separate syringe just after the pentane solution. Molar acid concentrations were varied from $3x10^{-4}$ to $3x10^{-2}$ mole/mole. The serum cap was then reinserted and the vacuum reestablished. After all the pentane (and ether) was evacuated, leaving the high boiling stannous octoate (and lactic acid) in a thin coating at the bottom of the polymerization tube, the reactor was torch sealed.

The sealed and evacuated vessel was then placed in an oven or oil bath at the required polymerization temperature which was necessarily above the melting point of the monomer. The polymerization temperatures studied ranged from 100 C (exclusively for L-lactide) to 200 C. On melting, the lactide was allowed to flow to the bottom of the polymerization tube at which time the tube was gently hand shaken to mix the stannous octoate with the monomer. Typical polymerization times were on the order of 60 hours. For the kinetics studies, both shorter and longer reaction times were

of interest.

3.2.3 REACTION SCALE-UP

With some experience in successful polymerizations well in hand, scale-up from a nominal one gram scale to 300 gram batches was undertaken. A larger reactor design is shown schematically in Fig. 3.14. Some modifications to the set-up procedures were necessary in order to accommodate the larger batch size.

First, the monomer was charged to a side flash in order to separate the sublimation residue from the reaction mixture. This residue was thought to consist largely of lactic acid that was more evident as separation from larger amounts of lactide was attempted. In addition, longer exposures to heat necessary for the sublimation of larger baths may also be responsible for increased observation of sublimation residue. After the monomer was charged to the side flask under dry nitrogen conditions, the open ports were serum capped and the reactor was attached to the vacuum line.

Again, a vacuum was then established in the reactor assembly by breaking the seal with a magnetic stir bar. The long side arm used for monomer charge was torched sealed. Sublimation heat was applied to the small side flask via a thermostated oil bath nominally 3-5 centigrade degrees below monomer melting points. Condensation of monomer on the inside of the large reaction flask was facilitated by the cold finger design and the larger cooling collar which held

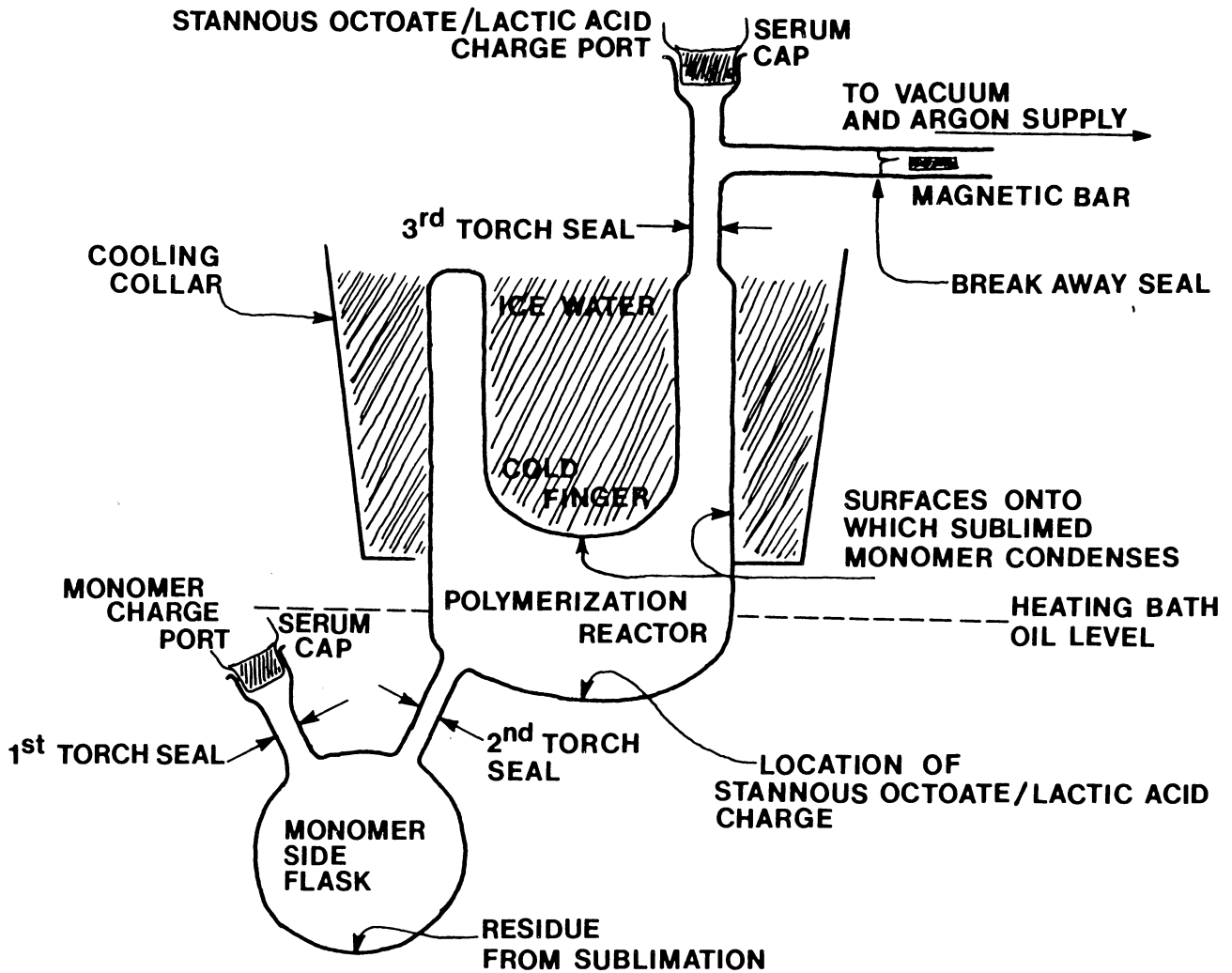

Figure 3.14. Large scale polymerization reactor.

the ice water. After sublimation was complete (30 hours) and the heating bath and the cooling collar were removed, the side flask was separated from the reactor by torch sealing the glass connecting tube, see Fig. 3.14. The stannous octoate/pentane solution was then added through the second serum port under a positive flow of dry argon. The stannous octoate molar concentration used for the large batches was always $5x10^{-5}$ mole/mole. Molecular weight control was affected by changing lactic acid concentrations added in ethyl ether solutions. As with the smaller reactors, the vacuum was reestablished, drying the pentane and ether charges and leaving the stannous octoate and acid at the bottom of the vessel. The reactor was sealed under vacuum and separated from the vacuum line by a third torch seal at the point of connection shown in Fig. 3.14. Subsequent to placing the now isolated reaction vessel in an oven at a polymerization temperature of 130 C, periodic mixing of the molten monomer, stannous octoate, and lactic acid for the first hour of reaction time was crucial in this large volume reactor for reproducible and homogeneous products.

3.2.4 POLYMER SOLUTION TREATMENTS

Both poly(L-lactic acids) and poly(D,L-lactic acids) were separated from residual monomer and stannous octoate by dissolving in chloroform at room temperature and precipitating in ice cold ethyl ether. The reaction products were then dried under vacuum at 80 C for a minimum of 20 hours. When appropriate, percent conversions were calculated based on the weight of the product after drying and the weight of the monomer originally charged to the reactor. This precipitation procedure was later shown to effectively fractionate some low molecular weight samples by virtue of the fact that lowest molecular weight fractions in these samples remained in the ether/chloroform mixtures. A more effective non-solvent for the polymer was sought which would also continue to solubilize the residual monomer and stannous octoate, but without success.

When necessary, blends of poly(L-lactic acid) and racemic poly(lactic acid) were made by dissolving the appropriate ratios of the homopolymers in chloroform to a final concentration of 5% weight/volume and then coprecipitating in hexane. Hexane was determined to be a very effective non-solvent for the polymer as well as the monomer. The precipitated blend was then vacuum dried as previously described.

3.2.5 POST SYNTHESIS THERMAL TREATMENTS

In conjunction with the investigations of transesterification and thermal degradation mechanisms, samples were exposed to 200 C with and without the concurrent application of vacuum. The small scale vacuum reactors, previously described, were also used to heat the samples to the desired temperature with the application of vacuum to a final pressure of less than 1 millitorr. Previously purified and dried poly(lactic acids) (~0.5 gm portions) were charged to the bottom of a precleaned reactor under dry nitrogen conditions. Vacuum was established as discussed previously and the sample was heated through the glass reactor walls with the application of a thermostated silicon oil bath. Typically, degradation products were induced to precipitate on the reactor walls above the sample with the aid of the cooling jacket also previously described. Samples were heated without the application of vacuum by placing the poly(lactic acid) between two sheets of aluminum foil coated with teflon and placing the sandwich between the plattens of a thermostated press. Only enough pressure was applied to guarantee a good thermal contact. Timed exposures were terminated by quenching the foil/sample sandwich between two auxiliary aluminum plattens at room temperature.

3.2.6 ANALYTICAL TECHNIQUES

The following techniques were used to characterize the synthesized poly(lactic acids).

3.2.6.1 GEL PERMEATION CHROMATOGRAPHY

Molecular weight distributions were determined by gel permeation chromatography (GPC) methods using a Waters Model 150-C High Temperature GPC equipped with a differential refractive index detector. Five Styragel columns, installed in series with the following pore size ratings 500 A, $1x10^3$A, $1x10^4$A, $1x10^5$A, and 1x10+6A, were used to effect the separations. Operating conditions included column temperature of 28 C, injection volume 200 l, and a flow rate of 1 ml/min. Tetrahydrofuran was used as the solvent for the racemic polymer, while chloroform was used as the solvent for the optically active polymer. Universal calibration techniques were used with narrow molecular weight polystyrenes from Polymer Laboratories to convert elution volume times to poly(lactic acid) molecular weights.

3.2.6.2 VISCOMETRY

Solution viscosities were measured with semimicroviscometers of the Cannon-Ubbelohde type in a water bath thermostated to 30 C ± 0.1 C. Intrinsic viscosities were obtained from typical dilution series double extrapolation techniques (81). Poly(L-lactic acid) measurements were done in chloroform, while racemic poly(lactic acid) measurements were done in tetrahydrofuran. The appropriate Mark-Houwink parameters are listed in Table 3.1 along with the source references.

Table 3.1

Mark-Houwink Constants
Used to Calculate Viscosity Average Molecular Weight from Intrinsic Viscosity

			Mark Houwink Constants		
Polymer	Solvent	Temperature	K (dl/gm)	a	Reference
Poly(L-lactic acid)	Chloroform	30°C	5.45×10^{-4}	0.73	(41)
Racemic Poly (lactic acid)	Tetrahydrofuran	31°C	5.50×10^{-4}	0.64	(82)

$[\eta] = kM_v^a$

$[\eta]$, Intrinsic Viscosity dl/gm
k,a, Mark-Houwink Constants
Mv, Viscosity Average Molecular Weight

3.2.6.3 DIFFERENTIAL SCANNING CALORIMETRY

Differential scanning calorimetry (DSC) on selected samples was accomplished through the use of a Perkin-Elmer DSC-4. Sample weights were on the order of 5 milligrams and a scanning rate of 10 C/min was used exclusively. Baseline corrections were done digitally using a standard software package supplied by Perkin-Elmer.

3.2.6.4 SPECTROSCOPY TECHNIQUES

High resolution 67.92 MHz. ^{13}C nuclear magnetic resonance (NMR) spectra of poly(lactic acids) were obtained using a Bruker WP-270SY spectrometer through the courtesy and assistance of Raj Subramanian. The samples were run in deuterated chloroform solutions at a concentration of 7.5% (weight/volume) at room temperature. Chromium acetyl acetonate ($Cr(acac)_3$) was added to the solution at a 0.1 M concentration as a relaxing agent in order to reduce the spin-lattice relatation times of the various carbons to a common value of about 1 second. This was accomplished by replacing the rate determining relaxation time mechanism of dipolar interactions with a paramagnetic relaxation mechanism (80). Inverse gated decoupling was also used to counteract nuclear Overhauser effects. It has been previously determined that the combination of inverse gated decoupling with the addition of $Cr(acac)_3$ can yield quantitative ^{13}C spectra (80). Spectra were generated by Fourier transforming an accumulated signal of 2000 free induction decays. Peak areas were digitally integrated using instrumental software.

Infrared spectra were measured on an IBM spectrometer. Samples were prepared in potassium bromide (KBr) pellets by first mixing sample with KBr crystals and subsequently pressing into pellet form in a standard manner.

Two wavenumber resolution ($2cm^{-1}$) was typical.

3.3.0 RESULTS AND DISCUSSION

As suggested in the introduction, the goals of this project were threefold. The primary goal was to investigate the feasibility of tailoring a reaction scheme which would allow for the predictive control of molecular weight in the synthesis of poly(lactic acids). As a corollary to the main thrust, the potential effects of transesterification on the stereochemical sequence distribution in poly(lactic acids) and, the effects of thermal processing on the product molecular weight were also investigated. Each of these topics will be discussed under separate headings.

3.3.1 MOLECULAR WEIGHT CONTROL IN THE SYNTHESIS OF POLY(LACTIC ACIDS)

Investigations into the mechanism of the ring-opening polymerization of lactide with an active hydrogen initiator (lactic acid) used in conjunction with a transesterification catalyst (stannous octoate) are described. The results are discussed in terms of the effects of lactic acid concentration, stannous octoate concentration, polymerization temperature, and reaction profile.

3.3.1.1 LACTIC ACID CONCENTRATION

A previous investigation (12) concluded that the presence of the hydrolysis products of lactide most likely has a detrimental effect on the product molecular weight from the melt polymerization of poly(lactic acid). In deference to this previous conclusion, a series of polymerizations were carried out at varying degrees of monomer purity. The optically active L,L lactide monomer, which had been recrystallized once from ethyl acetate, was combined in various proportions with the as received unpurified monomer. The monomer mixtures were washed with dry ethyl ether in the standard way prior to polymerization. Stannous octoate concentration, 2 x 10^{-4} mole/mole, as well as polymerization temperature, 130 C, was held constant. After 30 hours polymerization time, the reactions were quenched to room temperature. All products were white crystalline solids, even at reaction temperature. Once the polymers had been separated from residual monomer, intrinsic viscosities were measured. The resulting viscosity average molecular weights were plotted as a function of monomer composition in Fig. 3.15. A very systematic trend was evident supporting the conclusions of Kohn et al. (12). Clearly, molecular weight increased sharply with monomer purity.

It is interesting to note the success of the polymerizations despite the fact that the polymer

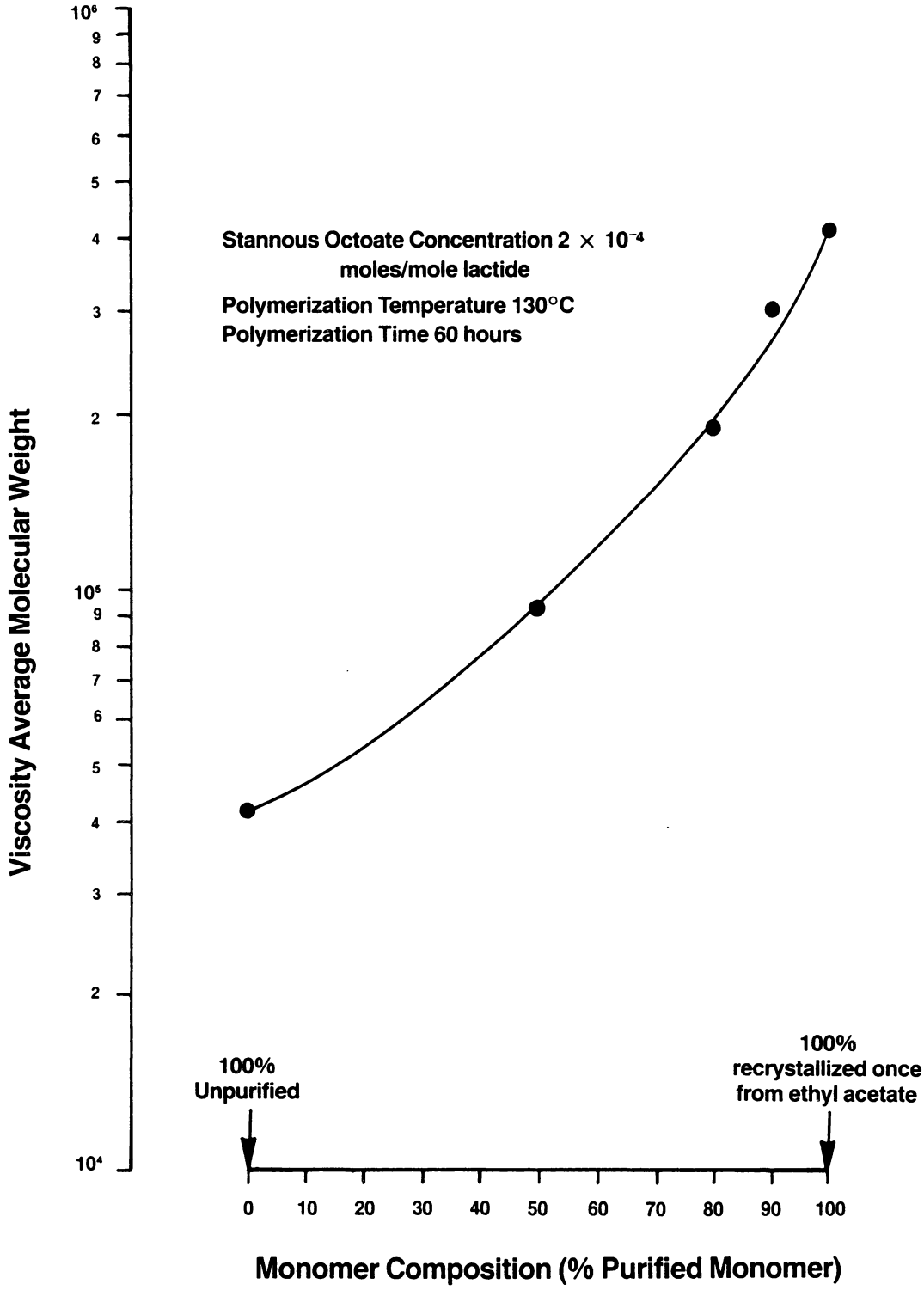

Figure 3.15. Effect of monomer purity on molecular weight in the polymerization of poly(L-lactic acid).

crystallizes in the reaction vessel. Apparently, the ability of the monomer to diffuse to the reaction site is not a rate limiting step. This observation has also been reported by other workers indicating high conversions in bulk polymerizations of poly(L-lactide) at temperatures well below the polymer melting point (42,43). However, in order to guarantee homogeneous reaction conditions, most of the balance of this work will deal with the polymerization of racemic poly(lactic acid) which does not crystallize and whose glass transition (57 C) is well below reaction temperatures.

It is generally known that the lactide monomer is produced by heating lactic acid in the presence of zinc-dust (38). The cyclic dimer is separated from the reaction mixture by sublimation (38). The similarity in vapor pressures between the lactide and the lactic acid suggested to this author that the major impurity in commercial grade lactide is lactic acid. Thus, a series of polymerizations were undertaken to investigate more directly the influence of lactic acid on molecular weight.

Table 3.2 shows the preliminary results from the lactic acid concentration study. Both the stannous octoate concentration and the polymerization temperature were maintained at 2×10^{-4} mole/mole and 130 C respectively for all four reaction schemes shown in Table 3.2. The as received racemic monomer stock was probably of higher purity

Table 3.2

Effect of Lactic Acid Charge on Molecular Weight of Racemic Poly(lactic acid)

Lactic Acid Charge (moles acid/mole lactide)	$[\eta]$ dl/gm	Mv	Mn $\frac{Mv}{1.8}$	*** 144/Mn Residual Acid Concentration	$\frac{144}{Mn} - 1.48 \times 10^{-3}$
None	1.25	175,000	97,200	1.48×10^{-3}	---
3×10^{-3}*	.627	59,500	33,100	4.36×10^{-3}	2.88×10^{-3}
5×10^{-3}*	.476	39,000	21,700	6.65×10^{-3}	5.17×10^{-3}
5×10^{-3}**	.512	43,500	24,200	5.96×10^{-3}	4.48×10^{-3}

* acid added after sublimation
** acid added before sublimation
*** 144 = molecular weight of lacticle monomer

Stannous Octoate Concentration 2×10^{-4} moles/mole lactide
Polymerization Temperature 130°C
Polymerization Time 60 hours

than the L,L lactide as judged by the higher molecular weight of the product polymerized from the racemic stock without recrystallization. Results of three additional reactions show the influence of racemic lactic acid which was added to the reactions at the concentrations indicated. Previous work on the polymerization of lactones may suggest that the molecular weight distribution in this type of reaction is "most probable" leading to a polydispersity of 2 (33). In addition, careful solution work on poly(lactic acids) with known polydispersities of 2 indicated that the ratio of M_v/M_n was approximately 1.8 (41). It was assumed that the number average molecular weight could be calculated from the viscosity average molecular weight and that the number of chains initiated in the polymerization was, in turn, inversely proportional to M_n. Thus, the fourth column reports the moles of chains initiated per mole of monomer charge based on the measured value of the viscosity average molecular weight. Note, assuming that lactic acid is an active hydrogen initiator, the unpurified monomer has a residual acid concentration of 1.48×10^{-3} moles acid/mole cyclic monomer. The last column of Table 3.2 shows the difference between the number of chains initiated in each reaction and the residual acid concentration in the monomer stock. With considerable accuracy, this calculation predicts the concentration of acid spiked to each reaction. The last entry in Table 3.2 reports an experiment in which, contrary

to standard procedure, the acid was added prior to sublimation. Only a small percentage of the acid (10%) is lost on sublimation. This would tend to confirm the similarity in vapor pressures of lactide and lactic acid. It thus appears that the lactic acid is an active hydrogen initiator which can be removed from the monomer by recrystallization procedures. Note that since both acids and alcohols have been shown to be active hydrogen initiators for lactone systems, lactic acid is probably difunctional. However, one lactic acid molecule will lead only to one growing polymer chain.

Figure 3.16 shows the anticipated initiation mechanisms whereby lactic acid can open a lactide ring. Either the acid functionality or the alcohol functionality may lead to the hydroxy propagating species typical of active hydrogen initiation. Since carboxylic acids will donate a proton more easily than an alcohol, the mechanism leading to structure I is probably the more prevalent mechanism. Continued addition of lactide to the growing chain will occur via the mechanism already described in the introduction and shown in Fig. 3.5. Structure I in Fig. 3.16 has dual hydroxy functionality and thus may propagate in both directions. Initial and propagating ring-openings are by acyl-oxygen cleavage as previously described.

The anhydride linkage shown in Fig. 3.17 (originating from structure I) may also undergo alcoholysis (or hydrolysis

INITIATION SCHEME I

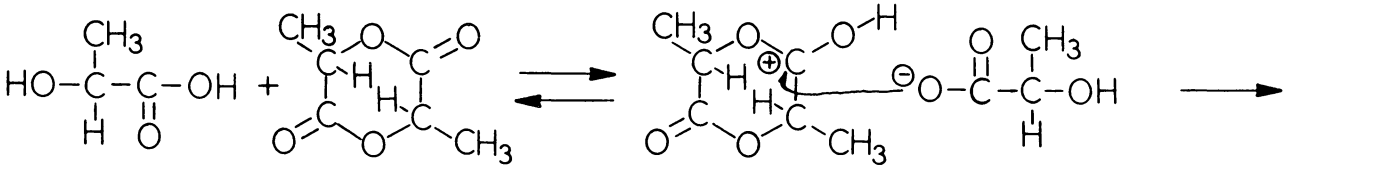

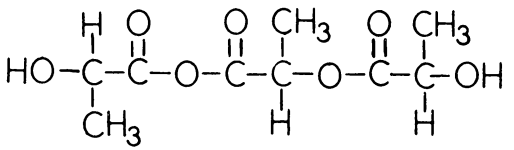

I

INITIATION SCHEME II

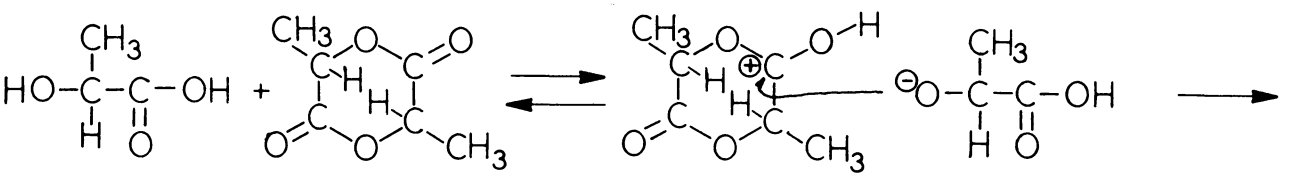

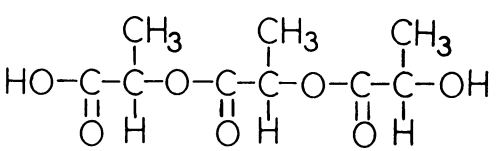

II

Figure 3.16. Active hydrogen initiation mechanisms for the polymerization of lactide with lactic acid.

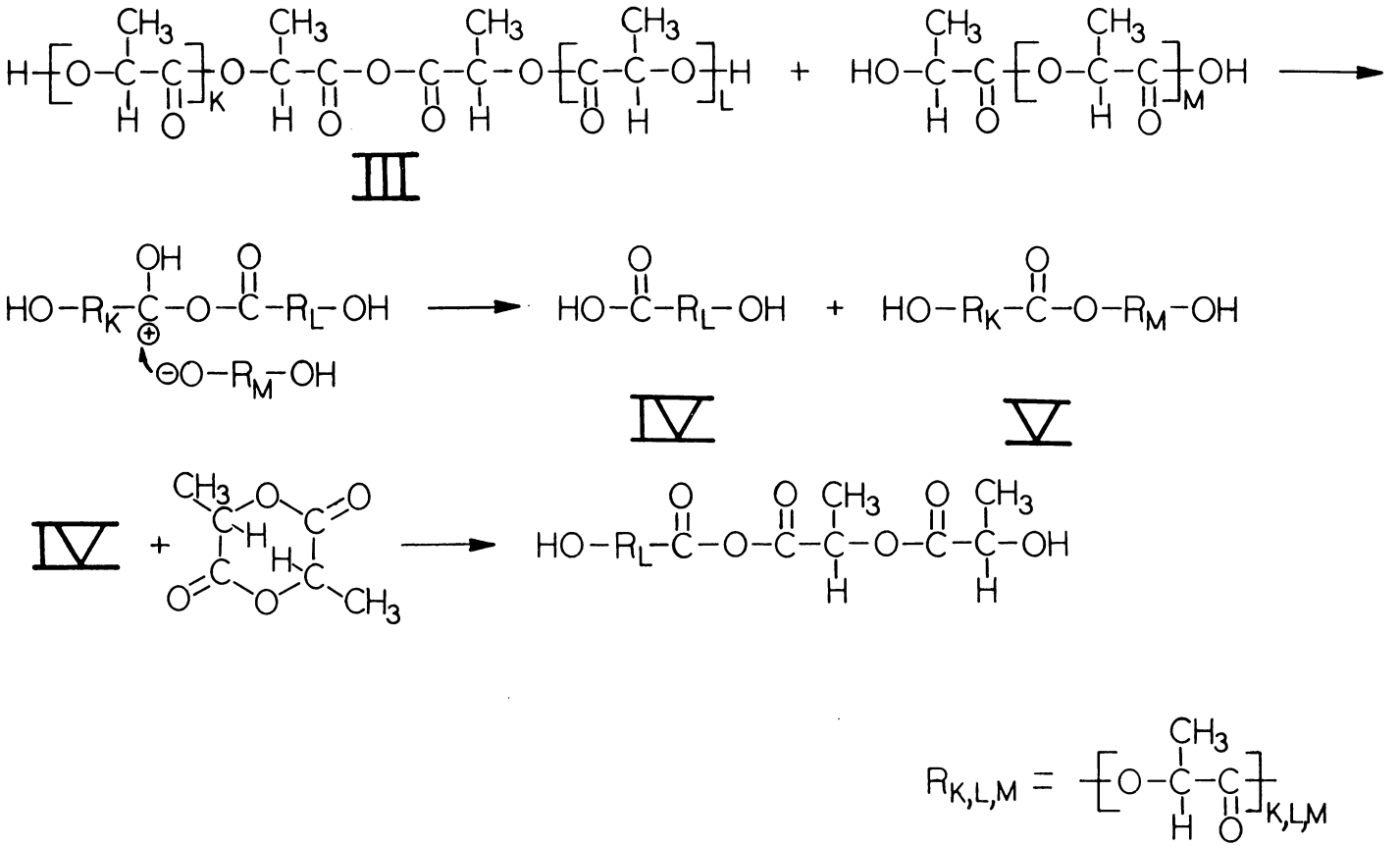

Figure 3.17. Reaction of anhydride linkage.

in the presence of water) to regenerate acid functionalities. These acid groups will, in turn, ring-open the monomer to generate a growing chain with the same anhydride linkage. Note, the alcoholysis of the anhydride linkage leads to the same number of reactive ring-opening functionalities in the products that were originally in the reactants. In fact, an anhydride linkage will be regenerated on subsequent reaction of structure IV with monomer as indicated in Fig. 3.17. Thus, the net effect of the recurring anhydride linkage is to transfer the growth center to a chain with a different molecular weight.

Any polymerization process whereby growing chains, whose numbers are constant with time, randomly add monomer until the growth center (hydroxyl group in this case) is terminated, provides the basis for the Schulz-Flory distribution (81). The original chain growth centers do not necessarily remain active, however, the overall growth center concentration must remain constant for the duration of the polymerization. Thus, if all the active hydrogen species (lactic acid) initiate lactide rings on a time scale which is short with respect to the propagation process so that the constant growth center concentration requirement is fulfilled, then the mechanisms outlined in Fig. 3.16, 3.5, and 3.17 should yield the "most probable distribution" as described by $M_w/M_n = 2$. It should be also stated that regardless of the polymerization mechanism, if

transesterification is operative at rates which are commensurate with the time scale of the reaction, then the polydispersity will also yield a polydispersity of 2.

Based on the preliminary results described above, a more detailed investigation of the influence of lactic acid at constant stannous octoate concentration was undertaken. All racemic lactide in subsequently described reactions was taken from the same feed stock which had been recrystallized from ethyl acetate twice to ensure that the residual acid concentration was minimized and the same for all reactions. The dry ethyl ether wash was performed just before reaction so that any aging effects of the monomer in the vacuum desiccator was also minimized.

The results of six reactions at various lactic acid charges ranging from 3×10^{-4} to 3×10^{-2} moles acid/moles monomer are discussed below. For the series of six reactions, polymer products were isolated from residual monomer by procedures previously described in the experimental section. Mass conversions are plotted in Fig. 3.18 as a function of lactic acid charge. Subsequently, molecular weight distributions were measured via gpc techniques and the results are summarized in Fig. 3.19. In addition, the results of the intrinsic viscosity measurements on each sample in the series are plotted as the calculated (via the Mark-Houwink equation) viscosity average molecular weight in Fig. 3.19.

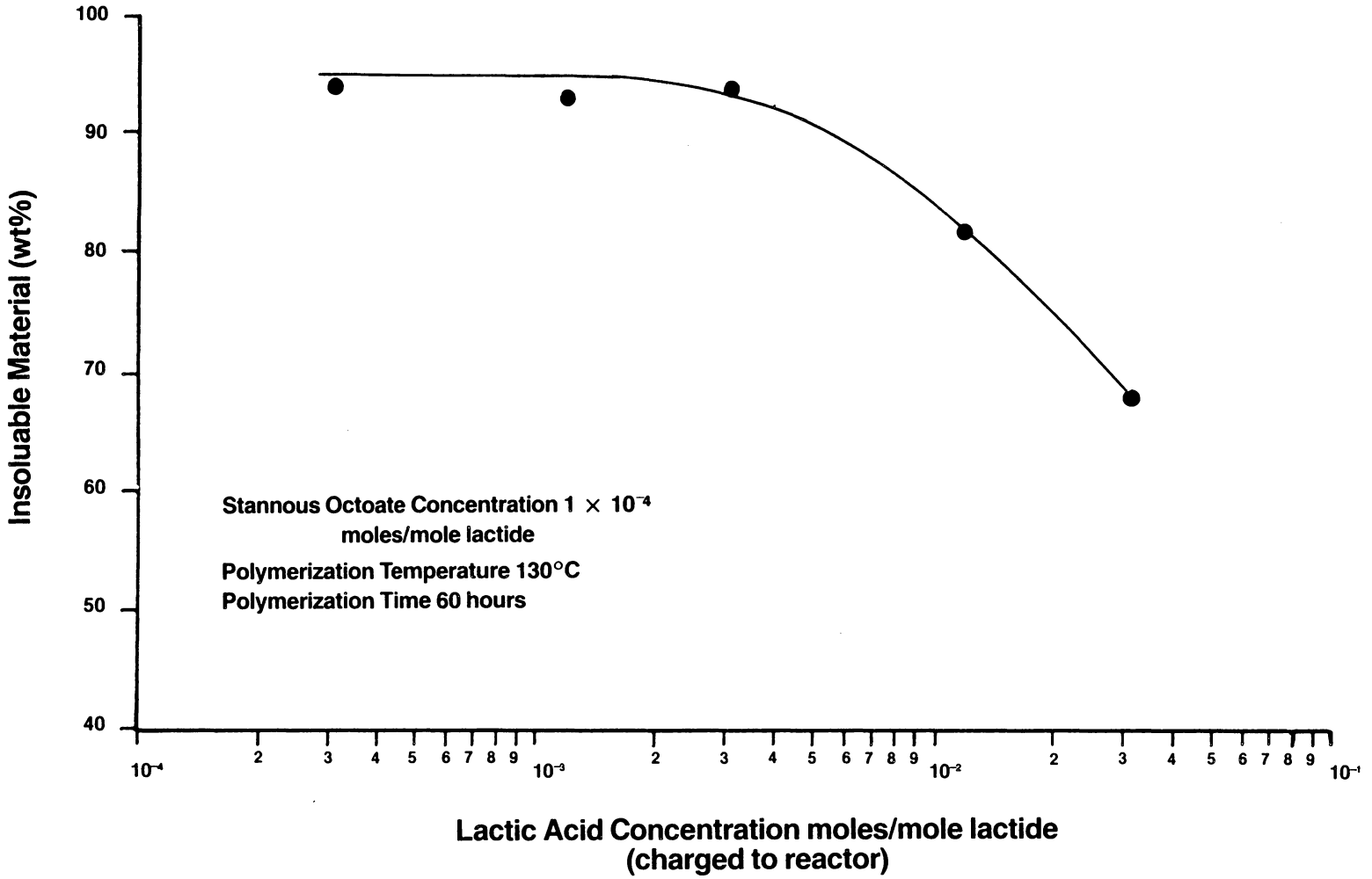

Figure 3.18. Mass conversion to polymer as a function of lactic acid charge in the polymerization of racemic poly(lactic acid).

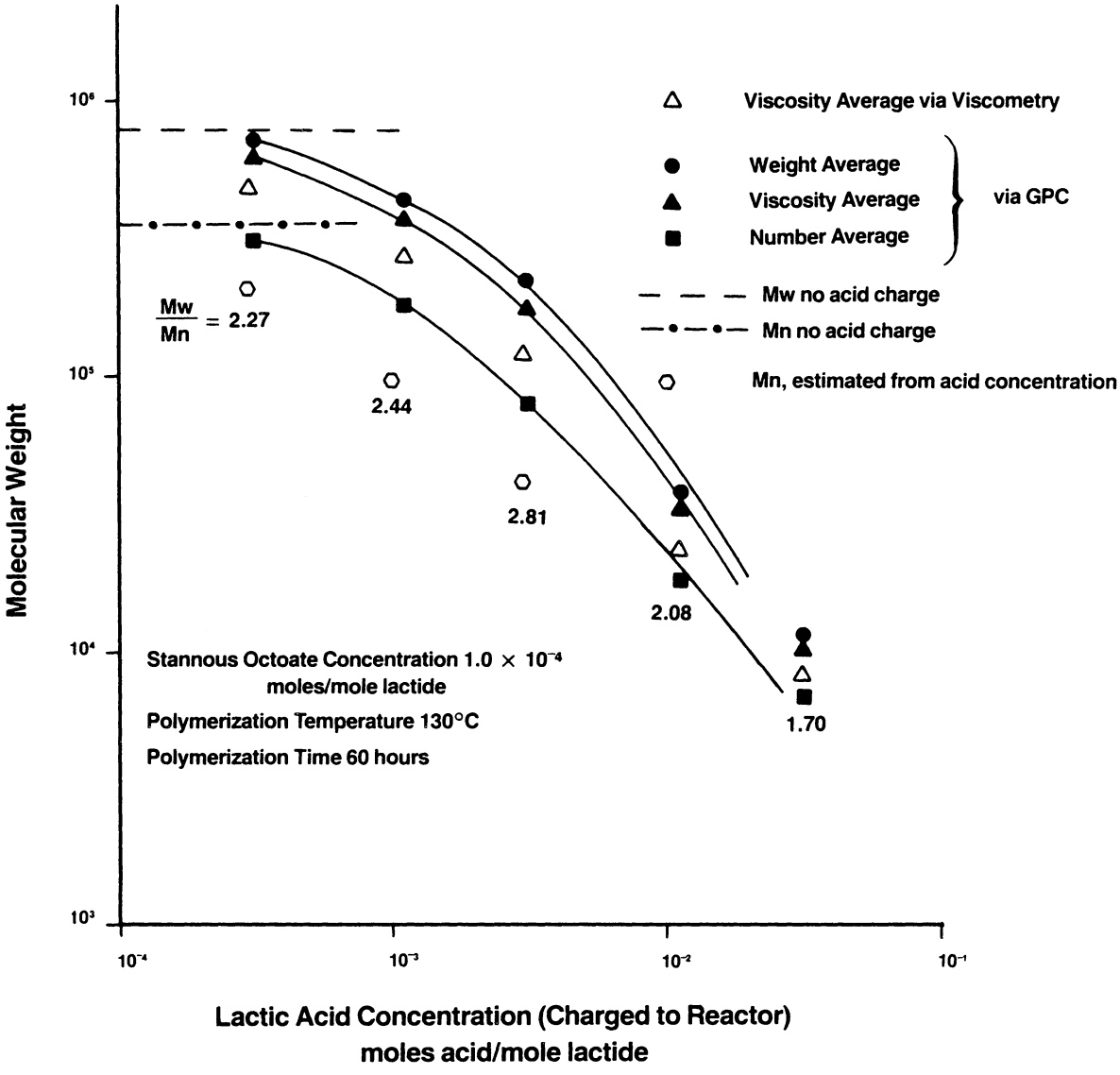

Figure 3.19. Molecular weight as a function of lactic acid charge in the polymerization of racemic poly(lactic acid).

The results in Fig. 3.18 would indicate a severe drop off in conversion above an acid concentration of 1×10^{-2} moles acid/mole monomer. However, as mentioned in the experimental section, the ethyl ether (cold) used to separate polymer from residual monomer was not efficient in precipitating low molecular weight species. This low end component appeared as a cloudy haze in the solvent/non-solvent mixture and could not be isolated by filtration. Thus, quantitative interpretation of the products from the reactions with the two highest acid concentration was not possible. The high, nearly constant, levels of conversion for the balance of the four reactions is consistent with a negative free energy of polymerization (42,43). Percent conversions, at the relatively high temperatures necessary for bulk conditions, was limited to 93% ±2% by the monomer/polymer equilibrium described previously in section 3.1.1.

Clearly, the decrease in molecular weight with increasing lactic acid change is consistent with the postulate that the acid behaves as an active hydrogen initiator. The correspondence between the viscosity average molecular weights as calculated via gpc results and more directly through intrinsic viscosity measurement could be better. This is a bit bothersome in light of the fact that the same Mark-Houwink constants used to convert the intrinsic viscosities to molecular weights were also used to convert

gpc universal calibration results to poly(lactic acid) molecular weights. However, both results confirm the same inverse dependence of molecular weight on initiator concentration.

With the exception of the two products at the highest concentration of lactic acid, the polydispersity also increases with lactic acid content. The two exceptions show artificially narrowed distribution due to the solubility of low molecular weight species in the non-solvent used to isolate the product. The increase in polydispersity was conjectured to result from a low molecular weight tail characteristic of lactone polymerizations (16). A backbiting mechanism shown in Fig. 3.11 is thought to occur during polymerization of lactones with the production of cyclic low molecular weight species. The full molecular weight distributions of products from the two reactions representing the extremes in polydispersity are plotted in Fig. 3.20. These indicate significant differences in distribution, however, both distributions appear exceptionally symmetric with no evidence of a low molecular weight tail. It might be argued that this low tail may have been removed by its solubility in ethyl ether. The high levels of conversion calculated previously would indicate that if cyclics were removed, they were of low concentration since the conversions quoted are thought to be close to the thermodynamic equilibrium (43). In any event, cyclics were not the cause

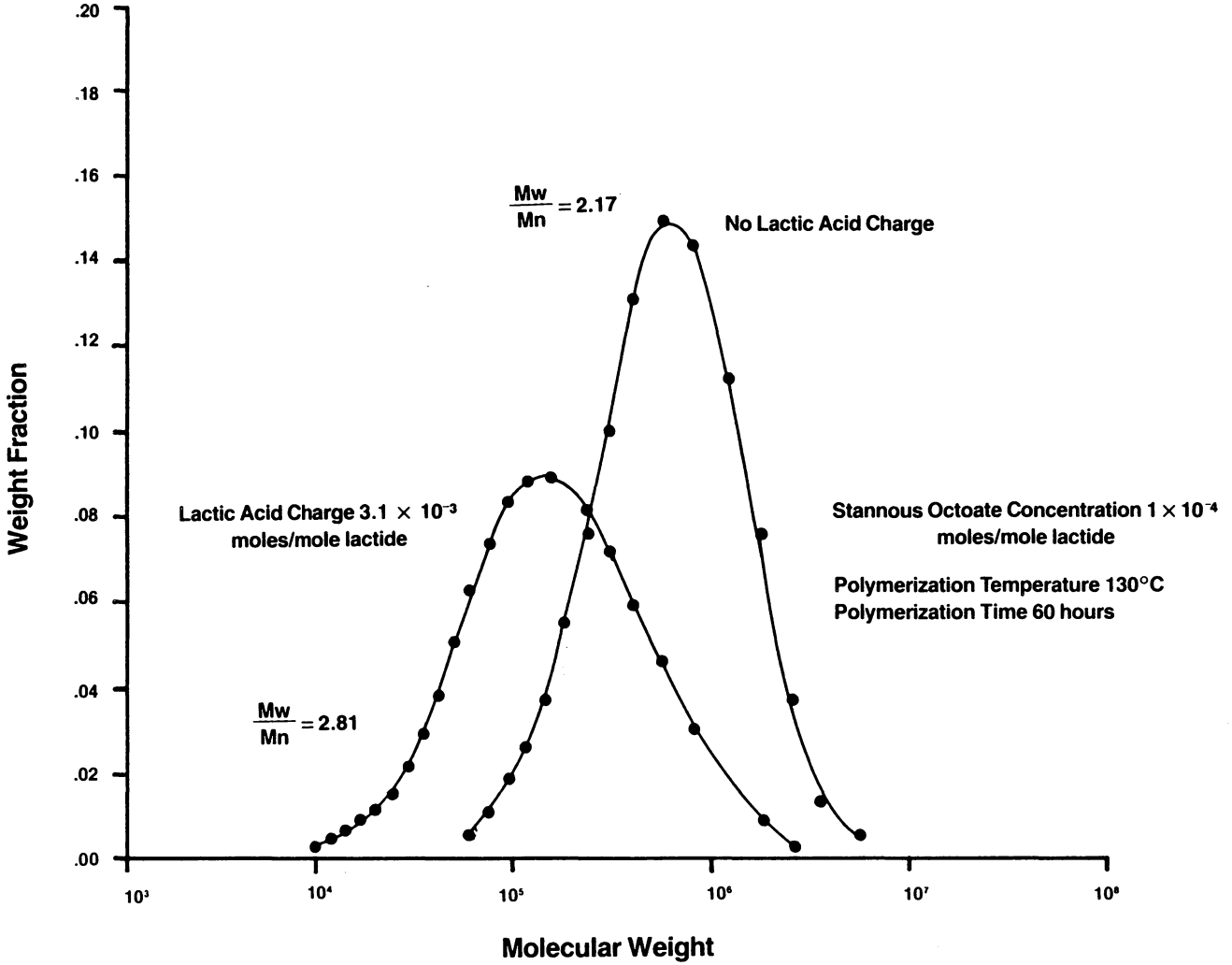

Figure 3.20. Detailed molecular weight distribution from selected samples in the lactic acid concentration series.

of the increase in the measured polydispersity with increasing acid concentration.

The progressive deviations from the Schulz-Flory distribution with increasing acid concentration can be rationalized in the framework of the basis for this type of distribution outlined previously. In particular, it is postulated that all active centers are not initiated early in the reaction scheme. If the rate constant for initiation is low enough, increasing the initial acid charge may defer complete consumption of the acid to later periods in the reaction. As more and more acid is added to the system at constant catalyst concentration, the initiation step of Fig. 3.16 is progressively extended into later periods in the polymerization. Thus, the high molecular weight region of the broad molecular weight distribution of Fig. 3.20 is populated with macromolecules which were initiated early in the reaction scheme. Similarly, the low molecular weight region of the distribution is due to chains initiated at high levels of monomer conversion.

The residual acid concentration in the purified monomer stock was calculated directly from the number average molecular weight of the product of polymerization in which no acid was added. This resulted in an estimated latent acid concentration of 4.00×10^{-4} moles acid/mole monomer. For all subsequent reactions in the series, the number average molecular weight was predicted based on the total lactic acid

concentration calculated as the sum of the latent lactic acid in the monomer feed stock and the amount of lactic acid changed to the reactor. The predicted number average molecular weight, as plotted in Fig. 3.19, is lower than the value measured by gpc. Clearly, if the assumed mechanism of acid initiation is correct, then apparently the effectiveness of initiation decreases with increasing acid content at constant stannous octoate concentration. This is consistent with the idea that the rate of initiation is comparable to the rate of propagation. It is quite reasonable to assume that the reactivity of the acid and hydroxyl groups on the lactic acid are not too different from the reactivity of the acid and hydroxyl groups on the propagating structures IV and V in Fig. 3.17. The conversion of lactic acid to propagating chains would not be complete in the time scale defined by the consumption of monomer as acid concentrations are increased. This would, in fact, explain the decreased efficiency of initiation at higher acid concentrations as well as the concomitant increase in polydispersity.

A second mechanism may be considered to explain the dependence of molecular weight on acid concentration. The typical hydroxy end groups could undergo a condensation reaction with the acid functionality of lactic acid as shown in Fig. 3.21. At high acid concentrations, the frequency of such a reaction would increase. The impact on the molecular weight of the chain undergoing condensation with the acid

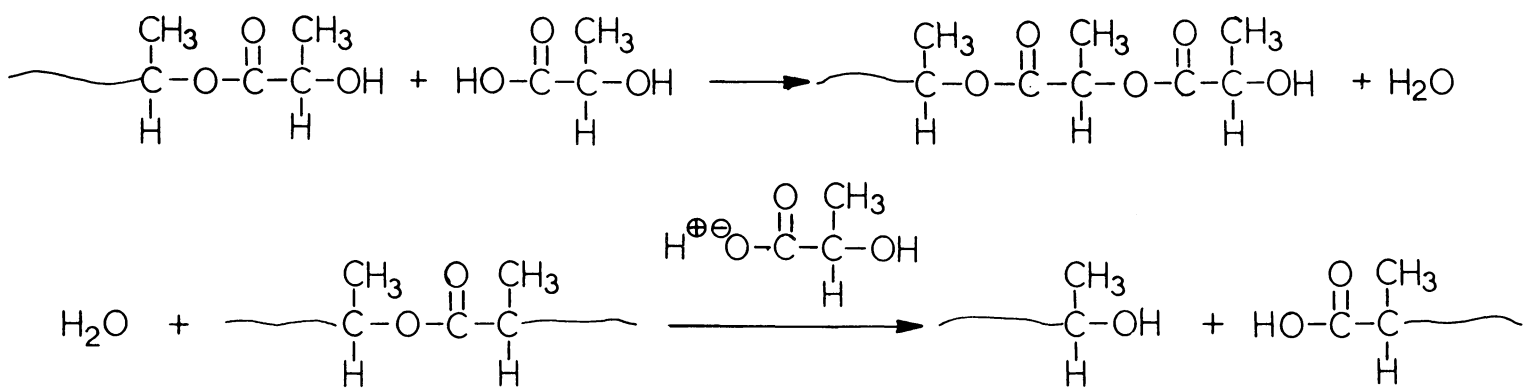

Figure 3.21. Proposed lactic acid condensation with hydroxy polymer end group and resulting hydrolysis.

would be slightly favorable, specifically the addition of one repeat unit. The production of water would, however, lead to the hydrolytic degradation of other chains, especially since the presence of excess lactic acid would tend to catalyze the hydrolysis. The overall impact of the hydrolysis mechanism on the number average molecular weight needs to be considered carefully. The condensation of the acid onto the growing chain effectively removes the potential for the initiation of a growing chain by removing a lactic acid molecule from the reaction medium. In compensation, the hydrolysis of an ester linkage in an existing chain will create two chains from one, each with active end groups capable of propagation. The net effect would be no change in the number of chains if the original acid molecule participating in the condensation would have otherwise initiated polymerization. Deviations from number averages predicted from original acid concentrations would occur if the lactic acid molecule participating in the original condensation would not eventually have initiated polymerization, in which case, the number average molecular weight would be lower than anticipated. The results in Fig. 3.19 indicate the opposite trend. In order to be consistent with the data, the water produced on condensation of an acid molecule with an active hydroxyl groups could not lead to hydrolysis. In such a case, the consumption of a lactic acid in condensation without subsequent ester linkage hydrolysis could, in fact,

lead to number average molecular weights higher than anticipated from known initial acid concentrations. However, this mechanism could not lead to the observed broadening of the molecular weight distribution.

Yet, a third mechanism may be considered to participate in the reaction mechanism. Figure 3.22 shows a proposed transesterification reaction between the hydroxyl functionality of the lactic acid and a mid chain ester linkage. Such a reaction would be considered to be self catalyzed in light of the necessary protonation of the carbonyl oxygen. Thus, this reaction may be expected to increase in frequency with increasing acid concentration. Clearly, the mechanism could be invoked to explain the decreasing molecular weight and increasing polydispersity with increasing acid content. However, if the mechanism were dominant, the correspondence between number average molecular weight and acid concentration would necessarily be closer. Certainly, this mechanism could not explain the positive deviation of the measured number average molecular weight from the anticipated number average molecular weight based on the proportionality to lactic acid concentration.

In summary, the proposed mechanism of lactic acid initiation of ring-opening polymerization of lactide is quite consistent with the molecular weight data. Although both the reactions of lactic acid with polymer end groups and mid chain ester linkages may occur to limited extents, deviations

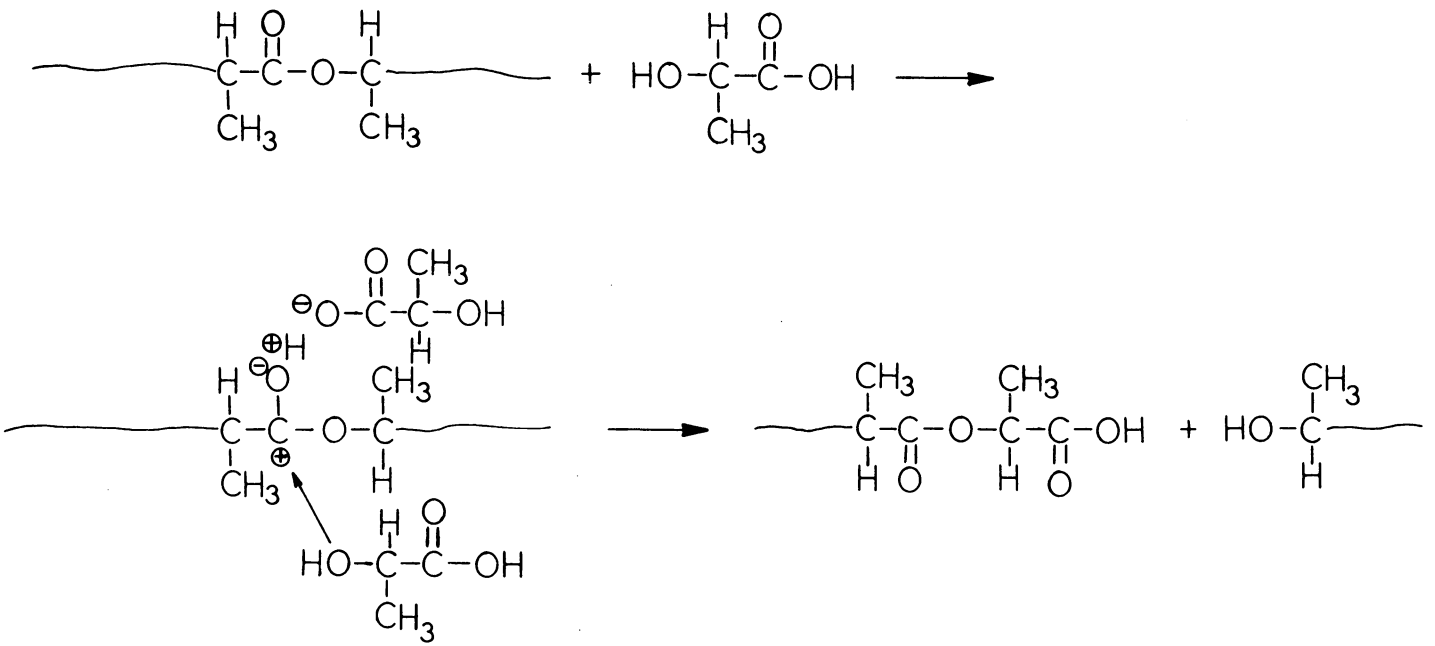

Figure 3.22. Ester interchange between lactic acid and mid-chain ester linkage.

from the Schulz-Flory distribution and decrease initiation efficiency are, to a large extent, attributed to the postulate that acid initiation rates are similar to propagation rates. Increasing acid concentrations accentuates the molecular weight distribution broadening and initiation inefficiency. Number average molecular weights are inversely related to acid concentrations with deviations from proportionality related to relatively low initiation rates.

3.3.1.2 STANNOUS OCTOATE CONCENTRATION

The fact that stannous octoate has been added to the reaction mixtures has been taken for granted. It is generally considered that the stannous octoate behaves as a catalyst for active hydrogen initiated polymerizations of lactones (14). The specific mechanism of activity has not been disclosed. However, stannous octoate is considered to complex with the carbonyl group on the lactone monomer to stabilize intermediate structures on ring-opening (14). In order to confirm the activity of the stannous octoate, a polymerization was run under conditions similar to those of Table 3.2 with the exception that no stannous octoate was added to the system. Lactic acid was added at a concentration of 5×10^{-3} moles acid/mole of racemic lactide monomer. After an exposure of 60 hours at 130 C, no polymer could be isolated from the reaction mixture. In addition, gpc results on the reaction product showed no signals above baseline for any elution volumes. The maximum sensitivity of the gpc detector and high reactant concentrations were used in the attempts to detect polymer.

Using a methodology similar to that used to investigate acid concentration effects, the influence of stannous octoate concentration on the conversion, molecular weight, and molecular weight distribution was investigated. The acid concentration was held nominally constant by using all

monomer from the purified feed stock without any additional acid change. Again, reaction temperature was constant at 130 C. Stannous octoate concentrations varied between 1 x 10^{-5} and 1 x 10^{-3} moles stannous octoate/mole lactide monomer.

Figure 3.23 represents the impact of stannous octoate concentration on the mass conversion in poly(lactic acid) polymerizations. Conversion remains unaffected until very high concentrations (1 x 10^{-3} mole/mole) are encountered. The lowering of conversion at high stannous octoate concentration is not an artifact of the procedure for isolating the polymer since the molecular weights are high enough as not to be dissolved by ethyl ether. The gpc results which describe the influence of stannous octoate concentration on the molecular weight are summarized in Fig. 3.24. For a broad range of stannous octoate concentrations, both absolute molecular weight and its distribution remain invariant with increasing stannous octoate concentration. At the highest levels of stannous octoate concentration, a decrease in molecular weight and increase in polydispersity clearly occur at approximately the same point at which the decrease in conversions are observed. Also shown in Fig. 3.24 are the viscosity average molecular weights calculated from intrinsic viscosity measurements. A discrepancy between the two methods employed for molecular weight determination is still apparent although the overall trend in the date is still withstanding.

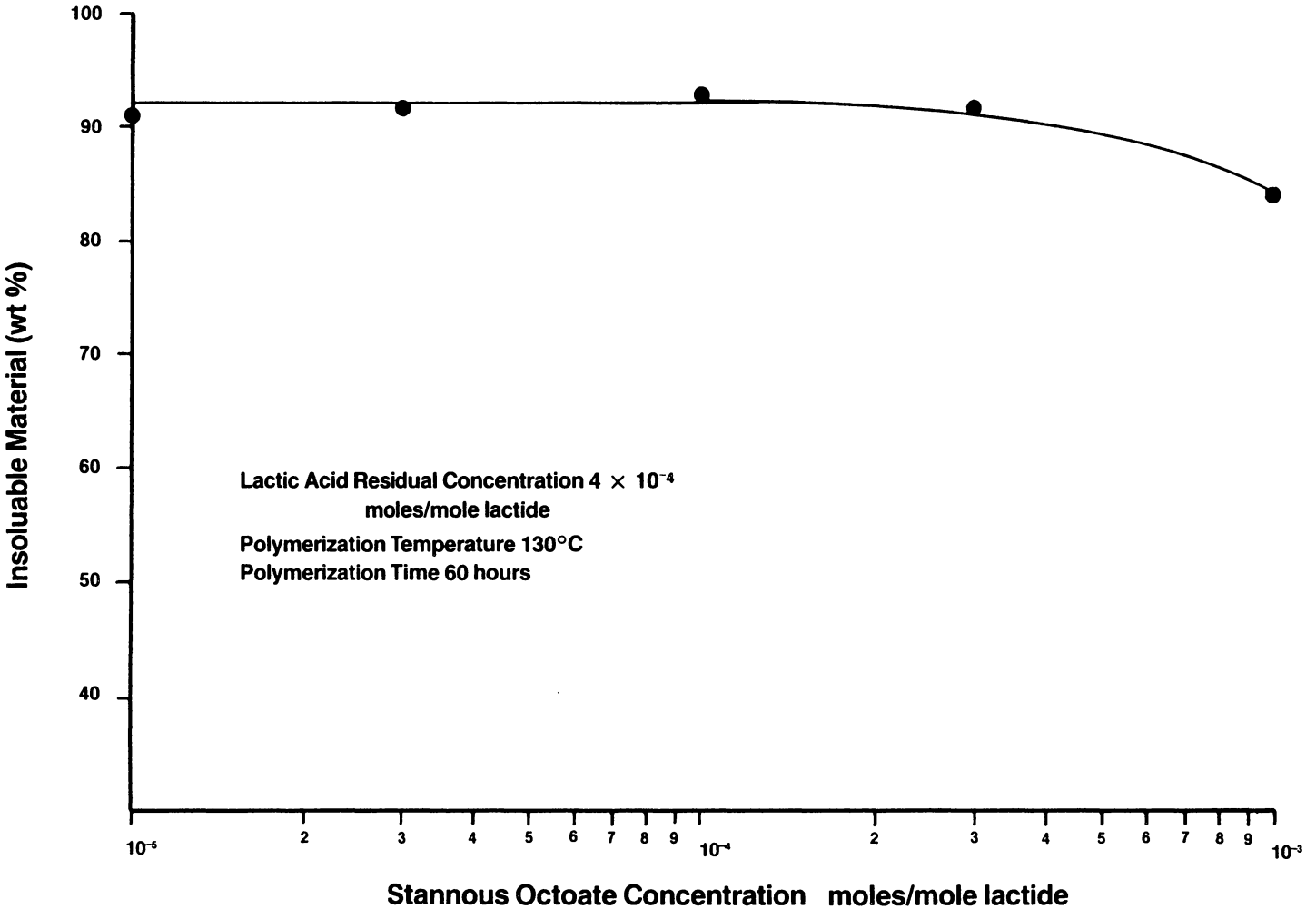

Figure 3.23. Mass conversion to polymer as a function of stannous octoate concentration in the polymerization of racemic poly(lactic acid).

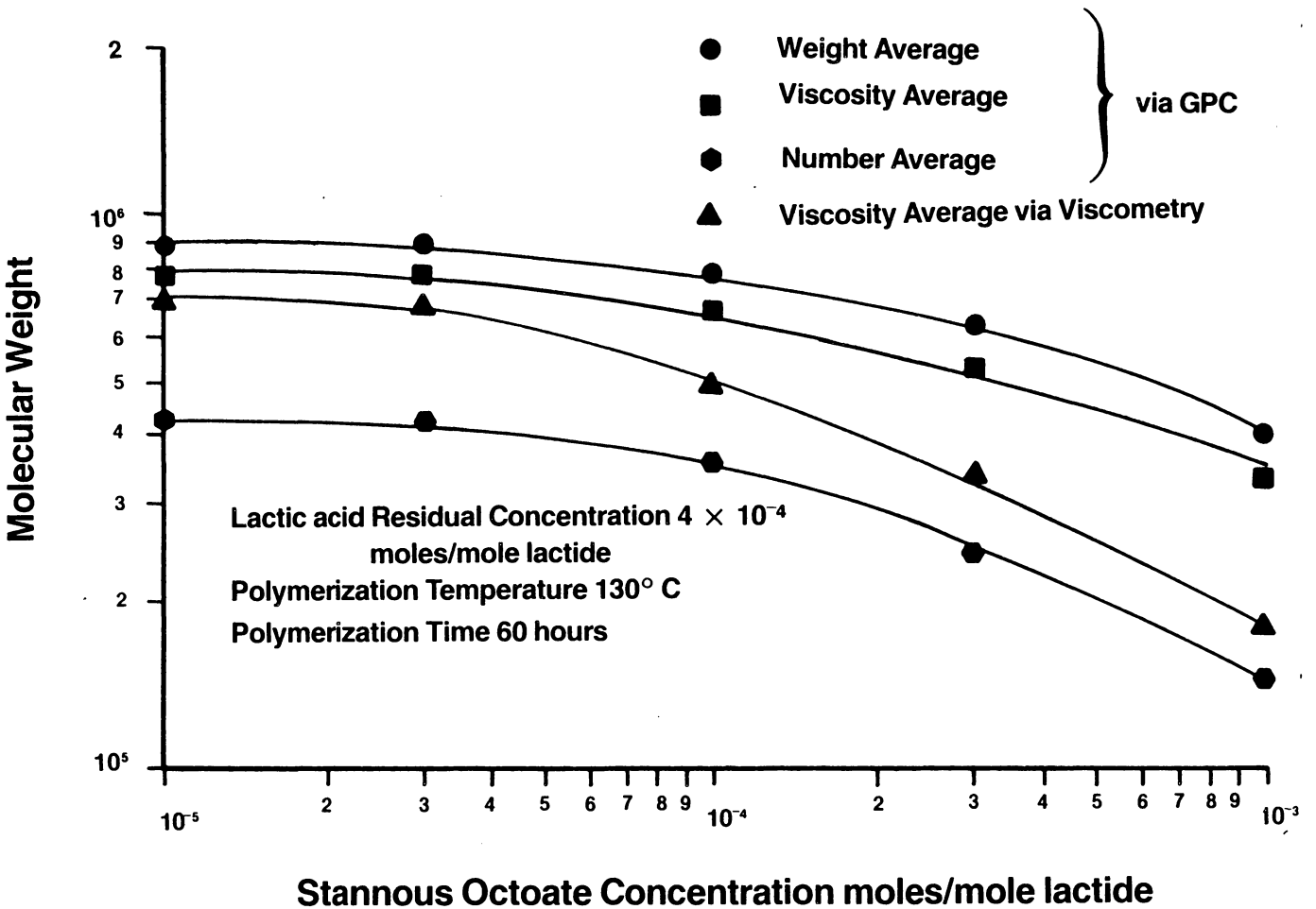

Figure 3.24. Molecular weight as a function of stannous octoate concentration in the polymerization of racemic poly(lactic acid).

The observation of decreasing molecular weight with increasing tin catalyst is consistent with the results of Brode and Koleske (14) which were discussed in section 3.1.4 of the introduction. Diminished thermal stability, as well as some initiation activity, was attributed to the presence of stannous octoate in lactone polymerizations although no particular mechanisms were proposed by Brode and Koleske (14). The extent of the data presented in this work is not comprehensive enough to determine any mechanisms absolutely, however, some discussion is still warranted.

As discussed in section 3.1.4, the major mechanism for the degradation of polylactones is the intramolecular transesterification reaction of Fig. 3.12. Since it has been postulated that stannous octoate is a transesterification catalyst (28), it seems reasonable that excess stannous octoate would promote this reaction. Certainly the increased level of monomer in the reaction products would support this mechanism. However, Sutton et al. (68-71) show that the influence of the intramolecular transesterification on molecular weight distributions is minimal and, thus, on the whole, this mechanism would be inconsistent with the results of Fig. 3.24. Along the same lines, stannous octoate may also be considered to catalyze the backbiting reaction of Fig. 3.11 which also involves an interchange mechanism. Production of the cyclic would result in a low molecular weight tail in the distribution obtained from reaction

products. Figure 3.25 shows the distributions, in detail, from the reactions with both the lowest and highest stannous octoate concentrations. Although no low molecular weight tail can be discerned, increasing the stannous octoate concentration has led to an increase in the breadth of the molecular weight distribution which is very similar to the increase in breadth realized at increased acid concentrations. The similarity is particularly acute in the continued symmetry of the distributions with increasing breadth. Thus, of the two potential effects of excess stannous octoate upon polymerization mechanisms advanced by Brode and Koleske (14), that of coinitiator activity seems the most probable.

Assuming that the excess stannous octoate behaves as an initiator as well as a catalyst in the polymerization of lactide, the rationalization of both the mechanism and the decreased conversion with increasing stannous octoate concentration remains. Figure 3.26 depicts an insertion type reaction involving the classic acyl-oxygen cleavage. This may be a reasonable first step in the reaction sequence. The subsequent alcoholysis of the anhydride structures of VII by lactic acid or hydroxyl terminated chain would lead to other propagating chains as per the mechanism in Fig. 3.17. Specifically, Fig. 3.27 shows such an alcoholysis with structure V of Fig. 3.17. Note that through this mechanism, the development of monofunctional structures like structures

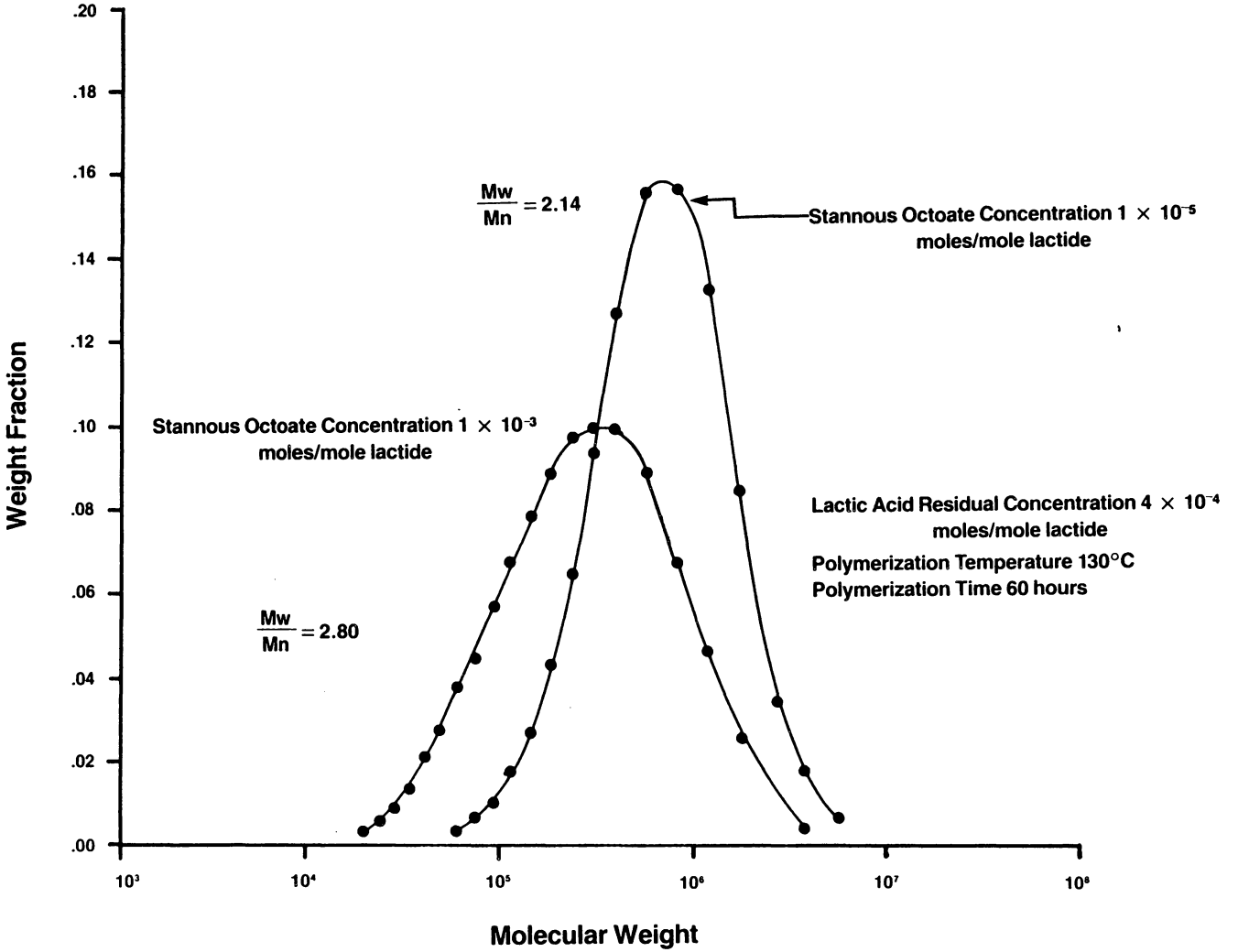

Figure 3.25. Detailed molecular weight distributions from selected samples in the stannous octoate concentration series.

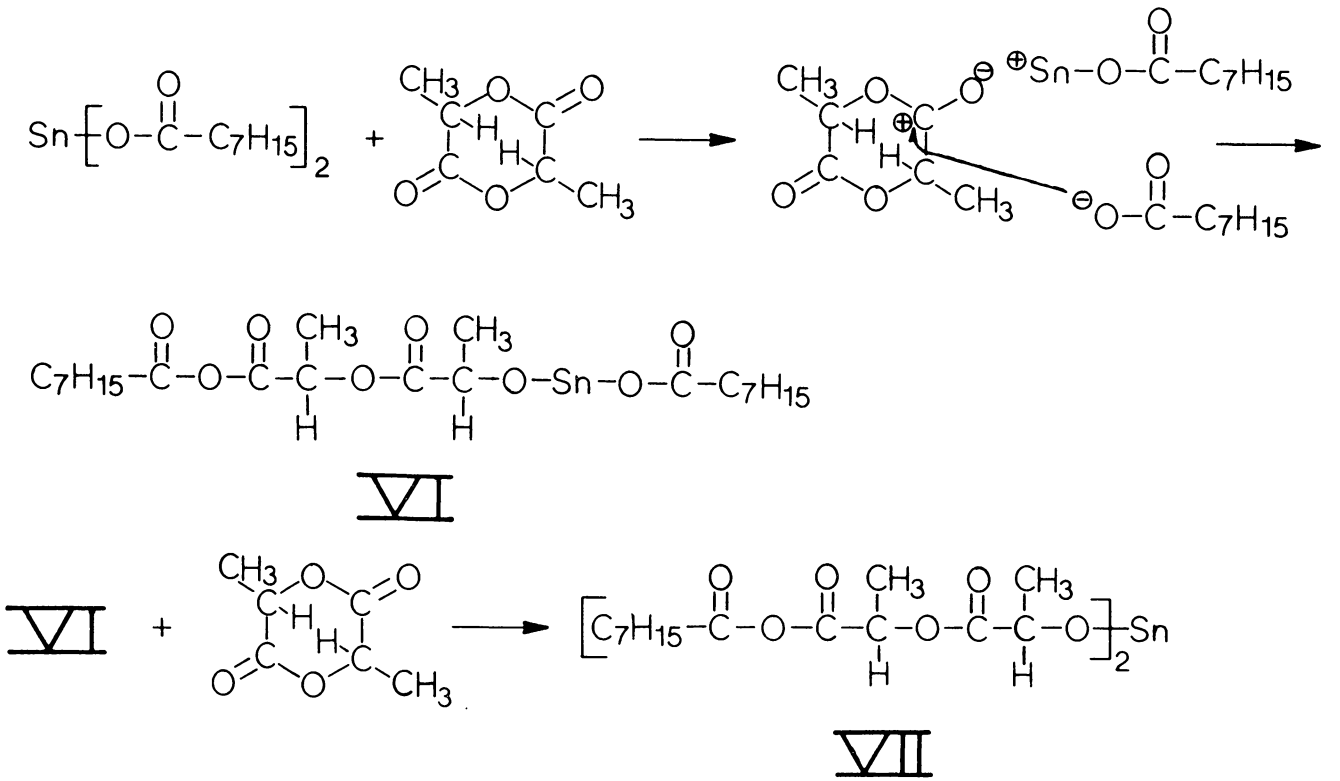

Figure 3.26. Insertion of lactide into stannous octoate as a possible initiation mechanism.

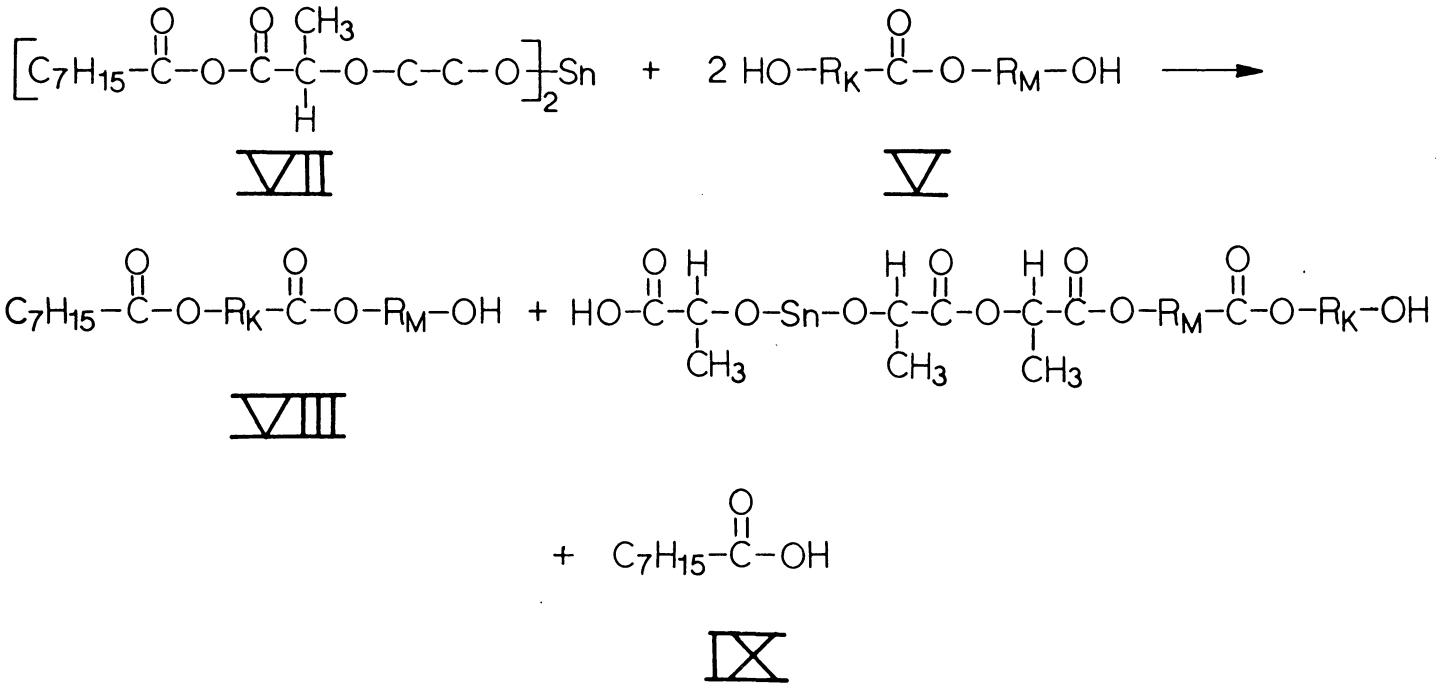

Figure 3.27. Alcoholysis of insertion product with hydroxy terminated chain.

VIII and IX of Fig. 3.27 are possible. Condensation of VIII and IX could lead to chain termination with the proposed stannous octoate initiation scheme. Such termination by combination in the lactic acid initiation scheme was not possible because of the difunctional nature of all the species in Fig. 3.16. Thus, if mechanisms in Fig. 3.26 and 3.27 dominate at very high stannous octoate concentrations and concomitant low lactic acid concentrations, it seems possible that termination may lead to lower conversions if not, at least, to lower reaction rates. In fact, the hydrolysis of ester linkages by the product of the proposed condensation type termination may not occur to significant extents in the low acid concentration reactions of Fig. 3.24. Thus, chain termination by combination would occur without any transfer expected via ester hydrolysis. This, then, supports the observation of lower conversions and, thus, necessarily lower overall molecular weights. Increased polydispersity would again be rationalized in the framework of the Schulz-Flory distribution theory. The complex initiation via insertion would ostensibly be a slow process so that the rate of initiation would be competitive with propagation rates. In addition, the termination by condensation would also tend to decrease the number of propagating chains. The combination of these two mechanisms would violate the Schulz-Flory stipulation that the concentration of active centers remains constant during

polymerization. Thus, the polydispersity would tend to broaden beyond the Schulz-Flory most probable distribution.

The mechanism of Fig. 3.26 requires lactide insertion into stannous octoate which Brode and Koleske were unable to detect in the analogous caprolactone system (14). This may be particularly relevant since a seven membered ring (caprolactone) may be expected to be more reactive than the six membered lactide ring. An alternate mechanism is proposed. Figure 3.28 shows an effective acid interchange reaction between stannous octoate and lactic acid. The resulting generation of 2-ethyl-hexanoic acid could lead to lactide ring-opening via mechanisms similar to Fig. 3.16, reproduced in Fig. 3.28. Note that the anhydride structure XI in Fig. 3.28 would also lead to monofunctional groups through alcoholysis. Thus, with any significant acid interchange, terminations via condensation could lead to a broadening of molecular weight distribution, and lowering of both conversion and molecular weight.

Corroboration of the proposed acid interchange mechanism was sought through the following experiment. Equivalent volumes of lactic acid and stannous octoate were mixed at ambient conditions. The resulting white precipitate was isolated from residual acid and stannous octoate by successive washing with fresh ethyl ether and hexane. The large pieces of the precipitate were then ground into a fine powder and washed again with ethyl ether and hexane. The

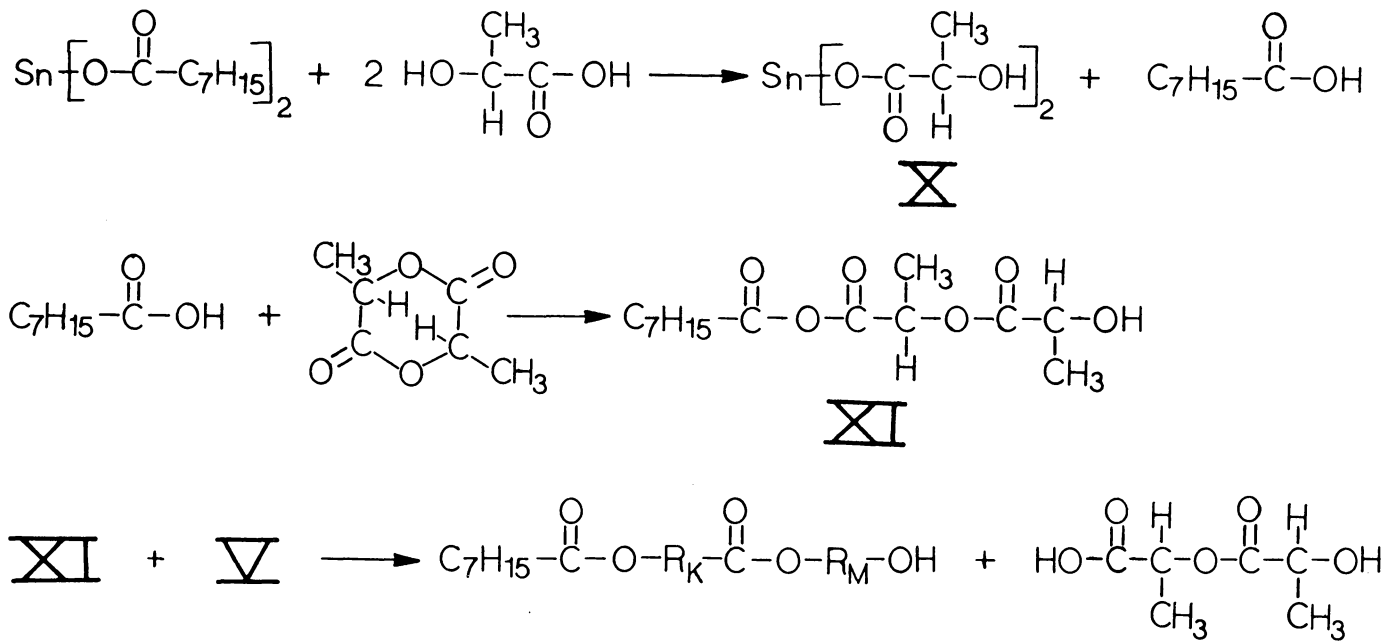

Figure 3.28. Acid interchange between stannous octoate and lactic acid.

powder was then vacuum dried at 80 C for 12 hours. Assuming the molecular weight of the precipitate was consistent with structure X of Fig. 3.28, a charge of $5x10^{-3}$ moles of precipitate/mole of monomer was added to a typical 1 gram scale polymerization in place of stannous octoate. Polymerization conditions were otherwise the same as those in Fig. 3.24. Gel permeation chromatography results from the polymerization product indicate molecular weights considerably higher than those expected from the curve in Fig. 3.24 for equivalent stannous octoate concentrations. Namely, the weight average molecular weight was $1.06x10^{6}$ and the number average was $4.80x10^{5}$. Similarly, the polydispersity ($Mw/Mn=2.2$) was narrower than that expected from the results in Fig. 3.23. In general, the use of this precipitate as a substitute catalyst may extend the low catalyst concentration trends of Fig. 3.24 and prevent both the decrease in molecular weight and increase in polydispersity at higher stannous octoate concentrations. It would seem reasonable that the tin salt of lactic acid could also catalyze the polymerization with a activity similar to that ascribed to the tin salt of 2-ethyl hexanoic acid (stannous octoate). Thus, the improvement in molecular weight may be credited to the lack of monofunctional groups generated by hexanoic acid which can be displaced from the stannous octoate by lactic acid.

The marked improvement in polymerizability of lactides

with the addition of stannous octoate is apparently associated with catalyst activity of tin salts of carboxylic acids in general lactone polymerizations (26-28). The displacement of 2-ethyl hexanoic acid from stannous octoate by the lactic acid initiator may result in the reduced molecular weight and increased polydispersity observed in polymerizations at high stannous octoate concentrations. The proposed mechanism of acid interchange between the lactic acid and stannous octoate may lead to monofunctional initiations which, in turn, leads to chain termination reactions detrimental to molecular weights. It is assumed that the white precipitate generated on mixing stannous octoate and lactic acid is, in fact, the tin salt of lactic acid. The addition of this white precipitate to lactide polymerizations was an effective catalyst substitute which did not lead to the decreased molecular weights at high catalyst concentrations associated with the aforementioned termination side reactions.

3.3.1.3 POLYMERIZATION TEMPERATURE

All the polymerizations described up to this point in the discussion have been performed at 130 C. This represents the effective lower limit since the melting point of the racemic monomer is 126 C. A four centigrade degree margin of error was deemed appropriate to prevent accidental cooling below the monomer melting point. Although control of molecular weight through initiator and catalyst control would seem to be well in hand, it was still deemed appropriate to investigate the effect of temperature on polymerization.

A series of polymerizations were undertaken at various temperatures from 130 C to 190 C. Stannous octoate concentration was held constant at $1x10^{-5}$ moles stannous octoate/mole monomer. No lactic acid was added beyond the latent concentration present in the stock lactide which had been recrystallized twice from ethyl acetate. Reaction times were maintained at 60 hours. Figure 3.29 shows the results of the gpc work up of each reaction product. Number average and weight average molecular weights decrease systematically with increasing temperature. Although polydispersity is not quite as systematic with temperature, the overall trend would seem to indicate an increase in breadth of distribution with increasing temperature.

In light of previous discussions concerning the thermodynamics of polymerization which describe the

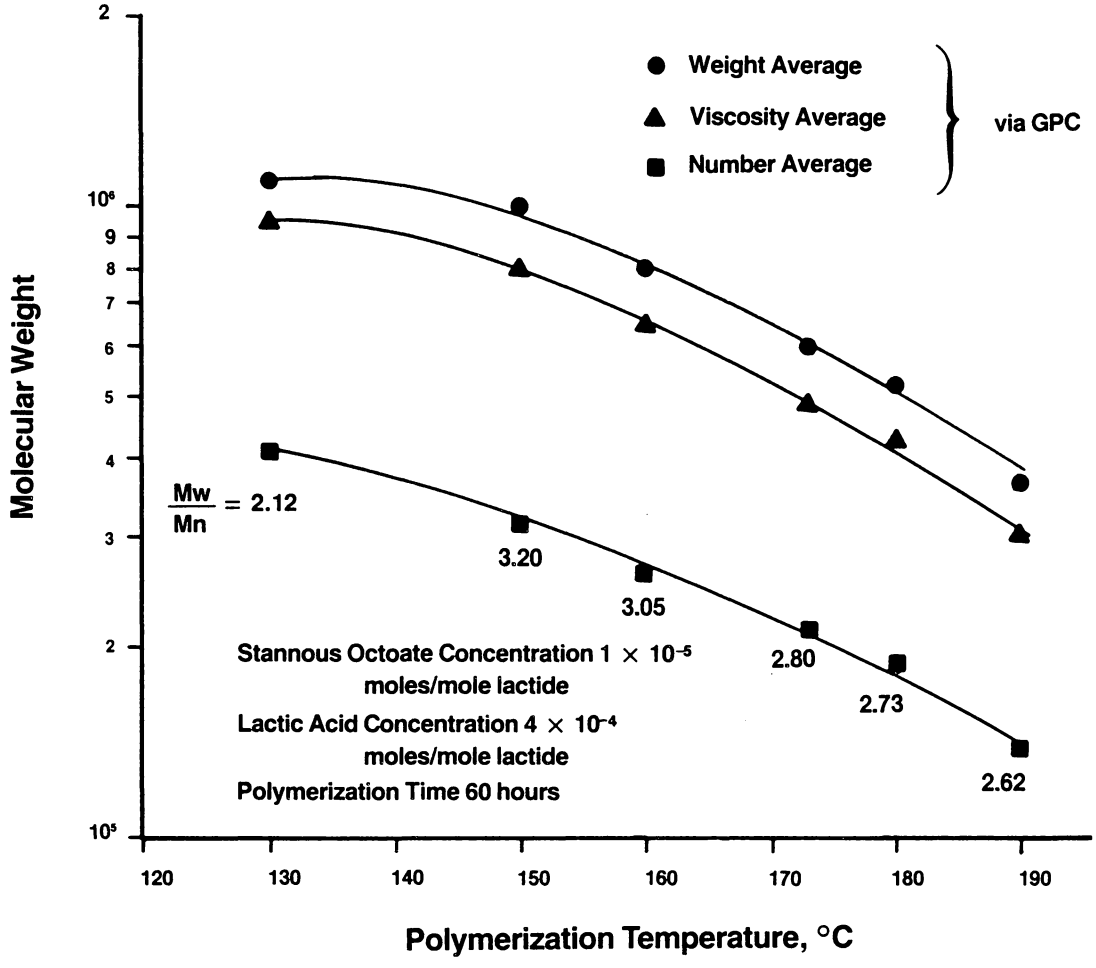

Figure 3.29. Molecular weight as a function of polymerization temperature in the polymerization of racemic poly(lactic acid).

relatively low driving force for polymerization associated with this six membered ring structure as compared to caprolactone and propriolactone, it may be expected that increasing the temperature of polymerization would necessarily decrease the equilibrium conversion. Simple intramolecular ester interchange and backbiting mechanisms would lead to the generation of cyclic dimers and would thus contribute to the dynamic equilibrium between polymer and monomer. Assuming a comparable level of initiation, decreasing conversions would necessarily decrease the average degree of polymerization. The approximately fourfold decrease in molecular weight seen on increasing the temperature from 130 C to 190 C would require a tremendous drop in conversion assuming this simple mechanism. Although the conversion levels in this series of polymerizations was not measured directly, qualitative observations of the nature of the polymerization products are inconsistent with large drops in conversion. A more drastic mechanism associated with chain scission would be more capable in explaining the temperature effects. Intermolecular transesterification reactions would tend to drive the molecular weight distributions toward the most probable and, thus, are not considered to be competitive with the scission reactions.

The increased yellowing of the product as polymerization temperature was increased would also tend to suggest that reactions beyond simple cyclization are operative at elevated

temperatures. Chain degradation would also be consistent with the increase in polydispersity previously described. Considering the limited data presented here, it is certainly beyond the scope of this work to conclude (a) specific chain scission mechanism(s). However, the extent of such mechanisms would not necessarily need to be severe in order to be consistent with the decrease in molecular weight and increase in polydispersity. Speculation on the mechanism(s) involved will be kept to a minimum.

Since the carboxylic acid autocatalytic hydrolysis of this polyester was probably not operative at lower temperatures, ostensibly due to the removal of water through the standard sublimation techniques, it would seem reasonable to discount its likelihood at elevated temperatures as well. Based on previous investigations of the degradation behavior of glycolide based polyesters (68-73), the two mechanisms next in probability of occurrence would be a homolytic mechanism and chain degradation due to a catalyst insertion. The free radical mechanism for this lactide system is particularly attractive in light of the tertiary hydrogen present on the alpha carbon which would be expected to lead to a free radical site. This is supported to some extent by previous workers who speculated on a free radical mechanism based on enhanced degradation rates of poly(lactic acid) with increasing oxygen exposure (70,73). Although previous authors (14) were unsuccessful in detecting caprolactone

monomer insertion into stannous octoate, the likelihood for lactide insertion and its well documented detrimental effects on polymer thermal stability (14) can not be totally discounted. Quite a few additional degradation mechanisms, previously discussed in the introduction, could also participate in the decrease of molecular weight at elevated polymerization temperatures. These mechanisms may include decarboxylation, decarbonylation, heterolytic chain scission, the elimination mechanism, as well as others as discussed in pertinent reviews (68-73).

The limited data presented here cannot discriminate among all possible degradation mechanisms. However, it would seem appropriate to state that the molecular weight realized from the polymerization of lactide, with lactic acid as initiator and stannous octoate as catalyst, is sensitive to polymerization temperature. The deleterious effect of temperature on molecular weight is more severe than would be anticipated from arguments of reduced conversions stemming from ceiling temperature. It is postulated that degradation reactions leading to chain scission are operative at elevated polymerization temperatures. In order to reduce chain scission during polymerization, the minimum reaction temperature, as dictated by monomer melting point, is recommended.

3.3.1.4 KINETICS OF POLYMERIZATION

As a final experiment in the investigation of the polymerization mechanism of poly(lactic acids), the kinetics of polymerization were measured and compared to previous suggestions that the polymerizations of lactones under ideal conditions should proceed via a "living" mechanism. A series of ten reactions were performed all under identical conditions. Stannous octoate concentration and reaction temperature were all maintained at the levels indicated in the legends of Fig. 3.30 and 3.31. Lactic acid was present only in concentrations indicative of the residual concentrations in the purified monomer stock. Reaction temperature was set at 140 C, approximately ten degrees above the normally recommended level to accommodate faster monomer melting and, thus, more accurate polymerization temperature control at short reaction times. Each of the ten reactions was terminated by a rapid quench of the tube reactors in ice water after various reaction times which ranged from 0.5 hours to 105 hours. Conversion levels were calculated in the standard manner and molecular weights were determined via the standard gpc method with a slight modification to sample preparation.

The procedure for obtaining the gpc results was slightly altered for these kinetic studies so that a critical evaluation of the low molecular weight species in the various

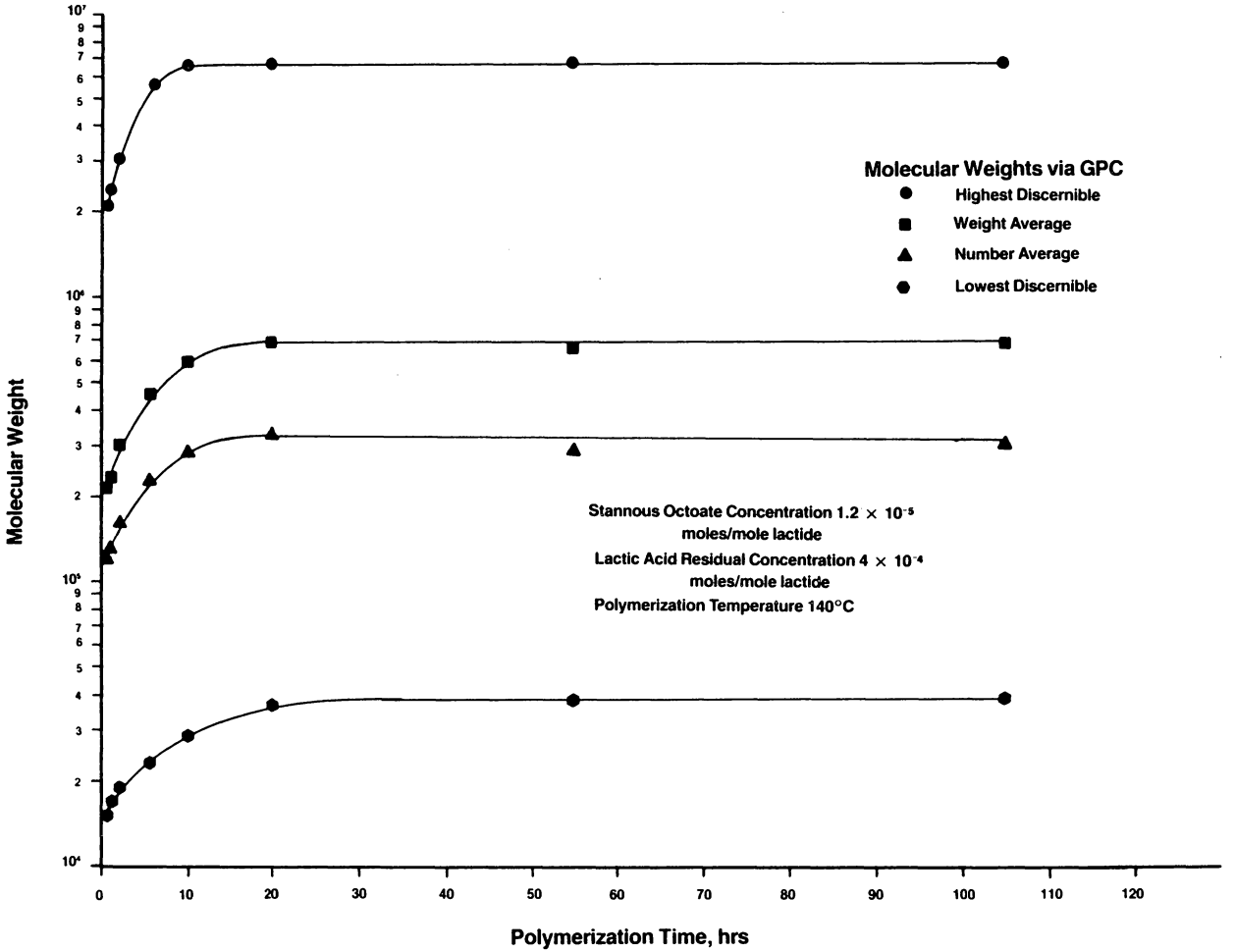

Figure 3.30. Molecular weight as a function of time in the polymerization of racemic poly(lactic acid).

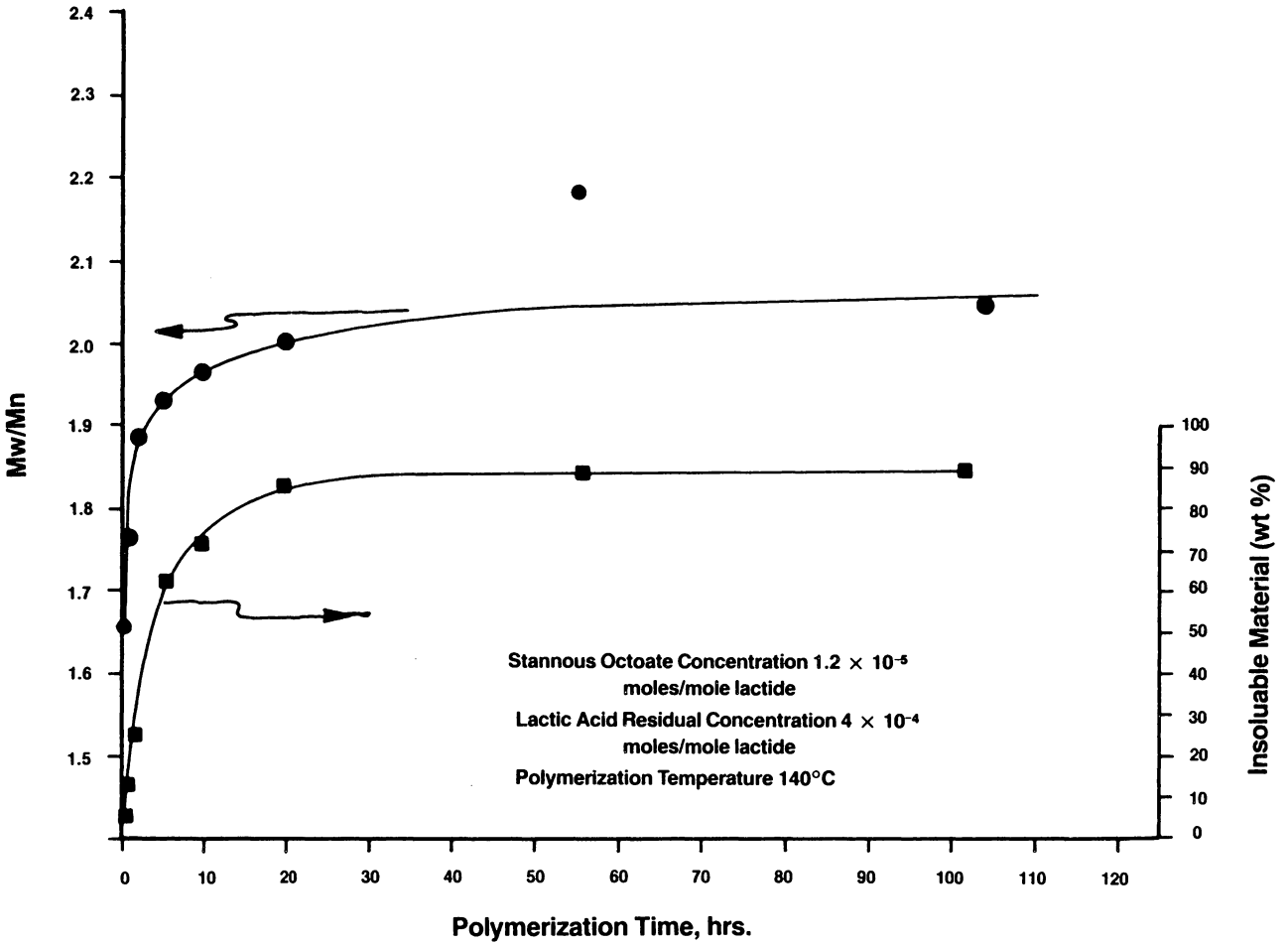

Figure 3.31. Conversion and Mw/Mn as a function of reaction time in the polymerization of racemic poly(lactic acid).

distributions was not obscured by the lack of an effective non-solvent. Small portions of the reaction products were obtained prior to the separation of insolubles. A sample of all reaction products was put into THF solutions and submitted for gpc analysis. Thus, there was no arbitrary fractionation of low molecular weight tail from any sample in the kinetic study prior to the molecular weight distribution measurement.

The results of the kinetic studies are reported in Fig. 3.30 and 3.31. Figure 3.30 shows a plot of the number average and weight average molecular weights as a function of reaction time. In addition, the highest and lowest discernible molecular weights in the distributions are also plotted. The conversion percentages, as well as the polydispersity numbers, are plotted as a function of reaction time in Fig. 3.31. In general, molecular weights, polydispersity, and conversion are seen to increase with reaction time up to maximum values realized at approximately 20 hours reaction time. After 20 hours, all the reported polymerization parameters reach a steady state value.

Figure 3.31 indicates that at low conversions the ratio of weight average molecular weight to number average molecular weight is already significantly greater than 1. The possibility of intermolecular reactions of the type described in Fig. 3.17 (alcoholysis of anhydride linkages) or intermolecular transesterification is surely a minimum when

the polymer concentration is at 6.5%. Thus, the breadth of the early molecular weight distribution would more likely be due to ongoing initiation rates.

It would be difficult to label the cutoff point beyond which initiation could be considered negligible and propagation is dominating. An initiation scheme in which the rate of initiation is first order in both lactic acid concentration and monomer concentration seems reasonable leading to the conclusion that initiation would occur, at least to diminishing extents, throughout the polymerization. The rate constant for initiation might depend on such variables as stannous octoate concentration and temperature. As discussed in section 3.3.1.1, the final molecular weight distribution breadth may depend on the rate of initiation in the latter stages of polymerization. If these rates tend to be very low at high conversions, then the polydispersity (Mw/Mn) would approach a value of two (2). If acid concentrations were high enough such that the initiation rate at high conversions was significant, then the distributions may be expected to broaden.

The appearance of very high molecular weight species at very low conversion levels may be the strongest argument yet for the proposal that the lactic acid initiation takes place over a time scale that is long compared to propagation rates. For example, after 0.5 hours reaction time and at a conversion of approximately 6.5%, there are macromolecules

present that have molecular weights as high as 2.09×10^6. The increase in the number average molecular weight and concurrent increase in conversion with time is certainly consistent with the mechanism of monomer addition to active centers on growing chains. However, since the time scale across which the conversion reaches the thermodynamic equilibrium value of approximately 90% is 20 hours, the appearance of molecular weight species which are considerably higher than the final number average molecular weight in a time scale of 30 minutes is inconsistent with the initiation of all active sites at polymerization onset.

Note, the molecular weight of the longest macromolecules present in the polymerization only increases from 2.09×10^6 at 6.5% conversion to 6.61×10^6 at 90% conversion. This apparent slowing of the addition of monomer units to an existing growing chain can also be explained with the stipulated ongoing initiation rates. Increasing the number of active propagating sites during the course of the reaction would necessarily increase the competition for the given amount of monomer. This would then lead to the nonlinearity between molecular weight increase and monomer conversion for a given chain in the polymerization batch.

The ability of "tagging" a molecule by calling it the highest molecular weight species in the reaction batch may not be quite accurate because of the potential for the anhydride alcoholysis reaction sequence in Fig. 3.17. and

transesterification. However, structures of type III in Fig. 3.17 can undergo alcoholysis just once and the resulting structures of type V cannot undergo further alcoholysis. Thus, assuming little potential for intermolecular transesterification and that the high molecular weight species are of type V of Fig. 3.17, the "tag" is still valid and the arguments for finite initiation rates through the course of the reaction are still intact. Support for the assumption of minimal intermolecular transesterification has been given in subsequent discussions, see section 3.3.2.

The persistence of low molecular weight species throughout the course of polymerization may also be due to ongoing initiations. Clearly, as short chains grow to become larger molecular weight species, new short chain species must have been generated to take their place. The lack of any measurable gpc signal above an elution volume corresponding to a molecular weight of 1.52×10^4 may be due to the inherently low concentration of these very low molecular weight species. Note, the amount of time spent by a growing chain at a particular molecular weight is inversely proportional to that molecular weight. In other words, it takes a macromolecule ten times as long to grow from a molecular weight of 50,000 to 100,000 as it does to grow from 5,000 to 10,000. Thus, in a hypothetical situation in which there is a constant initiation rate and a rate of growth which is independent of molecular weight, there will be 10

times as many chains at 50,000 as there are at 5,000. Since the value of dn/dc for poly(lactic acid) in THF was observed to be rather low, it stands to reason that there may be a lower limit to the molecular weight observed in the kinetics series samples.

The upward swing in the observed lower limit molecular weight is probably due to the fact that the rate of initiation is necessarily decreasing as both monomer and lactic acid concentrations decrease throughout the course of the reaction. Thus, the lower concentration limit for gpc detection would shift to higher molecular weights as the molecular population of the very low molecular weight regimes falls off.

The final polydispersity of 2.2 is very consistent with the results of section 3.3.1.1, in that, for the low concentration of acid in the kinetics series, a relatively narrow distribution approaching 2.0 is expected. Some effect of increasing the reaction temperature from 130 C to 140 C for this kinetics series might be expected due to the very deleterious effect of temperature demonstrated in section 3.3.1.3. In fact, the steady state value of molecular weight is a bit lower than predicted in sections 3.3.1.1 and 3.3.1.2 for comparable lactic acid and stannous octoate concentrations.

In addition, previous authors (33) have correlated the occurrence of side reactions with a maximum in molecular

weight/time profile in the polymerization of caprolactone. Such maxima were not seen in this work at the low reaction temperature (140 C) employed for the kinetics study. The slight maximum in the molecular weight curve in Fig. 3.30 is not large enough to consider as significant in the context of typical gpc error. Thus, reaction profile studies are also recommended for higher temperatures which were shown in this work to favor lower molecular weights. If the maximum in molecular weight with time can be reproduced, correlation between elevated temperature and degradation and/or side reactions may be reinforced.

The discussion above is somewhat tentative due to the limited data available. Certainly, the conclusions regarding the initiation mechanisms as they influence the increase in molecular weight with conversion need to be further substantiated with additional experiments. Reaction profiles for other lactic acid concentrations and stannous octoate concentrations would go a long way toward this end. However, it may be stated that the initiation mechanism proposed and the stated correspondence between lactic acid concentrations and molecular weight are consistent with the reaction profile described above.

3.3.1.5 REACTION SCALE-UP RESULTS

As testimony to the integrity of the trends stated above, the results of the scale-up of the reaction scheme will be briefly described. The large scale reactions were necessary for generating poly(lactic acids) for another study in this dissertation, see chapter 4.0. Based on the proposed lactic acid initiation mechanism, the addition of lactic acid was used as the mechanism for controlling the molecular weight for both the polymerization of L-lactide as well as racemic lactide. Molecular weight control was deemed especially crucial since it was desired to generate a total of six products in three pairs of equivalent molecular weights. Each pair was to contain one optically pure species, poly(l-lactic acid), and the racemic poly(lactic acid).

Approximately, one kilogram of each of the two monomer species was purified by repeated recrystallization from ethyl acetate. All polymerizations were done at 3 to 4 centigrade degrees above the melting points of the respective monomers. Thus, the L-lactide was polymerized at 100 C and the racemic monomer was polymerized at 130 C. The temperatures were minimized in order to obviate any side reactions thought to occur at elevated temperatures. Stannous octoate was the chosen catalyst and was used at concentration levels below those previously shown to lead to increased polydispersities.

Initially, each of the two one kilogram monomer feed stocks was individually homogenized by crushing the crystals separated from the ethyl acetate and thoroughly hand mixing. This was done to guarantee a uniform lactic acid content in the feed stocks. The acid content was characterized by polymerizing a small one gram portion of each. Molecular weight of the products was characterized by intrinsic viscosity techniques. The acid concentration was determined from the number average molecular weight which was, in turn, estimated from the viscosity average molecular weight as described in section 3.3.1.1.

Large scale polymerizations of the L-lactide and the racemic lactide were done in pairs at equivalent acid concentrations. Each 300 gram polymerization was carried out in the procedure described in the experimental section. The results of the six polymerizations are summarized in Table 3.3 in which the total lactic acid concentrations and viscosity average molecular weights are reported. The total acid concentration represents the sum of the latent acid in the monomer feed stock and the acid intentionally added for molecular weight control. Clearly, molecular weights are almost identical in each pair, reflecting the inverse relationship between acid content and molecular weight. The inverse relationship is not truly proportional due to the kinetic effects of initiation described earlier. The molecular weights of the racemic polymers are generally

Table 3.3

Summary of Poly(lactic acid) Polymerization Scale-Up Products

Poly(lactic acid) Stereochemical Configuration	Lactic Acid Concentration Moles/Mole Lactide		Intrinsic Viscosity dl/gm	Viscosity Average Molecular Wt.
Racemic	1×10^{-2}		.458*	36,500
L	1×10^{-2}		1.21 **	38,300
Racemic	3×10^{-3}		1.04 *	130,000
L	3×10^{-3}		3.25 **	148,000
Racemic	4.7×10^{-4}	***	2.61 *	550,000
L	5×10^{-4}		8.06 **	515,000

* Chloroform

** Tetrahydrofuran

*** Residual Acid Concentration in Purified Monomer (i.e. No Acid Added)

slightly lower than those in its optically pure counterpart. This may be the result of the lower polymerization temperatures employed for the L-lactide. Thus, accurate control of molecular weight was obtained principally through the tailoring of lactic acid concentration.

3.3.2 TRANSESTERIFICATION OF POLY(LACTIC ACIDS)

The potential of transesterification in poly(lactic acids) was investigated using ^{13}C NMR techniques. Quantitative ^{13}C NMR characterization of stereochemical sequences in poly(lactic acids) of various tacticities have been attempted in two previous publications (38,41,60), as described in the introduction. Neither of these two previous works was conclusive in its assessment of the potential for or extent of transesterification mechanisms in disrupting the stereosequence distributions nascent to the polymerization of lactides of various stereochemical compositions.

A more quantitatively correct approach was undertaken in this work. Generally, there are two major complications in use of quantitative ^{13}C NMR techniques (80). Variations in spin-lattice relaxation times and variable nuclear Overhauser effects, (NOE), across different ^{13}C nuclei in different environments can make non-protonated carbon atoms very insensitive to signal detection. By combining the techniques of inverse gated decoupling with the addition of a shiftless relaxation agent, these problems have been overcome and good quantitative ^{13}C NMR results are possible (80). The solution preparations and instrumental conditions appropriate for the implementation of these techniques are described in the experimental section.

Figure 3.32 is a ^{13}C NMR spectrum obtained from a

racemic poly(lactic acid) with viscosity average molecular weight of 36,500. The three different carbon atoms present in the carbonyl, methine, and methyl groups should appear in equal proportions consistent with their appearance in the polymer repeat unit. In fact, the integration curves above each of these three peaks located at 169.3, 69.2, and 16.7 ppm, respectively, bears this out. Note, the digitally integrated areas are reported above each curve as a percentage of the total area under all three curves. It may be worth noting that previous reports on the ^{13}C NMR investigations of stereosequence distributions in poly(lactic acids) which claim to be quantitative show very unequal areas under these three carbon peaks (60). This leaves some doubt as to the validity of the results of Chabot et al. (60). Possibly, the effects of spin-lattice relaxation times and NOE were not correctly compensated.

Of the three peaks in Fig. 3.32, the carbonyl and the methine show some fine structure indicative of stereochemical sequence distributions. Since the methine peak showed only dyad resolution, the majority of this work will concentrate on the carbonyl peak whose fine structure was dominated by three major peaks and, thus, offers the highest potential for discrimination between pair addition statistics and single addition statistics. Figure 3.33 shows the level of resolution for the carbonyl group that could be obtained

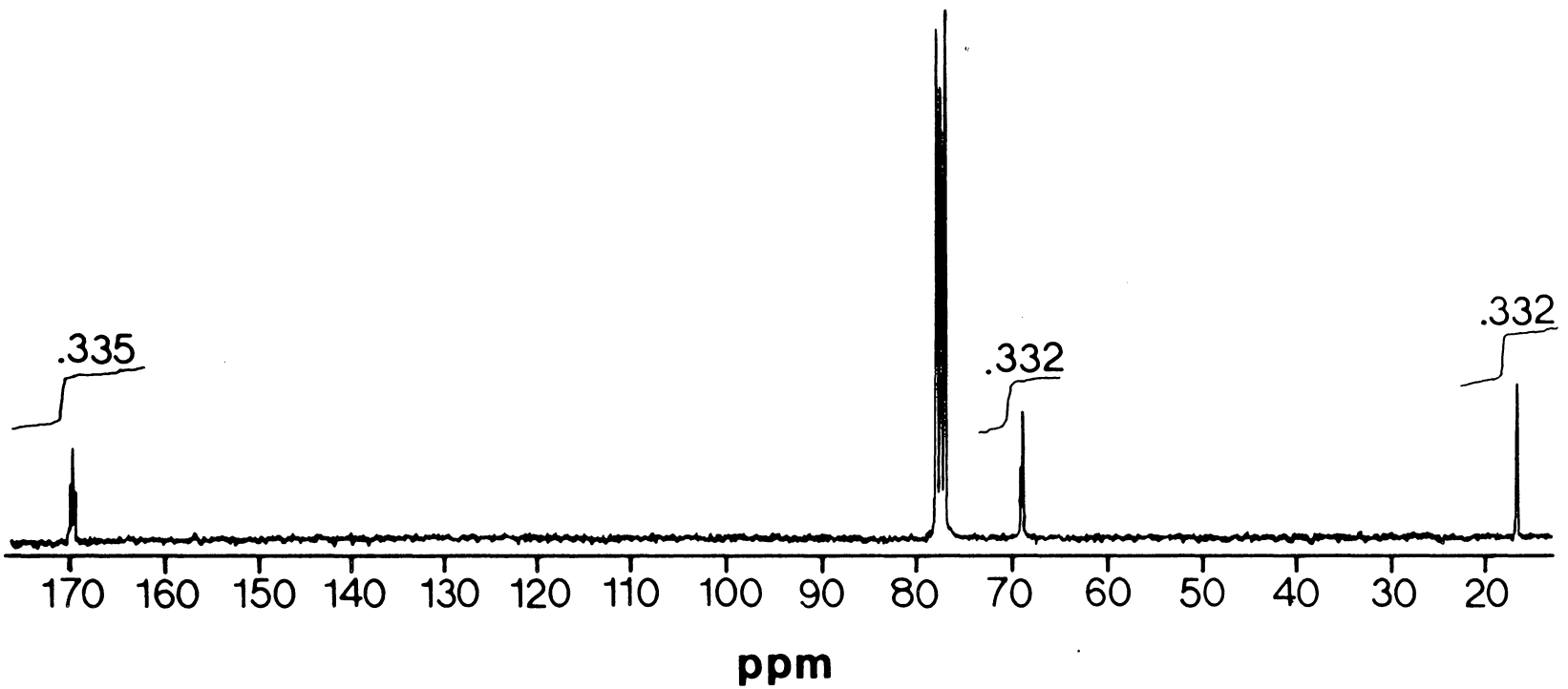

Figure 3.32. ^{13}C NMR spectra of racemic poly(lactic acid) 67.92 MHz, 2000 scans.

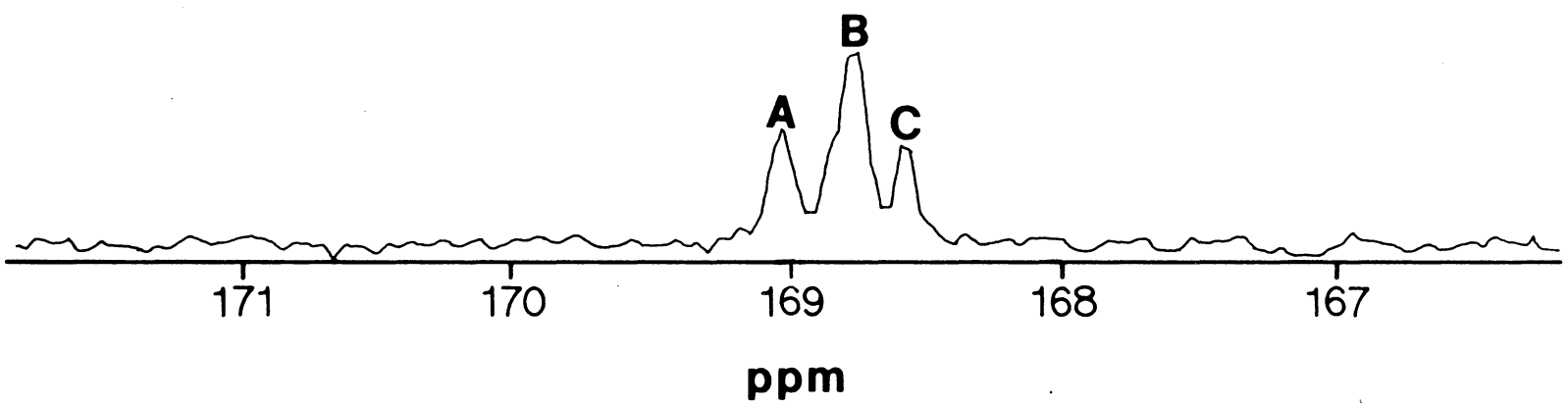

Figure 3.33. Fine structure resolution for carbonyl peak in racemic poly(lactic acid) at 67.92 MHz.

using the 67.92 MHz field strength employed in this work. Fine structure for all three peaks, including the methyl peak, was claimed by Lillie and Schulz (38), however, no such fine structure in the methyl region was observed in the data presented here. In contrast, Chabot et al. (60) saw no fine structure in either the methyl or methine peaks.

The resolution that was obtained in the ^{13}C NMR spectra of the carbonyl region does not compare favorably with previous results at equivalent field strengths. Chabot et al. (60) show more than seven peaks at 62.86 MHz. This is consistent with Lillie and Schulz (38) who also show more than seven peaks at field strengths as low as 25.2 MHz. Chalot et al. (60) report a carbonyl spectra very similar to that in Fig. 3.33, however, the field strength employed in this relatively low resolution spectra was 20.11 MHz. The improved resolution in the previous high resolution work discussed is attributed to resolution enhancement techniques employed by the authors prior to transformation of the experimental decay. Similar enhancement techniques were not used in this work.

As will be recalled from discussions in the introduction, racemic lactide is the molecular 1:1 compound of both enantiomers, L-lactide and D-lactide. It is generally assumed that the presence of both enantiomers should not affect the mode of ring-opening polymerization so that retention of configurations during monomer addition is

fully expected. This mode of polymerizing isotactic dyads involving either D-lactide or L-lactide in random growth steps has been described by Bernoullian D,D and L,L pair addition statistics (41). Stereosensitivity to triads, tetrads, and pentads should give 3, 5, and 7 NMR lines, respectively, for the carbonyl spectra in racemic poly(lactic acid). If significant levels of ester interchange occur, then the stereochemical sequence of D and L units will be randomized along the chain. In such an instance, the well known case of Bernoullian single addition statistics should hold which will give 4, 8, and 16 components to the carbonyl spectra for triad, tetrad, and pentad sensitivity, respectively. These differences are the basis upon which the occurrence of transesterification can be determined (38,41,60).

Following the previous work of Chabot et al. (60), the carbonyl spectrum of racemic poly(lactic acid) will be divided into three regions labeled A, B, and C as in Fig. 3.33. A is considered to be an isolated peak specific only to isotactic sequences due to its correspondence to the unique peak observed for poly(L-lactic acid), see Fig. 3.34. The high field peak C was considered by Chabot et al. (60) to be an isolated heterotactic peak, while the intermediate peak B is assumed to be a multiplet of the remainder of the possible heterotactic peaks. These two latter peak assignments seem to be somewhat arbitrary. In order to more

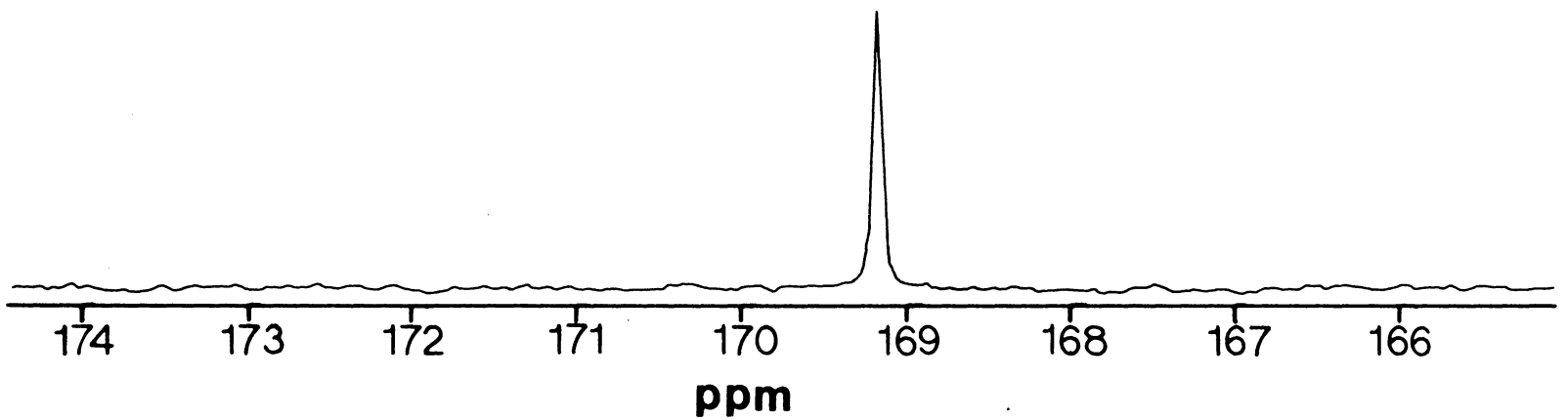

Figure 3.34. Fine structure resolution for carbonyl peak in poly(L-lactic acid) at 67.92 MHz.

adequately consider all possibilities, the analysis will be expanded to include single addition statistics. It still is quite reasonable to consider peak A as an isolated isotactic peak. The high field peak C may now be considered to be a syndiotactic peak while the intermediate peak is again considered to be a multiplet of all heterotactic peaks. Note, syndiotactic sequences for pair addition statistics were denied. Table 3.4 is a comparison of theoretical and experimentally determined peak areas expressed as fractions of the total carbonyl intensity. Triad, tetrad, and pentad sensitivity are considered in the theoretical calculations. Both results obtained in this work on racemic poly(lactic acid), as well as those of Chabot et al., are listed for comparison.

Clearly, there is a difference between the results obtained in this work and those of previous studies (60), especially in the high field intensity (peak C). This difference may be linked to the improved and more quantitative techniques used to measure the NMR response. If pair addition statistics are assumed to be operative, then Chabot's et al. 20.11 MHz. spectra correlated well with pentad sensitivity while the data in this work do not find a good match with theoretical intensity calculations. If single addition statistics are assumed to dominate, then data generated in this work correlate well with triad resolution.

Putting aside for the moment the discrepancies

Table 3.4

Comparison of Peak Areas from NMR Analysis of Racemic Poly(lactic acid) to Single and Pair Addition Bernoullian Statistics

	I_A/I_{total}*	I_B/I_{total}*	I_C/I_{total}*
Single Addition Bernoullian Statistics	(25, 12.5, 6.25)** (a, b, c)	(50, 75, 87.5)	(25, 12.5, 6.25)
Pair Addition Bernoullian Statitics	(50, 37.5, 25)	(25, 50, 62.5)	(25, 12.5, 12.5)
Chabot et. al. (60)	27	59	14
Data	26	52	22

*I_A/I_{total} ratio of peak intensity to total carbonyl intensity expressed as a percentage.

**(a, b, c) triad, tetrad, pentad theoretical intensities.

associated with differences in resolution and technique, there is an additional contrast to be noted. The racemic poly(lactic acid) synthesized in the previous work was done with the aid of zinc powder catalyst, while the material in this work was synthesized with stannous octoate. The activity of the stannous octoate is considerably higher than that of the zinc dust as judged by the longer polymerization times (744 hours) required for the zinc based polymerizations at 140 C. Note from the kinetic studies above, that polymerization time of twenty hours at 140 C was sufficient to reach final conversion and reactions were seldom run in excess of 60 hours. In addition, the stannous octoate is also known to promote transesterification (26,28). It would be tempting to attribute the single addition statistics in the poly(lactic acid) synthesized in this work to the enhanced ester interchange promoted by stannous octoate. However, this reasoning would be offset somewhat by the increased exposure to heat endured by the materials synthesized by Chabot et al. It would stand to reason that increased exposure to heat would promote ester interchange even at the potentially lower rates in the absence of stannous octoate. In fact, Chabot et al. (60) discussed the potential of transesterification in the polymerized samples in order to correlate their 20.11 MHz. NMR results with mixed single addition and pair addition Bernoullian statistics assuming tetrad sensitivity (instead of pentad sensitivity).

In other words, the NMR spectrum is also consistent with tetrad resolution if the material is considered partially transesterified so that neither single addition or pair addition statistics hold.

A series of racemic poly(lactic acid) samples were annealed at 200 C for times of 100, 300, 1000, and 3000 seconds and then quenched to room temperature. The technique for this heat treatment is detailed in the experimental section. It suffices to say that the intent of the exposure to 200 C was aimed at promoting transesterification and subsequently investigating any changes in NMR carbonyl fine structure. Table 3.5 details the results of the experiment in terms of peak intensities under A, B, and C again expressed as fractions of the total carbonyl intensity. Clearly, there was no overall change in the peak areas with only minor variations due to experimental error. This would tend to reinforce the idea that single addition statistics are prevalent in the material received from the reaction vessel and that stannous octoate promotes ester interchange in the course of the reaction. All spectra for this series are reproduced in Fig. 3.35 and the general lack of change supports the results of Table 3.5. One further observation is worth noting. There appears to be a very reproducible shoulder on the down field side of the heterotactic multiplet (peak B) possibly indicating the existence of two peaks in this region. This would be very consistent with an overall

Table 3.5

Effects of Annealing Racemic Poly(lactic acid) at 200 C
on the Fine Structure of the Carbonyl ^{13}C Spectrum, 67.92 MHz

Annealing Time of 200°C Seconds	I_A/I_{total}^*	I_B/I_{total}	I_C/I_{total}
0	26.2	52.3	21.5
100	27.4	55.2	17.4
300	22.3	56.1	21.6
1000	24.6	57.9	17.5
3000	22.9	53.5	23.6

$^*I_{A,B,C}/I_{total}$ ratio of peak intensity to total carbonyl intensity expressed as a percentage.

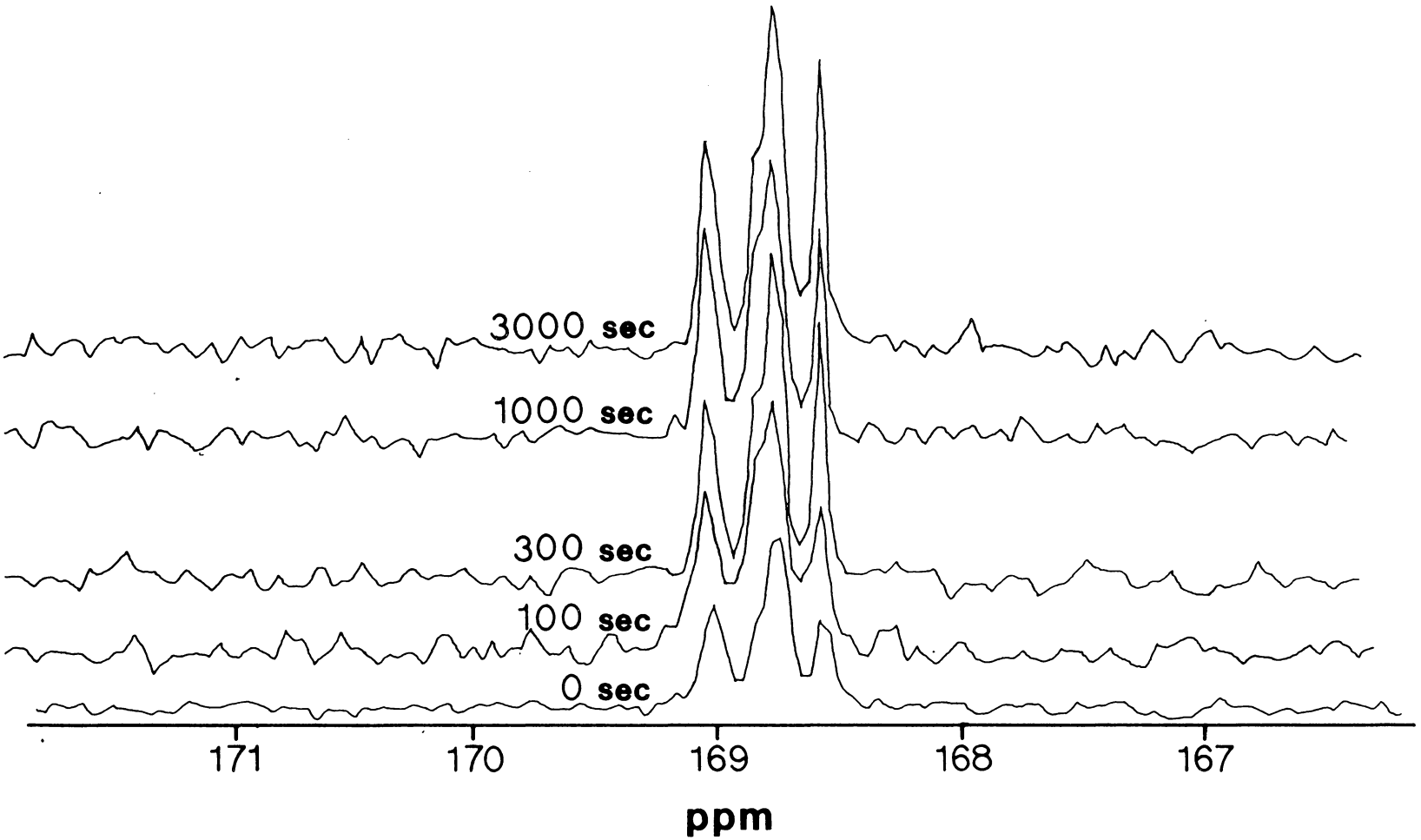

Figure 3.35. Effects of annealing racemic poly(lactic acid) at 200 C on the fine structure of the carbonyl ^{13}C NMR spectrum, 67.92 MHz.

peak count of four expected from single addition statistics and a triad resolution.

Assuming the extensive transesterification associated with stannous octoate catalyzed polymerization, there was no driving force for observing sequence distribution changes on annealing racemic poly(lactic acid). Thus, a second annealing series was undertaken in an attempt to induce sequence distribution changes observable in NMR spectra. A blend of 20% by weight poly(l-lactic acid) (isotactic) in 80% racemic poly(lactic acid) was made with the methodology previously described in the experimental section. This starting material was considered to contain enough isotactic sequence length that, if transesterification was to take place, significant changes in the carbonyl spectra were expected. This blend was expected to be miscible at least at the temperatures of annealing (200 C). Table 3.6 and Fig. 3.36 show the results of annealing at 200 C for times of 100, 300, 1000, and 3000 seconds. Clearly, no measurable change in peak areas was observed, and it must be concluded that transesterification did not take place on a scale that could be measured with NMR, in the time frame indicated, and under the conditions of this experiment.

The conclusion of no transesterification is further reinforced with differential scanning calorimetry results. Figure 3.37 shows scans of the blend before and after the thermal treatment. Both samples were slow cooled from 200 C

Table 3.6

Effects of Annealing a Blend of 20% Poly(L-lactic acid) and 80% Racemic Poly(lactic acid) at 200 C on the Fine Structure of the Carbonyl ^{13}C NMR Spectrum, 67.92 MHz

Annealing Time at 200°C Seconds	I_A/I_{total}*	I_B/I_{total}	I_C/I_{total}
0	39.0	43.1	17.9
100	40.1	45.7	14.2
300	40.5	39.1	20.4
1000	38.9	44.8	16.4
3000	40.0	44.6	15.4

*I_A, I_B, I_C/I_{total} ratio of peak intensity to total carbonyl intensity expressed as a percentage.

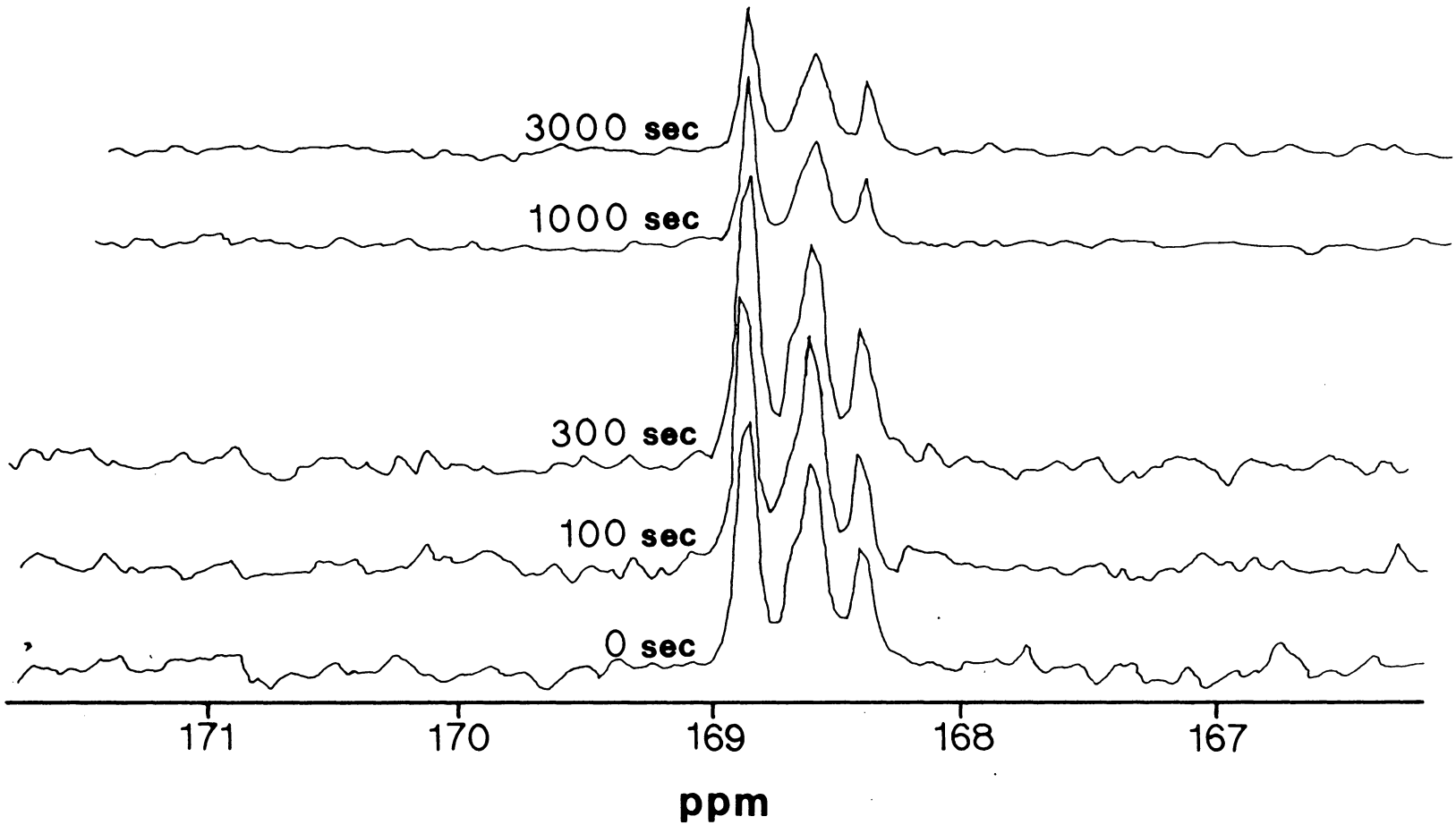

Figure 3.36. Effects of annealing a blend of 20% poly(L-lactic acid) and 80% racemic poly(lactic acid) at 200 C on the fine structure of the carbonyl ^{13}C NMR spectrum, 67.92 MHz.

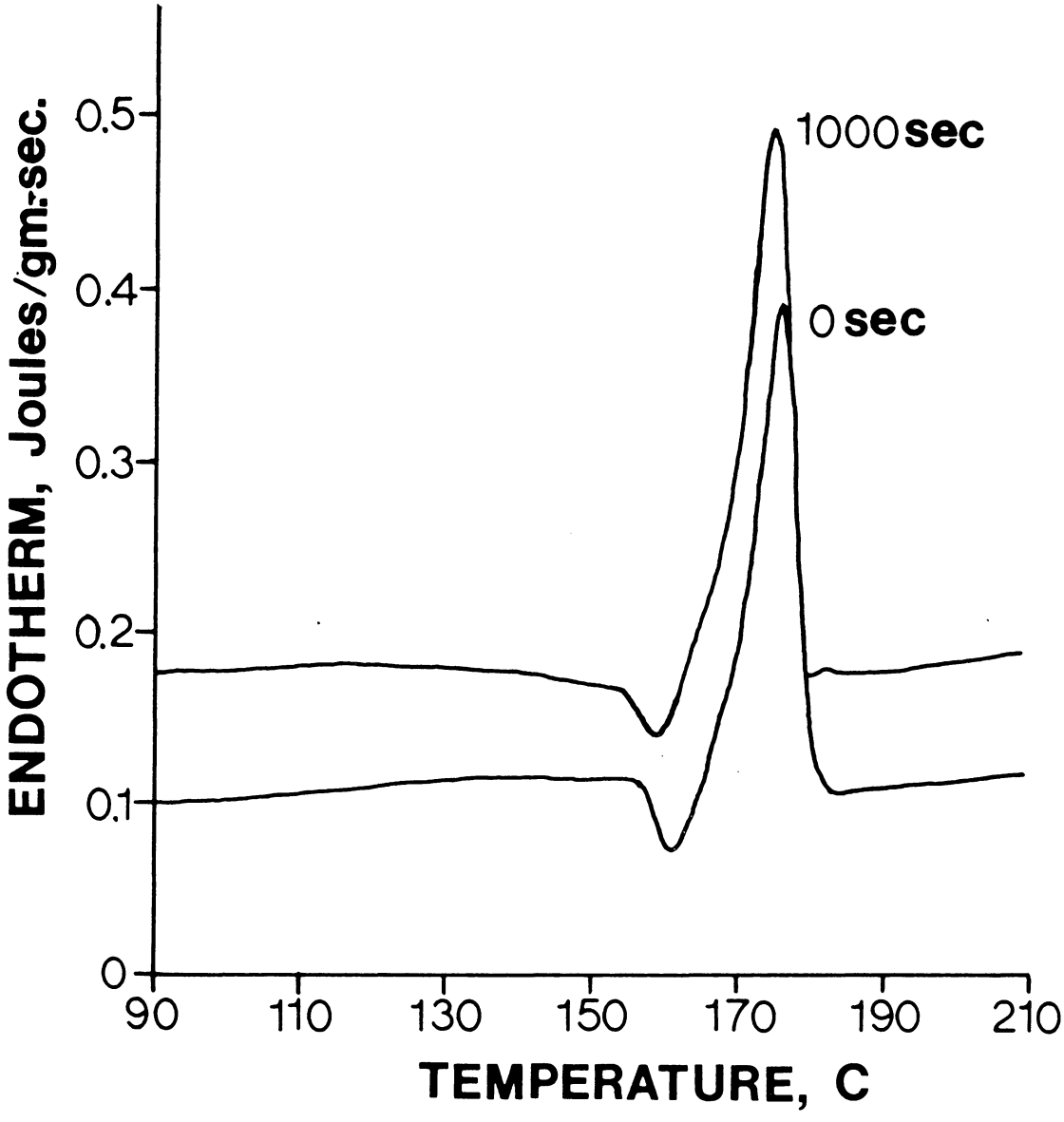

Figure 3.37. DSC heating scans (10 C/min) of 20% poly(L-lactic acid)/80% racemic poly(lactic acid) blends after 0 seconds and 1000 seconds at 200 C.

in the calorimeter to induce as much crystallinity as possible. The melting point and heat of fusion do not change indicating that the crystallizable material in the blend has no significant D unit copolymer character. Note that a copolymer content as small as 2% D units has been shown to drop the melting point of poly(L-lactic acid) by 13 centigrade degrees (60).

If the conclusion regarding the lack of measurable transesterification is correct, then the rationalization of the racemic poly(lactic acid) spectra in terms of required pair addition statistics remains. At field strengths of 62.86 MHz., Chabot et al. (60) compare the spectra of poly(lactic acids) polymerized from racemic lactide monomer and racemic lactic acid monomer. The ring-opening lactide polymerization is expected to give the standard pair addition statistics (barring any significant transesterification reactions) while the condensation of the racemic acid should give true random single addition statistics. Even though the resolution obtained by Chabot et al. is greater than that obtained in this work, the similarity between the assumed pair addition spectra and the spectrum in Fig. 3.33 is strong enough to give convincing arguments for pair addition. The spectra of the condensation polymer and the ring-opening polymer are so radically different that interpretation of the results in Table 3.4 needs to be reconsidered. The original discussion of the peak intensities in Table 3.4 was based on

the assumption, originally postulated by Chabot et al. (60), that the high field peak C is a single heterotactic peak and would necessarily carry a normalized intensity of 12.5 (expressed as a percentage of the overall carbonyl intensity) if pentad sensitivity is assumed. This would be very consistent with the intensity of 14 measured by Chabot et al. (60). It appears that this is the only a priori reasoning for assuming that peak C was not a multiplet. If it is assumed that peak C contains two equal intensity heterotactic peaks, then the theoretical pentad intensity distribution shifts to 25, 50, 25. This is as close to the measured values as can be experimentally expected. Note, this is indistinguishable from single addition statistics for triad resolution with the exception of the overall spectra shape comparison mentioned above. It would necessarily be expected to obtain pentad sensitivity at equivalent field strengths. Note that the field strength employed in this work, 67.92 MHz, is close to that employed by Chabot et al. (60) (62.86 MHz.). The discrepancy in the details of resolution between the spectra in this work and those obtained by Chabot's et al. can be attributed to the resolution enhancement techniques employed by Chabot et al. (60). The difference between the intensity measured for the high field peak C in the two spectra may be due to the improved quantitative techniques of combining inverse gated decoupling with the addition of a shiftless relaxation agent employed in the

generation of this NMR data.

Based on the literature data available, and the best interpretation of this NMR study, it is concluded that no sequence distribution rearrangement can be detected due to ester interchange in both the synthesis of poly(lactic acid) and in the post synthesis thermal processing of the polyester. Bernoullian pair addition statistics appear to hold for the ring-opening polymerization of racemic poly(lactic acid) although an improved resolution spectrum allowing for more peak definition would go a long way toward data interpretation. It appears that at a field strength of 67.92 MHz, pentad resolution of the carbonyl carbon may be expected for poly(lactic acid). With a view toward chapter 4 of this dissertation, it may be stated that no significant transesterification takes place in heating blends of poly(L-lactic acid) and racemic poly(lactic acid) to 200 C for as long as 3000 seconds.

3.3.3 THERMAL DEGRADATION OF POLY(LACTIC ACIDS)

A very utilitarian approach was undertaken to investigate the thermal degradation of the poly(lactic acids). The major objective was not to improve on the information already available in the literature on the mechanisms and chemistry of the thermal stability of this material. Rather, methods were sought to facilitate the thermal processing of poly(lactic acid) that would prevent significant molecular weight loss.

An especially high molecular weight poly(L-lactic acid) was chosen for the study with the reasoning that even subtle thermal instabilities can be more easily detected by concomitant changes in molecular weight the higher the molecular weight of the system. Put in more rudimentary terms, a given number of molecular chain ruptures will have a larger impact on a high molecular weight system than in a low molecular weight system. The viscosity average molecular weight of the optically active polymer was 716,000 as determined in chloroform at 30 C (see experimental section).

The first experiment that seemed appropriate was a thermalgravimetric analysis. The results of heating the polymer under a dry nitrogen purge is shown in Fig. 3.38. Significant weight loss at a heating rate of 10 C/min. is detected at approximately 310 C. Similar results are shown in Fig. 3.39 for the heating of the poly(lactic acid) under

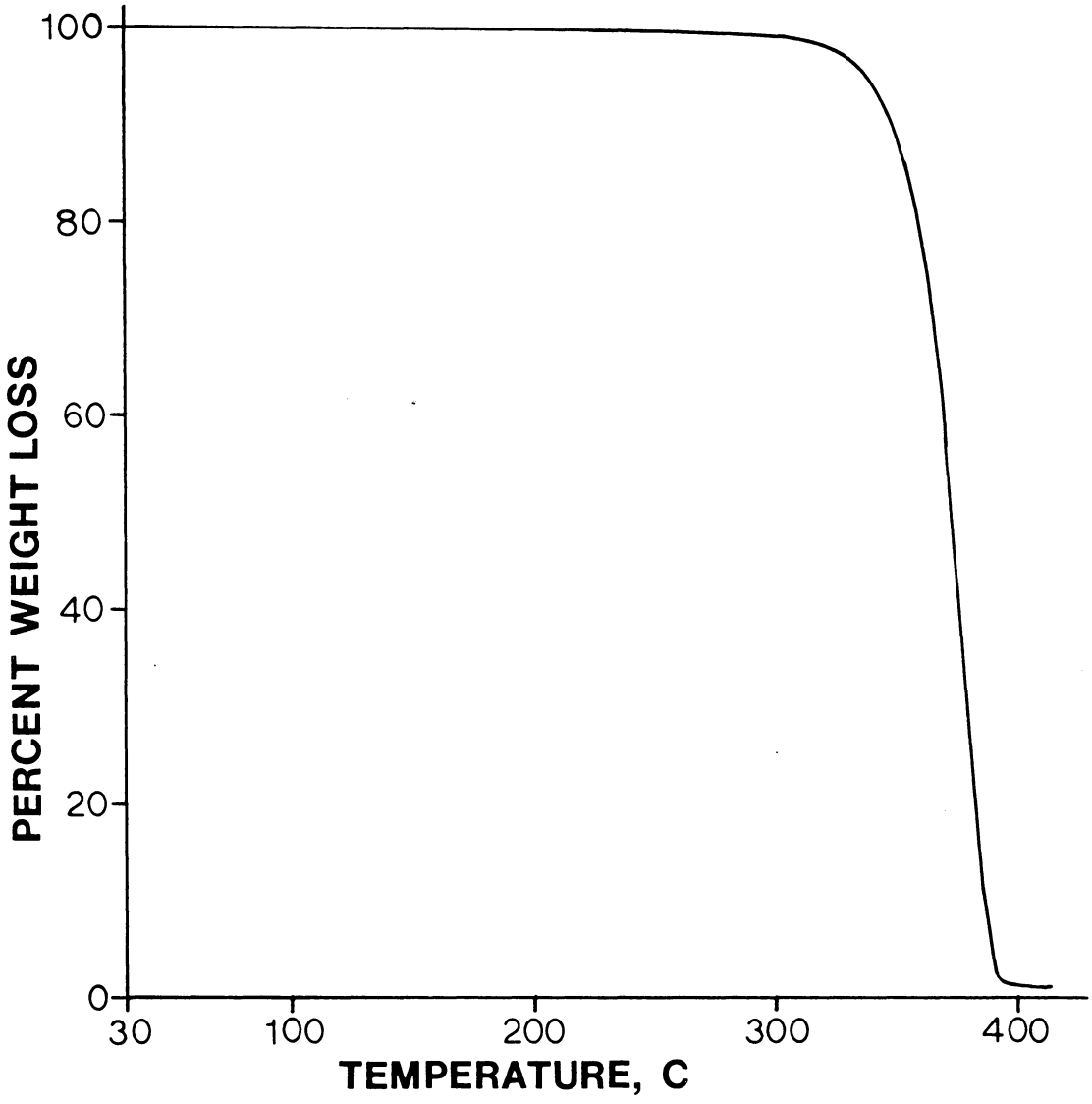

Figure 3.38. Thermalgravimetric analysis of poly(L-lactic acid) under a nitrogen atmosphere at 10 C/minute scan rate.

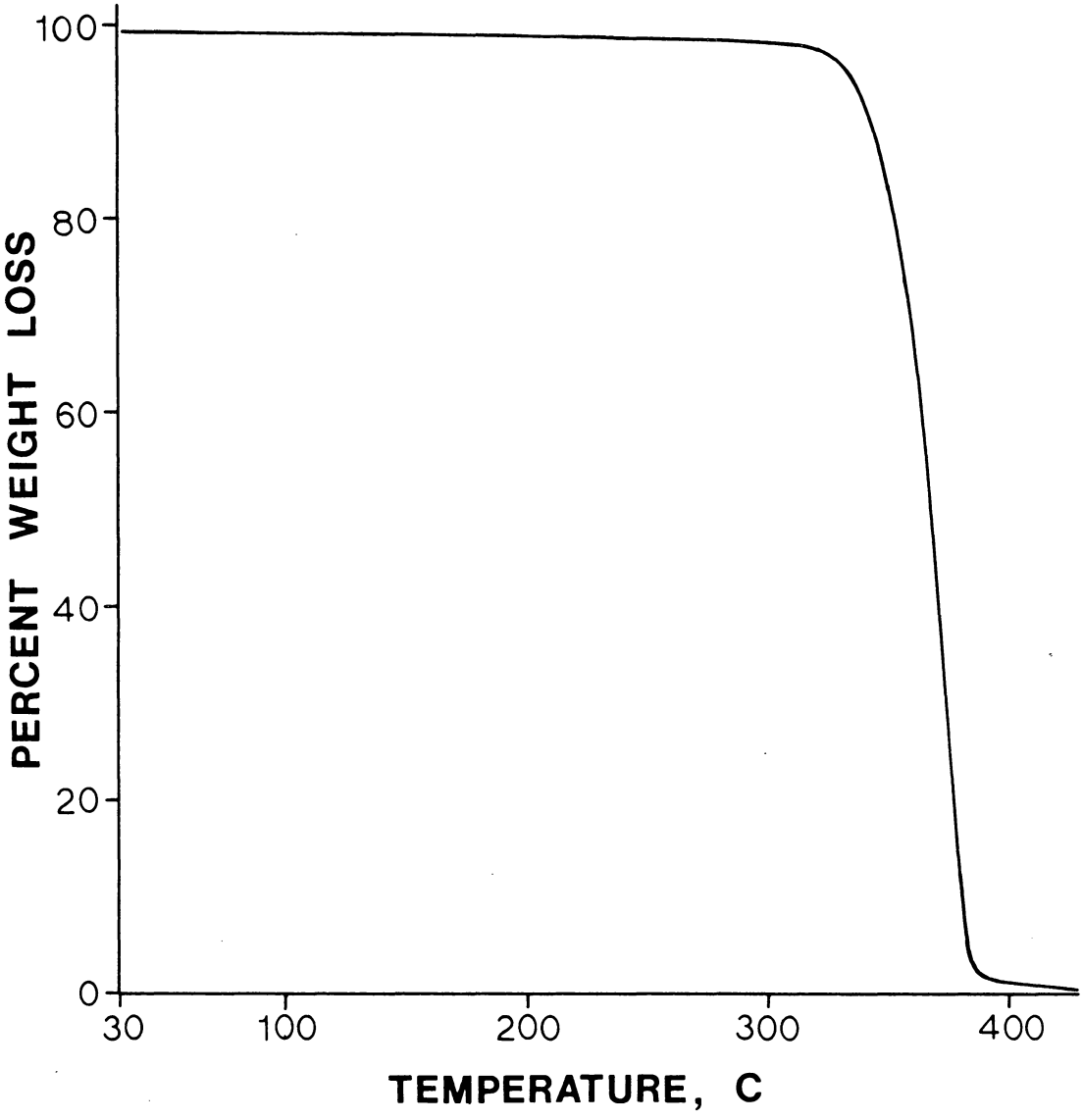

Figure 3.39. Thermogravimetric analysis of poly(L-lactic acid) under an oxygen atmosphere at 10 C/minute scan rate.

an oxygen atmosphere. However, the degradation in an oxygen atmosphere is a bit more severe with significant weight loss occurring as early as 285 C. On careful inspection of both curves, detectable weight loss is seen as a slight and increasing negative slope as early as 200 C. Since the melting point of the material is 180 C, 200 C seems a minimum temperature for processing and the weight loss seen in the TGA is indicative of the problems seen by other workers in the melt processing of this polymer (75).

In light of previous studies in the degradation mechanisms of the family of polymers derived from the ring-opening polymerization of cyclic dimers of -hydroxy-acids (68-72), three potential modes of improving degradation characteristics in the poly(lactic acid) system were chosen for investigation. Aside from the intramolecular transesterification mechanism of degradation mentioned in the introduction, the mechanisms of backbiting to form cyclics, homolytic chain cleavage, and hydrolysis are the three mechanism that are most often considered to participate in the degradation of poly(lactic acid) and lactone polymers in general. Since the intramolecular transesterification mechanism has no known counter treatment, the investigation is limited to the remedy of the three previously mentioned mechanisms.

Acetyl end capping of terminal hydroxyl groups was previously determined to improve thermal stability in

valerolactone systems (16) as well as in this poly(lactic acid) system (75). This end capping is considered to prevent a backbiting mechanism in the formation of cyclic byproducts of depolymerization by removing the hydroxy end groups which result from the polymerization chemistry. End capping of poly(lactic acid) with acetic anhydride and pyridine was affected by a simple procedure already published (75).

The accelerated degradation of this polyester in an oxygen atmosphere as demonstrated in the TGA experiments, as well as conjecture by previous workers that homolytic chain cleavage may be a particularly acute thermal degradation mechanism for poly(lactic acid) (72), suggested that the addition of a free radical scavenger may prevent molecular weight loss. A commercial grade antioxidant called Irgonox 1010 was blended with the poly(L-lactic acid) to a final concentration of 1% by weight by dissolving both in chloroform and casting a film from the solution. The film was dried under vacuum overnight at 80 C.

Thirdly, hydrolysis of lactone based polyesters may be especially acute in the presence of acid groups. This, in fact, has been known to lead to an autocatalytic effect since acid is a byproduct of the hydrolysis reaction (70). Hydrolysis of the polyester might be alleviated by meticulous drying of the material prior to exposure to thermal processing temperatures. This was accomplished by drying the polymer under a continuous vacuum at 80 C for 30 hours just

prior to thermal processing. More severe drying conditions were avoided in order to prevent concurrent degradation. Complete removal of all acids may not be feasible since the typical active hydrogen initiation of these systems will lead to a finite number of acid end groups (26-28).

Table 3.7 shows the results of the degradation study in which the potential for molecular weight stability was evaluated for the three treatments described above. The viscosity average molecular weight for each treatment was measured before and after exposure to 210 C for 10 minutes. The control for the experiments was taken as a sample of the same polymer which had been stored in a vacuum desiccator over phosphorous pentoxide after the standard post polymerization clean-up. Prior to heating, all three treatments show molecular weights similar to the original polymer indicating no change in molecular weight due to the treatment alone. When the untreated sample was heated to 210 C for 10 minutes, a significant molecular weight loss was measured. Similar molecular weight loss was observed on heating the end capped sample and the sample blended with the free radical scavenger. Only the polymer which had been meticulously dried showed any significant improvement in molecular weight stability on heating. This is a strong indication that hydrolysis makes a significant contribution to the overall degradation mechanism. However, despite the improvement on drying, there was still a great deal of

Table 3.7

Effects of Several Post Synthesis Treatments on the Thermal Degradation of Poly(L-lactic acid) Molecular Weight

Polymer Treatment	VISCOSITY AVERAGE MOLECULAR WEIGHT	
	Prior to Thermal Treatment	After Exposure to 210°C/10 Minutes
None	716,000	79,000
Irgonox 1010	707,000	76,000
Acetic Anhydride End Capping	660,000	80,000
Meticulous Drying	703,000	493,000

molecular weight loss.

In an effort to try and ascertain whether the molecular weight loss beyond that attributed to hydrolysis is due to the mechanism of intramolecular transesterification, a high vacuum heating experiment was performed. Approximately 0.5 grams of the poly(L-lactic acid) was placed in the bottom of a standard vacuum tube reactor (see section 3.2.2) and heated to 220 C. The material was previously dried at 80 C for 30 hours under a continuous vacuum. Vacuum was applied throughout the high temperature exposure to maintain the pressure below one millitorr. As discussed in the experimental section, the upper portion of the tube was kept cool via ice water to facilitate the condensation of the degradation byproducts. After a timed exposure to 220 C, the vacuum tube was allowed to cool to room temperature prior to repressurization to ambient conditions. Several portions of the same poly(L-lactic acid) were exposed to 220 C for periods of 10, 60 and 250 minutes. The molecular weight of these samples, as well as the unheated material, as determined by gpc, are plotted in Fig. 3.40. Within the first 10 to 20 minutes of exposure, the number average molecular weight has dropped from the original value of 4.3×10^5 to a value just above 2.7×10^5 which remains almost invariant for the remainder of the time scale investigated. A similar trend is obvious for the weight average molecular weight. Thus, the polydispersity remains at approximately 2,

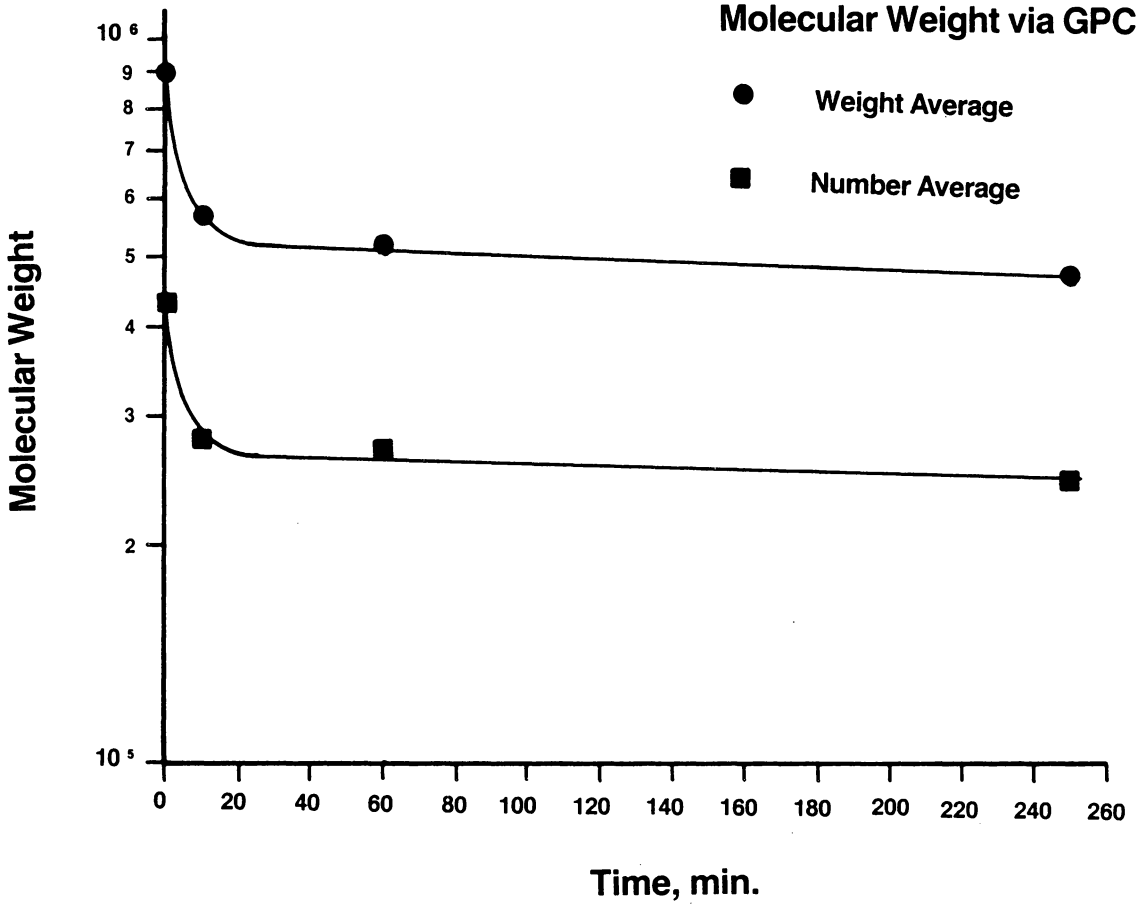

Figure 3.40. Molecular weight loss kinetics at 220 C exposure under a vacuum of approximately 1 millitorr.

independent of the change in molecular weight.

Two distinct bands of condensate are formed on the inner surface of the vacuum tube and are most obvious for the samples exposed to 220 C for the longest times. Material from each of the two bands in the 250 minute sample was collected and mixed with KBr to form a pressed pellet for IR analysis. Figures 3.41 and 3.42 represent spectra from the higher condensate and the lower condensate, respectively. From the positioning in the vacuum tube, it is assumed that the high condensate (farthest from the sample) had the highest vapor pressure. The high condensate was present at significantly higher proportions.

Previous molecular weight studies on the thermal degradation of glycolide based polymers have shown that the dominant mechanism of degradation is intramolecular transesterification. Two characteristics of this mechanism are the production of cyclic monomer and the slow decrease in molecular weight. The high condensate IR spectrum is a perfect match for lactide monomer which is consistent with this mechanism. The slow molecular weight loss in the long time portions of the trace in Fig. 3.40 is also consistent with the intramolecular transesterification mechanism. The initial steep and short-lived drop in molecular weight still begs explanation. It is assumed that this decrease is due to the residual water content in the material and the resulting hydrolytic degradation suffered until the water was

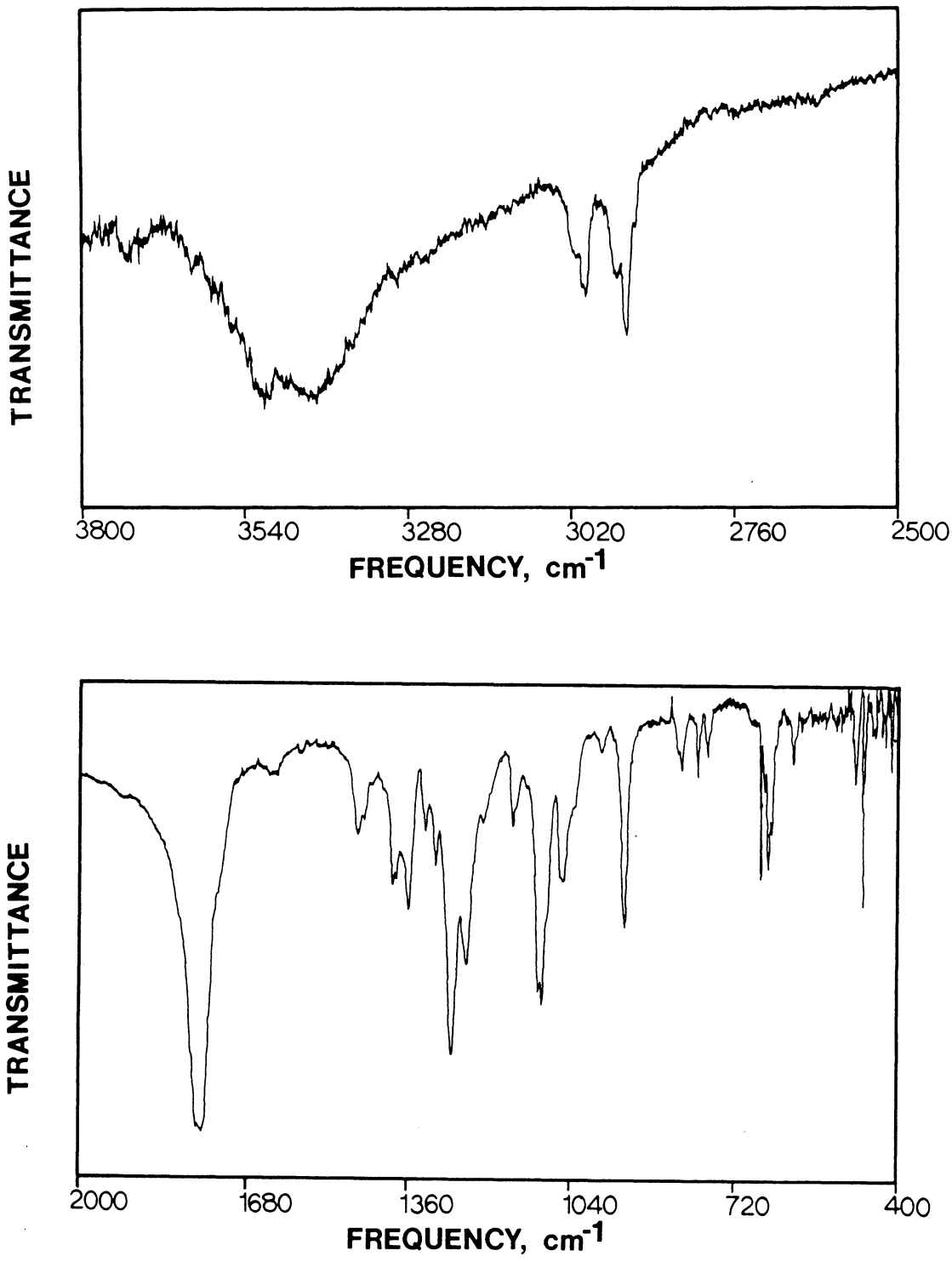

Figure 3.41. Partial infrared spectrum from high condensate obtained during vacuum treatment at 220 C (2 cm^{-1} resolution).

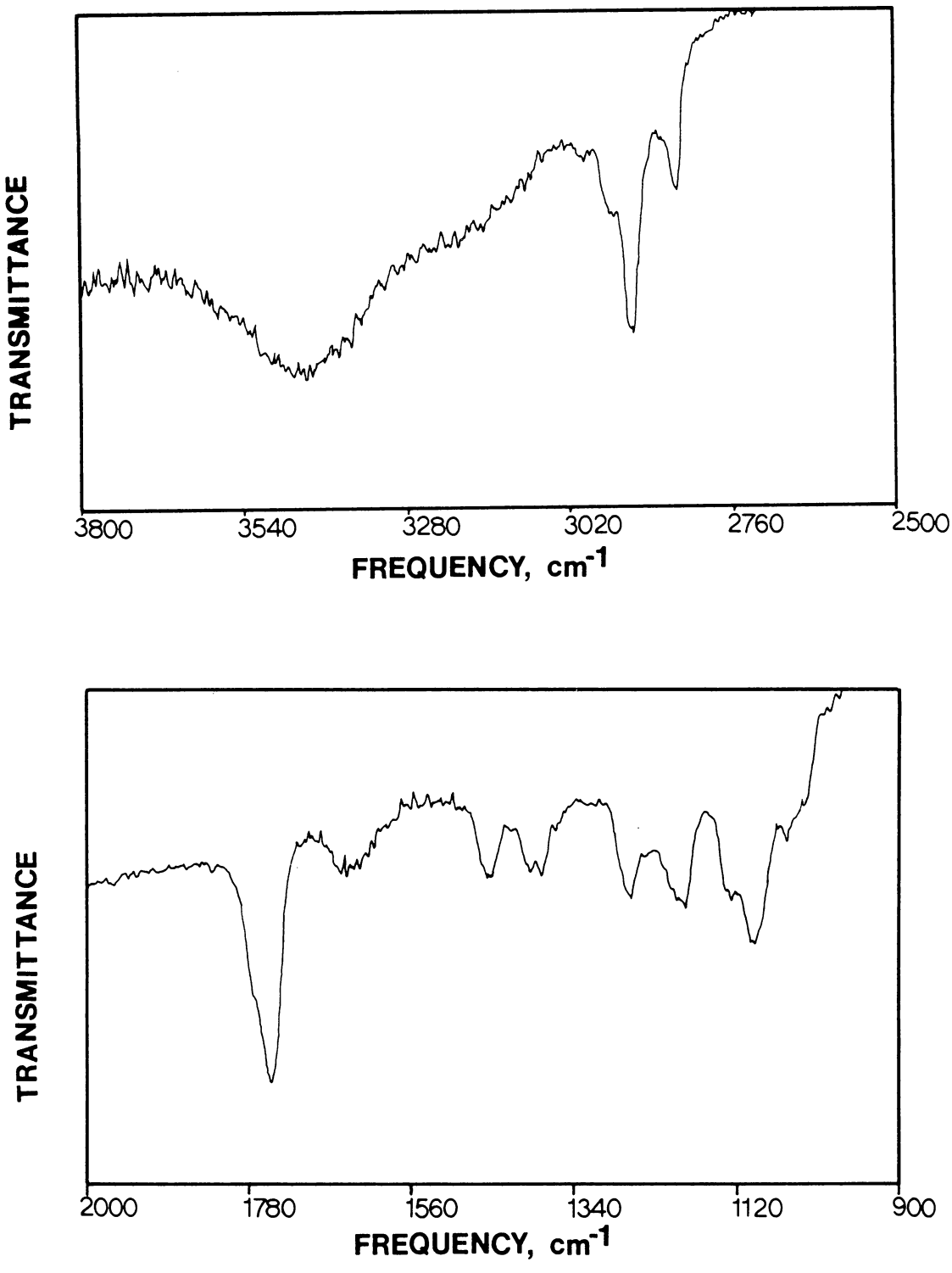

Figure 3.42. Partial infrared spectrum from low condensate obtained during vacuum treatment at 220 C (2 cm^{-1} resolution).

eventually removed by the vacuum. In partial support of this, the IR spectrum in Fig. 3.42 is very similar to the spectrum obtained from pure poly(lactic acid). Although some discrepancy exists between the low condensate spectra and poly(lactic acid), the broad OH peak at 3445 cm^{-1} may indicate carboxylic acid or hydroxy termination. Thus, it is supposed that the low condensate (low vapor pressure material) may be oligomeric byproducts of the hydrolytic degradation. Note that there is an OH stretch peak in the lactide spectra as well. This may suggest a lack of perfect separation during condensation.

The constancy of the polydispersity in Fig. 3.40 may be explained by two mechanisms. First, the cyclic dimer formation mechanism is molecular weight independent so that high and low molecular weight species are equally likely to lose repeat unit sequences. Thus, no change is expected in the ratio of Mw/Mn. The second possibility of intermolecular transesterification which would inherently maintain the polydispersity at 2, is discounted based on the results in section 3.2.2. The original polydispersity of 2 in the sample is attributed to the polymerization mechanism as described in section 3.3.1.1.

In summary, there are two dominant mechanisms in the thermal degradation of poly(lactic acids). First, the material is susceptible to hydrolytic degradation if even trace amounts of water are present. This will lead to

catastrophic loss of molecular weight at temperatures commensurate with the thermal processing of the crystalline poly(L-lactic acid). This can be minimized to some extent by the vacuum drying of the material at 80 C for 30 hours. The elevated temperatures needed to remove all the water will lead to concurrent degradation of the material. A second mechanism of degradation which will lead to the production of the cyclic dimer is the intramolecular transesterification discussed in detail in section 3.1.4 of the introduction. This mechanism does not lead to significant molecular weight loss in time scales expected in thermal processing. With a view toward the handling of these materials at elevated temperature as described in chapter 4 of this dissertation, molecular weight loss can be best minimized by vacuum drying the materials under mild conditions just prior to thermal treatment.

3.4.0 CONCLUSIONS

3.4.1 LACTIC ACID INITIATES THE POLYMERIZATION OF LACTIDE

Lactic acid initiation of the polymerization of lactide to poly(lactic acid) is proposed based on an active hydrogen mechanism typical of other lactone polymerizations. Molecular weight control was adequately affected by tailoring the lactic acid concentration in the melt phase polymerization. Deviations from the anticipated inverse proportionality between number average molecular weight and lactic acid concentrations is attributed to slow initiation rates. Incomplete conversion of lactic acid to propagating chains at reaction completion leads to higher than expected molecular weights. Molecular weight distributions tend toward the most probable as described by the Shulz-Flory distribution at low acid concentrations (less than $3x10^{-4}$ moles acid/mole lactide). In this case, near complete initiation can be expected early in the reaction scheme so that a constant concentration of active species may be anticipated for the majority of the reaction. Acid initiation of the ring-opening polymerization is thought to lead to anhydride linkages which are considered to undergo alcoholysis by active hydroxyl chain ends and/or lactic acid. This effectively leads to chain transfer, but this is not inconsistent with the requirement of constant active growth

site concentration stipulated by the Shulz-Flory distribution. At higher lactic acid concentrations, deviations from the most probable distribution ($M_w/M_n = 2$) are attributed to finite initiation rates throughout the polymerization reaction. This changes the number of active growth sites during the course of the reaction and, thus, at high acid concentrations broader molecular weight distributions may be expected.

3.4.2 STANNOUS OCTOATE BEHAVES AS A CATALYST IN THE POLYMERIZATION OF LACTIDE

The catalytic activity of stannous octoate is suspected although a mechanism for such was not postulated. Without the presence of stannous octoate, the polymerization of lactide to poly(lactic acid) could not be detected in reasonable time scales. The effect of stannous octoate on molecular weight and molecular weight distribution is nil at low to moderate concentrations up to $1x10^{-4}$ moles stannous octoate/mole lactide. Above this concentration stannous octoate causes a drop in the molecular weight and conversion realized from the polymerization. This deleterious effect is attributed to a acid interchange reaction between the lactic acid initiator and the stannous octoate. On acid interchange, a production of monofunctional initiation species, such as 2 ethyl-hexanoic acid, occurs which may result in termination reactions due to condensation of monofunctional acids with hydroxy chain end groups. The increase in termination reactions adequately explains the observed drop in molecular weight and conversion.

3.4.3 OPTIMUM POLYMERIZATION TEMPERATURES ARE JUST ABOVE THE MONOMER MELTING POINT

Increase in polymerization temperatures above the minimum allowed by the melting point of the monomer causes a drop in molecular weight and increase in molecular weight distribution. This is thought to result from chain scission type of degradation mechanisms known to be promoted by higher temperatures. Best molecular weight control and the narrowest distributions can be expected from running polymerizations at temperatures as low as possible, ie. just above the melting point of the monomer of interest.

3.4.4 SIGNIFICANT DEVIATIONS FROM A "LIVING" MECHANISM ARE SEEN FOR THE MELT PHASE RING-OPENING POLYMERIZATION OF LACTIDE

The limited investigation into the kinetics of the polymerization scheme for poly(lactic acid) based on lactic acid initiation and stannous octoate as a catalyst yielded reaction profiles which were consistent with the proposed initiation mechanism. The steep rise in molecular weight with time and conversion is indicative of some living character to this ring-opening polymerization. However, the deviations from narrow molecular weight distributions even at low conversions early in the reaction profile suggest that true living polymerization is not the case. In order to maintain a Poisson distribution necessary for a true living mechanism, all active centers for monomer addition must be born at polymerization onset. This premise is violated by the finite initiation rates postulated to be operative throughout the course of the polymerizations studied.

3.4.5 POLYMERIZATIONS WERE SUCESSFULLY SCALED UP WITH CONTOL OF MOLECULAR WEIGHT MAINTAINED

Reactions were successfully scaled-up to 300 gram levels with good molecular weight control maintained through control of lactic acid concentration. Although a direct inverse relationship between molecular weight and acid concentration was not operative across large acid concentration ranges, reproducibility was demonstrated even at the large scales employed.

3.4.6 NO TRANSESTERIFICATION IN POLY(LACTIC ACIDS) COULD BE DETECTED VIA ^{13}C NMR TECHNIQUES

In the best interpretation of the ^{13}C NMR experiments described, no stereochemical sequence redistribution could be detected due to ester interchange in either the synthesis of racemic poly(lactic acid) or in the post synthesis thermal treatment of the polyester. In particular, Bernoullian pair addition statistics appear to hold for the ring opening polymerization of racemic poly(lactic acid) and are maintained after heating to 200 C for as long as 3000 seconds. In addition, no significant transesterification was detected via NMR in heating blends of poly(L-lactic acid) and racemic poly(lactic acid) up to 200 C for as long as 3000 seconds. This was confirmed through DSC melting endotherms of the blend containing the crystallizable component, poly(L-lactic acid).

3.4.7 MOLECULAR WEIGHT LOSS IN POLY(LACTIC ACID), AT TEMPERATURES COMMENSURATE WITH PROCESSING, IS MINIMIZED MOST EFFECTIVELY BY DRYING UNDER MILD CONDITIONS

Thermal degradation of molecular weight in poly(lactic acid) was determined to occur primarily through hydrolysis. The molecular weight loss on heating to temperatures commensurate with typical thermal processing could be minimized by drying at milder conditions (vacuum at 80 C). However, it was difficult to remove all water without heating to temperatures that concurrently degraded the polyester. At these elevated temperatures (220 C) and under a vacuum of less than 1 millitorr, lactide monomer was also removed from poly(lactic acid). This suggested that intramolecular transesterification leading to weight loss through regeneration of monomer was occurring. This second mechanism, typical of many lactone systems, led to relatively slower rates of molecular weight loss.

3.5.0 RECOMMENDATIONS FOR FUTURE WORK

3.5.1 MONOFUNCTIONAL ACTIVE HYDROGEN INITIATORS

It is proposed to investigate monofunctional active hydrogen initiators to determine the effects of chain termination via condensation on molecular weight and molecular weight distributions. With the inevitable residual concentration of lactic acid, a monofunctional carboxylic acid initiator could be used to investigate the potential of chain termination between active acid end groups and active hydroxy end groups. If the termination by condensation occurs to significant extents, then molecular weights and conversions should be limited to values below those realized in this study.

3.5.2 NON-CARBOXYLIC ACID ACTIVE HYDROGEN INITIATORS

In order to investigate the potential for the proposed formation of anhydride linkages in the initiation of poly(lactic acid), it is proposed to use a dialcohol to control molecular weight. The residual lactic acid concentration not withstanding, the alcohol initiation should not lead to the formation of the anhydride linkages, thus denying the chain transfer mechanism described in section 3.3.1.1. It is proposed to investigate this influence on molecular weight distributions.

3.5.3 ANALYTICAL TECHNIQUE FOR DETECTING LOW LACTIC ACID CONCENTRATIONS IN LACTIDE MONOMER

If a technique could be developed for determining the lactic acid concentration in lactide monomer, a more reliable estimate could be made of the molecular weight anticipated from any given polymerization employing the active hydrogen/stannous octoate scheme described in this study.

3.5.4 CATALYTIC EFFECTS OF STANNOUS OCTOATE ON OVERALL REACTION KINETICS

If, in fact, stannous octoate behaves as a catalyst in the polymerization scheme for poly(lactic acid), it should have a profound effect on polymerization kinetics. It is recommended to study the influence of stannous octoate concentration on the reaction profiles in the ring-opening polymerization of lactide within the range of concentrations in which no side reactions are suspected of occurring.

3.5.5 ALTERNATE TIN BASED SALTS OF CARBOXYLIC ACIDS TO BE EVALUATED AS POLYMERIZATION CATALYSTS

Acid interchange between stannous octoate and lactic acid was suspected to result in the formation of the tin salt of lactic acid. The isolated product from the assumed acid interchange was determined to be a more effective catalyst for the polymerization of lactide. In fact, fewer side reactions were attributed to the new catalyst ostensibly due to the dual functionality of lactic acid as compared to the monofunctional 2-ethyl hexanoic acid displaced from the stannous octoate. A more detailed study of this phenomenon is recommended. Other monofunctional and difunctional tin salts of carboxylic acids are suggested for investigation.

3.5.6 THE INFLUENCE OF STANNOUS OCTOATE ON TRANSESTERIFICATION IN POLY(LACTIC ACIDS)

It was determined that no transesterification in poly(lactic acids) could be detected by changes in stereosequence distributions as measured by ^{13}C NMR spectra. However, in light of the fact that stannous octoate is a known transesterification catalyst, it is proposed that the investigation of transesterification be extended to poly(lactic acids) in which the stannous octoate has not been removed by post polymerization clean-up. If transesterification can be induced by the presence of stannous octoate, a comparative study may clear up some questions concerning NMR spectra interpretation discussed in section 3.3.2.

3.5.7 DEVELOPMENT OF A MELT PHASE "LIVING" POLYMERIZATION OF LACTIDE

The development of an active hydrogen initiation/catalyst system, in which the relative rates of initiation and propagation are more favorable for molecular weight control and narrower distributions, seems worthwhile in light of the growing interest in this type of polymer. If a system could be discovered in which initiation takes place exclusively in the earliest stages of melt phase polymerization without side reactions, it would be more likely to obtain a truly "living" character. This could be of special utility in constructing well controlled block copolymer systems based on glycolide systems. Note, this has been reported for solution phase polymerizations which are of less industrial importance.

REFERENCES

1) R.L. Kronenthal, in Polymers in Medicine and Surgery, R.L. Kronenthal, Z. Oser, and E. Martin, Eds., Plenum, New York, 1975.

2) J.W. Hodge, U.S. Natl. Tech. Inform. Serv., AD report No. 742,719, 1971.

3) J.B. Gregory, A.D. Schwope, and D.L. Wise, U.S. Natl. Tech. Inform. Serv., AD Report No. 759,381, 1973.

4) L.C. Anderson, D.L. Wise, and J.F. Howes, Contraception, **13**, 375 (1976).

5) R.K. Kalkarn, E.G. Moore, A.F. Hegyeli, and F. Leonard, J. Biomed. Mat. Res., **5**, 169 (1971).

6) T. Asahara, S. Katayama, J. Chem. Soc., **67**, 956 (1964).

7) E.M. Filachioni and C.H. Fisher, Ind. Eng. Chem., **36**, 223 (1944).

8) P.J. Flory, Principles of Polymer Chemistry, Cornell Univ. Press, Ithaca, N.Y., 1953.

9) J. Kleine and H.H. Kleine, Makromol. Chem., **30**, 23 (1959).

10) R.C. Schulz, IUPAC Int. Symp. on Macromolecular Chemistry, Budapest, 185 (1969).

11) J.L. Brash and D.L. Lyman, Cyclic Monomers, High Polymers, Vol. XXVI, K.C. Frisch, Ed., Wiley-Interscience, New York, 1972.

12) F.E. Kohn, J.W.A. Van den Berg, G. Van de Ridder, and J. Feijen, J. Appl. Polym. Sci., **29**, 4265 (1984).

13) G. Odian, Principles of Polymerization, McGraw-Hill, New York, 1970.

14) G.L. Brode and J.V. Koleske, J. Macromol. Sci.-Chem., **A6**, 1109 (1972).

15) R.D. Lundberg and E.F. Cox, in Ring Opening Polymerization, K.C. Frisch and S.L. Reegen, Eds., Dekker, 1969.

16) K. Saotome and Y. Kodaira, Makromol. Chem., **82**, 41 (1965).

17) F.S. Dainton, T.R.E. Devlin, and P.A. Small, Trans. Faraday Soc., **51**, 1710 (1955).

18) F.S. Dainton and K.J. Ivin, Quart. Rev. (London), **12**, 61 (1958).

19) P.A. Small, Trans. Faraday Soc., **51**, 1717 (1955).

20) H.K. Hall and A.K. Schneider, J. Am. Chem. Soc., **80**, 6409 (1958).

21) D.K. Gilding and A.M. Reed, Polymer, **20**, 1459 (1979).

22) H.K. Hall, M.K. Brandt, and R.M. Mason, J. Am. Chem. Soc., **80**, 6420 (1958).

23) H.G. Brown, R.S. Fletcher, and R.B. Johannesen, J. Am. Chem. Soc., **73**, 212 (1951).

24) Ya.I. Gol'dfurb and L.I. Belen'kii, Russ. Chem. Rev., **29**, 214 (1960).

25) F. Korte and W. Glet, J. Polym. Sci., **B4**, 685 (1966).

26) D.M. Young and F. Hostettler (to Union Carbide Corp.), U.S. Pat. 2,890,208 (1959).

27) Belgium Patent 743,123 (to Union Carbide Corp.) (1970).

28) E. F. Cox and F. Hostettler, U. S. Patent 3,021,310 (to Union Carbide Corp.) (1964).

29) T. Ouhadi, C. Stevens, and P. Teyssie, Die Makromol. Chem., Suppl., **1**, 191 (1975).

30) J. Heuschen, R. Jerome, and P. Teyssie, Macromolecules, **14**, 242 (1981).

31) F. Hostettler and D.M. Young (to Union Carbide Corp.), U.S. Pat. 3,169,945 (1965).

32) F. Hostettler, G. Magnus, and H. Vineyard (to Union Carbide Corp.), U.S. Pat. 3,284,417 (1966).

33) R.H. Young, M. Matzner, and L.A. Pilato

34) H. Cherdron, H. Ohse, and F. Korte, Makromol. Chem., **56**, 179 (1962).

35) H. Cherdron, H. Ohse, and F. Korte, Makromol. Chem., **56**, 187 (1962).

36) H. Ohse and H. Cherdron, Makromol. Chem., **97**, 139 (1966).

37) Y. Yamashita, T. Tsada, M. Okada, and S. Iwatsuki, J. Polym. Sci., A-1, **4**, 2121 (1966).

38) E. Lillie and R.C. Schulz, Makromol. Chem., **176**, 1901 (1975).

39) M. Vert, F. Chabot, J. Leray, and P. Christel, Makromol. Chem., Suppl. **5**, 30 (1981).

40) R.G. Sinclair and G.M. Gynn, U.S. Natl. Tech. Inform. Serv., AD Report No. 748411 (1972).

41) A. Schindler and D. Harper, J. Polym. Sci., Poly. Chem. Ed., **17**, 2593 (1979).

42) R. Dunsing and H. R. Kricheldorf, Polymer Bulletin, **14**, 491 (1985).

43) H. Kricheldorf and A. Serra, Polymer Bulletin, **14**, 497 (1985).

44) S. Inoue, Y. Tomo, T. Tsuruta, and J. Furukawa, Makromol. Chem., **48**, 229 (1961).

45) E.F. Cox and F. Hostettler (to Union Carbide Corp.), U.S. Pat. 3,021,316 (1962).

46) E.F. Cox and F. Hostettler (to Union Carbide Corp.), U.S. Pat. 3,021,317 (1962).

47) R.D. Lundberg, J.V. Koleske, and K.B. Wischmann, J. Polym. Sci., **7**, 2915 (1969).

48) D.M. Young, F. Hostettler, L.C. Shriver, and R.W. McLaughlin, Division of Paint, Plastics, and Printing Ink Chemistry, Amer. Chem. Soc. Meeting, **16**, 108 (1956).

49) F.E. Kohn, J.G. van Ommen, and J. Feijen, Eur. Polym. J., **19**, 1081 (1983).

50) A. Cosani, E. Peggion, E. Scaffone, and A.S. Verdini, Makromol. Chem., **97**, 113 (1966).

51) T.M. Jackanicz, H.A. Nash, D.L. Wise, and J.B. Gregory, Contraception, **8**, 227 (1973).

52) A.K. Schneider (to Ethicon, Inc.), U.S. Pat. 3,797,499 (1974).

53) J. Kleine and H.H.Kleine, Makromol. Chem., **30**, 23 (1959).

54) C.G. PiH, A.R. Jeffcoat, R.A. Zweidinger, and A. Schindler, J. Biomed. Mater. Res., **13**, 497 (1979).

55) B. Eling, S. Gogolewski, and A.J. Pennings, Polymer, **23**, 1587 (1982).

56) G.S. Sanina, M.V. Fomina, A.K. Khomyakov, V.S. Livshits, V.A. Savin, and E.B. Lyudvig, Vysokomol. Soyed, **A17**, 2726 (1975).

57) E.F. Cox, F. Hostettler, and R.R. Kiser, Makromol. Synthesis, N.G.G. Gaylord, Ed., Wiley, New York, 1968.

58) K. Chujo, H. Kobayashi, J. Suzuki, S. Tokahara, and M. Tanabe, Makromol. Chem., **100**, 262 (1967).

59) B. Kalband and A.J. Pennings, Polymer, **21**, 607 (1980).

60) F. Chabot, M. Vert, S. Chapelle, and P. Granger, Polymer, **24**, 53 (1983).

61) R.K. Kulkarni, K.C. Pani, C. Neuman, and F. Leonard, Arch. Surg., **93**, 839 (1966).

62) L. Sedel, F. Chabot, P. Christel, X. Charentenay, J. Leray, and M. Vert, Rev. Chir. Orthop., **64**, 92 (1978).

63) R.K. Kulkarni, E.G. Moore, A.F. Hegyeli, and F.J. Leonard, Biomed. Mat. Res., **5**, 169 (1971).

64) M. Vert, F. Chabot, J. Leray, and P. Christel, Makromol. Chem., **5**, 30 (1981).

65) V.W. Dittrich and R.C. Schulz, Ang. Makromol. Chem., **15**, 109 (1971).

66) A. Schindler and D. Harper, J. Polym. Sci., Polym. Lett. Edn., **14**, 729 (1976).

67) W.H. Carothers, G.L. Dorough, and F.J. von Natta, J. Amer. Chem. Soc., **54**, 761 (1932).

68) G.J. Sutton and B.J. Tighe, J. Polym. Sci., Polym. Chem. Ed., **11**, 1069 (1973).

69) G.J. Sutton, B.J. Tighe, and M. Roberts, J. Polym. Sci., Polym Chem. Ed., **11**, 1079 (1973).

70) A.J. Lovett, W.G. O'Donnell, G.J. Sutton, and B.J. Tighe, J. Polym. Sci., Polym. Chem. Ed., **11**, 2031 (1973).

71) P.R. Cooper, G.J. Sutton, and B.J. Tighe, J. Polym. Sci., Polym. Chem. Ed., **11**, 2045 (1973).

72) I.C. McNeill and H.A. Leiper, Poly. Degrad. and Stabil., **11**, 267 (1985).

73) I.C. McNeill and H.A. Leiper, Poly. Degrad.and Stabil., **11**, 309 (1985).

74) E.E. Sommers and J.I. Crowell, J. Amer. Chem. Soc., **77**, 5443 (1955).

75) S.H. Hyon, K. Jamshidi, and Y. Ikadu, Polymer Preprints, **24(1)**, 6 (1983).

76) I.S. Mega and A. Koroscil, J. Polym. Sci., Part B, **6**, 653 (1968).

77) D.A.S. Ravens and J.M. Ward, Trans. Faraday Soc., **75**, 150 (1961).

78) J.G. Noltes, F. Verbeek, H.G.J. Overmars, and J. Boersma, J. Organometal. Chem., **24**, 257 (1970).

79) V. Stannett and M.S. Szware, J. Polym. Sci., **10**, 587 (1953).

80) R. Subramanian, B.K. Carter, and G.L. Wilkes, submitted for publication.

81) H. Elias, Macromolecules, Vol. 1, Plenum Press, New York, 1977.

82) J.A.P.P. Van Dijk, J.A.M. Smit, F.E. Kohn and J. Feijen, J. Polym. Sci., Polym. Chem. Ed., **21**, 197 (1983).

4.0 THE RELATIONSHIP BETWEEN STRAIN INDUCED CRYSTALLIZATION AND STRAIN HARDENING IN THE BIAXIAL DEFORMATION OF AN IDEAL POLYMER BLEND

4.1.0 INTRODUCTION

In the manufacture of biaxially oriented semicrystalline polymer films, highly anisotropic properties are developed by the crystallization of the materials under the influence of deviatoric stresses. During a biaxial stretch, the deforming stresses can be resolved into two orthogonal principal stresses which can be applied simultaneously or sequentially to a final strain state that produces either a balanced or unbalanced film. Typically, the biaxial strain of a supercooled polymer melt promotes the crystallization of the material. This strain induced crystallization guides the development of the oriented crystalline morphology and this, in turn, has a strong influence upon the final film properties. Among the enhanced film properties realized through the crystallization of polymer films from a strained supercooled melt are higher mechanical properties, increased film clarity, and improved barrier properties.

Reviews of biaxial film orientation have been supplied by a number of authors including Park (1,2), Schuur and Van Der Vegt (3), and Sweeting (4). Although these references describe film manufacturing processes and the properties of the resulting oriented films, little or no discussion is offered as regards to the effects of biaxial stress on crystallization kinetics, biaxially oriented crystalline morphology, and mechanical properties. In fact, with a few exceptions briefly reviewed in the following paragraphs, little information is currently available in the open literature dealing with this very important aspect of biaxial film manufacturing.

Since a large majority of the early work on strain induced crystallization in uniaxial extension was performed on crosslinked systems, it seems a natural extension that Oono, Miyasaka, and Ishikawa (5) reported on the crystallization kinetics of biaxially stretched natural rubber. Lightly crosslinked rubber sheets were stretched at temperatures well above the crystallization range of the material. Stretched sheets of various elongations were clamped to metal frames to lock in the entropically unfavorable orientation and subsequently quenched to crystallize isothermally at a constant extension ratio. Although the equilibrium level of crystallinity reported decreased with extension ratio, the kinetics of crystallization were substantially accelerated as elongations

were increased. Upon reheating, the melting of the restrained rubber sheets was recorded over a broad temperature range with the final melting point also increasing with extension ratio.

Lindenmeyer and Lustig (6), as well as Nagasawa et al. (7), investigated the strain induced crystallization of molten supercooled polyethylene experiencing a biaxial strain in a tubular blown film operation. Crystalline orientation was the primary emphasis of the studies as opposed to crystallization kinetics. Wide angle X-ray scattering techniques were employed to correlate crystalline orientation distributions with the mechanical properties of the semicrystalline biaxial films. Although the morphology was not studied directly, the crystal orientation pattern determined by Lindenmeyer and Lustig (6) was rationalized with the classic row nucleation model often described in direct morphological investigations of uniaxial strain induced crystallization studies.

Garber and Clark (8) clearly demonstrated the row nucleation morphology in unbalanced, but simultaneous biaxial films, blown from poly(oxymethylene). Nucleating crystalline fibers were seen oriented in the preferred stretch directions with traverse lamellar overgrowths also clearly visible in the reported micrographs. The associated anisotropic mechanical properties of the resulting film were well correlated to the observed oriented crystalline morphology.

As distinct from the blown film processes described above, wherein the biaxial orientation has been introduced to a supercooled melt, the bubble process for producing biaxially oriented copolymers of poly(vinylidene chloride) and poly(vinyl chloride) (Saran) is quite different (9,10). Often a tube of Saran melt is directly quenched to temperatures below Tg preventing any crystallization and, thus, forming a completely amorphous glass. The tubular material is then reheated to temperatures just above the glass transition temperature and inflated with positive air pressures. The resulting biaxial stretching sets off an accelerated crystallization at relatively high degrees of supercooling to yield an oriented semicrystalline film.

The process for manufacturing poly(ethylene terephthalate) films is very analogous to that of Saran. As described by Heffelfinger and Knox (11), molten poly(ethylene terephthalate) is extruded and quenched to an amorphous ductile sheet. Often, the sheet is reheated in a continuous process to temperatures just above the glass transition and stretched sequentially, first in the machine direction and then in the traverse direction to yield an oriented crystalline film. Morphological characterization of the biaxial character is inferred from both wide angle X-ray scattering and the mechanical properties of the product film. Jabarin (12) reports quite a comprehensive and systematic study of biaxial orientation of poly(ethylene terephthalate)

films. The temperature, and rate and degree of extension of poly(ethylene terephthalate), as well as molecular weight, was investigated. These variables were shown to influence the final film properties as determined by molecular orientation, crystal morphology, mechanical properties, transport properties, and thermal shrinkage.

Although the various authors listed above describe widely different techniques for introducing biaxial strain induced crystallization into polymeric films, one common theme is quite clear. The first stage of an industrial drawing process aimed at manufacturing a semicrystalline biaxial film is most often performed on a mainly amorphous precursor. This precursor may be either a slightly supercooled melt, as in the case of tubular blown films of polyethylene, or an amorphous film just above the glass transition, as in the case of tentering poly(ethylene terephthalate). Consequently, molecular orientation in the amorphous phase will precede and affect the formation of more or less perfectly oriented crystalline regions. These crystalline regions are produced at temperatures, rates, and morphologies which would otherwise be extremely uncommon if the material was crystallizing quiescently (ie. from an unoriented amorphous phase). It is these highly oriented crystalline regions which have been shown to impart the highly desirable film properties described above.

4.1.1 ORIGINS OF STRAIN HARDENING IN BIAXIAL DEFORMATIONS OF THERMOPLASTIC POLYMERS

Motivated by the importance of the orientation of the amorphous phase to the biaxial strain induced crystallization of semicrystalline polymers, De Vries et al. (13) investigated both the uniaxial and biaxial deformation of amorphous polymer films and sheets under well-defined thermal and mechanical conditions. Some of the principal parameters common to all mechanical stretching operations were discussed. The extent of molecular orientation induced in amorphous polymers strongly depends on the temperature of deformation as well as the extensional strain rate. The most appropriate temperature suited for orienting amorphous materials, such as atactic polystyrene, polyvinylchloride and poly(ethylene terephthalate), was just above the glass transition. In this particular temperature range all amorphous polymers behave as viscoelastic rubbers. The breadth of this temperature range may vary, depending on the nature of the polymer, the molecular weight, and the rate of deformation. The rate of deformation needs to be high enough compared to the reciprocal of the characteristic relaxation time of the polymer (dictated by the temperature and molecular weight) in order to avoid disorientation during stretching. In effect, the amorphous polymer just above the glass transition may be thought of as a polymer network with

molecular entanglements acting as physical crosslinks. De Vries et al. (13) have confirmed the rubberlike behavior of amorphous polymers in this temperature regime by demonstrating that the biaxial strains were almost completely recoverable after stress release.

In contrast to the behavior of ideal crosslinked networks, the relationship between stress and strain for thermoplastic polymers in the rubbery state depends on strain rate, temperature, and molecular weight. Generally, the stress at a specific level of strain increases with increasing strain rate and molecular weight, as well as with decreasing temperature. This behavior has been classically interpreted in terms of two competing molecular level mechanisms. The formation and destruction of molecular entanglements often occurs in conjunction with the stretching and alignment of molecular segments between entanglements. The former process of disentanglement will lead to mechanical energy dissipation as strain is increased. The latter process of molecular orientation will foster the buildup of elastic potential energy (ie. stress) as strain is increased. The rise in stress with a given strain increment is often termed strain hardening. The relative contributions of molecular disentanglement and molecular orientation were used to describe the onset of strain hardening in polyethylene melts in elongational flows, as discussed in Chapter 1. Extending this previous discussion, the energy dissipation

becomes of greater relative importance compared to the storage of elastic energy as temperatures are increased because of the concomitant reduction in the lifetime of a molecular entanglements. Decreasing the strain rate experienced by the material has the same overall effect as increasing temperature since the longer time scale of the experiment allows for greater number of disentanglements. Note, the time scale of disentanglement under deformation is closely associated with the relaxation spectrum of the material. Both increasing temperature and decreasing strain rates will tend to promote a viscous response, while decreasing temperatures and increasing strain rates will promote an elastic response and increased strain hardening. Molecular weight of the material will also have a profound effect on the mechanical response. Generally, increasing molecular weight will tend to augment the number of intermolecular entanglements and, thus, enhance the elastic response of the material (ie. more rubberlike).

As suggested from the above arguments, an increase in the strain hardening characteristics (ie. elastic energy storage) resulting from an increase in strain rate, a decrease in temperature, or an increase in molecular weight may be expected to be associated with a greater extent of molecular orientation. A correlation between biaxial stretching stress and molecular orientation, as measured by birefringence, has been reported in the literature for

atactic polystyrene (14). As will be discussed in subsequent paragraphs (see section 4.1.2), increased molecular orientation causes a decrease in molecular entropy. This reduction in entropy strongly promotes the phenomenon of strain induced crystallization, if, in fact, the initially amorphous polymer is capable of crystallizing. The strain induced nucleation of small highly oriented fiber-like crystallites is thought to involve the collapse of many highly oriented amorphous molecular segments into a fringed micellar type of structure (15). As such, these crystallites act as additional physical crosslinks restricting the mobility of the participating chains. If this crystallization takes place during the time scale of the deformation, the strain hardening and molecular orientation will be enhanced due to the increase in network structure, as, for example, in the biaxial deformation of poly(ethylene terephthalate) (16,17).

Chain extended crystal fibril structures observed in transmission electron microscopy (32,83) are generally made up of many shish crystals aligned end to end such that the lattice orientation of the crystalites does not change over distances as large as 10 nm (32). The morphology of shish crystals grown under flow conditions from a supercooled melt can be characterized by the length and diameter of these high aspect ratio structures. Mechanisms involving defect clustering (85) and multiple nucleation (53) have been used

to describe the limited length of the shish crystals. Typically, these lengths have been reported to be in the range of a few hundred angstroms up to several thousand angstroms (83). Based upon the free energies of crystal nucleus formation, Hoffman (53) has proposed a theory of strain induced shish crystal formation which predicts the smallest stable crystal nucleus diameter as a function of supercooling, nucleus surface free energy, and volume strain energy. This theory predicts that shish diameters vary inversely with supercooling. The supercooling can be increased by dropping the crystallization temperature or by incrementing the flow field. In addition, a higher concentration of a miscible second component in the melt will lower the supercooling at a constant crystallization temperature, asssuming a significant melting point depression due to the presence of the second blend constituent (86).

Within the context of Hoffman's theory, the melting point depression induced through the presence of a miscible blend constituent should decrease the supercooling and, thus, increase the metastable shish crystal diameter. In fact, an opposite trend has been reported in both blends of isotactic polystyrenes with poly(phenylene oxide) (86) and atactic polystyrene (83). Although, in the latter case, the melting point depression may be expected to be negligible due to the fact that the enthaply of mixing is expected to be nil, the decreasing shish crystal diameter with increasing

noncystallizable blend constituent must be explained. Recently, Feit et al. (83) have determined that the lateral diffusion of extended macromolecules into a shish crystal structure is the size controlling mechanism in determining crystallite diameter. In particular, the dependence of isotactic polystyrene shish crystal diameter upon the square root of atactic polystyrene concentration confirms a diffusion controlling mechanism.

An experimental program has been carried out in order to investigate the strain hardening of an initially amorphous crystallizable polymer in biaxial flow. Poly(lactic acid) was the polymer system of choice. The ring opening polymerization of this material was described in detail in chapter 3 and was shown to provide a means of synthesizing polymers of controlled tacticities. Two polymer tacticities were of interest, specifically, the isotactic poly(L-lactic acid) and the racemic poly(lactic acid) were synthesized. The optically active polymer is crystallizable with a Tg of 60 C and an observed melting point of 180 C. This relatively narrow temperature window for crystallization facilitates the ability to quench this material from temperatures above the melting point to room temperature without crystallization. The racemic polymer is the atactic analog of the optically active polymer. The racemic poly(lactic acid) remains amorphous exhibiting a Tg of 53 C. Each of these two polymers was synthesized, in quantity, to two molecular

weights, 40,000 and 120,000, as measured by intrinsic viscosity techniques.

A novel methodology was adopted using this polymer system in order to investigate the effects of strain induced crystallization on the strain hardening phenomenon during biaxial orientation of amorphous poly(L-lactic acid) in the rubbery region just above Tg. By blending racemic poly(lactic acid) with the optically active poly(L-lactic acid), it was intended to determine the contribution of strain induced crystallization to the extent of strain hardening above and beyond the strain hardening anticipated from stretching a purely amorphous poly(lactic acid).

The overall intent was to keep the viscoelastic response of the blends and pure component constituents the same by closely matching both glass transition temperature and molecular weight. In addition, it was assumed that the blends would be miscible due to the fact that the blend components had the identical polymer repeat units with only subtle differences in tacticities. Note, similar attempts at blending vinyl polymer isomers (differing only in tacticity) have shown that such systems are, in fact, miscible and produce glass transitions intermediate to the blend constituents (18-21). Due to the similarity in Tg between the two materials of different tacticities, miscible blends of the two components would not show any significant differences in rubbery behavior when compared at identical

stretching temperatures. By virtue of the fact that blend constituents were the same molecular weight, any differences in intermolecular entanglement densities and associated differences in relaxation spectra were again minimized upon blending. Thus, on comparing the strain hardening characteristics of various blends of racemic poly(lactic acid) with poly(L-lactic acid) of similar molecular weight, any differences in the strain hardening characteristics associated with changing blend composition might be attributable to strain induced crystallization of the poly(L-lactic acid) component.

From a practical point of view, the study of stress-strain relationships under variable conditions of temperature and strain rate is of interest for several reasons. First, as previously discussed, increased strain hardening has been associated with increased molecular orientation, and, thus, with improved film properties. Further, strain hardening is known to improve the uniformity of biaxial deformations and prevent strain instability phenomena (22). The particular problem of strain instability has been addressed in some detail in a study by Hart-Smith and Crisp (23) for the biaxial deformation of rubber sheets and is of great importance for orientation processes of thermoplastic polymers in the rubbery state (24). In order to reduce thickness gradients and to avoid excessive thinning in biaxially extended sheets, conditions must be chosen so that

the slope of the stress-strain curve is as high as possible (25). In the case of completely amorphous polymers, such as racemic poly(lactic acid), this may be best achieved by lowering the temperature of stretch towards the glass transition. Additional strain hardening is often achieved in polymer processing by stretching amorphous crystallizable polymers such as quenched poly(L-lactic acid). Thus, the overall purpose was to investigate the strain hardening phenomenon in crystallizable and non-crystallizable poly(lactic acids) and their blends as a function of temperature, strain rate, and molecular weight.

Typically, the stress and deformation trajectories are difficult to record during a programmed biaxial deformation, primarily because of instrumental deficiencies. Unlike the situation with mechanical characterization of uniaxial deformation, whereby a plethora of commercial instruments are available, the measurement of stress and strain during biaxial deformation is hampered by a marked deficiency in such instrumentation. Through the courtesy of Eastman Kodak in Kingsport, Tenn., an instrument was made available for measuring biaxial stress and strain in a constant crosshead speed deformation. A brief description of the instrument is given in the experimental section, 4.2.0. It was with the aid of this instrument and the technical assistance of the scientists and technicians at Eastman Kodak that this work was made possible.

Before delving into the experimental aspects, it is appropriate that a brief theoretical review of strain induced crystallization be presented with a view toward how the stress-strain history can affect molecular entropy and, in turn, accelerate the oriented crystallization of materials like poly(L-lactic acid). In addition, the influences of polymer blending on the crystallization of a blend constituent will be reviewed in light of the methodology adopted for investigating the strain hardening of poly(lactic acid) blends.

4.1.2 THEORETICAL CONSIDERATIONS OF STRAIN-INDUCED CRYSTALLIZATION

In contrast to studies of strain induced crystallization, the development of molecular level models for quiescent polymer crystallization has been characterized by a very balanced approach between theory and experiment. Initial treatments of the temperature dependence of melt phase crystallization rates have been based on general nucleation theory arguments by Turnbull and Fisher (26). These initial theories have been superseded by more detailed rate theories for chain folding and molecular nucleation (27-31). A relative abundance of kinetic data and cross correlations of this data with morphology and property studies has served as an important basis and guide for the now developing theories of strain induced crystallization.

With flow induced crystallization one needs to consider, in addition to thermodynamic nucleation processes, chain transport, orientation, and fluid flow. In particular, the interactions between crystal size and flow kinematics have been shown to be of extreme importance (32). Since flow kinematics are generally not involved in quiescent crystal growth, and further, since relatively few kinetic data are available on crystallization in the presence of deformation fields, current theoretical analyses of strain induced growth mechanisms have been based upon an ad-hoc extension of

quiescent crystal nucleation theories. The objective of this short review will be to focus attention on some of the fundamentals of quiescent crystallization nucleation theories and to show how these have been adapted to predict the crystallization of polymers undergoing strain. The primary emphasis will be upon the correlation between crystal nucleation rates and the stress-strain relationships associated with the deformation of the polymeric materials. Although, by far and away, the theoretical developments of strain induced crystallization have been developed for the case of uniaxial deformation and shear, it should be mentioned that these fundamental ideas are applicable in principle to the case of biaxial deformation as well.

Most quantitative analyses of strain induced nucleation and growth have been based on the idea that stretching a polymer molecule reduces its conformational entropy and, therefore, leads to an effective increase in the equilibrium melting temperature (33-38). As a consequence of this increased supercooling, nucleation and growth rates are predicted to increase by many orders of magnitude while the crystallite length decreases. A number of studies of strain induced crystallization of crosslinked melts have demonstrated just such effects (39,40) and, in several cases, comparison of the temperature dependence of the crystallization rate with kinetic theory predictions has been quite good. Although the application of this approach to

strain induced crystallization in thermoplastic systems seems intuitively reasonable, there are fundamental differences between crosslinked and thermoplastic systems which generally render the comparison invalid.

Turnbull and Fisher (26), by combining the absolute reaction rate theory developed by Evans (41) with the fundamentals of nucleation developed for the condensation of the vapor phase pioneered by Becker and Doring (42), derived an expression describing the kinetics of nucleation which is even now used to interpret nucleation phenomenon in the condensed state. For the case of a solid nucleating from a liquid phase, Turnbull and Fisher (26) obtained the rate of formation of nuclei, $\dot{N}$, as follows:

$$\dot{N} = N_o \exp\left\{-\left(\Delta F^* + \Delta G^*\right)/KT\right\} \qquad (4.1)$$

where $\dot{N}_o$ is a term dependent on molecular parameters; ΔF^* is the activation energy barrier affecting transport of material across the liquid-crystal interface; ΔG^* is the critical free energy required for the formation of the critical sized nucleus; k is Boltzmann's constant; and T is the absolute temperature. Note, a critical size nucleus is a nucleus of the size beyond which energetics favor further growth. This size corresponds to the point where the energy reduction of bulk transformation surpasses the free energy elevation due to nucleus formation. Thus, $\dot{N}$ actually corresponds to the

rate at which these critically sized nuclei transform into stable nuclei as expressed in Eq. 4.1.

The overall nucleation rate as shown in Eq. 4.1 is controlled by the rate of transport of material to the nucleation site and the rate of formation of the critically sized nucleus. The rates of these two processes have opposite temperature dependencies. At very high degrees of supercooling, the term containing ΔF^*, which describes the energy barrier affecting the transport of material across the liquid/crystal interface, overrides the second exponential causing the nucleation rate to drop. According to Williams, Landel, and Ferry (43), the effective barrier involving segment motion may be expected to be significant and temperature dependent at low temperatures and insignificant and temperature independent at high temperatures. Thus, when supercooling is not too great, the second exponential term is dominant and predicts an exponentially decreasing nucleation rate as the thermodynamic melting point is approached (44). This gives a maximum in the realized rate of nuclei production at an intermediate temperature between the melting point (rate of formation of nuclei large enough to be stable =0) and the glass transition temperature (rate of material transport to the nucleation site=0). These results were first presented by Frenkel (45) and later by Mandelkern et al. (30).

In order to use this classical nucleation theory to make

quantitative predictions, the specific mechanism of nucleation must be specified in order to fix the form of the second exponent in Eq. 4.1. A relatively convenient and general expression for ΔG^* derived by several investigators (26,28,30) takes the following form:

$$\Delta G^* = \frac{K \gamma^2 \gamma_e}{\Delta G_v} \tag{4.2}$$

where K is a constant dependent on the shape of the nucleus; γ and γ_e are surface interfacial free energies per unit area for the side surface and end surface of the embryo respectively; and ΔG_v is the bulk free energy difference between the embryo and the melt per unit volume. Substitution of Eq. 4.2 into Eq. 4.1 results in the popular form for the rate of nucleation of crystals from a quiescent melt:

$$\dot{N} = \dot{N}_0 \exp\left\{-\left(\frac{\Delta F}{KT} + \frac{K \gamma^2 \gamma_e}{KT \Delta G_v^2}\right)\right\} \tag{4.3}$$

Quiescent crystalline growth processes in polymers are usually described in terms of secondary nucleation on the surface of an established growing crystal. The general formulation of isothermal, steady state, linear growth rates is developed from Eq. 4.1 with appropriate free energies (44). For example, a number of different theories have been proposed for coherent nucleation of macromolecules on the

growth face of folded chain lamellae. Some of the most recent work on this problem has centered around the nature of the fold surface at the growing face of the lamellae (46). This is in contrast to the very earliest theories which advocated that the chain folds were all of the same length (47). It has been proven that lamellae actually crystallize with an irregular fold period with the thickness of the growth surface fluctuating around a mean value equal to the nominal lamellar thickness. The base case formulation represents the results of Hoffman and coworkers (46) which considers a rudimentary approach assuming a smooth chain fold surface and adjacent reentry. Under these assumptions the crystalline growth rate, $\dot{G}$, can be expressed as:

$$\dot{G} = \dot{G}_o \exp\left\{ \frac{-\Delta E_a}{KT} - \frac{4 b_o \gamma \gamma_e T_m^o}{\Delta H_f (\Delta T) K T} \right\} \qquad (4.4)$$

where $\dot{G}_o$ is a preexponential term again incorporating molecular parameters; ΔE_a is the energy barrier opposing the movement of a chain segment to the growth interface; b_o is the nucleation layer thickness; ΔT is the level of supercooling defined as the difference between the equilibrium melt temperature, T_m^o, and the crystallization temperature, T, and finally; ΔH_f is the specific enthalpy of fusion. The balance of the variables has been defined previously. Equation 4.4 is applicable for growth rates from melt for both bundle type of nuclei as well as folded nuclei.

Extension of Eq. 4.4 to describe the growth rate kinetics from an oriented melt seems a bit unlikely since the following assumptions would be necessary (48):

(1) The mechanism of secondary nucleation on existing crystal surfaces has to remain essentially unaffected, i.e. the mode of crystal growth has to remain simple chain folding.

(2) The orientation of the molecules in the melt phase would not affect the transport of chain segments to the growth interface.

(3) The bulk free energy change on crystallization would remain unchanged as a function of chain orientation.

Since it is well established that polymer molecules crystallize in a whisker-like morphology when substantial strain is imparted to a supercooled melt (15), the viability of the first assumption is quite out of the question. Although row nucleated structures from oriented polymer melts and shish kebab structures from oriented polymer solutions are known to involve chain folding, the dominant crystallization phenomenon during deformation (at higher strains and strain rates) is considered to be extended chain crystals. In addition, it has been shown that transport of long chain molecules through a melt has been substantially altered by imposing a deformation gradient (49) which violates the second assumption. Although the free energy of crystallization is known to decrease with polymer

deformation, the reduction in entropy, in particular, can be estimated by increasing the value of the equilibrium melting point. Thus, only the third assumption can be accommodated by Eq. 4.4. In general, a simple extension of growth rate theory from the quiescent case to model strain induced growth rates is not possible.

It may serve to note that some limited progress has been made in the development of crystal growth kinetics from strained melts. Several qualitative models exist describing the molecular growth mechanism (50,51), but only marginal success has been obtained in predicting the typically small lateral size of the whisker-like crystals obtained from a highly strained melt (32,52). Recently, Hoffman (53) put forward a model which predicts the diameters as well as the length of the shish crystals on the basis of nucleation theory, but without comment on kinetics. Tiller and Shultz (54) have treated the fibrillar growth of shish crystals as similar to the dendritic growth of low molecular weight materials where heat transport away from the growth surface is the size controlling parameter, but as growth rates were not measured, accurate verification of the theory was not possible. In general, the growth process of shish crystals from the melt or solution has not been accessible to experiment and, thus, computational study has been quite limited.

The acceleration of both primary crystal nucleation

rates and overall crystallization growth rates by the deformation of crystallizable polymer melts will, in turn, influence the strain hardening characteristics of a material. As discussed in the previous section, the number of crystallites formed during strain will have the controlling influence upon the number of additional physical crosslinks. It is these additional crosslink sites that contribute to enhancement of the strain hardening phenomenon. Therefore, the thrust of this study will be to investigate the enhancement of primary crystalline nucleation rates and overall crystallization rates as a function of temperature, strain rate, molecular weight, and blend composition implicitly by measuring the strain hardening phenomenon of poly(lactic acids) in biaxial deformation.

As opposed to the growth rate expression of Eq. 4.4, the form of expression derived for nucleation rate in the quiescent case has generally been assumed applicable for the case of strained melts with appropriate modification of certain parameters (33,55,56). Application of Eq. 4.3 is centered around several assumptions outlined as follows:

(1) The bulk free energy change associated with nucleation from a strained melt or solution, ΔG_v(strained), can be written as the sum of the bulk free energy change between liquid and solid under quiescent conditions, ΔG_v, plus the elastically stored free energy resulting from the deformation of the polymer chains by the flowing polymer

solution or melt, ΔG_{def}.

$$\Delta G_v(\text{strained}) = \Delta G_v + \Delta G_{def} \tag{4.5}$$

(2) The effect of a deformation field on the transport term is small compared to the effects on the bulk free energy so that small changes in ΔF^* will be overwhelmed by the anticipated larger changes in ΔG_v.

(3) The nucleus type, as well as the preexponential factor of Eq. 4.3, is similar for both the quiescent crystallization and the strain induced crystallization.

Pennings (55) has advocated the substitution of Eq. 4.5 into the expression for nucleation rate in Eq. 4.3 to yield the nucleation rate for the strain induced crystallization case:

$$\dot{N}(\text{Strained}) = \dot{N}_o \left\{ \frac{-\Delta F^*}{KT} - \frac{K\gamma^2\gamma_e}{KT(\Delta G_v + \Delta G_{def})^2} \right\} \tag{4.6}$$

A very similar approach has been taken by Kobayashi and Nagasawa (33), and more recently by Yeh and Hong (56), to illustrate the strain enhancement of nucleation rates in polymer melts which does not require knowledge of the mass transport term ΔF^*, or the preexponential constant $\dot{N}_o$. The ratio of strained to quiescent nucleation is formulated as:

$$\frac{\dot{N}(\text{strained})}{\dot{N}(\text{quiescent})} = \exp\left\{\frac{K\gamma^2\gamma_e}{KT}\left(\frac{1}{\Delta G_{def}^2} - \frac{1}{\Delta G_V^2}\right)\right\} \quad (4.7)$$

Although this ratio appears simpler in form than Eq. 4.6, all the same assumptions including similar nucleus type, mass transport term, and preexponential factor are required in order to justify the expression.

In the application of Eqs. 4.6 and 4.7, an estimate of ΔG_{def} is pivotal. Several methodologies have been adopted in estimating this quantity and, as will be demonstrated, most of these methodologies reduce to relating the change in the amorphous chain entropy to the state of stress in the melt.

The best known and most thoroughly examined case of correlating state of deformation with change in free energy is in the study of crosslinked polymer materials. The mechanisms of strain induced crystallization for this important case was first considered by Flory (57) and then later by Krigbaum and Roe (58), Kim and Mandelkern (59), and Yamamoto and White (60). Flory (57) set the stage for all subsequent work by deriving an equation for the equilibrium melting temperature of a permanently crosslinked polymer network subjected to uniaxial deformation. It was assumed that this network was stretched to a fixed elongation prior to crystallization. Additional simplifying assumptions in Flory's analysis are that crystallization occurs under equilibrium conditions, crystallites are perfectly oriented

in the stretch direction, all chains traverse through the crystallite in the same direction as their end to end vectors, and amorphous chain segments between network junctions obey Gaussian statistics. In all the analyses listed above, an increase in supercooling is associated with the elongation of the elastomer and a concomitant increase in nucleation rate is predicted. More quantitatively, the evaluation of ΔG_{def} for these crosslinked polymers can be made assuming that the effect of stress on the enthalpy of fusion is approximately zero (33), hence

$$\Delta G_{def} = -T\Delta S_{def} \tag{4.8}$$

where ΔS_{def} is the reduction of melt entropy due to the orientation and T is the temperature of deformation. The theory of rubber elasticity evaluates ΔS_{def} directly as a function of elongation as:

$$\Delta S_{def} = -\frac{KN}{2}\left(\lambda^2 + \frac{2}{\lambda} - 3\right) \tag{4.9}$$

where N equals the number of network chains per unit volume; λ is the elongation ratio; and k is Boltzmann's constant.

The theory of rubber elasticity gives an upper limit for the effect of deformation on the reduction of amorphous entropy (free energy) for uncrosslinked systems. In polymer melts, and polymer solutions, as well as highly supercooled

amorphous polymers slightly above Tg, the end to end distance of the polymer chains tends to relax back towards the unstretched condition during the time scale of deformation. This relaxation and associated gain in entropy will vary as the mobility of the chains is known to be affected by temperature, molecular weight, and state of dissolution. Thus, the extent of chain extension in the uncrosslinked case is less than the macroscopic draw ratio. Typically, a steady state may be reached in which the degree of chain extension and the orientation can be maintained, provided there is an ongoing deformation with velocity gradients parallel (elongation) or perpendicular (shear) to the flow direction. In such cases, the extent of chain deformation has proven to be difficult to analyze theoretically.

Pennings (55) has used an expression relating ΔG_{def} to the square of the shear rate in dilute polymer solutions to interpret experimental results (61):

$$G_{def} = \frac{1}{2}\left(\tau_{11} - \tau_{22}\right) = J_e \eta^2 \dot{\gamma}^2 \qquad (4.10)$$

where $\tau_{11} - \tau_{22}$ is the first normal stress difference; Je is the equilibrium compliance factor; η is the shear viscosity; and $\dot{\gamma}$ is the shear rate.

Mchugh (62) has pointed out the increased efficiency of polymer chain orientation in elongational flows as compared to the effectiveness of shear flows. As Peterlin (87) has

demonstrated through molecular modeling, this is primarily due to the fact that elogational flows do not involve any rotational components. Thus, applied mechanical energy is converted more effectively to the reduction of molecular entropy in elongational flows. The free energy was related to polymer solution stretch ratio in elongational flow as the area under the stress strain curve:

$$G_{def} = 1/c \int_0^{\lambda} (\tau_{11} - \tau_{22}) \frac{d\lambda}{\lambda} \tag{4.11}$$

where λ is the extension of the melt and c is the polymer concentration.

In the case of polymer melts, Haas and Maxwell (63) assumed that the stored energy in a shear experiment could be written as:

$$\int_0^{\gamma} \tau_{12} \, d\gamma \tag{4.12}$$

where γ is the elastic or recoverable shear strain and τ_{12} is the associated shear stress. Hass and Maxwell (63) combined this result with the work of Krigbaum and Roe (58) to estimate the effective supercooling of the system as an implicit measure of ΔG_{def}.

In summary, the estimate of ΔG_{def} for a crosslinked polymer is a straight forward function of the macroscopic draw ratio. This is due to the one to one correspondence

between the macroscopic draw ratio and true molecular chain deformation. Through the theory of rubber elasticity the change in entropy (and therefore free energy) can be estimated from chain dimensions. In a polymer solution or melt, the molecular chains relax making the estimate of ΔG_{def} from macroscopic deformations impossible. This lack of adequate treatment to predict the G_{def} in polymer melts from externally controlled variables makes the quantitative prediction of primary nucleation rates difficult. The preferred way has been to relate the quantity ΔG_{def} to the state of stress in the melt. A general evaluation of this form has been suggested by Jarecki and Ziabicki (64) as a series expansion of the trace of the stress tensor:

$$\Delta G_{def} = a_{11}\,\mathrm{tr}\,\underline{\underline{\tau}} + a_{21}\,\mathrm{tr}\,\underline{\underline{\tau}}^2 + a_{22}\left(\mathrm{tr}\,\underline{\underline{\tau}}\right)^2 + a_{31}\,\mathrm{tr}\,\underline{\underline{\tau}}^3 + \cdots \qquad (4.13)$$

As a specific example of this idea, Marrucci (61,65) and Jarecki (66) have developed a simple expression relating G_{def} and the extra stress tensor for an arbitrary flow field under isothermal conditions. The result is general, in that, it applies to both network systems as well as to uncrosslinked systems:

$$\Delta G_{def} = \tfrac{1}{2}\,\mathrm{tr}\,\underline{\underline{\tau}} \qquad (4.14)$$

Equations 4.3 and 4.14 offer a theoretical basis for

attempting to correlate measured stresses in biaxial flow to the decrease in free energy of the amorphous chains and, consequently, to the anticipated increase in strain induced crystalline nucleation rates. Although no quantitative analysis will be attempted, the experimental methodology described in the previous section offers a qualitative route to characterizing the effects of strain induced crystallization upon strain hardening phenomenon. As such, the experimental program involves the blending of the optically active and crystallizable poly(L-lactic acid) with the racemic noncrystallizable poly(lactic acid). Thus, a quick review of the fundamentals of polymer blend thermodynamics will be addressed in the next section with a view towards the question of polymer miscibility between the two tactic systems of poly(lactic acid) and the associated effects of polymer blending on polymer crystallization.

4.1.3 SOLUTION AND CRYSTALLIZATION THERMODYNAMICS FOR MISCIBLE POLYMER BLENDS

The state of miscibility in binary mixtures of polymeric materials was first investigated when most of the known miscible polymer blends involved only amorphous constituents. Paul and Newman (67) have reviewed the most rigorous statement of the thermodynamic criteria for miscibility in these systems as:

$$\left[\frac{\partial^2 \Delta G_{mix}}{\partial \phi_1^2}\right]_{T,P} > 0 \qquad (4.15)$$

Simply stated, this relationship dictates that if a polymer mixture is to be considered miscible on a molecular level for the full composition range between the extremes of pure component constituents, then the second partial derivative of the free energy of mixing, ΔG_{mix}, with respect to the volume fraction of a chosen component, i.e. component 1, must be everywhere positive at constant pressure, P, and temperature, T. Paul and Barlow (68) state that this is, in fact, the only thermodynamically valid definition of miscibility. Although many experimental observations can be directly related to the free energy of mixing, direct measurements of this quantity are not possible. Thus, most theoretical considerations of polymer-polymer miscibility have been centered around a necessary, but insufficient requirement for

miscibility stated as follows:

$$\Delta G_{mix} = \Delta H_{mix} - T\Delta S_{mix} \leq 0 \qquad (4.16)$$

where ΔH_{mix} is the enthalpy change on mixing and ΔS_{mix} is the entropy change on mixing.

One of the simplest models describing the thermodynamics of polymer mixtures is the Flory-Huggins theory (69) which was first applied to polymer systems by Scott (70) and recently discussed in a comprehensive review of miscible polymer mixtures by Paul and Barlow (68). In effect, the thermodynamics of mixing was discussed based on the assumption of a regular solution (70) with the excess enthalpy of mixing described by a van Laar expression and the combinatorial entropy estimated from the Flory-Huggins lattice model. Specifically, the excess enthalpy of mixing was expressed as:

$$\Delta H_{mix}^{excess} = BV\phi_1\phi_2 \qquad (4.17)$$

where V is the volume of the mixture; B is the mixing energy density characteristic of polymer-polymer segmental interactions in the blend; and ϕ_1, ϕ_2 represent the volume fractions of each constituent in the blend. From the Flory-Huggins lattice model the combinatorial entropy of mixing was expressed as:

$$\Delta S_{mix}^{ideal} = -\frac{RV}{V_r}\left[\frac{\phi_1 \ln \phi_1}{x_1} + \frac{\phi_2 \ln \phi_2}{x_2}\right] \qquad (4.18)$$

where R is the ideal gas law constant; V_r is the reference volume; and x_1, x_2 are the degree of polymerization of each component.

Theoretically, it is thermodynamics that dictates whether a polymer mixture is in fact miscible. Practically, the experimentalist is faced with the problem of proving the miscibility of a polymer mixture in the face of insufficient thermodynamic information. As is often the case, parameters such as the mixing energy density, B, cannot, in general, be predicted by theory. One of the most useful methods of determining polymer-polymer miscibility is to observe the glass transition behavior of blends using a variety of experimental techniques including differential scanning calorimetry, dynamic mechanical spectra, and dilatometery (71). The glass transition is considered to represent a change in the motional freedom of main chain segments. The temperature at which this transition occurs is affected by the local environment of the chain segments. Kaplan (72) discusses the idea that an intimate mixture of two segment types in a miscible binary polymer blend would experience a single glass transition. This new transition would transpire at a temperature intermediate between the glass transition temperatures of constituent segments in an unmixed state. In

contrast, a mixture which results in two glass transitions is considered to be composed of two amorphous phases of differing segmental environments (differing compositions). Thus, the ability to discern two glass transitions is considered to be indicative of immiscibility, at least at the prevailing overall compositions, temperatures, and pressure.

There are a number of alternate techniques which have been employed to verify the level of miscibility of polymer mixtures. These include small angle neutron scattering (73), nuclear magnetic resonance (74), eximer fluorescence (75), and inverse chromatography (76). It is beyond the scope of this cursory review to detail the results of these techniques. However, it may be worth noting that, in general, the polymer miscibility is related to the exothermic heat of mixing of the polymer pairs.

A rationale for the observation that the overwhelming number of miscible polymer pairs exhibit exothermic heat of mixing (negative value of B) is based on the thermodynamic model described in Eqs. 4.15-4.17. As discussed by Koningsveld et al. (77), the combinatorial entropy of mixing two polymers is substantially less than that associated with mixing two low molecular weight compounds. In the limit of very high molecular weights, the combinatorial entropy of mixing is essentially zero. The enthalpy of mixing on the other hand is primarily dependent upon the energy associated with nearest neighbor contacts made during mixing and, to a

first approximation, is independent of molecular weight (78). Thus, unless the excess enthalpy of mixing can show a negative contribution to the overall free energy of mixing, the polymer mixture is typically immiscible. Specific examples of this are the immiscibility of linear polyethylene with both low density polyethylene (79) and polypropylene (80).

There are a number of apparent exceptions to the rationale that miscibility is restricted to polymer pairs that are structurally different, but which complement each other and promote favorable exothermic interactions. As mentioned previously, isotactic/atactic pairs in the styrene and propylene systems are thought to be miscible, at least at elevated temperatures where the amorphous nature of both constituents is guaranteed (18-21). It may be argued that the heat of mixing need only be slightly negative for polymer miscibility to occur and that considerably less intense interactions between constituents would suffice. It has been shown that changing the stereo configuration of poly(methyl methacrylate) from syndiotactic to isotactic causes a more exothermic enthalpy of mixing in blends with poly(vinylidene fluoride) (81). Thus, the subtle changes anticipated from stereo sequence redistribution have been shown to significantly affect polymer miscibility. The miscibility of the atactic/isotactic pairs may be rationalized by considering that there is a small but finite exothermic

interaction between two differing stereo configurations.

In addition, enthalpic heats of mixing which are only very slightly positive or zero may be offset by the small but finite negative contribution of entropy to the free energy of mixing. As an example, Paul and Barlow (68) consider the mixing of two polymers which only interact via dispersive or van der Waals type bonding between segments. In such a case, the mixing energy density, B, may be replaced by the square of the difference of the solubility parameters of the components, δ_i :

$$\Delta H_{mix}^{excess} = V\left(\delta_1 - \delta_2\right)^2 \phi_1 \phi_2 \qquad (4.19)$$

For the case in which both polymer species participating in the intended blend are monodisperse, are of equal molecular weight, and have specific gravities close to 1.0, the thermodynamic model of Eqs. 4.15, 4.17, and 4.18 predicts an interesting result. For very similar solubility parameters that might be expected from blending two polymers which differ only in tacticity, the model predicts a small endothermic enthalpy of mixing. The negative entropy of mixing can offset this positive result only for limited molecular weights. If the solubility parameters differ by 0.1 $(cal/cm^3)^{1/2}$, then miscibility will be maintained only for molecular weights below 120,000.

The discussion of polymer miscibility for blend systems

in which the components differ only in tacticity is particularly relevant since the work reported here deals with blends of optically active poly(L-lactic acid) and racemic poly(lactic acid). Clearly, the enthalpy of mixing for this case can be expected to be approximately zero so that miscibility may be anticipated for this blend system for at least a limited range of molecular weights.

The blend system involving the two tacticities of poly(lactic acid) is of further interest because the isotactic component is expected to crystallize from the mixture. In principle, the mixed amorphous state may be of a lower overall free energy than a two phase system with crystals of pure poly(L-lactic acid) in equilibrium with a mixed amorphous state naturally depleted in the isotactic component. Paul and Barlow (82) consider a detailed analysis of polymer crystallization from miscible polymer blends and derive a thermodynamic criteria predicting the conditions under which crystallization may be thermodynamically unfavorable. If the inequality:

$$\frac{\Delta H_f}{-\Delta G_{mix}}\left(1-\frac{T}{T_m^o}\right) < 1 \qquad (4.20)$$

is maintained, then crystallization will be thermodynamically denied. Note, ΔH_f represents the enthalpy of fusion, and T_m^o represents the equilibrium melting point of the pure component crystalline polymer poly(L-lactic acid). For the

system under consideration, it is anticipated that G_{mix} is just slightly negative due to the offsetting contribution of the combinatorial entropy suggesting that the ratio $\Delta H_f/(-\Delta G_{mix})$ is considerably larger than 1. Still, the inequality can always be satisfied for a finite level of supercooling. Due to the small absolute value of G_{mix}, any T significantly below Tm will result in crystallization.

Paul, Barlow, and Bernstein (76) describe the appropriate thermodynamics for predicting the melting point depression due to the lower free energy of the mixed amorphous phase. The melting point depression is divided between the energetic contributions stemming from the enthalpic part of the mixing process and the entropic contributions. Due to the fact that the enthalpy of mixing for the blends of racemic and optically active poly(lactic acids) is, to a first approximation, either zero or just slightly positive, the entropic contribution to the melting point depression will be considered as the limiting case.

$$\Delta T_m = -R\frac{V_{2u}}{\Delta H_{2u}}\left(T_{m2}^{\circ}\right)^2\left[\frac{\rho_2 \ln \phi_2}{M_2}+\left(\frac{\rho_2}{M_2}-\frac{\rho_1}{M_1}\right)\phi_1\right] \quad (4.21)$$

As before, the numerical subscripts refer to the blend component where the crystallizable component is referenced as component 2. The as yet undefined variables are listed as follows:

H_{2u} = enthalpy of crystallization per repeat unit

V_{2u} = volume of polymer per repeat unit

ρ_1, ρ_2 = densities of each component

M_1, M_2 = molecular weight of each component

For all calculations, wherein the component molecular weights are greater than 10,000, the melting point depression is less than 1°C. Thus, for all poly(lactic acid) blends considered in this work, the depression of the equilibrium thermodynamic melting point is nil.

It has been established in considering blends of poly(L-lactic acid) with racemic poly(lactic acid), that if the blends are miscible, the optically active component is thermodynamically favored to crystallize from the blend with negligible depression of the melting point. The remainder of the discussion in this section will be focused on some considerations of how the kinetics of crystallization might be affected by blend composition. With the exception of some limited work by Feit et al. (83), there has been very little done in considering the consequences of polymer blending on strain induced crystallization. Thus, the formalism developed for quiescent crystallization will be relied upon to structure the discussion. The general principles as developed can be related qualitatively to strain induced crystallization.

The presence of a miscible polymer diluent can influence the crystalline nucleation rate decried in Eq. 4.1. In the following discussion a binary polymer blend is assumed. Only

one constituent in the blend is crystallizable. Clearly, this serves as a model for the poly(lactic acid) blend systems investigated. Both the activation free energy of the transport process, ΔF^*, and the free energy of formation of a nucleus of critical dimensions, ΔG^*, will, in general, depend on the composition.

The influence of a diluent on the transport term can be predicted using the WLF equation and assuming that the mixture of miscible polymers should present a single glass transition temperature intermediate between those of the pure components. If the Tg of the blend is greater than that of the pure component crystalline polymer, then ΔF^* will also increase resulting in a retardation of the crystallization rates a high supercooling. Conversely, if the glass transition of the blend is below that of the pure component crystalline polymer, then the crystallization rates of the blend will be enhanced at large supercoolings. To a first approximation, these arguments have been avoided in considering blends of optically active and racemic poly(lactic acids) due to the fact that the glass transition temperature of these two blend components are so close. Recall that the Tg of optically active poly(L-lactic acid) is 60 C and the Tg of racemic poly(lactic acid) is 53 C.

The effect of a noncrystallizable polymer diluent will also influence the energy required for the formation of a critically sized nucleation cluster, ΔG^*. In principle, the

diluent will affect both the surface free energies and bulk free energy difference between the crystal nucleus and the melt, see Eq. 4.2. Generally, these influences are measured by a depression in the crystalline melting point. From the previous discussion concerning solution thermodynamics, this effect is anticipated to be minimal for the polymer blend system under study. Boon and Azeue (84) and Mandelkern (44) point out that an additional term must also be considered in order to obtain a rigorous expression for ΔG^*. This additional term stems from an entropic contribution to ΔG^* which represents the probability of selecting the required number of crystalline sequences from a blend of crystallizable and noncrystallizable chain sequences. Overall, the entopic contribution to ΔG^* is positive and should, therefore, lead to diminished nucleation rates. Thus, for the nearly ideal blend system considered in this work, the effects of the noncrystallizable diluent upon nucleation rate equation is restricted to the entropic contributions of selecting a crystallizable sequence length from a melt blend also containing noncrystallizable molecules.

It should be pointed out that spherulitic growth rate data reported in the literature concerning blends of polymer isomerism, such as isotactic polystyrene/atactic polystyrene, show decreasing growth rates with increasing non-crystallizable components ostensibly due to diffusion effects

at the growth front (18,19). Based on the discussion of spherulitic growth mechanisms in chapter 2, the diffusion effects are associated with the long time development of an impurity rich layer at the spherulitic growth front. The primary nucleation mechanism may not occur on a size scale which facilitates the development of this impurity rich layer. It is only the subsequent growth from the nucleus (spherulitic growth, for instance) that would lead to the development of a diffusion mechanism at a crystal growth front. Still, diffusion phenomenon may be a critical issue when considering primary nucleation kinetics from polymer blends undergoing strain induced crystallization. Recent work reported by Feit et al. (83) demonstrates that the lateral size of shish crystal nuclei grown from strained melts of isotactic/atactic polystyrene melts follow with the square root of isotactic polystyrene concentration. This was adequately modeled by considering a diffusional lateral growth of the shish crystals which was independent of the molecular mechanism acting for the longitudinal growth of those crystals (83). These conclusions were made under experimental circumstances not unlike those designed for the poly(lactic acid) blend systems.

In summary, it is anticipated that mixtures of optically active and racemic poly(lactic acids) should be miscible to at least some limiting molecular weight of the constituents. Due to the fact that the glass transition for the poly(lactic

acid) isomer blends investigated varies by just a few centigrade degrees and that the energetics of mixing are such that very little melting point depression is expected, differences in the primary nucleation rate processes of poly(L-lactic acid) crystallization from the blend should be minimized. The largest anticipated effect of blending racemic poly(lactic acid) with optically active poly(lactic acid) will be on the diffusion limiting size of the strain induced shish crystals.

In fact, blends of optically active and racemic poly(lactic acids) were chosen in order to try and minimize the effects of composition on crystallization thermodynamics and kinetics. Section 4.1.1 also points out that these miscible blends should not show any significant differences in rubbery behavior when compared at identical stretching temperatures. Thus, the effects of strain on molecular orientation and the associated entropy reduction of the crystallizable component should remain invariant with blend composition. This will again insure that the driving force for crystallization will remain unchanged by blend composition even when considering strain induced crystallization in biaxial flow. It is under these special experimental circumstances that the influences of strain induced crystallization upon the strain hardening phenomenon in biaxial flow will be discussed. It is the ideal thermodynamics associated with blends of optically active and

racemic poly(lactic acids) that make this a unique study.

4.2.0 EXPERIMENTAL

As pointed out in the introduction, the overall scheme in this study has been to investigate the strain hardening characteristics of optically active poly(L-lactic acid) and its blends with racemic poly(lactic acid) in biaxial flow. The synthesis and the characterization of the poly(lactic acids) was described in chapter 3.0. The ensuing discussion of experimental techniques begins with the preparation of the amorphous poly(lactic acid) films from the feed stock of material generated in the synthesis scheme. This is followed by a cursory description of the apparatus used to biaxially stretch these amorphous films. Differential scanning calorimetry and wide angle X-ray scattering techniques were employed to characterize the nature of strain crystallization induced during the biaxial deformation. Finally, tensile mechanical properties were utilized as a measure of overall orientation in the stretched films.

4.2.1 SAMPLE PREPARATION

Both optically active poly(L-lactic acid) and racemic poly(lactic acid) were synthesized in each of two molecular weights, 40,000 and 120,000. Blends composed of both stereo chemical species were prepared by solution mixing the two tacticities with identical molecular weights. The two polymeric isomers, at the desired weight ratio, were placed in chloroform and allowed to dissolve at room temperature for 1 week to a final solution concentration of between 5 and 10% solids (weight/volume). Gentle agitation was supplied intermittently once or twice a day. The solutions were then precipitated in ice cold hexane at a 10/1 volume ratio of nonsolvent (hexane) to solvent (chloroform). The polymer solution was added slowly to the highly agitated hexane in order to augment a rapid precipitation with minimum phase separation due to crystallization of the poly(L-lactic acid) constituent. The solid was recovered by filtration and vacuum dried at 60 C for two days. Upon removal from the vacuum oven, the "fluff" samples were stored in a vacuum desiccator over phosphorous pentoxide.

The blends targeted for study have been labeled according to composition and molecular weight. Table 4.1 reports the scheme for labeling these mixtures. Note that the compositions have been described in terms of weight percent poly(L-lactic acid). Clearly, the pure component

Table 4.1

Molecular Weight and Composition
of Poly(lactic acid) Blends

Molecular Weight	COMPOSITION (wt. % poly (L-lactic acid)) 100%	95%	90%	75%
40,000	100/40K	95/40K	90/40K	75/40K
120,000	100/120K	95/120K	90/120K	75/120K

species of poly(L-lactic acid) and racemic poly(L-lactic acid) did not undergo the solution preparation described above. As an example of the labeling scheme, 90/40k is a blend consisting of 90 weight percent 40,000 molecular weight poly(L-lactic acid) and 10 weight percent 40,000 molecular weight racemic poly(lactic acid).

The materials recovered from solution were pressed into amorphous films with the use of a heated laboratory hydraulic press. In order to minimize moisture content, the fluff material recovered from solution was dried under vacuum at 60 C for 8 hours just prior to pressing. The platens of the press were controlled to a temperature of 200 C ($\pm$ 0.2 C). Exposure to 200 C was minimized to 100 seconds in order to prevent sample degradation and transesterification in the blends (see discussions in section 3.3.2). A maximum platen force of 10,000 lbs. was applied to a final film area of approximately 10 square inches. Final film thickness was controlled with the aid of a 15 mil brass shim. Immediately upon removing the molten film from the press, the sample was quenched between an auxiliary set of platens cooled with circulating water at 20 C. The film was then peeled from the aluminum foil and cut to square samples which where 2 3/8 inches on a side for subsequent biaxial stretching. Wide angle X-ray diffraction patterns of the quenched films indicated that the materials were indeed amorphous. The films were stored in a vacuum desiccator over phosphorous

pentoxide at room temperature until the time they were to be stretched.

4.2.2 BIAXIAL STRETCHING

The biaxial orientation was performed on a Long Extensional Stretcher (LES) outfitted with capabilities for measuring stress and strain on both axes of stretch. A stress transducer placed in line on each cross head hydraulic pull rod produced a dc voltage signal proportional to force. Similarly, a linear variable differential transducer was used to record each cross head displacement as a dc voltage signal proportional to distance of travel. Access to this specially instrumented LES was supplied through the courtesy of the Eastman Kodak Co. in Kingsport, Tenn. The voltage signals representative of stress and draw ratio were digitalized and recorded on computer disk with a Bascom-Turner programmable chart recorder (model 4120). All data manipulation was performed on computer after uploading the data from the Bascom-Turner.

Simultaneous and balanced biaxial stretching was performed under various conditions of temperature and strain rate for each of the various samples described in section 4.2.1. Unless otherwise indicated, all samples were drawn to a final extension ratio of 4 X 4. The temperatures of stretch were 75 C, 80 C, 85 C, and 90 C. The cross head stretching speeds employed were 1.27 cm./sec., 5.72 cm./sec., and 25.4 cm./sec. For an initial sample gauge dimension of 5.08 cm. X 5.08 cm. between the LES grips, these cross head

velocities correspond to initial strain rates of 0.25 $sec.^{-1}$, 1.12 $sec.^{-1}$, and 5.00 $sec.^{-1}$, respectively.

The thermal history of every sample was made as reproducible as possible. Sample temperatures were carefully controlled in the oven of the LES to within 0.5 C during the biaxial orientation. Upon initially loading, the film sample was allowed to equilibrate in the oven for a time period of no shorter than 100 seconds and no longer than 120 seconds before stretching the material. After the stretch was complete, the oven was opened and the sample was quenched with a forced cool air source while the sample was held at the final biaxial strain in the crosshead clips. The sample was then released from the clips with little or no visible shrinkage and stored in a vacuum desiccator until further testing.

Superimposed upon the force-displacement measurement for each sample was a significant amount of frictional force stemming from the movement of the instrument cross head. In order to compensate for this frictional force, a force-displacement measurement was made from the LES during a dry run just before loading each sample. The dry run force-displacement curve was later subtracted from the force-displacement curve acquired during a sample stretch. It is the difference between these two data sets that yields the stress-draw ratio curves which will be used to characterize the relative strain-hardening characteristics of the various

samples. An example of such a pair of data sets is given in Figs. 4.1 and 4.2. Figure 4.1 represents the force and displacement curves for both the dry run and the sample 100/40k stretched at 80 C at a cross head rate of 1.27 cm./sec. Figure 4.2 shows the results of subtracting the curves and converting the corrected force displacement data to stress and draw ratio. Note, the draw ratio is calculated as:

$$\lambda = \frac{l + l_o}{l_o} \tag{4.22}$$

where λ represents the biaxial draw ratio; l is the measured cross head displacement; and l_o is the initial film width. The true sample stress an be calculated simply as:

$$\sigma_b = \left(\frac{F - f}{l_o t_o}\right)\lambda \tag{4.23}$$

where σ_b represents the true biaxial stress; F is the measured sample run force; f is the friction force from the dry run; and t_o is the initial sample thickness. It is assumed implicitly in Eq. 4.23 that the material remains at constant density and deforms homogeneously. The stress-draw ratio curves so calculated will serve as the basis of the strain hardening characterization.

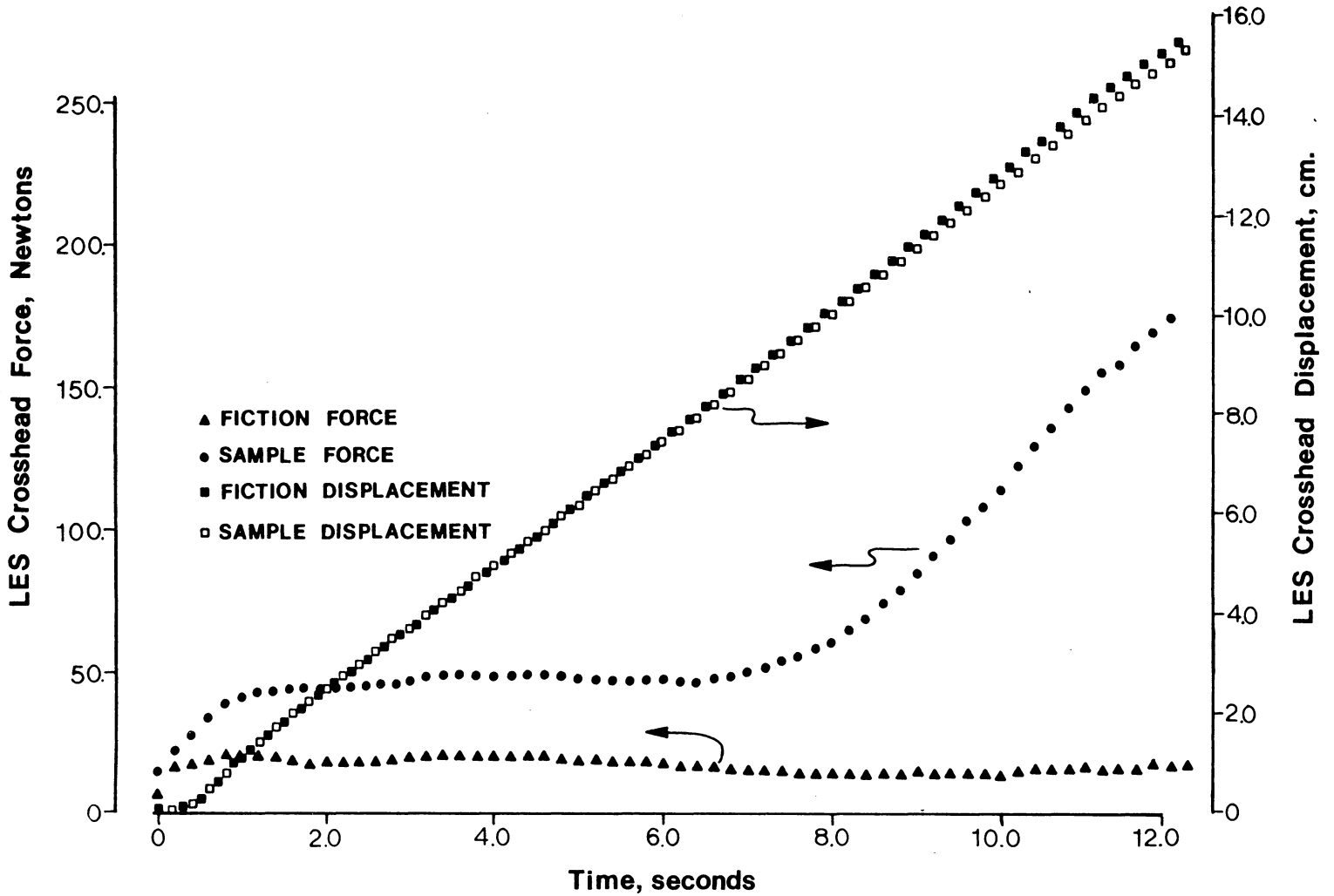

Figure 4.1. Composite force and displacement data demonstrating typical instrumental friction and sample runs.

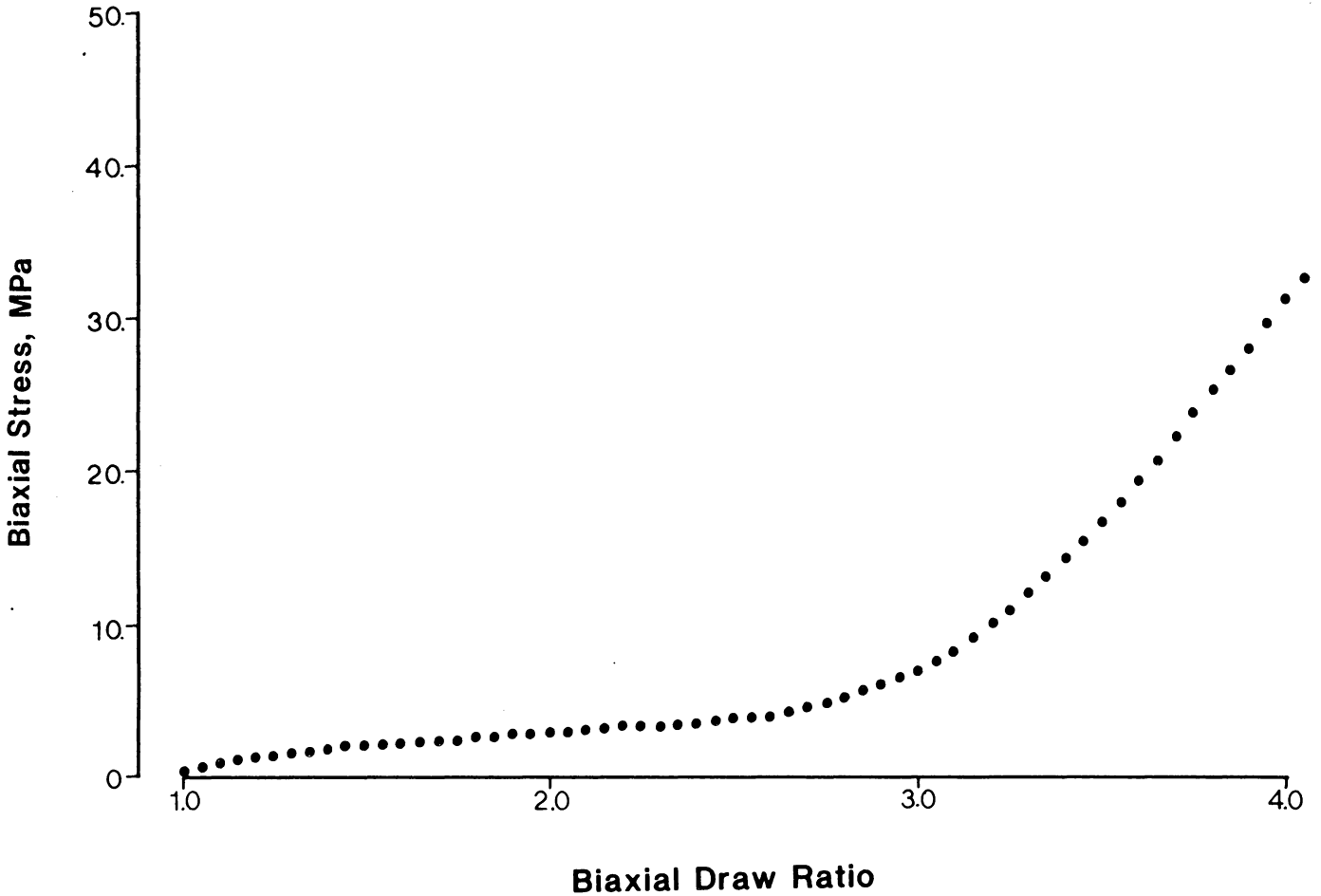

Figure 4.2. Biaxial stress-draw ratio results based on Fig. 4.1 data (corrected for instrumental friction).

4.2.3 ANALYTICAL TECHNIQUES

The following techniques were used to characterize the biaxial films. Differential scanning calorimetry (DSC) was used in order to try and determine the amount of crystallinity induced through the biaxial strain. In addition, DSC was used to characterize the glass transition of the unstretched blends in order to determine the degree of miscibility between the poly(lactic acid) isomers. Wide angle X-ray scattering (WAXS) patterns corroborated the crystallinity determination from DSC and also qualitatively characterized the level of crystal orientation in the biaxial films. Finally, mechanical properties of the biaxial films were measured to characterize the relative overall orientation of the polymer molecules.

4.2.3.1 DIFFERENTIAL SCANNING CALORIMETRY (DSC)

DSC scans on selected samples were acquired through the use of a Perkin-Elmer DSC-4. Sample weights were on the order of 10 to 20 milligrams and a scanning rate of 10 C/min. was used exclusively. Baseline corrections were done digitally using the standard software package supplied by Perkin-Elmer. Calibration of the instrument was checked and corrected on a daily routine. Both temperature shifts and

peak areas were standardized using an indium standard. Endotherm and exotherm heats used to estimate net crystallinity were calculated through the use of curve integration software routines supplied through Perkin-Elmer.

4.2.3.2 WIDE ANGLE X-RAY SCATTERING (WAXS)

WAXS patterns were obtained at room temperature using a Phillips diffractometer with Ni filtered CuK radiation at 40 KV and 20 MA. An evacuated Warhus camera with a pinhole collimator was used to expose a photographic negative. The final pinhole diameter was always 0.51 mm. Exposure times were 5 hours for all the samples. Two sample orientations were used to generate diffraction patterns. First, the beam was oriented normal to the film surface. By consistently stacking films in this first orientation to a final thickness of approximately 0.40 to 0.45 mm., a constant scattering volume was maintained. Scattering patterns from different samples are comparable since all exposures in this orientation were taken at a constant sample to film distance of 109 mm. Due to the balanced biaxial stretch, this first orientation gave rise to WAXS patterns similar to those obtained from isotropic materials and, thus, allowed comparison of ring intensity between samples without the confusion of orientation effects. Secondly, film samples

were cut into thin strips and stacked edge on to the beam with a preferred stretch direction vertical to the reported diffraction patterns. In this case, the X-ray sample thickness (width of strips) was maintained at 1.2 to 1.3 mm and stacked to cover the full pinhole diameter. Sample to film distances were again held constant to 153 mm. so that comparisons between samples would be facilitated. This second orientation of the sample with respect to the X-ray beam leads to WAXS patterns which highlight orientation effects, i.e. diffraction arcs are evident instead of rings.

4.2.3.3 MECHANICAL PROPERTIES

The tensile modulus was determined for selected film samples with an Instron tensile testing apparatus (model 1122) at room temperature. "Dog bone" type samples which were cut from the biaxial films had a gauge length of 10 mm. and a width of 2.5 mm. A crosshead speed of 1.0 mm/min. was employed to yield a 0.10 $min.^{-1}$ initial strain rate for the tensile test. Young's modulus was measured by estimating the slope of the linear, low deformation region of the stress-strain curve. The reported moduli represents an average of at least five measurements taken on each of the selected samples. In order to avoid variations in modulus due to the physical aging of the predominantly amorphous biaxial films,

all tensile tests were performed 72 hours ($\pm$ 2 hours) after the quench from the LES oven. In this way the time period of sub Tg annealing was maintained the same for each sample and changes in modulus could be solely attributed to orientation effects.

4.3.0 RESULTS AND DISCUSSION

As pointed out in the introduction, the most efficient temperature for biaxially orienting an amorphous polymeric material is just above the glass transition. Within this rubbery plateau regime, the most important variables affecting the strain hardening phenomenon are strain rate, temperature, and molecular weight. In addition, strain induced crystallization is expected to enhance strain hardening characteristics. Each of these four topics will be discussed under separate headings as to their respective influences on the strain-hardening behavior and molecular orientation in blends of optically active poly(L-lactic acid) and racemic poly(lactic acid) stretched biaxially at temperatures just above 60 C (Tg). The results of the strain hardening in biaxial flow are discussed first as a function of blend composition to show the dramatic effect of strain induced crystallization. Temperature and strain rate influences are then summarized principally for blends in the 40,000 molecular weight blend series. Extension of the experimental work to higher molecular weights was somewhat limited due to the break down of polymer miscibility. However, some limited discussion of higher molecular weight immiscible blends will serve as an instructive comparison. The discussion begins with a characterization of the state of miscibility in the poly(lactic acid) blends.

4.3.1 CHARACTERIZATION OF POLYMER MISCIBILITY IN BLENDS OF POLY(LACTIC ACID) ISOMERS.

As is most often the case, the characterization of polymer blend miscibility is not amenable to direct thermodynamic analysis and the verification of miscibility between the poly(lactic acid) isomers was determined through the glass transition behavior. Amorphous films of both the pure components and the blends were prepared as indicated in the experimental section. The glass transitions of these films were determined via DSC heating thermograms. In order to avoid complications associated with physical aging, the samples were flash heated from 20 C to 90 C at 100 C/min., held at 90 C for 10 seconds, and then quick cooled to 20 C at 100 C/min. in the DSC sample chamber just prior to the final heating scan at 10 C/min.

Figure 4.3 reports the glass transition behavior of blends of poly(L-lactic acid) and racemic poly(lactic acid) at 40,000 molecular weight. Although the pure component Tgs are very close, there is a systematic increase of a single transition with increasing content of poly(L-lactic acid) for 20% increments in composition. The optically active polymer is obviously the higher Tg constituent.

Although a comparable blend series at 120,000 molecular weight was not available, blends at this higher molecular weight employed in biaxial stretching experiments

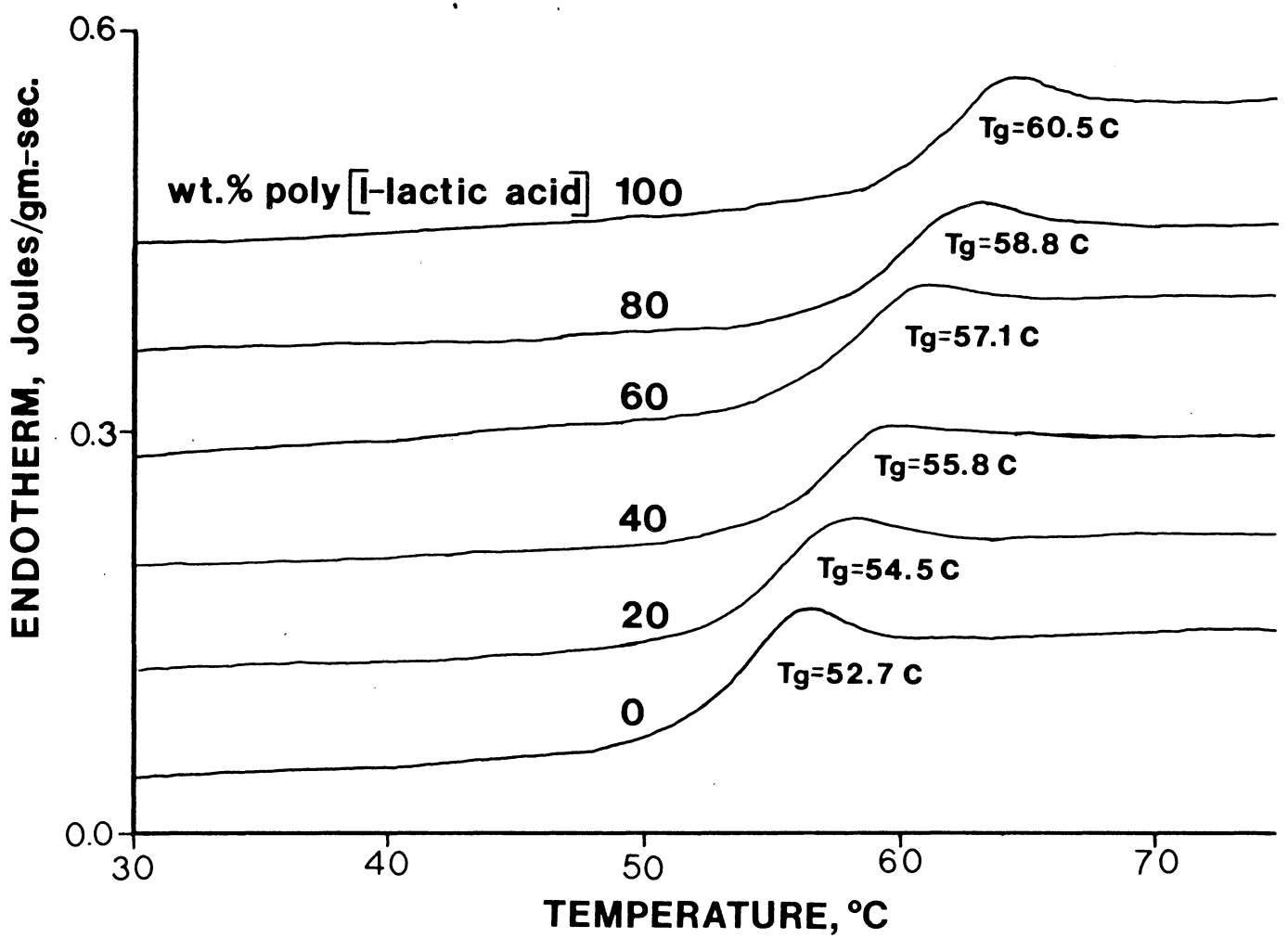

Figure 4.3. DSC thermograms of the glass transition behavior of poly(lactic acid) binary isomer blends.

systematically showed two Tgs. This point will be demonstrated and further emphasized in the dicussion of the DSC thermograms of the 120,000 molecular weight biaxial films. Clearly, a change in molecular weight has significantly changed the thermodynamics of mixing between the two isomers of poly(lactic acid).

The discussion of solution thermodynamics in section 4.1.3 suggests that the enthalpy of mixing for this system is just slightly positive. At lower molecular weights (40,000), the small entropy of mixing apparently adequately compensates for the positive contribution of the excess enthalpy of mixing to give an overall negative free energy of mixing. Recall that an overall negative free energy of mixing is necessary (not sufficient) for polymer/polymer miscibility, see Eqs. 4.16 and 4.17. As the molecular weight is increased, the combinatorial entropy decreases in direct proportion to molecular weight until finally the free energy of mixing becomes positive. Thus, at a molecular weight of 120,000, miscibility is thermodynamically prohibited.

The possibility of kinetic arguments contributing to the apparent phase behavior was briefly investigated. It was considered that during the precipitation from hexane the poly(L-lactic acid) blend constituent crystallized. Thus, phase separation, at least on a scale commensurate with lamellar (crystallite) structure, was unavoidable. The reestablishment of phase homogeneity as the films are in the

melt state during pressing is contingent upon intermolecular diffusion. It has been well established that polymer diffusion is a strong function of molecular weight. For example, deGennes (88) predicts that diffusivity varies inversely with the square of molecular weight. Thus, the possibility that the 40,000 molecular weight blends were reestablishing a homogeneous mixture faster than the 120,000 molecular weight species was investigated. A 50%/50% blend of 120,000 molecular weight poly(lactic acid) isomers was annealed in the melt for 10 minutes and then quenched to 20 C before the Tg thermogram was run. The increased opportunity for intermolecular diffusion did not diminish the separation of constituent Tgs initially observed. This would indicate that it was the solution thermodynamics and not the kinetics of diffusion which was responsible for the immiscibility at a molecular weights of 120,000.

Although the results of immiscibility at the higher molecular weights are disappointing in light of the intent of this study to investigate miscible blends, the result would tend to suggest that the excess enthalpy of mixing for this particular blend system is indeed just slightly positive. As long as relatively low molecular weights are considered so that there is a dominant effect of combinatorial entropy on the overall free energy of mixing, a miscible polymer blend is expected. For example, it has been demonstrated that the 40,000 molecular weight blend series is miscible at all

compositions as detected by DSC Tg analysis. In addition, these lower molecular weight blends are expected to be miscible without the melting point depression attributed to a negative enthalpy of mixing which is typical of most known miscible polymer pairs.

As previously discussed in detail, the crystallization rates are governed by the degree of undercooling (thermodynamic driving force) and the resistance to segmental motions (as characterized by the glass transition temperature). Thus, to a first approximation, polymer crystallization rates can be characterized by the separation of the melting point, Tm, and the glass transition temperature, Tg. Generally, blending two miscible polymers has a strong effect on this crystallization window (Tm-Tg) (82). The poly(lactic acid) isomer pair offers a very unique situation in which a crystallizable polymer is miscible with an amorphous polymer and the crystallization window is very nearly unaltered in the blend at all compositions.

4.3.2 THE EFFECT OF STRAIN INDUCED CRYSTALLIZATION ON THE STRAIN HARDENING OF MISCIBLE POLY(LACTIC ACID) ISOMER BLENDS IN BIAXIAL DEFORMATION

Figure 4.4 depicts the stress-draw ratio characteristics of the biaxial stretch of 40,000 molecular weight blends of the poly(lactic acid) isomers at four compositions, 100/40k, 95/40k, 90/40k, and 75/40k. The applied cross head speed was 1.27 cm./sec., and the temperature of deformation was 80 C. Clearly, as the amount of crystallizable material is increased in the blends, the amount of strain hardening increases concomitantly. Since the molecular weights of the constituents are nearly identical and the glass transition of the unoriented amorphous material changes by less than 2 C across the range of compositions studied (see Fig. 4.3), the viscoelastic properties of the blends (initially amorphous) should be very nearly the same. It should be mentioned that the conformational chain statistics of poly(lactic acids), as characterized by the measurement of unperturbed chain dimensions, indicate differences between the optically active polymer and the racemic polymer (97-99). These differences in polymer chain mean-square end-to-end distance would suggest at least small differences in solid state viscoelastic behavior. However, the differences associated with chain statistics would certainly be small when compared with molecular weight and glass transition effects. Thus,

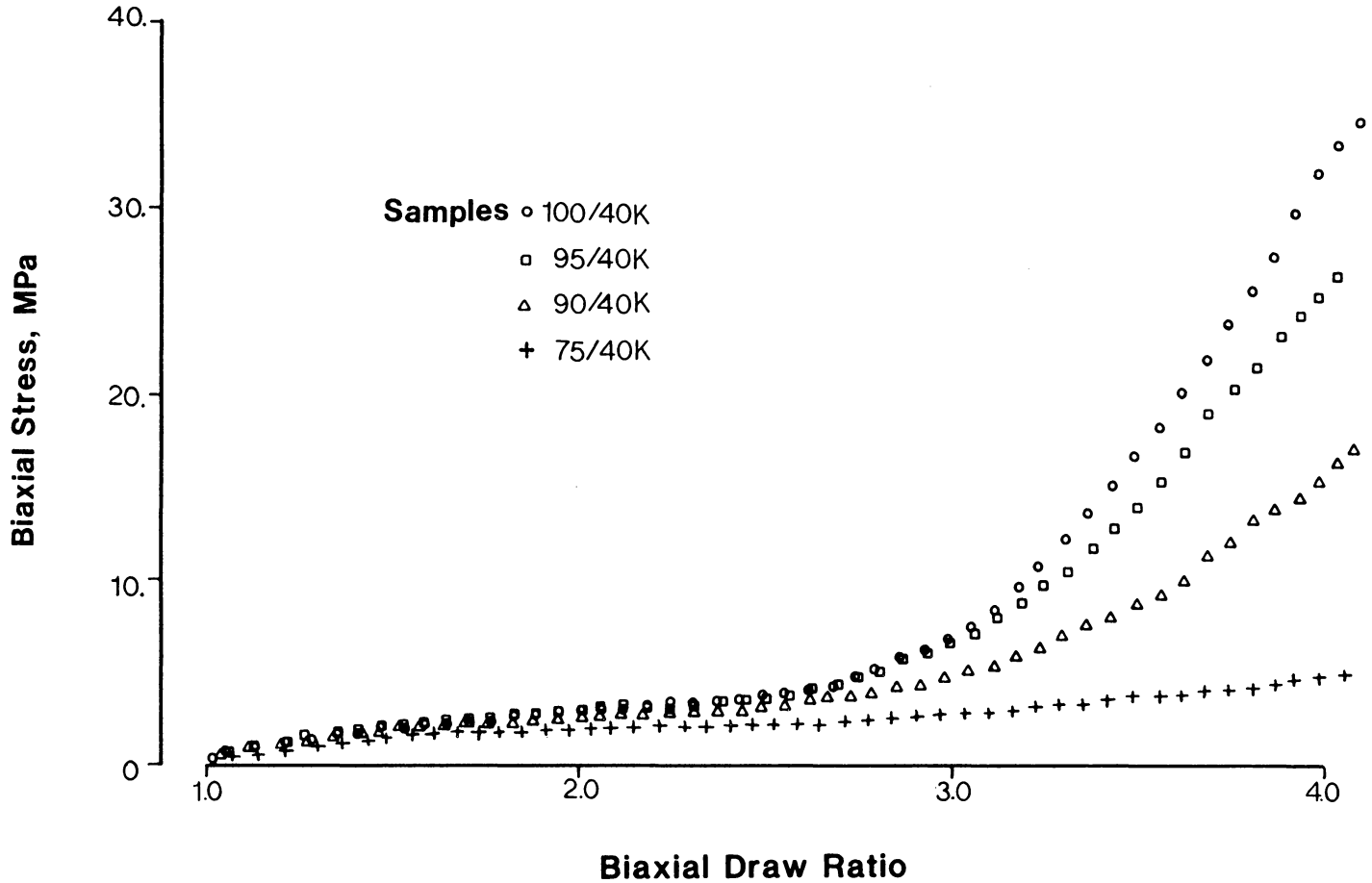

Figure 4.4. Biaxial stress vs. biaxial draw ratio for 40,000 molecular weight poly(lactic acid) blends.
Temperature: 80 C
Crosshead Speed: 1.27 cm./sec.
Final Biaxial Draw Ratio: 4 x 4

the increase in strain hardening must be due to strain induced crystallization at the higher concentrations of poly(L-lactic acid). Strain induced nucleation will increase the number of physical crosslinks above the number associated with molecular entanglements. This will, in turn, improve the effectiveness of the biaxial draw in inducing amorphous orientation. The theory of rubber elasticity, briefly discussed in section 4.1.2, predicts that the improved amorphous orientation will decrease the entropy of the network chain and, thus, increase the force required for further deformation. Strain hardening is, therefore, a consequence of higher amorphous orientation brought about by the enhancement of the network crosslinks by strain induced nucleation. This is the rationale used to explain the extremely steep rise in stress at the highest concentrations of poly(L-lactic acid). In fact, the stress strain behavior is very similar to previous reports of biaxial deformation of network polymers above Tg (5,89).

In order to determine the amount of crystallinity in each of the four samples of Fig. 4.4, a series of DSC scans was taken at a 10 C/min. heating program from 20 C to 200 C. However, before these results can be described in detail, it will be convenient to describe some general attributes of DSC scans from this type of sample.

The DSC scan for sample 100/40k biaxially drawn at conditions in Fig. 4.4 is singled out for discussion and is

shown in detail in Fig 4.5. There are several general characteristics to this DSC trace that are representative of many of the scans reported throughout this work. First, the glass transition temperature is elevated due to orientation of the amorphous phase and the presence of some crystallinity. Immediately after the Tg, a sharp endotherm is seen followed directly by a crystallization exotherm. The low temperature endotherm is believed to be due to the gain of entropy associated with the shrinkage of the sample at temperatures above the Tg where molecular mobility is enhanced. After shrinkage the amorphous chains assume a higher entropy conformation approaching that of a random coil. There is a significant overlap between this entropy peak and the ensuing crystallization exotherm. At higher temperatures, approaching 180 C, the large endothermic heat of fusion is representative of the sum of the original crystallinity in the sample and the crystallinity induced on heating in the DSC scan. The observed melting point is consistent with previous DSC results reported for this polymer (90). Note that an elevation of the melting point, often seen from oriented crystalline samples, is not realized in these DSC traces due to the fact that the amorphous orientation is allowed to relax during the heating scan.

The original sample crystallinity was estimated in this type of DSC scan by drawing the baseline indicated in Fig. 4.5, and calculating the net endotherm of fusion as area A

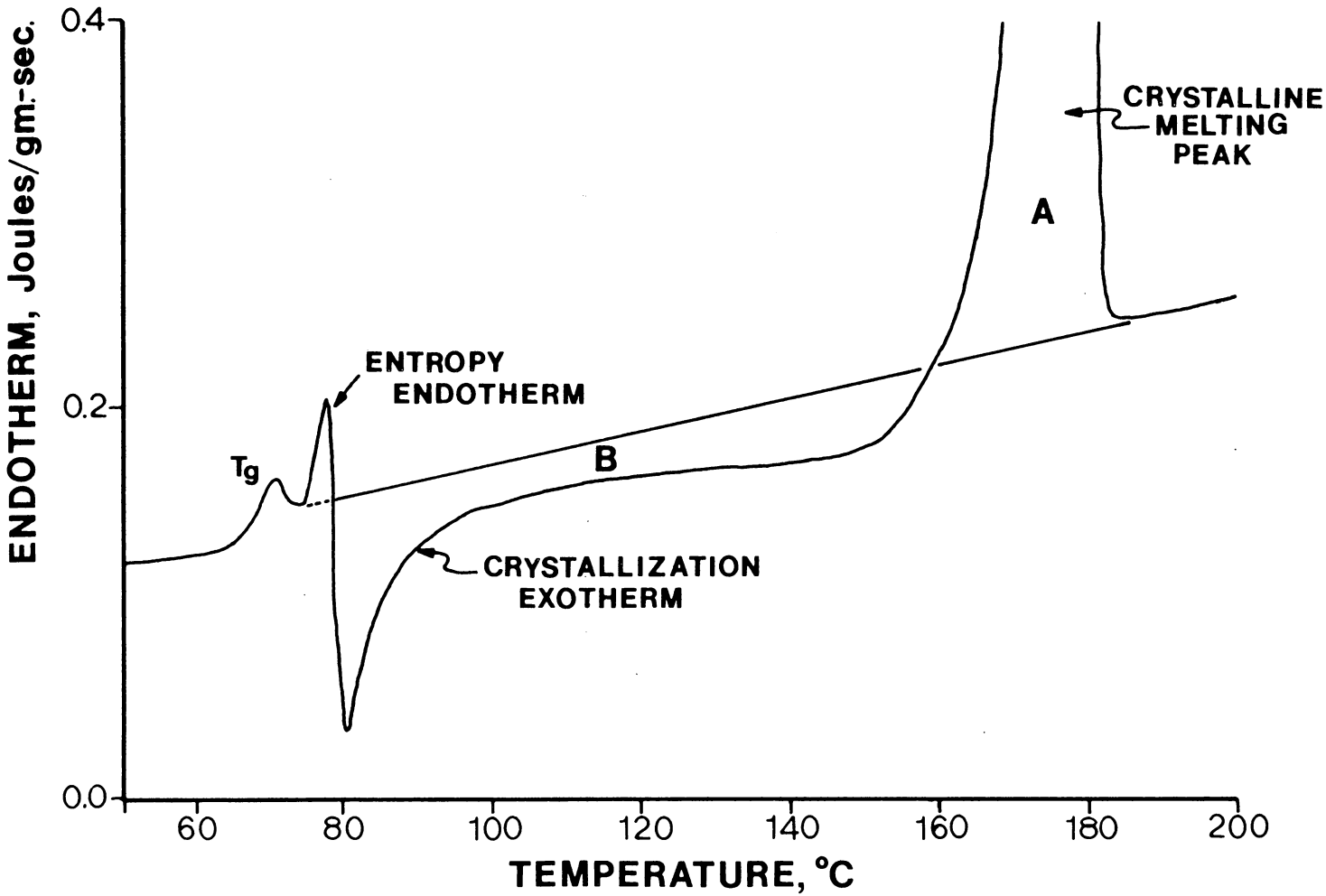

Figure 4.5. Typical DSC thermogram of poly(lactic acid) isomer blend biaxial film showing baseline construction for crystallinity calculation.

less area B. The enthalpy of fusion of poly(L-lactic acid), ΔH_f, has been previously estimated to be 20.5 cal./gm. (90). Thus, the crystallinity in the biaxial films may be expressed on a percent basis through the following simple formula:

$$\%\,\text{Crystallinity} = \frac{A-B}{\Delta H_f} \times 100\% \qquad (4.24)$$

The baseline was constructed by connecting the flat response after the melting endotherm to the minimum in the thermogram between the glass transition and the entropy peak. The heat associated with the area under the entropy peak is not included in the calculation of sample crystallinity. The accuracy of this calculation suffers from the aforementioned overlap between the entropy endotherm and the crystallization exotherm. Clearly, the estimate of the crystallinity generated during the DSC heating scan (area B) may be a bit low due to the strong effect of the entropy peak. Thus, it is anticipated that the crystallinities calculated by Eq. 4.24 will error toward higher values.

Returning now to the comparative discussion of the DSC traces of the samples stretched under the stress-draw ratio histories described in Fig. 4.4, a number of trends are worth mentioning. Figure 4.6 shows a composite of the four DSC traces. In general, there is a larger shift in the glass transition as a function of composition in the stretched materials than was demonstrated in the amorphous unstretched

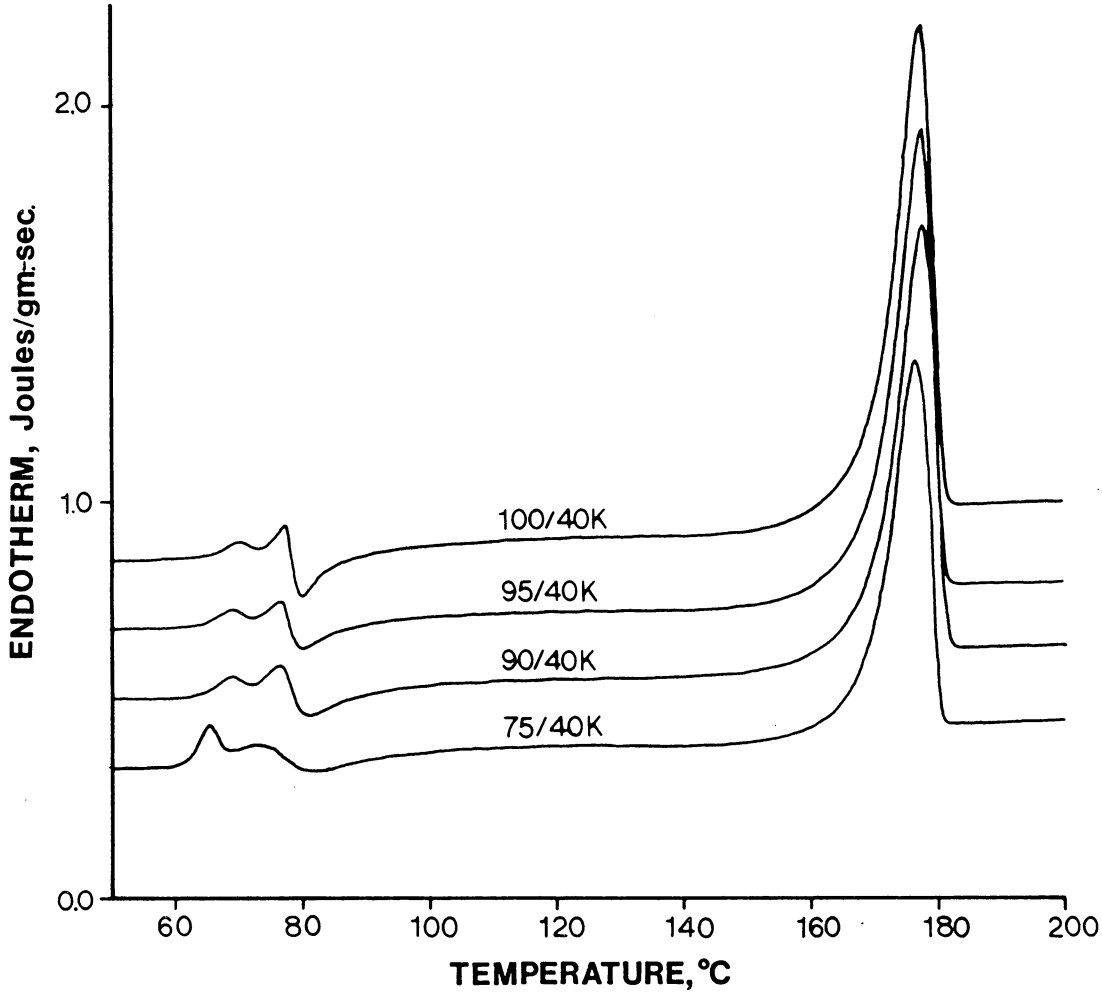

Figure 4.6. DSC thermograms of poly(lactic acid) 40,000 molecular weight biaxially stretched at 80 C and 1.27 cm./sec. to a final biaxial draw ratio of 4 x 4.

DSC traces reported in section 4.3.1. The larger increase in Tg with increasing poly(L-lactic acid) content is attributed to the higher orientation and crystallinity associated with the higher degrees of strain hardening. As testimony to the increased amorphous orientation expected at higher levels of strain hardening, the DSC entropy peak becomes more pronounced as the strain hardening depicted in Fig. 4.4 increases. As expected, there are no temperature shifts in the melting point with blend composition. It may serve to reiterate that since the excess enthalpy of mixing is expected to be very small and positive that the melting points are not expected to be depressed.

Figure 4.7 is a plot of the percent crystallinity calculated by Eq. 4.24 for the DSC traces in Fig. 4.6 as a function of poly(L-lactic acid) content. As expected, the overall crystallinity is decreased in the biaxial films as the content of poly(L-lactic acid) is decreased. Also shown in Fig. 4.7 are the crystallinities normalized for poly(L-lactic acid) content. Interestingly, the normalized crystallinities remain the same for each of the four films. This would suggest that the presence of the noncrystallizable racemic material did not influence the ability of the poly(L-lactic acid) to crystallize under strain. Note that the insensitivity of the normalized crystallinity to racemic poly(lactic acid) blend content does not necessarily contradict the results of Feit et al. (83). Recall this

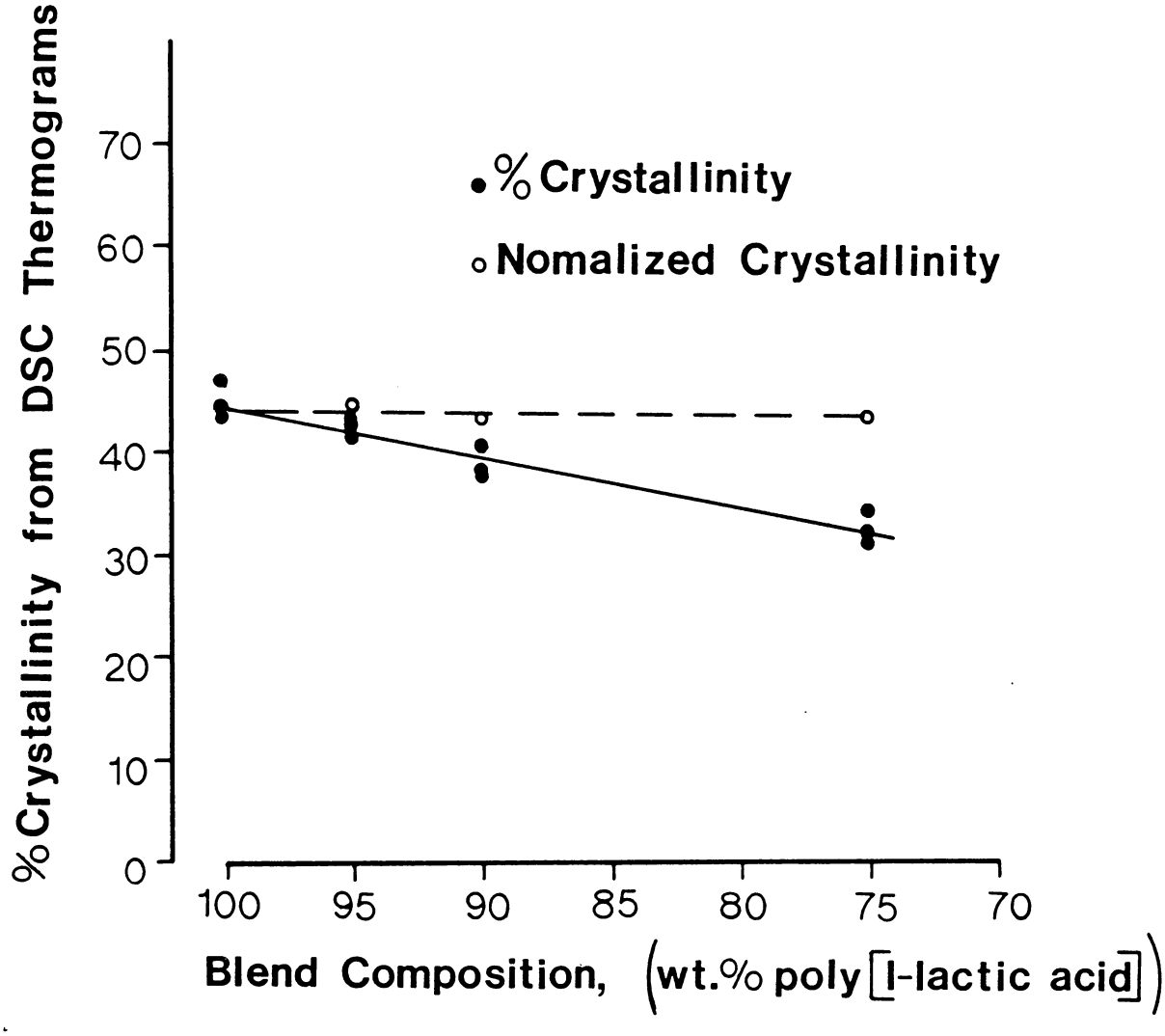

Figure 4.7. % crystallinity vs. blend composition for 40,000 molecular weight biaxial films stretched at 80 C and 1.27 cm./sec. to a final biaxial draw ratio of 4 x 4.

previous research demonstrated a decreasing shish crystal diameter with increasing dilution of the crystallizable component in strained polymer blends. A decreasing shish crystal diameter in the poly(lactic acid) isomer blends can be rationalized if the number of crystals increases to ensure a constant normalized crystallinity.

Figures 4.8 and 4.9 present the WAXS patterns developed for the X-ray beam oriented normal to the biaxial film surface and parallel to the biaxial film surface, respectively. Before examining these patterns in detail, a brief discussion of the unit cell characteristics of poly(L-lactic acid) will be presented.

Analysis of the diffraction patterns is hampered by the fact that there is some discrepancy in the literature as to the unit cell for poly(L-lactic acid). In fact, no definitive labeling of diffraction rings is available. De Santis and Kovacs (91) proposed a pseudo-orthorhombic unit cell from a layer line analysis of fiber diffraction patterns. More recently, Kalb and Pennings (92) investigated solution grown single crystals of the polymer by electron diffraction techniques and concluded a hexagonal unit cell. The latter authors rationalized these discrepancies in diffraction results by assuming that the fiber patterns of de Santis and Kovacs (91) suffered from lattice distortions due to cumulative strain in the crystal phase.

An exacting analysis of the unit cell crystallization

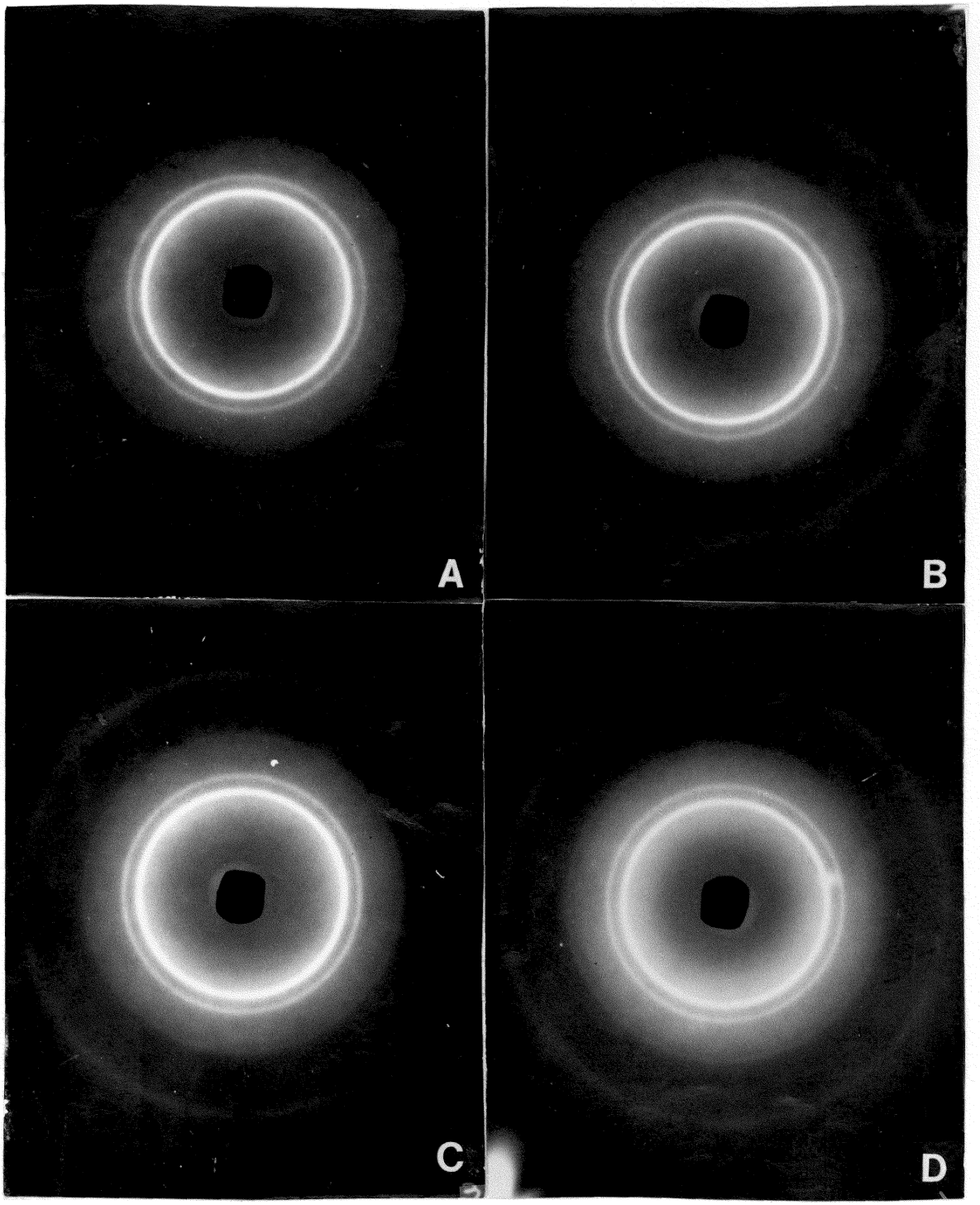

Figure 4.8. WAXS patterns for 40,000 molecular weight biaxial films stretched at 80 C and 1.27 cm./sec. to a final biaxial draw ratio of 4 x 4, X-ray beam oriented normal to film surface.
A) 100/40k B) 95/40k C) 90/40k D) 75/40k

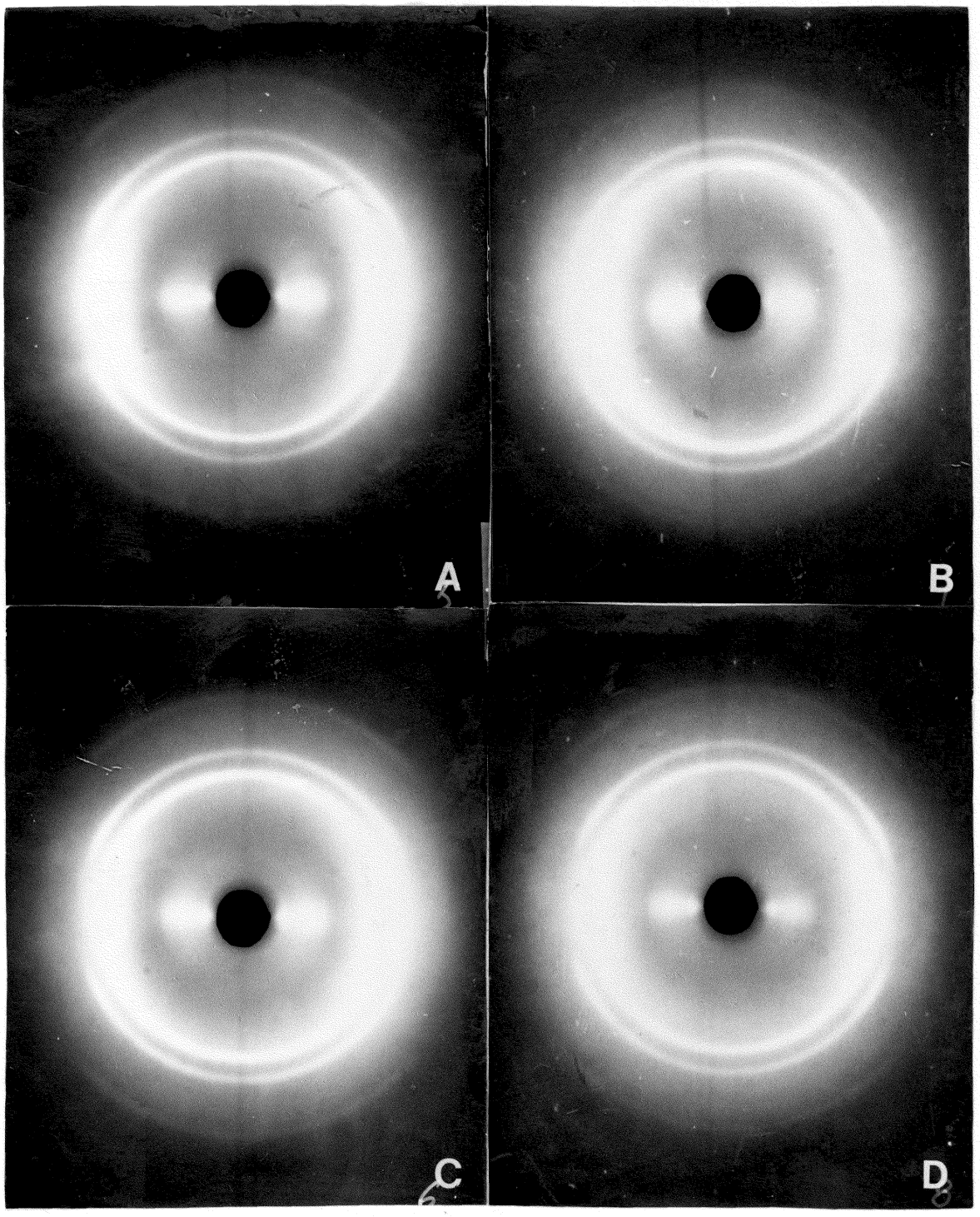

Figure 4.9. WAXS patterns for 40,000 molecular weight biaxial films stretched at 80 C and 1.27 cm./sec. to a final biaxial draw ratio of 4 x 4, X-ray beam oriented parallel to film surface.
A) 100/40k B) 95/40k C) 90/40k D) 75/40k

habit of poly(L-lactic acid) was beyond the scope of the present work. However, by calibrating diffraction patterns obtained from the Warhus camera with a quartz standard, the diffraction spacings for some of the strongest reflections from crystalline poly(L-lactic acid) could be calculated. A diffraction pattern from an unoriented sample of 100/40k which was crystallized at 130 C for 3 hours was used to calculate these diffraction spacings, see Fig. 4.10. Subsequently, Miller indices were assigned to the strongest reflections. The two strongest intensity rings in Fig. 4.10 are consistent with the pseudo-orthogonal unit cell proposed by de Santis and Kovacs (91). The diffraction peak marked A in Fig. 4.10 is considered to arise from the (110) and (200) crystallographic planes, while the diffraction peak marked B in Fig. 4.10 is considered to arise from the (113) and (203) crystallographic planes. These two diffraction peaks were isolated for discussion because they also appear in the biaxially oriented film patterns with the strongest intensity.

The diffraction patterns from the biaxially oriented films are discussed in the context of this limited assignment of Miller indices. Looking first at Fig. 4.8, the balanced pattern seen at all four poly(L-lactic acid) concentrations would indicate that there was a uniform in-plane orientation of the crystal phase. This is quite consistent with the balanced biaxial deformation imposed on the sample in the

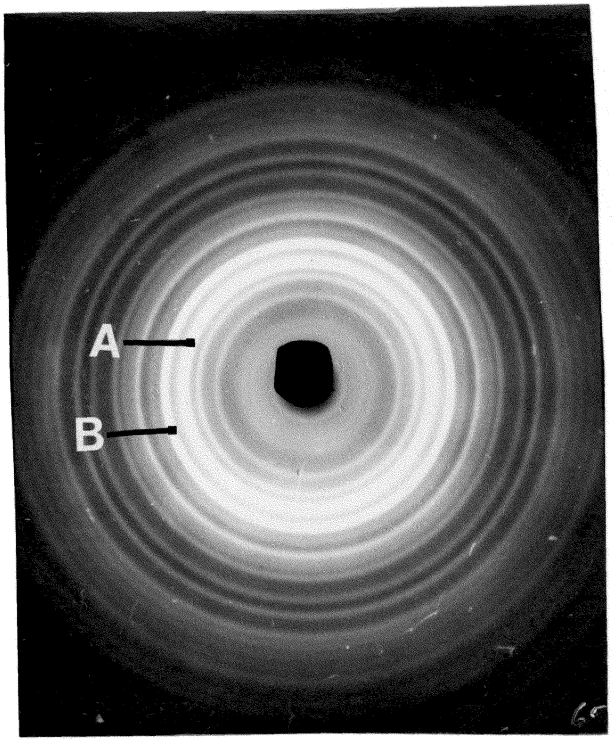

Figure 4.10. WAXS pattern of unoriented poly(L-lactic acid) crystallized isothermally at 130 C for 3 hours.

LES and the fact that the two intensity diffraction peaks of interest are associated with crystallographic planes whose normals are either perpendicular to the c-axis ((110),(200)) or nearly perpendicular to the c-axis ((113),(203)). As the concentration of the poly(L-lactic acid) component is decreased in favor of the racemic polymer, the crystal diffraction rings remain at approximately the same intensity while the amorphous halo increases in intensity. This would seem inconsistent with the DSC results that predict a decrease in overall crystallinity from 44% to 32% as the concentration of poly(L-lactic acid) is decreased from 100% to 75%. However, the qualitative nature of Warhus camera patterns may not be sensitive enough to reproduce this trend. There does appear to be a slight broadening of the diffraction rings with increasing racemic content suggestive of smaller crystallite sizes. This is consistent with the previous discussion of the anticipated decreasing shish diameter with increasing dilution of the crystallizable constituent in these polymer blends.

Heffelfinger and Knox (11) have classified various types of film orientation into six different types. The diffraction patterns in Fig. 4.9 indicate that of these six catagories the "planar orientation" best describes the biaxial character of poly(L-lactic acid) films. Planar orientation is described by a preferred crystal axis (in this case, the crystallographic c axis) parallel to the plane of

the film. Figure 4.9 also indicates that the level of orientation of the crystal phase is approximately the same in each of the four compositions. This latter observation is a bit surprising, especially for sample 75/40k, where the strain hardening has been shown to be comparatively low.

It may now be instructive to construct a simple model that can tie together some of the observations described above. During the early stages of deformation, the initially amorphous polymer chains begin to align themselves in the plane of the film. A steady state amorphous structure is approached which is characterized by an equilibrium entanglement density and chain orientation (entropy). The relative approach to this steady state is, for now, unimportant. It suffices to say that the preferred chain orientation is along the lines of strain (in plane), and that a specific entanglement density is experienced.

As crystal nucleation rates are known to be accelerated by chain orientation, chain extended crystallites begin to form in the films at finite biaxial strains probably well before the onset of strain hardening. The chain axis of the crystallite is also oriented in plane. A finite amount of chain mobility is required so that a cooperative number of chain segments can collapse into a shish type of structure. In the case where two highly extended amorphous chains are in proximity, but are not in exact parallel registry, the chain pair will not participate in a common crystallite unless

there is some relative chain mobility to allow cooperative realignment. This situation may be particularly acute in simultaneous biaxial orientation where two highly oriented amorphous chains could be orthogonal to one another. However, assuming conditions amenable to strain induced crystallization with some chain mobility allowing cooperative alignment of chains, extended chain nuclei will begin to form.

As the number of chain extended nuclei grow, they will act as physical crosslinks between elongated amorphous chain segments and contribute, along with the simple amorphous chain entanglements, to an overall network structure. In contrast to the entanglements which are capable of slipping by one another, the network junctions formed by extended chain crystallites are a good deal more permanent in nature. As the number of crystalline crosslinks grows relative to the number of entanglements, the network becomes more and more elastic with less and less of a mechanism available for energy dissipation (chain entanglement slippage). Given enough extended chain nuclei, the material will behave as a network structure (i.e. rubber) and strain hardening will occur.

The higher the concentration of crystallizable poly(L-lactic acid), the more likely is the onset of stain hardening under the given conditions of stretch. At lower concentrations of poly(L-lactic acid), the extended chain

nuclei probably still form under the influences of the imposed strain, but there will be a larger number of chain entanglements relative to crystalline crosslinks allowing for more energy dissipation through entanglement slippage. Thus, for blends with higher racemic contents, the same initial strain induced crystallization will occur in the optically active component at the onset of deformation. However, the inherently higher ratio of entanglements crosslinks compared to chain extended nuclei crosslinks will guarantee a mechanism for energy dissipation and, thus, lower strain hardening for materials like 75/40k, see Fig. 4.4.

Clearly, prior to strain hardening, the optically active poly(L-lactic acid) molecules in all four samples (100/40k, 95/40k, 95/40k and 75/40k) undergo approximately the same chain extension. Recall from section 4.3.2 that the similarity in the glass transitions and molecular weights ensures that the mechanical response of all the amorphous blends will be approximately the same. Given the same stress-draw ratio history, a poly(L-lactic acid) molecule in any blend will experience the same local rheological environment. In effect, the enhanced supercooling associated with molecular orientation will be the same for every poly(L-lactic acid) molecule independent of racemic polymer content. Due to the fact that $\Delta H_{mix} = 0$, there is no effect of blend composition on thermodynamic driving force for crystallization. Diffusional effects on crystallization

kinetics should be minimized since the Tgs of the blends are nominally the same. Under similar conditions of biaxial deformation (i.e. temperature and strain rate), the propensity for a given poly(L-lactic acid) molecule to crystallize under strain is, therefore, equivalent at all blend compositions. Possibly the outstanding influence of the racemic poly(lactic acid) diluent upon strain induced crystalline morphology is the reduced shish crystal diameter predicted by Feit et al. (83) and suggested by the increased breadth of the WAXS diffraction peaks.

It is further assumed that most of the strain induced nuclei are established prior to strain hardening. This postulate is supported by Oono et al. (5) who report that the equilibrium level of crystallinity in natural rubber films decreased with increasing biaxial extension ratio. At high molecular extensions in biaxial films, the mobility of taut, highly oriented chain segments is minimized preventing crystallization. Crystallization is, therefore, restricted to relatively low molecular alignments in biaxial deformation. The chain mobility may be high enough in the early part of the stress-draw ratio trajectory to allow crystallization to occur. As the amorphous chains become highly oriented in the strain hardening regime, further crystallization is restricted.

Given the hypotheses that the propensity for strain induced crystallization is independent of blend composition,

and that the crystallization process is arrested at higher levels of strain hardening, the DSC crystallinity data can be rationalized. Note that in Fig. 4.4 the onset of strain hardening is more or less independent of blend composition. Thus, given the same thermodynamic driving force for crystallization and the same time scale in which to crystallize (prior to strain hardening), it may well be expected that the level of crystallinity, once normalized to poly(L-lactic acid) content, is the same for all four samples stretched at conditions in Fig. 4.4.

Recall that the WAXS diffraction patterns from all four compositions in the biaxial deformation series of Fig. 4.9 showed approximately the same level of crystal phase orientation. In fact, given the proposed model described above, strongly different levels of crystal orientation might be expected. As the amorphous chain segments between shish crystal nuclei are drawn tight in the strain hardening regime of the biaxial stress draw ratio curve, the tension transmitted back to the shish crystal network junction would tend to orient the crystal c axis parallel to the plane of the film. Generally, the level of preferred orientation would be expected to increase in concert with enhanced strain hardening. The rationalization of this disparity was not clear until it was realized that a significant amount of stress relaxation was occurring just after the biaxial draw during the quench operation. Figure 4.11 reports the stress

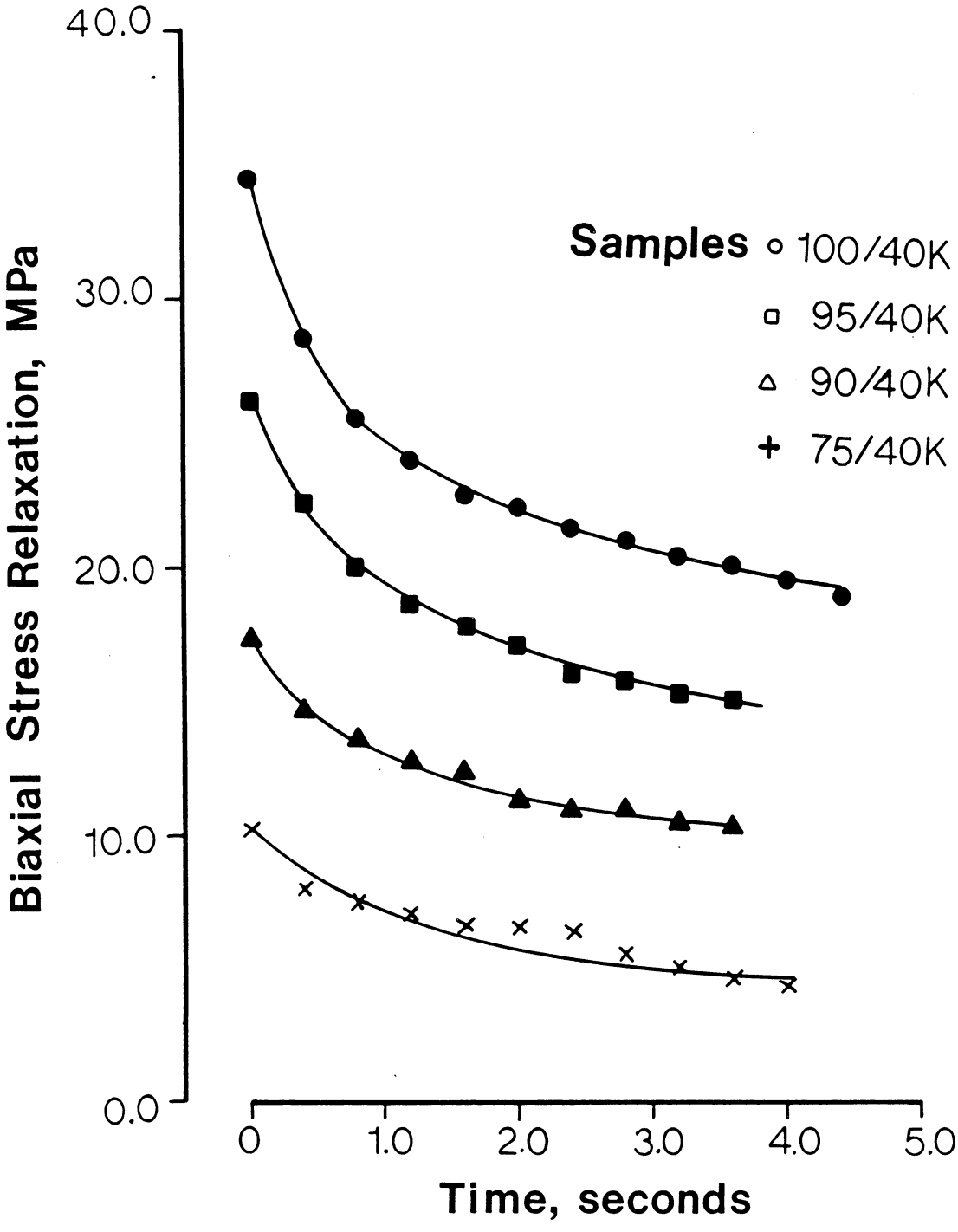

Figure 4.11. Biaxial stress relaxation at termination of biaxial stretch.
Temperature: 80 C
Crosshead Speed: 1.27 cm./sec.
Final Biaxial Draw Ratio: 4 X 4

relaxation occurring after a final biaxial strain of 4 X 4 in samples 100/40k, 95/40k, 90/40k, 75/40k stretched at a crosshead speed of 1.27 cm./sec and a temperature of 80 C. The initial stress data point in Fig. 4.11 corresponds to the final stress reported in Fig. 4.4. Clearly, there are not enough extended crystal nuclei to prevent relaxation of oriented amorphous chain segments by entanglement slippage after deformation ceases. Unfortunately, the forced air quench applied to the film was insufficient to prevent this rapid molecular relaxation. The highest level of strain hardening in sample 100/40k sample is counterbalanced with the highest level of stress relaxation. Similarly, the lowest level of strain hardening in sample 75/40k leads to the lowest potential for stress relaxation. Thus, the relaxation of the oriented molecules in the composition series stretched at 1.27 cm./sec. and 80 C leads towards the convergence of molecular orientation. The relaxation of the amorphous network chain segments can lead to the slight rotation of the shish crystals out of the plane of the film. Thus the stress relaxation is also associated with the slight relaxation of the shish crystal orientation and would tend to explain the overall similarity of crystal orientation in all four samples of Fig. 4.9.

Figure 4.12 reports the modulus measurements derived from the room temperature tensile testing of the finished films. The modulus data agrees with the crystal phase

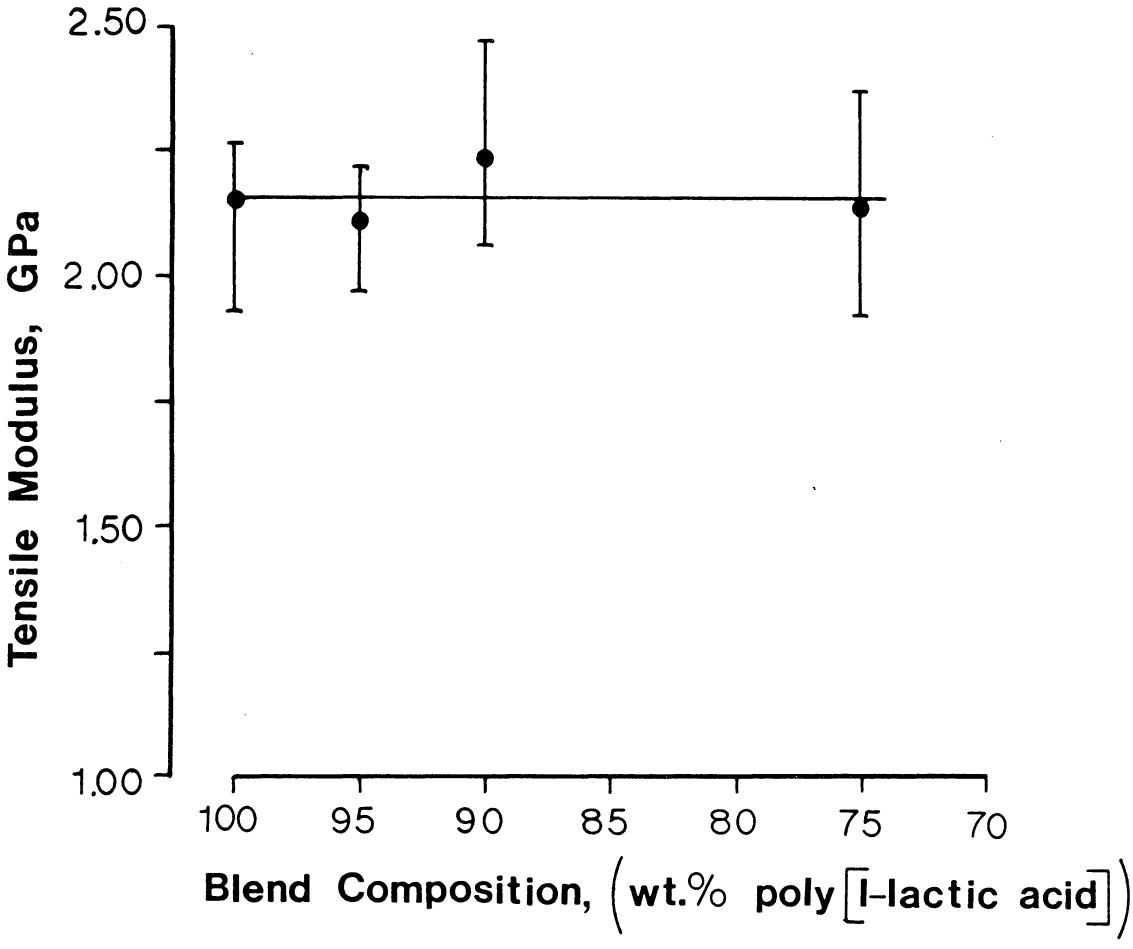

Figure 4.12. Tensile modulus vs. blend composition for 40,000 molecular weight biaxial films stretched at 80 C and 1.27 cm./sec. to a final biaxial draw ratio of 4 X 4.

orientation patterns of Fig. 4.9 in suggesting that there is less of an orientation difference between samples of different compositions than would be anticipated from the strain hardening curves in Fig. 4.4. Again, this phenomenon is rationalized with the stress relaxation data reported in Fig. 4.11 which indicates that all four films relax in proportion to the level of strain hardening. This, in turn, drives all samples toward an equivalent level of orientation. In addition, it should be noted that since the tensile measurements were done at room temperature, nearly 40 C below the glass transition, that the predominantly amorphous phase will behave as a relatively high modulus glassy material which could possibly dominate over any orientation effects.

In summary, the effects of changing the proportions of isomers in blends of optically active poly(L-lactic acid) and racemic poly(lactic acid) upon the strain hardening phenomenon in biaxial deformation above the glass transition can be solely attributed to strain induced crystallization of the optically active component. Crystallinity remains in direct proportion to the amount of poly(L-lactic acid) present in the blend. Both chain extended crystallites and amorphous chain entanglements contribute to a physical crosslink structure. A network structure made up of amorphous chain segments between these physical crosslinks is set up early in the stress-draw ratio trajectory. Further deformation of the network leads to the development of the

strain-hardening phenomenon and overall higher molecular orientations in biaxial deformation. However, the beneficial effects of enhanced orientation are, at best, difficult to realize due to the extreme propensity for molecular relaxation after the LES crossheads stop at the end of the stretch experiment.

4.3.3 THE EFFECT OF TEMPERATURE ON THE STRAIN HARDENING OF ISOMER BLENDS OF POLY(LACTIC ACIDS) IN BIAXIAL DEFORMATION

Although strain induced crystallization has been demonstrated to enhance strain hardening phenomenon in biaxial deformation of films, amorphous chain entanglements also contribute to the support of stress as evidenced by the stress relaxation at the end of the stretch experiment at 80 C described in the previous section. In order to demonstrate the relative influences of polymer chain entanglement and strain induced crystallization upon biaxial strain hardening, the effect of stretch temperature has been investigated. Specifically, film samples of the same composition and molecular weight, 100/40k, 95/40k, 90/40k, and 75/40k, were stretched at 75 C and 90 C. In order to facilitate comparison with data presented in section 4.3.2, the rate of stretch was held at 1.27 cm./sec. Although stretch temperature will affect crystallization, the dominant effect of changing temperature upon strain hardening phenomenon will be tied to its influences on the number of operative chain entanglement network sites.

Figure 4.13 depicts the relative degrees of strain hardening measured on biaxially stretching films from the 40,000 molecular weight blend materials at 75 C. On comparison with the stretch data at 80 C in Fig. 4.4, the same general increase in strain hardening with increasing

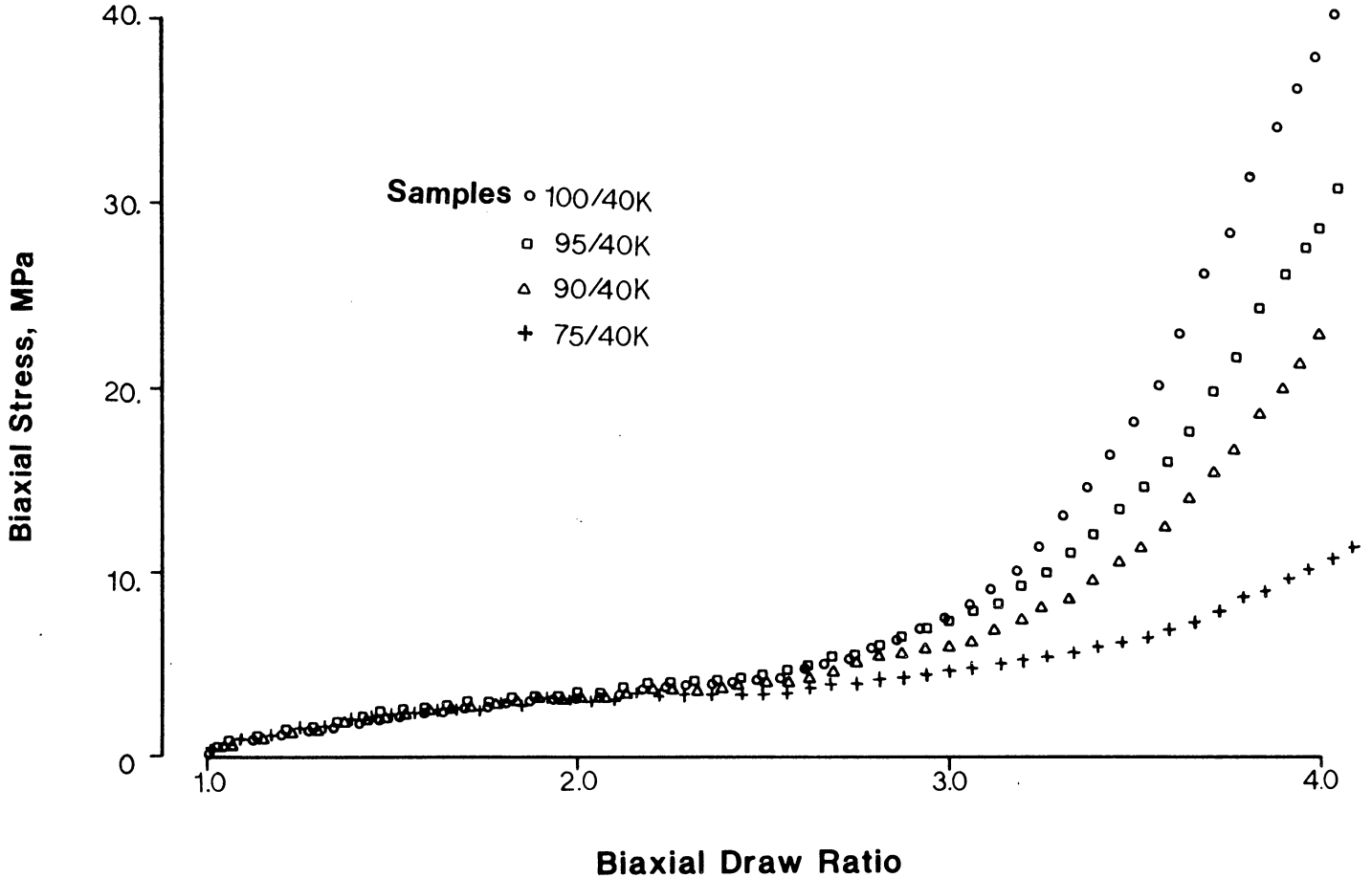

Figure 4.13. Biaxial stress vs. biaxial draw ratio for 40,000 molecular weight poly(lactic acid) blends.
Temperature: 75 C
Crosshead Speed: 1.27 cm./sec.
Final Biaxial Draw Ratio: 4 x 4

poly(L-lactic acid) content was seen, however, the stress levels are generally higher at 75 C. Also, the time scale necessary for the onset of strain hardening is nearly unchanged from that observed at 80 C.

The DSC thermograms for each of the four films stretched at 75 C are shown in Fig. 4.14. Recall the comparable DSC data for the 80 C stretch is reported in Fig. 4.6. The generally larger entropy endotherms for the 75 C stretch indicate considerably larger amorphous phase orientation. In addition, the larger crystallization exotherm would suggest a lower overall crystallinity of the films stretched at 75 C. In fact, the crystallinities and normalized crystallinities calculated from the net endotherms of the DSC traces are plotted as a function of composition for the 75 C films in Fig. 4.15. Although there is significantly more scatter to the data, the film crystallinity still increases in proportion to poly(L-lactic acid) content. Within the error bars, the normalized crystallinity remains independent of composition and is generally lower than the normalized crystallinities determined for the films stretched at 80 C. The increased error is believed to stem from the inability to separate the overlapping entropy endotherms from the crystallization exotherms. Note that the partial superposition of these two effects is more critical at 75 C due to their increased size over those measured at 80 C.

The higher degrees of strain hardening measured at lower

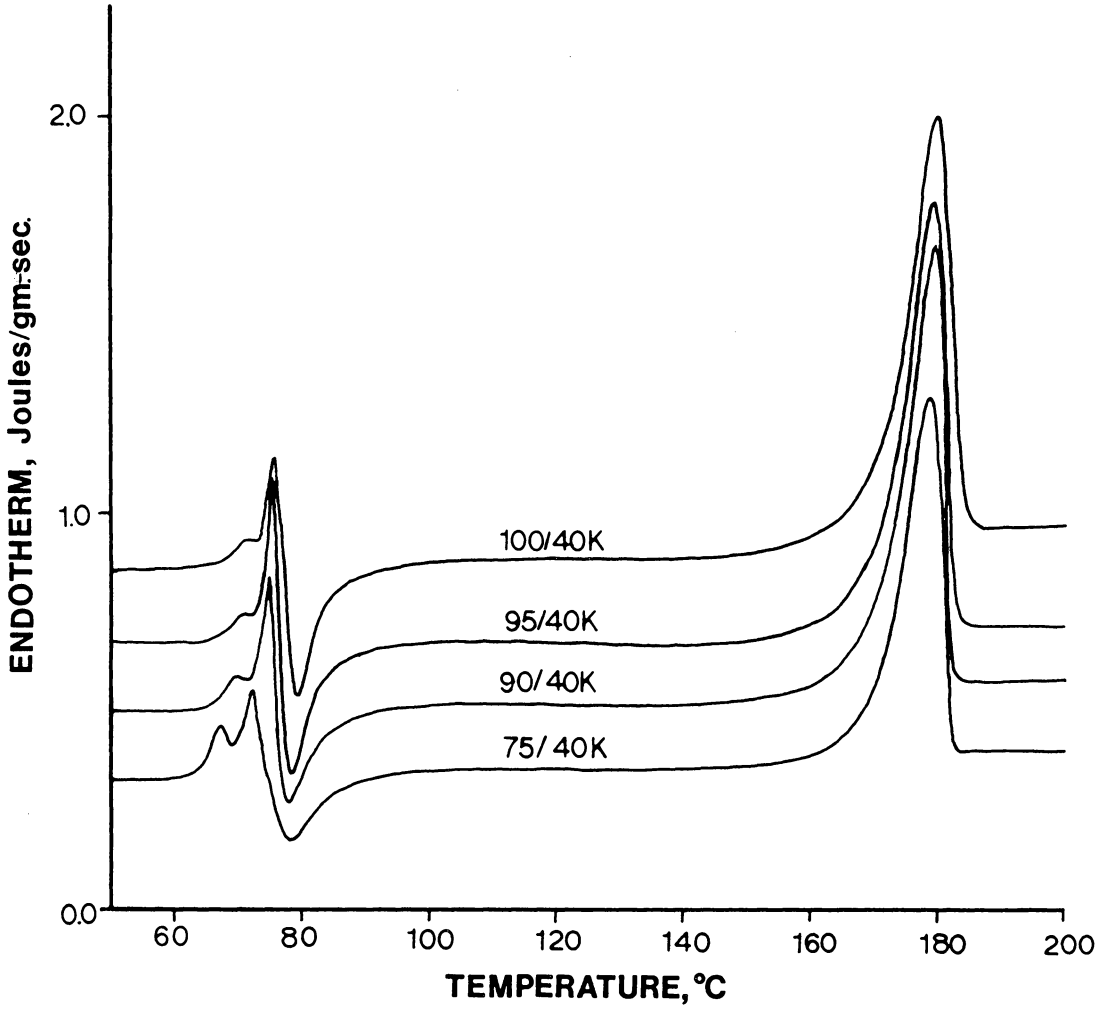

Figure 4.14. DSC thermograms of poly(lactic acid) 40,000 molecular weight blends biaxially stretched at 75 C and 1.27 cm./sec. to a final biaxial draw ratio of 4 x 4.

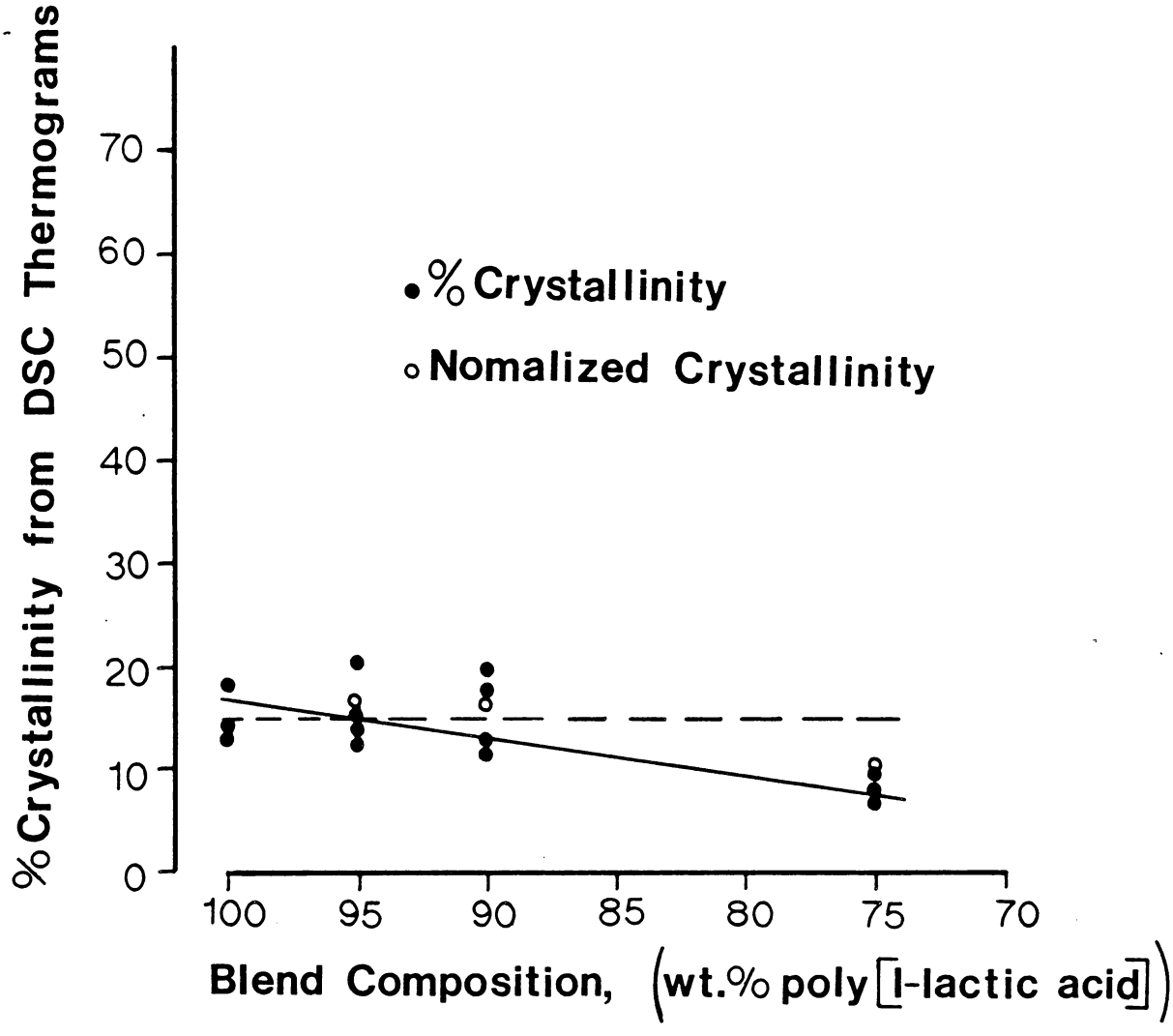

Figure 4.15. % crystallinity vs. blend composition for 40,000 molecular weight biaxial films stretched at 75 C and 1.27 cm./sec. to a final biaxial draw ratio of 4 x 4.

deformation temperatures must be rationalized with the increased tenacity of the amorphous chain entanglements. Since the crystallinity of the biaxial films stretched at 75 C is significantly lower than the crystallinities measured in the films stretched at 80 C, the distribution of network junction population between extended chain shish crystal junctions and chain segment entanglements at 75 C must be biased toward chain entanglements. Molecular relaxation times are longer at lower temperatures causing chain entanglements to become more permanent on the time scale of the deformation at 75 C.

During the early stages of deformation prior to strain hardening, strain induced crystallization mechanisms form the extended chain crystal network junctions. Due to the closer proximity of Tg at 75 C, the crystallization nucleation rate is expected to be lower. However, due to the increased tenacity of the entangled network, few numbers of extended chain crystallites are required in order to cause the network to become elastic in nature. In other words, there is less energy dissipation associated with chain entanglement slippage at 75 C than at 80 C. These two effects apparently offset one another leading to the onset of strain hardening on approximately the same time scale as that measured at the 80 C stretch.

The WAXS patterns of the biaxial films stretched at 75 C are depicted in Figs. 4.16 and 4.17. In agreement with the

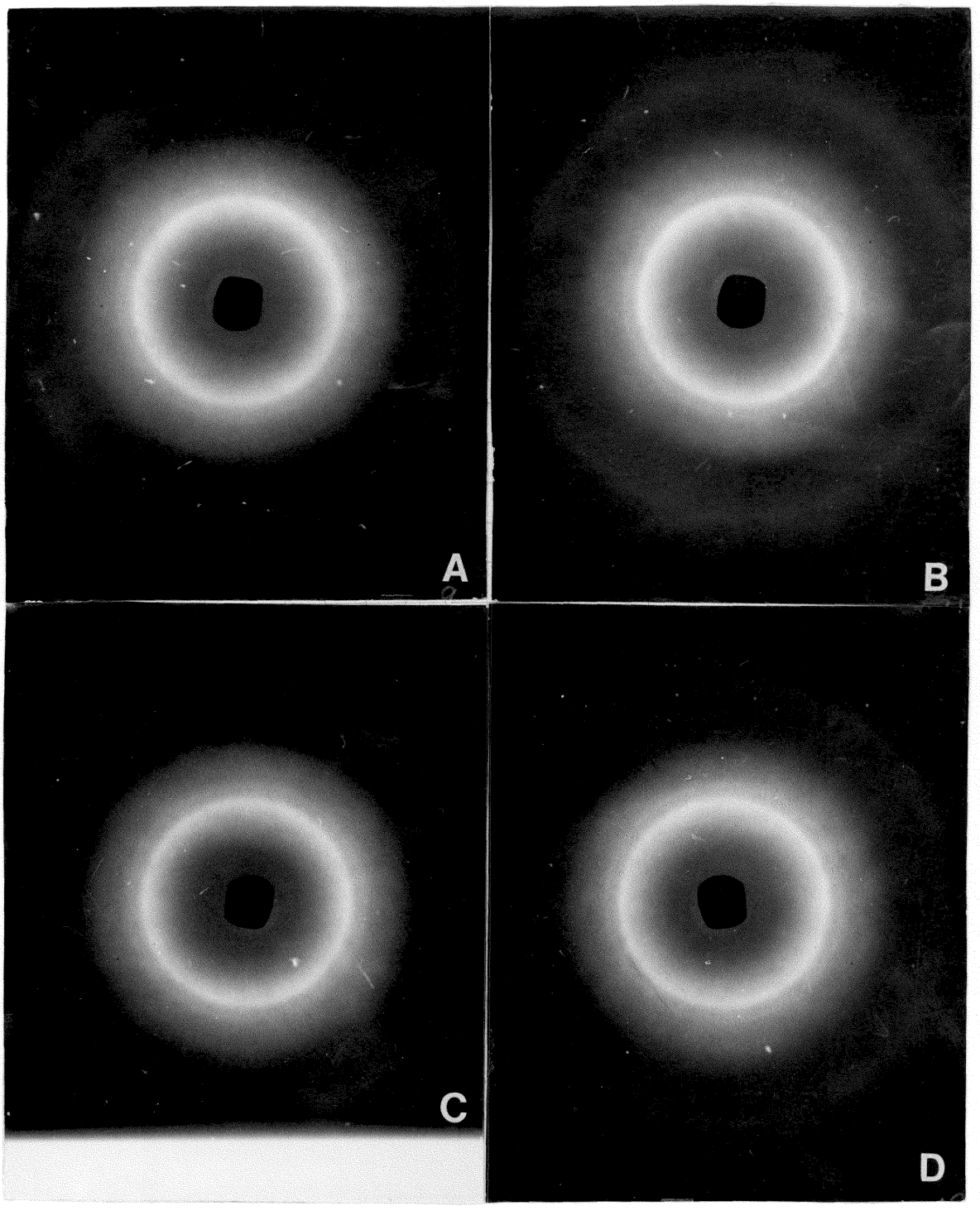

Figure 4.16. WAXS patterns for 40,000 molecular weight biaxial films stretched at 75 C and 1.27 cm./sec. to a final biaxial draw ratio of 4 x 4, X-ray beam oriented normal to film surface.
A) 100/40k B) 95/40k C) 90/40k D) 75/40k

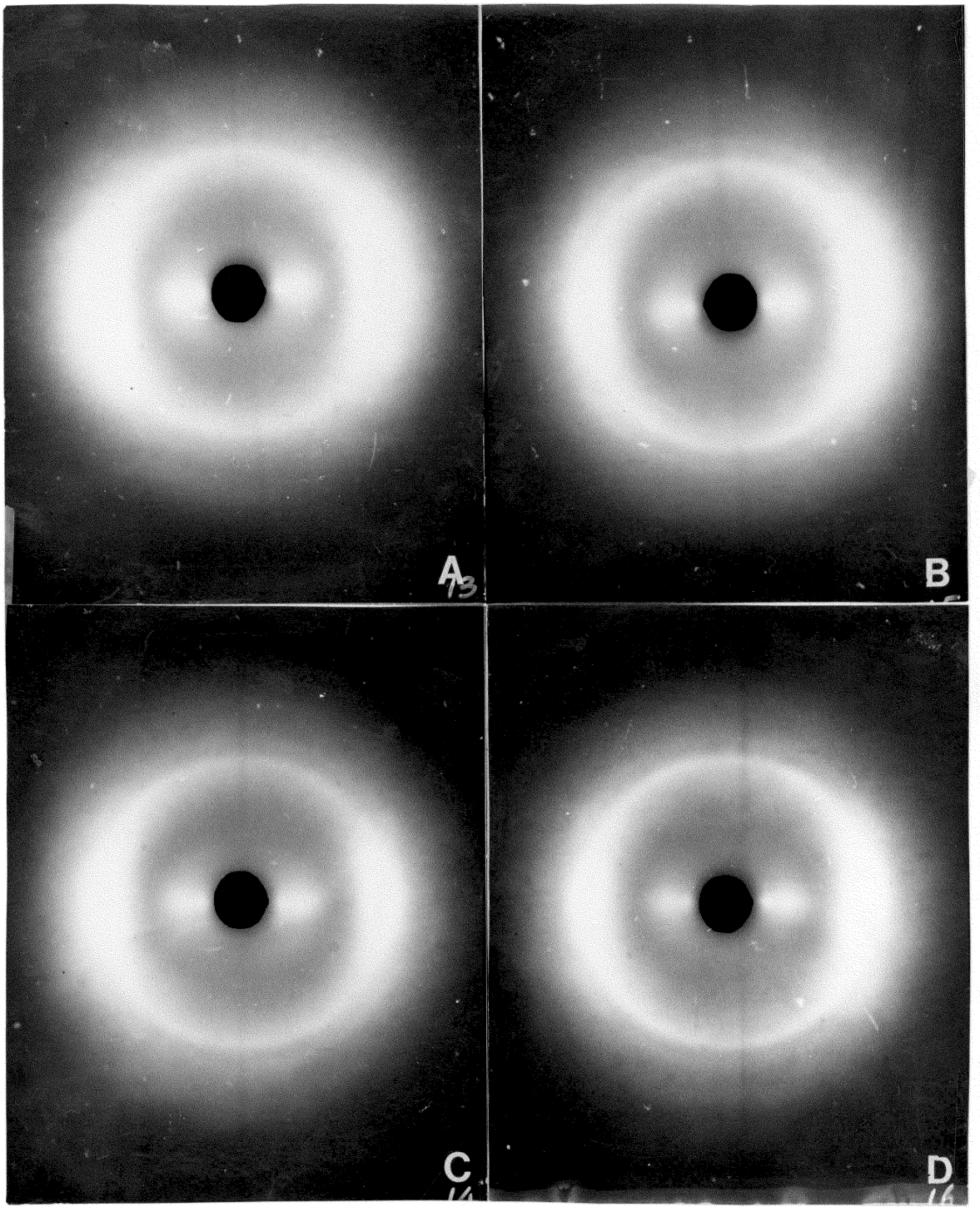

Figure 4.17. WAXS patterns for 40,000 molecular weight biaxial films stretched at 75 C and 1.27 cm./sec. to a final biaxial draw ratio of 4 x 4, X-ray beam oriented parallel to film surface.
A) 100/40k B) 95/40k C) 90/40k D) 75/40k

DSC results, the crystal reflection intensities in the patterns taken with the incident X-ray beam normal to the film surface in Fig. 4.16 indicate a lower degree of crystallinity in comparison to the similar WAXS patterns in Fig. 4.8 for the 80 C stretch films. Again, the patterns are balanced indicating the balanced biaxial nature of the in plane orientation. The breadth of the diffraction rings would indicate either a smaller crystallite size and/or a less perfected crystal structure. In fact, given the lower temperature of stretch, both of these effects can be rationalized. Lower temperatures are generally considered to stabilize a smaller crystallite size. In addition, the decreased molecular mobility at 75 C may inhibit the migration of chain segments to perfect crystalline registry.

Figure 4.17 displays the WAXS patterns of the 75 C films taken with the incident X-ray beam parallel to the film surface. Clearly, the same type of planar orientation is displayed in Fig. 4.17 as was seen in Fig. 4.9 for the films stretched at 80 C. The increased breadth of the diffraction rings due to the lower temperature of stretch is a bit more pronounced in these diffraction patterns. Despite the significantly higher degrees of strain hardening at higher poly(L-lactic acid) contents, the level of orientation of the crystalline phase implied in Fig. 4.17 does not seem to change with blend composition. As was the case with the 80 C data, this anomaly can be rationalized once the stress

relaxation data is considered.

Figure 4.18 presents the stress relaxation data obtained for the 75 C stretch after the LES crossheads stopped. Clearly, the increased contribution of entanglements over extended chain nuclei to the network structure during strain hardening is reflected in the higher degrees of stress relaxation at 75 C compared to 80 C, see Fig. 4.11. Again, it is this stress relaxation which accounts for the similarity in crystal phase orientation in the four composition samples stretched at 75 C. In all likelihood, the crystal orientation prior to stress relaxation was probably highest for higher poly(L-lactic acid) concentrations due to the enhanced stain hardening. As a result of the stress relaxation, the molecular orientation is relaxed and crystal orientations converge toward similar lower values.

The modulus data from the room temperature tensile testing of the films stretched at 75 C is presented in Fig. 4.19. Modulus is again independent of blend composition supporting the supposition that after stress relaxation the molecular orientation of the films stretched under conditions of Fig. 4.13 are approximately the same.

The other extreme in stretch temperature is now addressed in a similar methodology. Figure 4.20 presents the stress draw ratio results obtained from the LES for stretching the same 40,000 molecular weight blend series at

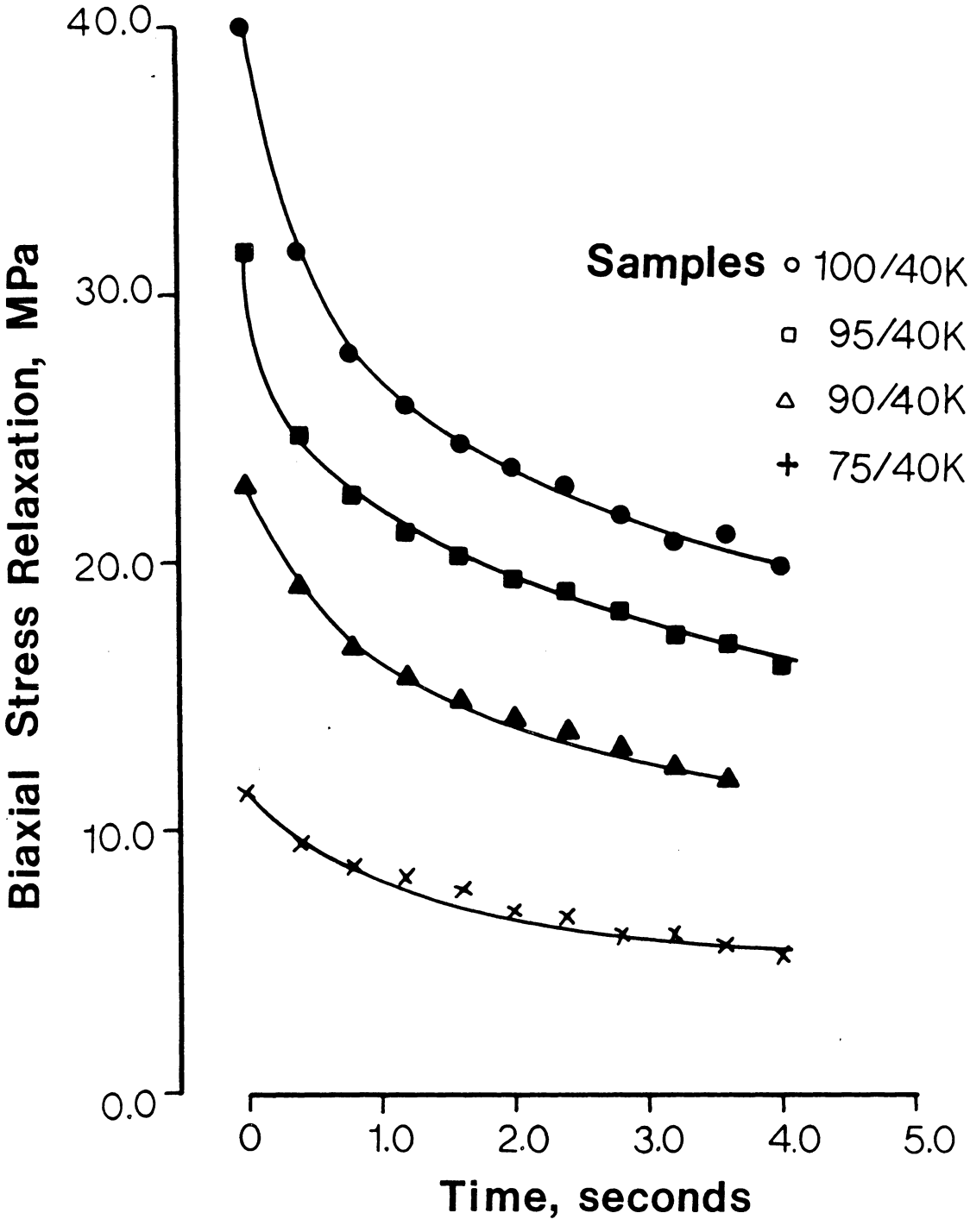

Figure 4.18. Biaxial stress relaxation at termination of biaxial stretch.
Temperature: 75 C
Crosshead Speed: 1.27 cm./sec.
Final Biaxial Draw Ratio: 4 x 4

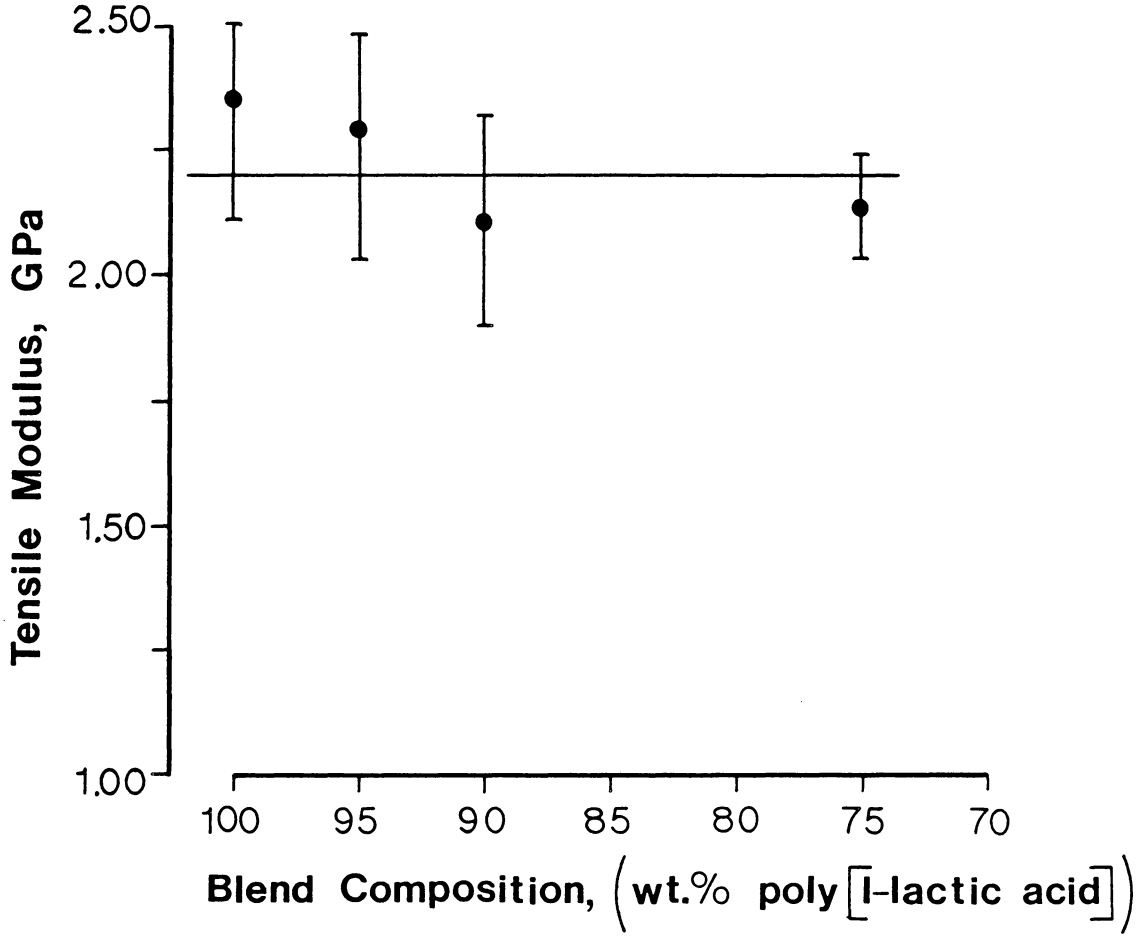

Figure 4.19. Tensile modulus vs. blend composition for 40,000 molecular weight biaxial films stretched at 75 C and 1.27 cm./sec. to a final biaxial draw ratio of 4 x 4.

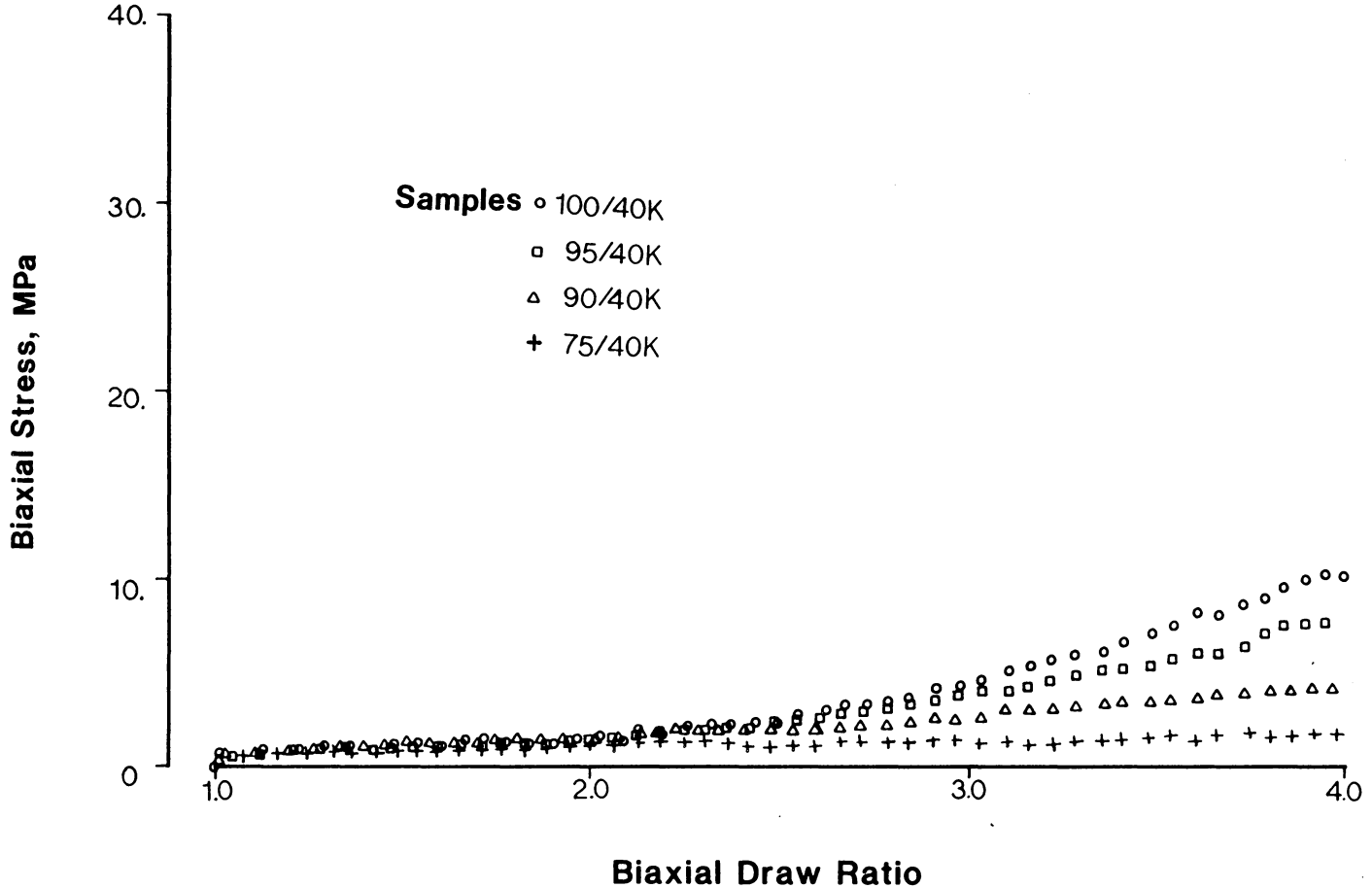

Figure 4.20. Biaxial stress vs. biaxial draw ratio for 40,000 molecular weight poly(lactic acid) blends.
Temperature: 90 C
Crosshead Speed: 1.27 cm./sec.
Final Biaxial Draw Ratio: 4 x 4

90 C and 1.27 cm./sec. to a final biaxial strain of 4 X 4. Clearly, at this highest temperature there is less of a difference in the strain hardening behavior as the content of poly(L-lactic acid) is increased from 75% to 100%. Again, this data will be discussed in terms of the relative contributions of both strain induced crystallites and amorphous chain entanglements to the network structure capable of supporting stress in biaxial flow. In order to determine the amount of crystallinity, the DSC data is reviewed.

The DSC thermograms reported in Fig. 4.21 for the film series stretched at 90 C are substantially different in behavior from the previous DSC results, see Figs. 4.6 and 4.14. There is an endotherm that occurs coincidentally with the glass transition of the material. This effect is particularly acute in the materials with low crystallinity (high racemic poly(lactic acid) content). It is considered that the peak is not the standard entropy peak associated with molecular relaxation for two reasons. First, there is very little strain hardening in these materials suggesting that there is very little amorphous orientation and, thus, no potential for an entropy peak. This is supported by the observation that these materials do not shrink during the DSC trace. Samples from the previous temperature series showed substantial dimensional changes on DSC heating. Secondly, this endotherm appears directly over Tg whereas the previous

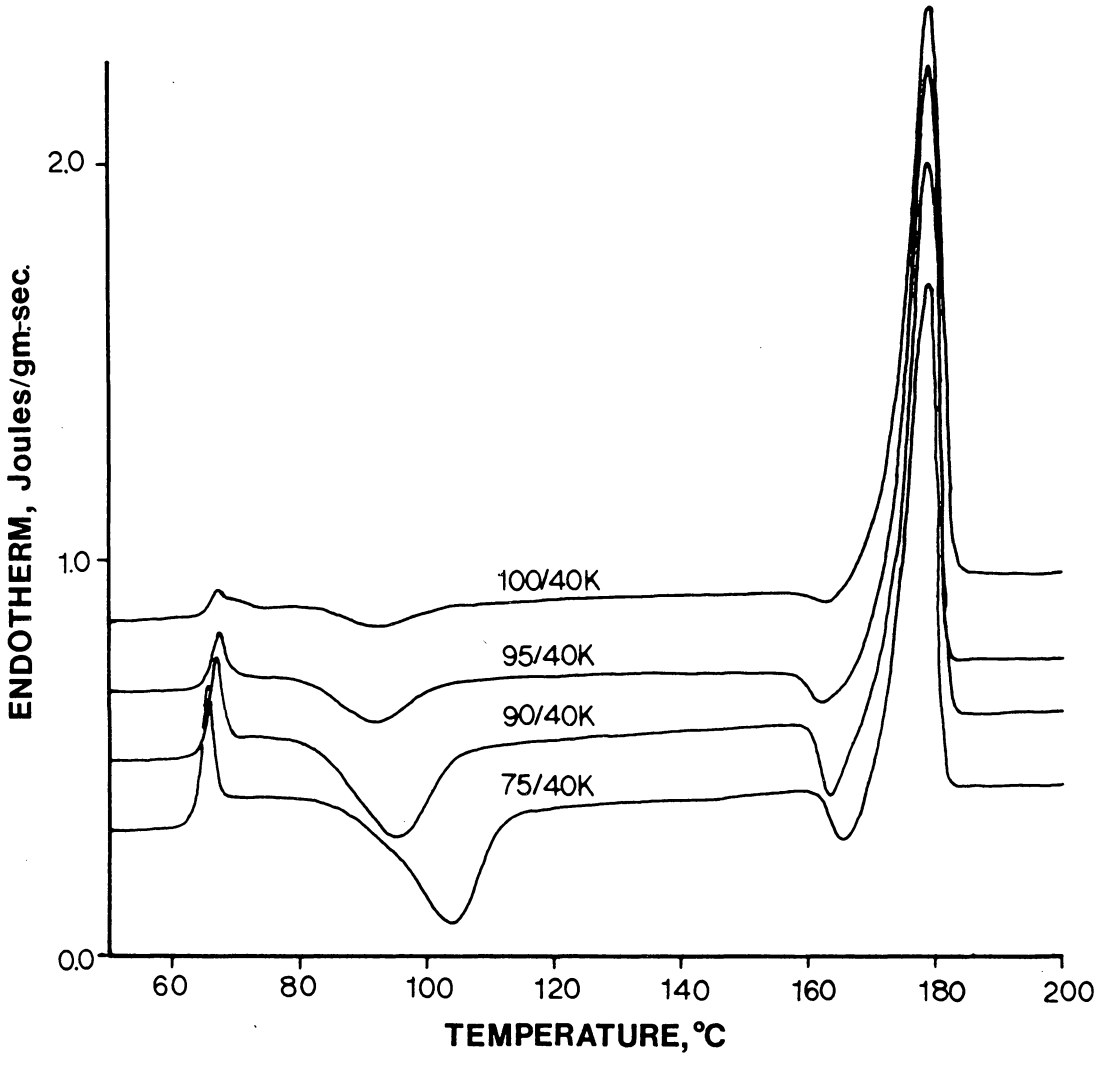

Figure 4.21. DSC thermograms of poly(lactic acid) 40,000 molecular weight blends biaxially stretched at 90 C and 1.27 cm./sec. to a final biaxial draw ratio of 4 x 4.

entropy peaks occurred after Tg. This last observation suggests that the low temperature endotherms in Fig. 4.21 are excess enthalpy peaks associated with free volume recovery of physically aged samples as they pass through the glass transition temperature (93). As would be expected, the free volume peak increases with increasing amorphous content. The absence of significant volume recovery peaks in previous DSC traces may be associated with the retardation of physical aging with the generally higher levels of crystallinity and orientation in the previous samples. The exotherm that immediately precedes the major melting peak is considered to be associated with a possible melting/recrystallization phenomenon and/or a crystalline unit cell change during the heating cycle. It is beyond the scope of this discussion to elaborate on these possible mechanisms. It will suffice to say that the appearance of both the free volume peak at Tg and the exotherm just prior to the major melting peak are both characteristics of thermograms run on unoriented amorphous poly(L-lactic acid).

Figure 4.22 is the calculation results of estimating the 90 C stretch biaxial film crystallinities from the DSC thermograms. The baseline for the calculation was drawn on the DSC trace with the same technique previously described. In contrast to the previous results (see Figs. 4.7 and 4.15), the crystallinity does not increase in proportion to the amount of poly(L-lactic acid) present in the blend. In fact,

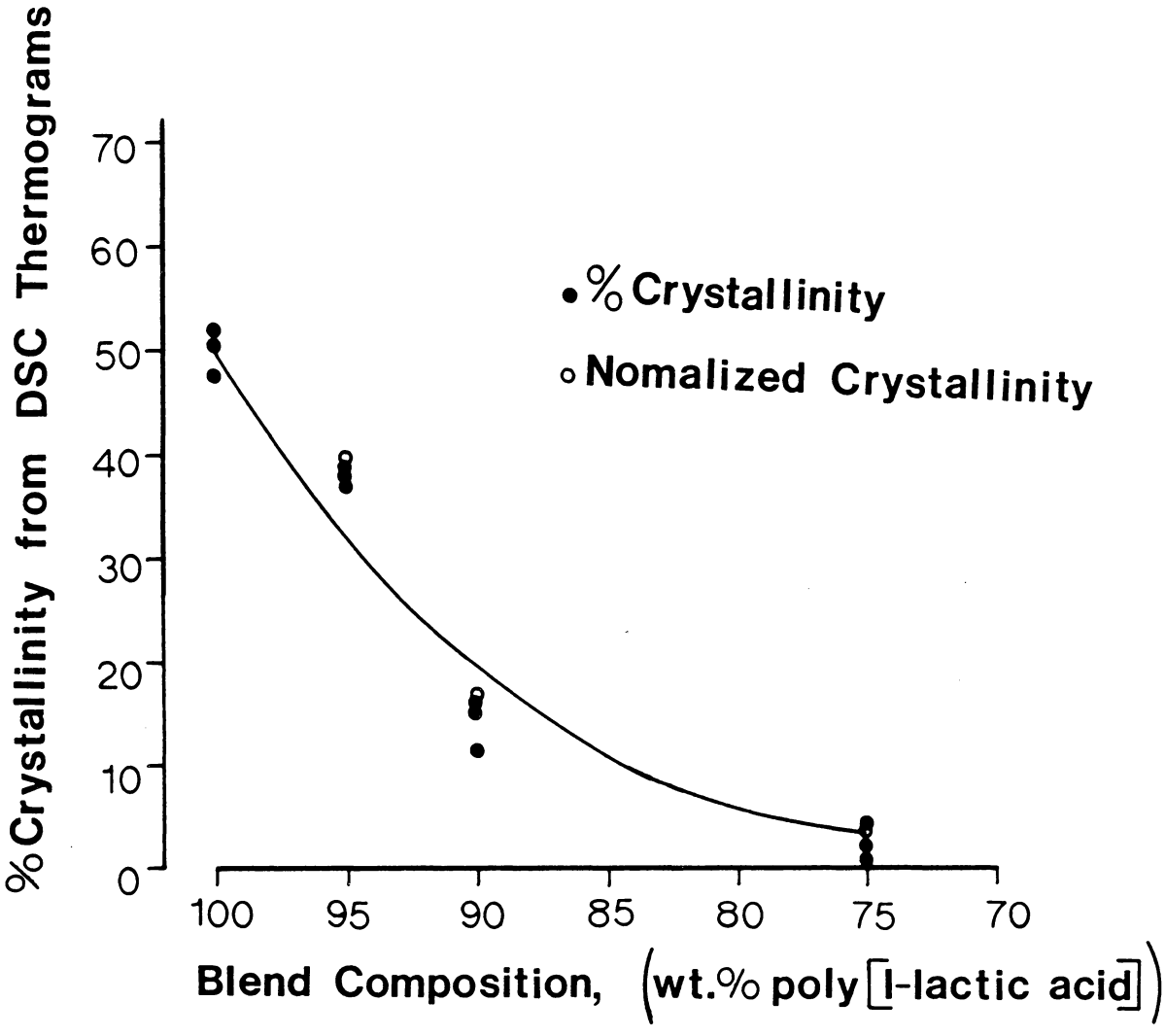

Figure 4.22. % crystallinity vs. blend composition for 40,000 molecular weight biaxial films stretched at 90 C and 1.27 cm./sec. to a final biaxial draw ratio of 4 x 4.

the crystallinity normalized to the optically active polymerconcentration does not remain constant with composition and decreases significantly with decreasing poly(L-lactic acid) concentration.

The severe and disproportionate drop off in crystallinity with decreasing poly(L-lactic acid) content in films stretched at 90 C may be due to a preferred chain folding crystallization mechanism as opposed to the extended chain crystallization phenomenon assumed at lower stretch temperatures. Due to chain entanglement slippage, highly oriented molecular segments may not be energetically favored. This may lead to some strain induced nucleation followed by a preferred and significant amount of subsequent chain folding crystallization. Keith and Padden (94) have shown that quiescent (chain folded) crystallization rates from polystyrene isomer blends are significantly slowed with increasing proportion of atactic species. It is suggested here without further proof that the crystallization in films stretched at 90 C is predominantly chain folding in nature. As such, the crystallization rates may be significantly slowed by racemic poly(lactic acid) content in direct analogy to Keith and Padden's work (94). This would account for the severe and disproportionate drop off in crystallinity in Fig. 4.22. The same drop off in crystallinity is not seen at lower draw temperatures due to the overriding effect of amorphous orientation on providing an enhanced thermodynamic

driving force for extended chain crystallization. It may be noted that previous work has shown that strain induced crystallization from isomeric polystyrene blends has shown that the dominant effect has been the reduction of lateral crystallite size (83).

The WAXS results for the films stretched at 90 C and 1.27 cm./sec. are shown in Figs. 4.23 and 4.24. The diffraction patterns for the incident X-ray beam normal to the film surface, shown in Fig. 4.23, corroborate the DSC results in that they indicate a severe drop off in crystallinity with decreasing concentration of poly(L-lactic acid). In addition, the line breadth, even at low levels of crystallinity in sample 75/40k, indicates relatively large and well organized crystals in comparison with the patterns in Figs. 4.8 and 4.16. The diffraction patterns from these same 90 C samples with the plane of the films positioned parallel to the incident X-ray beam shown in Fig. 4.24 indicate very little preferred orientation. This is the antithesis of the diffraction results for samples drawn at 75 C and 80 C and presented in Figs. 4.9 and 4.17, wherein some clearly significant orientations were demonstrated.

The tensile modulus of the poly(lactic acid) blend films drawn at 90 C and 1.27 cm./sec. are presented in Fig. 4.25. In comparison with previous results at draw temperatures of 75 C and 80 C (see Figs. 4.19 and 4.12), the moduli are significantly lower indicating an overall lower degree of

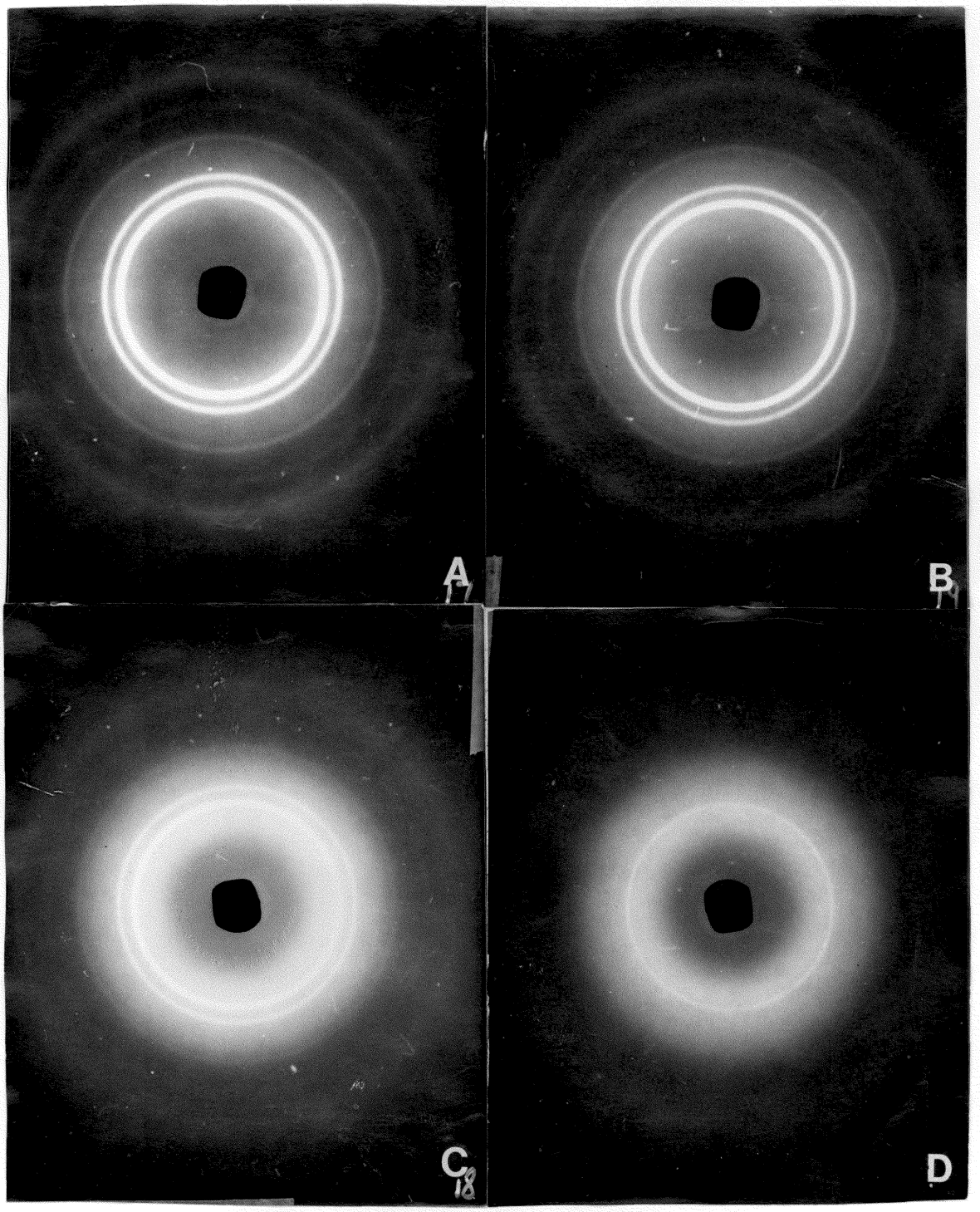

Figure 4.23. WAXS patterns for 40,000 molecular weight biaxial films stretched at 90 C and 1.27 cm./sec. to a final biaxial draw ratio of 4 x 4, X-ray beam oriented normal to film surface.
A) 100/40k B) 95/40k C) 90/40k D) 75/40k

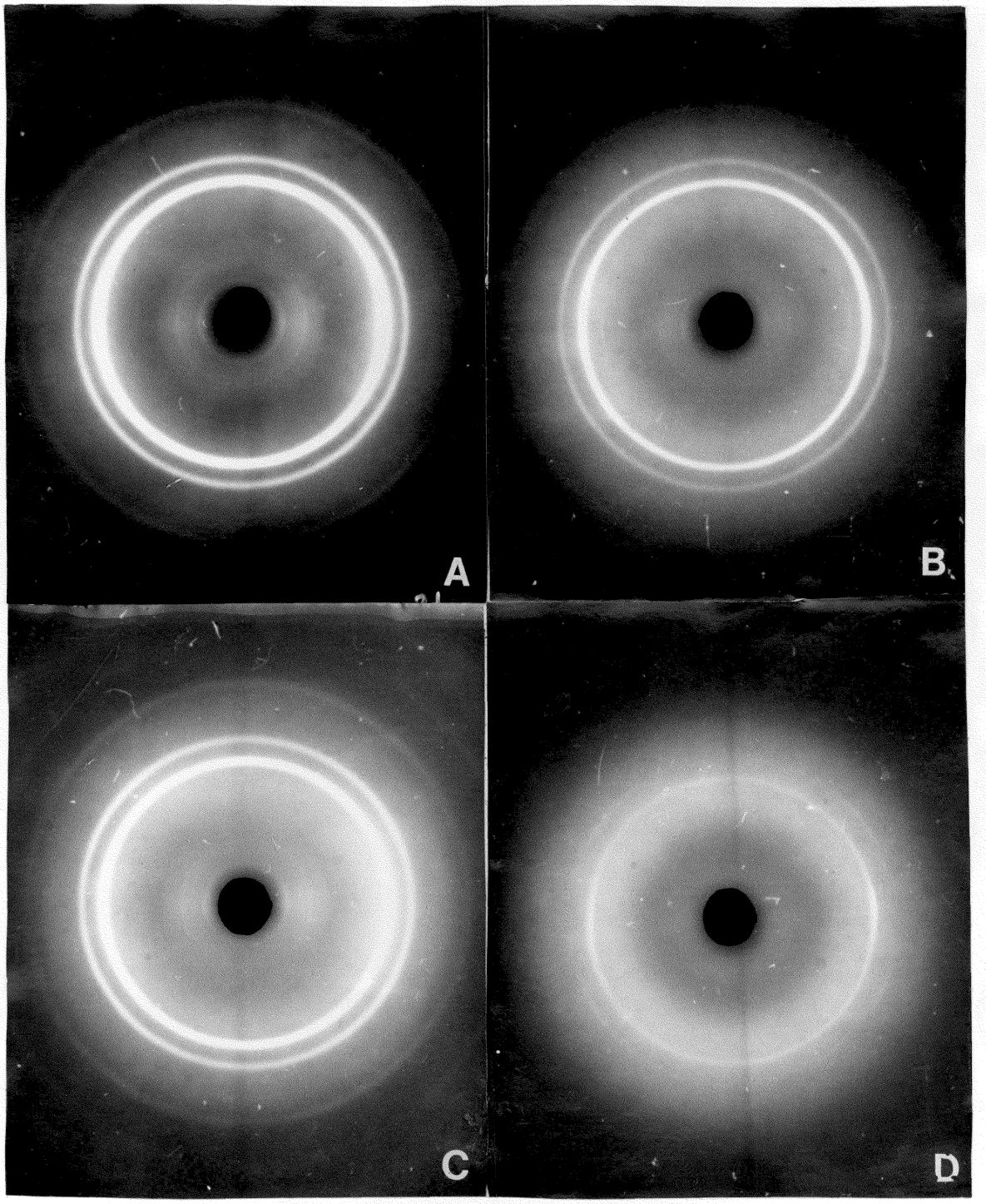

Figure 4.24. WAXS patterns for 40,000 molecular weight biaxial films stretched at 90 C and 1.27 cm./sec. to a final biaxial draw ratio of 4 x 4, X-ray beam oriented parallel to film surface.
A) 100/40k B) 95/40k C) 90/40k D) 75/40k

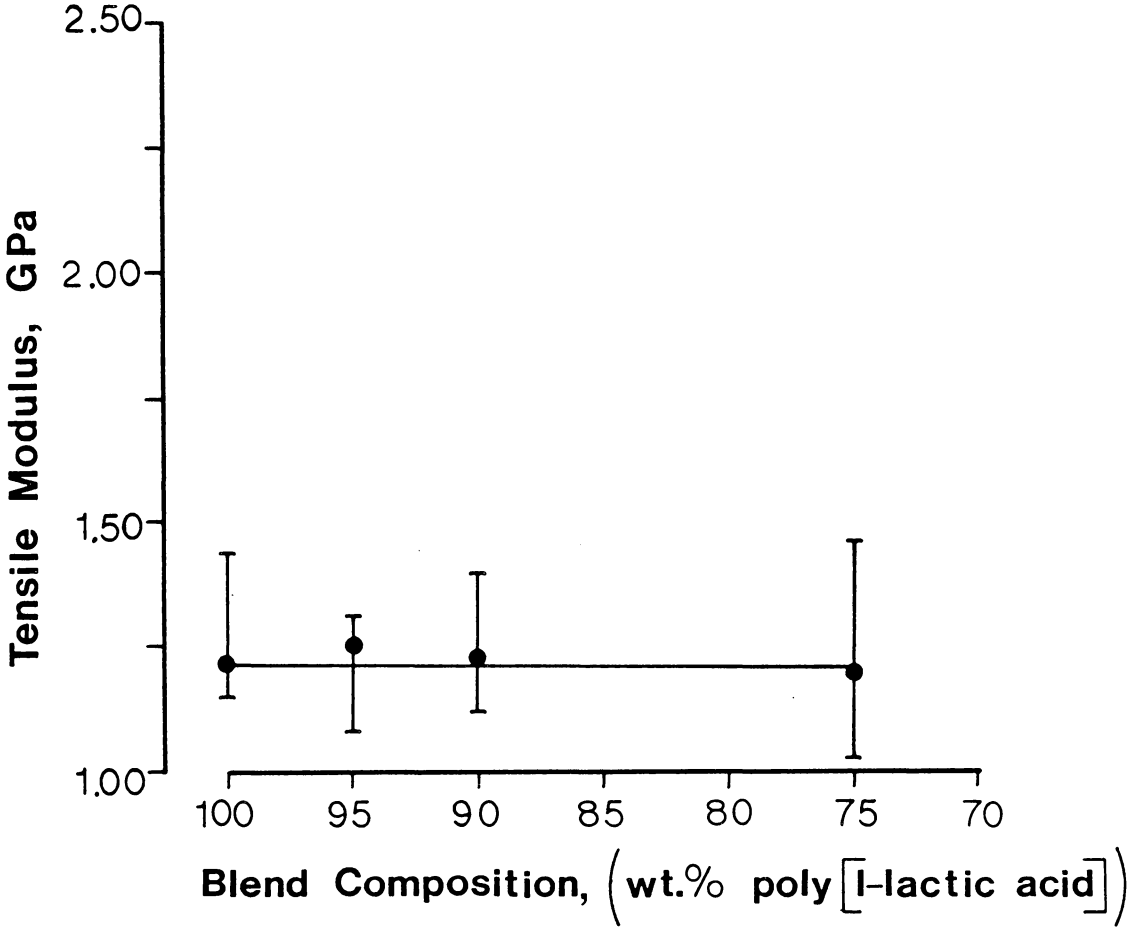

Figure 4.25. Tensile modulus vs. blend composition for 40,000 molecular weight biaxial films stretched at 90 C and 1.27 cm./sec. to a final biaxial draw ratio of 4 x 4.

molecular orientation. In addition, some dependence on blend composition is evident with moduli slightly higher for increasing poly(L-lactic acid) content. This dependence on composition is probably associated with crystallinity rather than molecular orientation.

With an estimate of the degree of crystallinity and crystal phase orientation in hand, some comments on the strain hardening behavior of the poly(lactic acid) blends biaxially stretched at 90 C are appropriate. The lack of significant strain hardening behavior at 90 C would suggest that there is very little molecular orientation occurring during the deformation. In fact, the lack of an entropy peak in DSC and only very small amounts of crystal orientation in the WAXS patterns support this conclusion. This result is particularly interesting in light of the relatively high levels of crystallinity induced in sample 100/40k. The lack of orientation is attributed to the increased mobility of amorphous molecular entanglements. At 90 C it appears that the mechanism of strain energy dissipation via entanglement slippage is very dominant, thus, preventing any support of stress through a long range network structure.

It seems reasonable to assume that both strain induced crystallization and low entanglement slippage on the time scale of the biaxial stretch are required in tandem for effective molecular orientation and strain hardening. Physical crosslinks due to strain induced crystallization and

the crosslinks due to entanglements are both required in order to enhance the elastic strength of the poly(lactic acid) blends. Thus, higher degrees of strain hardening and molecular orientation are realized at lower draw temperatures as a result of decreased entanglement slippage expected at the longer molecular relaxation times. However, strain induced crystallization also plays a crucial role in the strengthening of biaxial films as evidenced by the dependence of strain hardening on poly(L-lactic acid) concentration at the lowest temperatures of stretch (75 C). Interestingly, the influence of poly(L-lactic acid) concentration on strain hardening is the greatest at the lowest temperature suggesting that added crosslinks associated with the strain induced nuclei are more efficient in reinforcing the network at lower temperatures.

4.3.4 THE EFFECT OF STRAIN RATE ON THE STRAIN HARDENING OF ISOMER BLENDS OF POLY(LACTIC ACIDS) IN BIAXIAL DEFORMATION

As pointed out in the introduction, the strain energy dissipation by entanglement slippage, as well as strain induced crystallization, may also be altered by the rate of deformation. The effect of biaxial strain rate upon the strain hardening characteristics of poly(lactic acid) isomer blends will be addressed in this section. Whereas, in section 4.3.3 it was determined that changing the temperature of deformation at a constant deformation rate of 1.27 cm./sec. has an overriding effect on molecular entanglement tenacity, it will be demonstrated in this section that varying the deformation rate at constant temperature (80 C) has a strong influence on strain induced crystallization. Again, the biaxial stretch data for 1.27 cm./sec. and 80 C presented in section 4.3.2 will serve as a basis for comparison. In order to facilitate the comparison, the same series of four samples, 100/40k, 95/40k, 90/40k, and 75/40k, will be stretched at 80 C at two additional rates, 5.72 cm./sec. and 25.4 cm./sec.

In keeping with the previous formats, the biaxial strain hardening data from the LES will be presented first for each sample series at a given set of stretch conditions. The description of the DSC, WAXS, and mechanical data will follow. The stress relaxation of the biaxial film after the

4 X 4 stretch was not available for the experiments at the higher rates.

Figure 4.26 presents the biaxial stress-draw ratio results upon stretching the 40,000 molecular weight blend series at 80 C and 5.72 cm./sec. As all previous results have shown, strain hardening is seen to be dependent upon the blend composition with higher poly(L-lactic acid) contents favoring higher stresses. Clearly, strain induced crystallization plays a crucial role in setting up the elastic network that allows for strain hardening. The stress results, which are presented as a function of draw ratio, indicate that strain hardening at 5.72 cm./sec. has been deferred to slightly higher draw ratios as compared to the 1.27 cm./sec. data presented in Fig. 4.4. However, owing to the higher rates of deformation in Fig. 4.26, these slightly higher draw ratios, in fact, convert to a shorter time scale for the onset of strain hardening. A second point of comparison between the 80 C biaxial stretching results at 1.27 cm./sec. and 5.72 cm./sec. is critical for later points of discussion. Prior to strain hardening, in the low slope regime of the stress draw ratio curves, the stress levels at comparable blend compositions are higher at the elevated rate of deformation. Note, finally, that the final stress measured for the 1.27 cm./sec. deformation rates are higher than those measured at 5.72 cm./sec. These observations will be rationalized with the aid of the DSC and WAXS results to

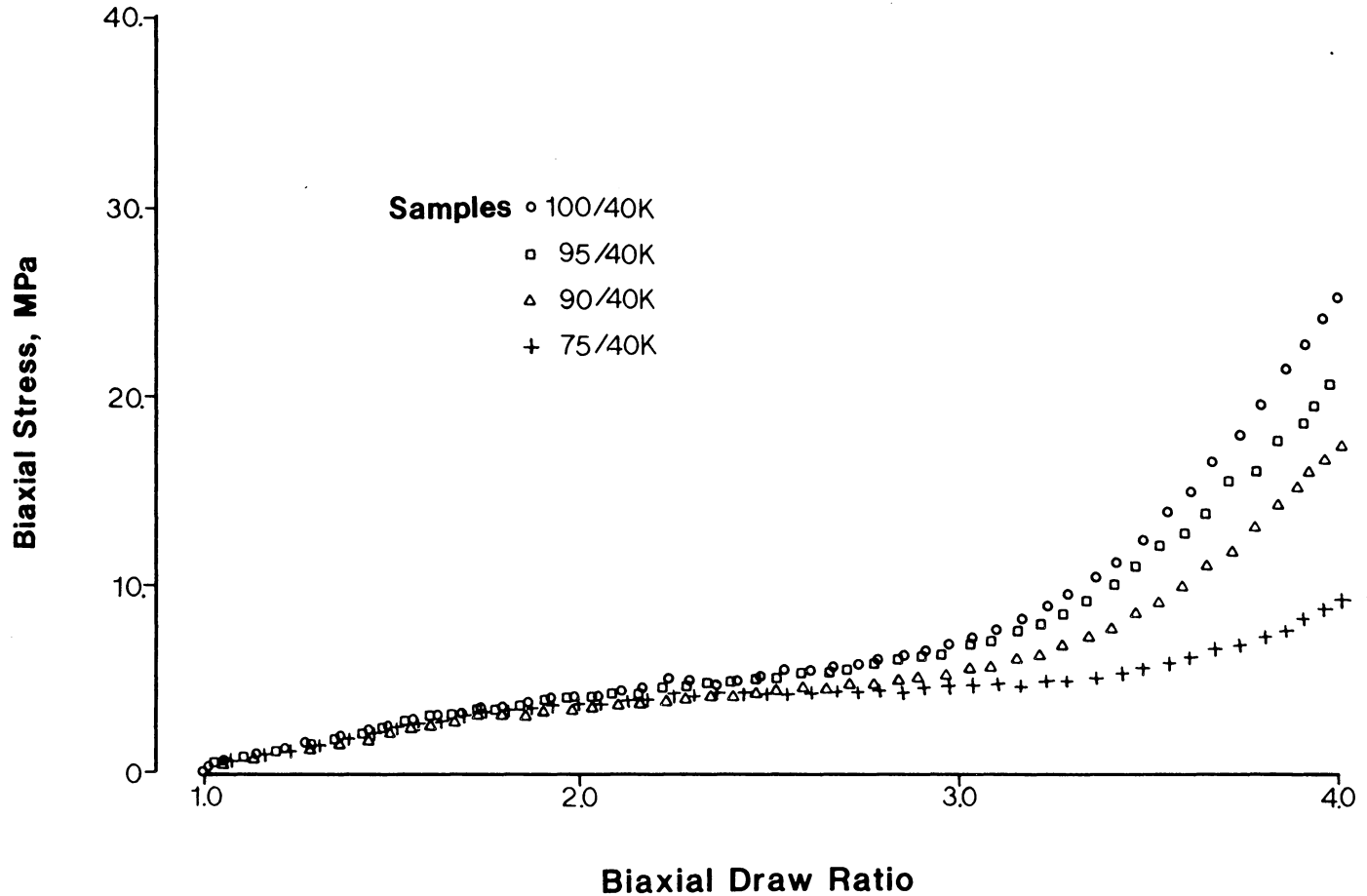

Figure 4.26. Biaxial stress vs. biaxial draw ratio for 40,000 molecular weight poly(lactic acid) blends.
Temperature: 80 C
Crosshead Speed: 5.72 cm./sec.
Final Biaxial Draw Ratio: 4 x 4

be presented next.

Figure 4.27 presents the DSC thermograms from the poly(lactic acid) blends biaxially deformed at 5.72 cm./sec. and 80 C. The general characteristics of these DSC traces are very similar in comparison to the DSC results presented in Fig. 4.6 for films stretched at 80 C and 1.27 cm./sec. The crystallinities calculated from the baseline construction as per Fig. 4.5 and measurement of the net endotherm are presented in Fig. 4.28. Within the breadth of the measurement error, the percent crystallinities in the films stretched at 5.72 cm./sec. are slightly lower than those in the films stretched at 1.27 cm./sec., see Fig. 4.7 for comparison.

Recall that in section 4.3.2, it was postulated that the majority of the chain extended crystallites were formed in the biaxially deforming films during the low slope portion of the stress draw ratio curve prior to strain hardening. In addition, it was supposed that the high level of biaxial orientation in the amorphous network chains induced during strain hardening arrested the crystallization process by restricting the mobility of the divergently oriented chain segments. This proposed mechanism is extended in order to rationalize the effects of increasing strain rates on the biaxial stress-draw ratio and DSC data.

As strain rates are increased from 1.27 cm./sec. to 5.72 cm./sec., the stress in the low slope regime of the stress

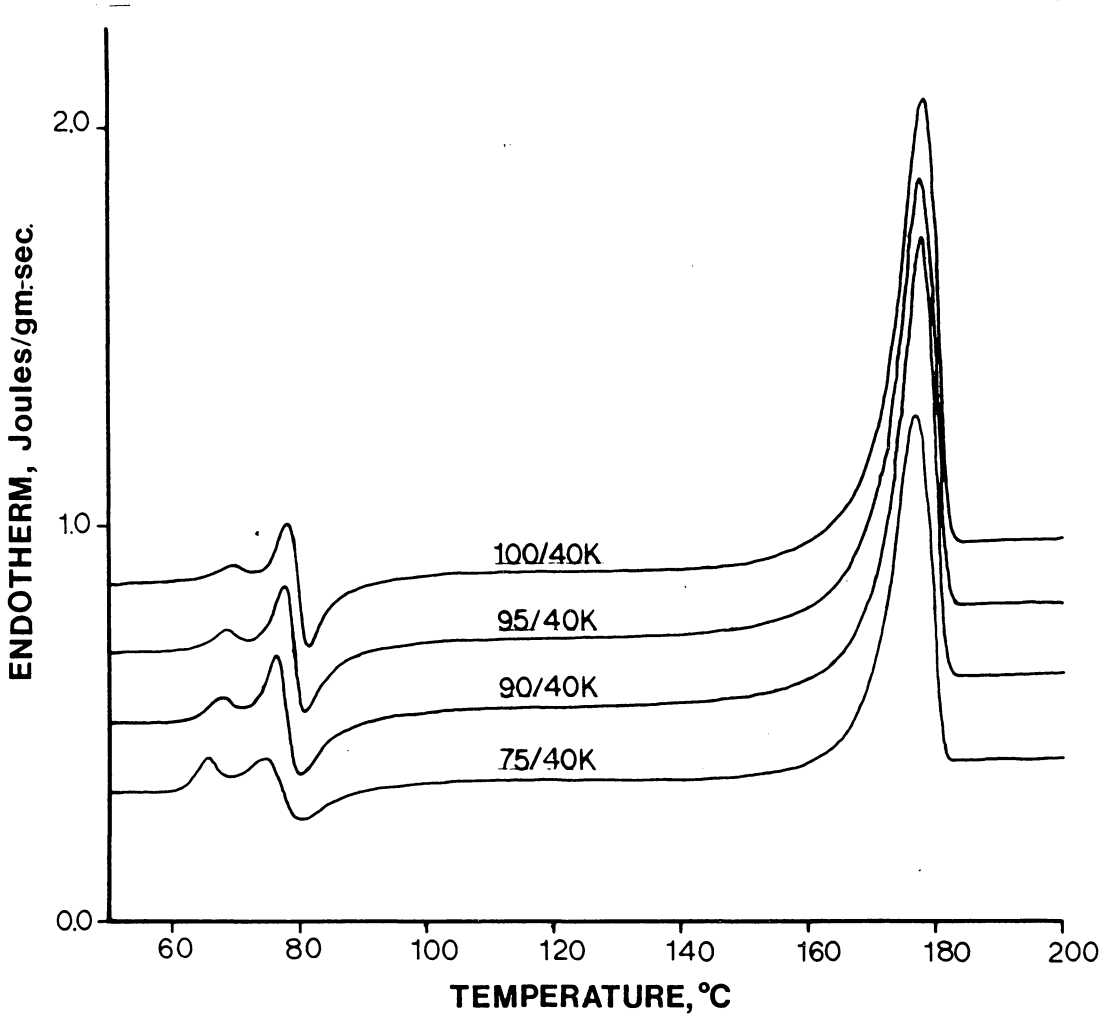

Figure 4.27. DSC thermograms of poly(lactic acid) 40,000 molecular weight blends biaxially stretched at 80 C and 5.72 cm./sec. to a final biaxial draw ratio of 4 x 4.

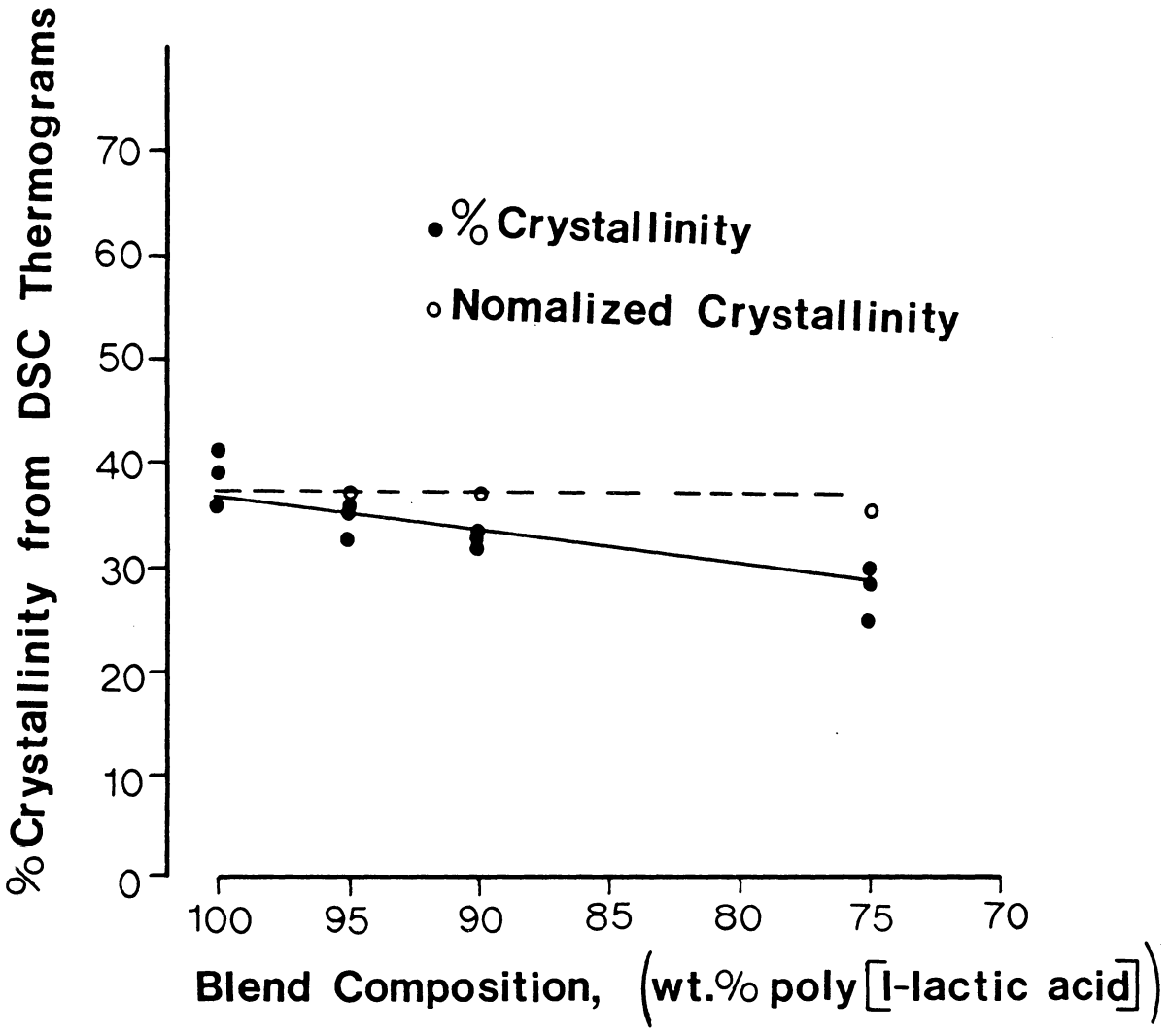

Figure 4.28. % crystallinity vs. blend composition for 40,000 molecular weight biaxial films stretched at 80 C and 5.72 cm./sec. to a final biaxial draw ratio of 4 x 4.

draw ratio curve increases. Equation 4.14 at the end of section 4.1.2 predicts that at higher stress levels the thermodynamic driving force for crystallization due to molecular orientation, ie. ΔG_{def}, is increased. As a result, the rate of strain induced nucleation predicted in Eq. 4.3 is also increased due to the functional dependence of nucleation rate on ΔG_{def}. Thus, the increased rate of strain induced crystal nucleation triggers the earlier upturn in stress at 5.72 cm./sec.

Due to the limited amount of strain allowed during the prescribed 4 X 4 stretch, the amount of deformation after the onset in strain hardening is smaller at 5.72 cm./sec. than at 1.27 cm./sec. Thus, the network set up by the strain induced crystallization is not deformed as far at 5.72 cm./sec. as it was at 1.27 cm./sec. This explains why the crystallization rates are faster at 5.72 cm./sec., however, the strain hardening is less.

At the higher strain rates the dissipation of elastic energy due to entanglement slippage is expected to be less. Therefore, at 5.72 cm./sec., a smaller number of strain induced nuclei is required in order to form an elastic network and trigger the onset of strain hardening than at 1.27 cm./sec. Recall that the since the crystallization is thought to be arrested during strain hardening, the amount of crystallinity measured by the DSC on the finished film is representative of the crystallinity required to set off

strain hardening. The slight decrease in finished film crystallinity of 44% to 40% on increasing the deformation rate rate from 1.27 cm./sec. to 5.72 cm./sec. may reflect the increased tenacity of entanglements with increasing strain rate.

The WAXS results from the blend materials stretched at 80 C and 5.72 cm./sec. are presented in Figs. 4.29 and 4.30. The diffraction ring patterns obtained with the X-ray beam normal to the film surface in Fig. 4.29 are more diffuse than the WAXS results from films stretched at 80 C and 1.27 cm./sec., see Fig. 4.8. The possibly smaller and/or less perfected crystals formed at 5.72 cm./sec. may reflect the increased crystal nucleation rates. To a first approximation the level of crystallinity in the films drawn at the two rates are the same. Equation 4.3 and 4.14 predict that the primary nucleation rates for the 5.72 cm./sec. film should be somewhat higher. Since the films stretched at 5.72 cm./sec. have a potentially greater number of crystallites, they must at the same time be smaller in order to give approximately the same overall heat of fusion on the DSC trace. Comparison of Figs. 4.30 and 4.9 indicates very little difference in orientation of the crystal phase in films stretched at 5.72 cm./sec and 1.27 cm./sec. This last result may not be of particular relevance in light of the previously demonstrated propensity for stress relaxation in these films prior to quenching from the LES. Although the stress relaxation

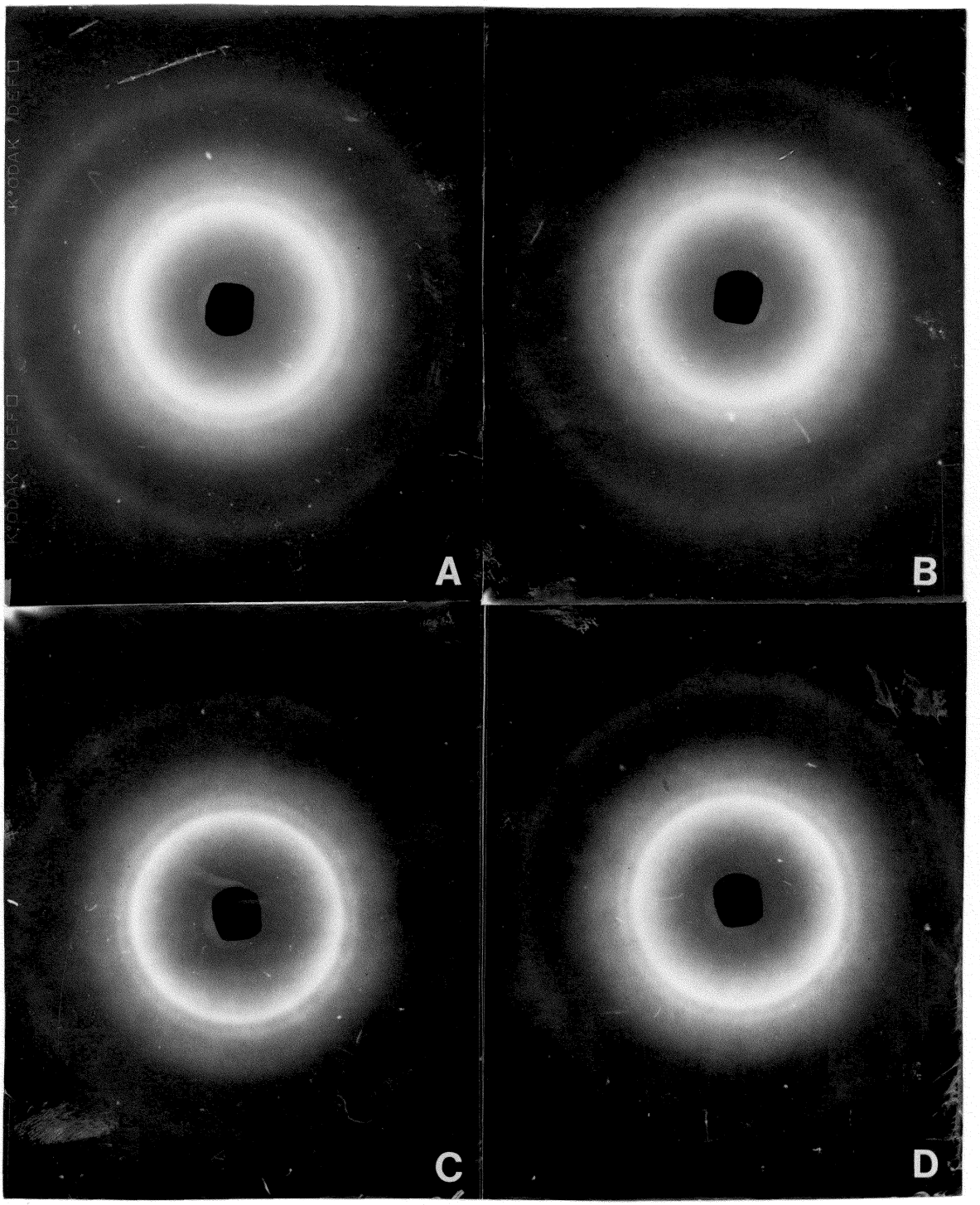

Figure 4.29. WAXS patterns for 40,000 molecular weight biaxial films stretched at 80 C and 5.72 cm./sec. to a final biaxial draw ratio of 4 x 4, X-ray beam oriented normal to film surface.
A) 100/40k B) 95/40k C) 90/40k D) 75/40k

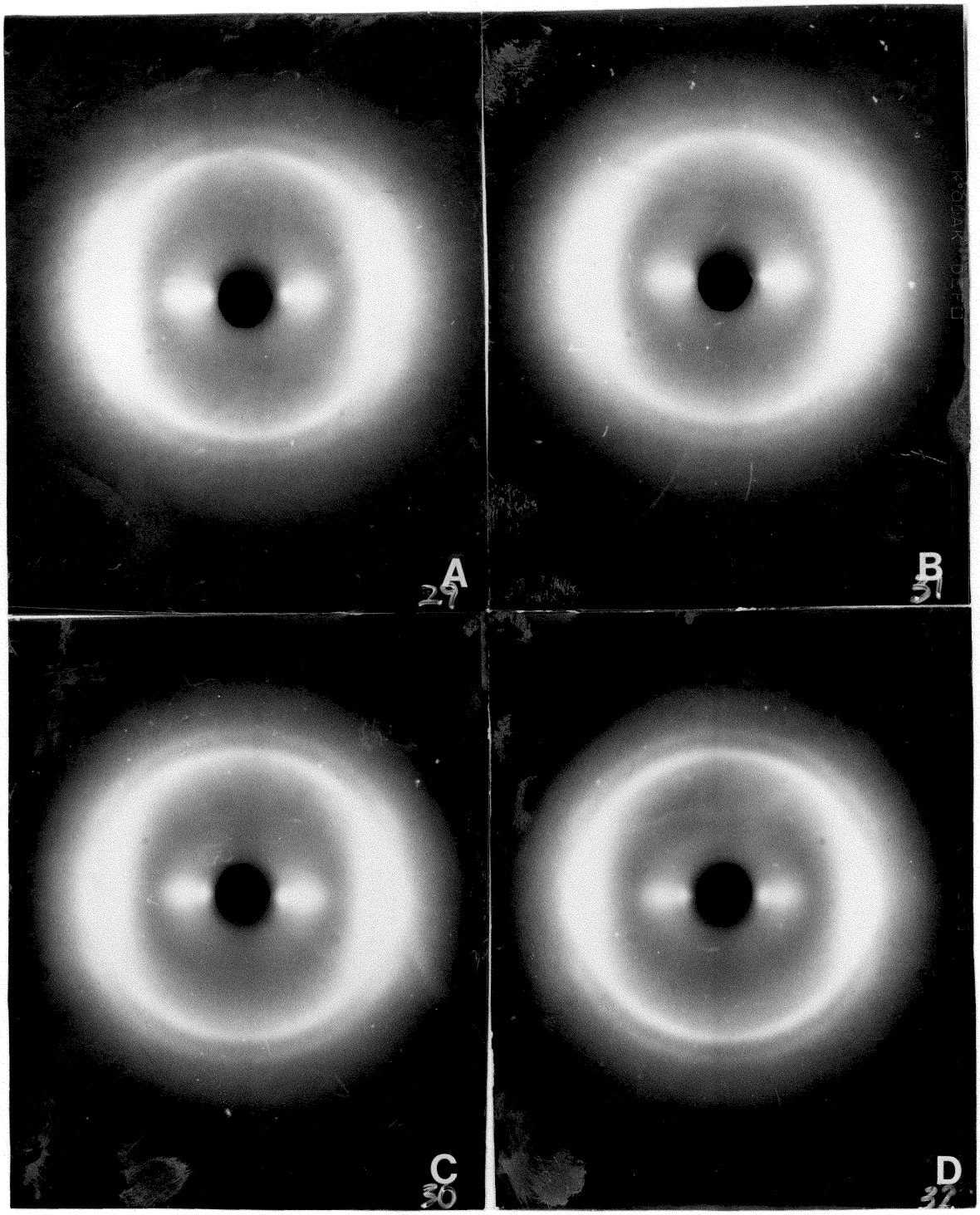

Figure 4.30. WAXS patterns for 40,000 molecular weight biaxial films stretched at 80 C and 5.72 cm./sec. to a final biaxial draw ratio of 4 x 4, X-ray beam oriented parallel to film surface.
A) 100/40k B) 95/40k C) 90/40k D) 75/40k

results are not available for the series of materials stretched at 5.72 cm./sec., it is suspected that a significant amount of relaxation is possible in these samples as well due to the similarity in crystallinity and stretch ratios.

The biaxial stress-draw ratio results, DSC thermograms, and WAXS diffraction patterns for the 40,000 molecular weight blend series stretched at 80 C and 25.4 cm./sec. are presented in Figs. 4.31-4.35. Without reiterating all the details of the rationale used to describe the data trends due to increasing the stretch rate from 1.27 cm./sec. to 5.72 cm./sec., it will suffice to say that these general trends continue up to a strain rate of 25.4 cm./sec. Note that in Fig. 4.31 at low levels of draw ratio, prior to significant strain hardening, the levels of stress continues to increase above those at 1.27 cm./sec and 5.72 cm./sec., see Figs. 4.4 and 4.26. This again enhances the rate of strain induced crystallization so that an elastic network in the biaxially deforming film is set up in a shorter time frame. Strain hardening is thus triggered faster at 25.4 cm./sec. than at either of the other two previous rates. However, the time frame in which strain hardening is initiated does not shorten in direct proportion to the increase in strain rate which defers the onset of strain hardening to higher draw ratios. The network structure is set up too late in the limited draw ratio experiment to allow for significant network

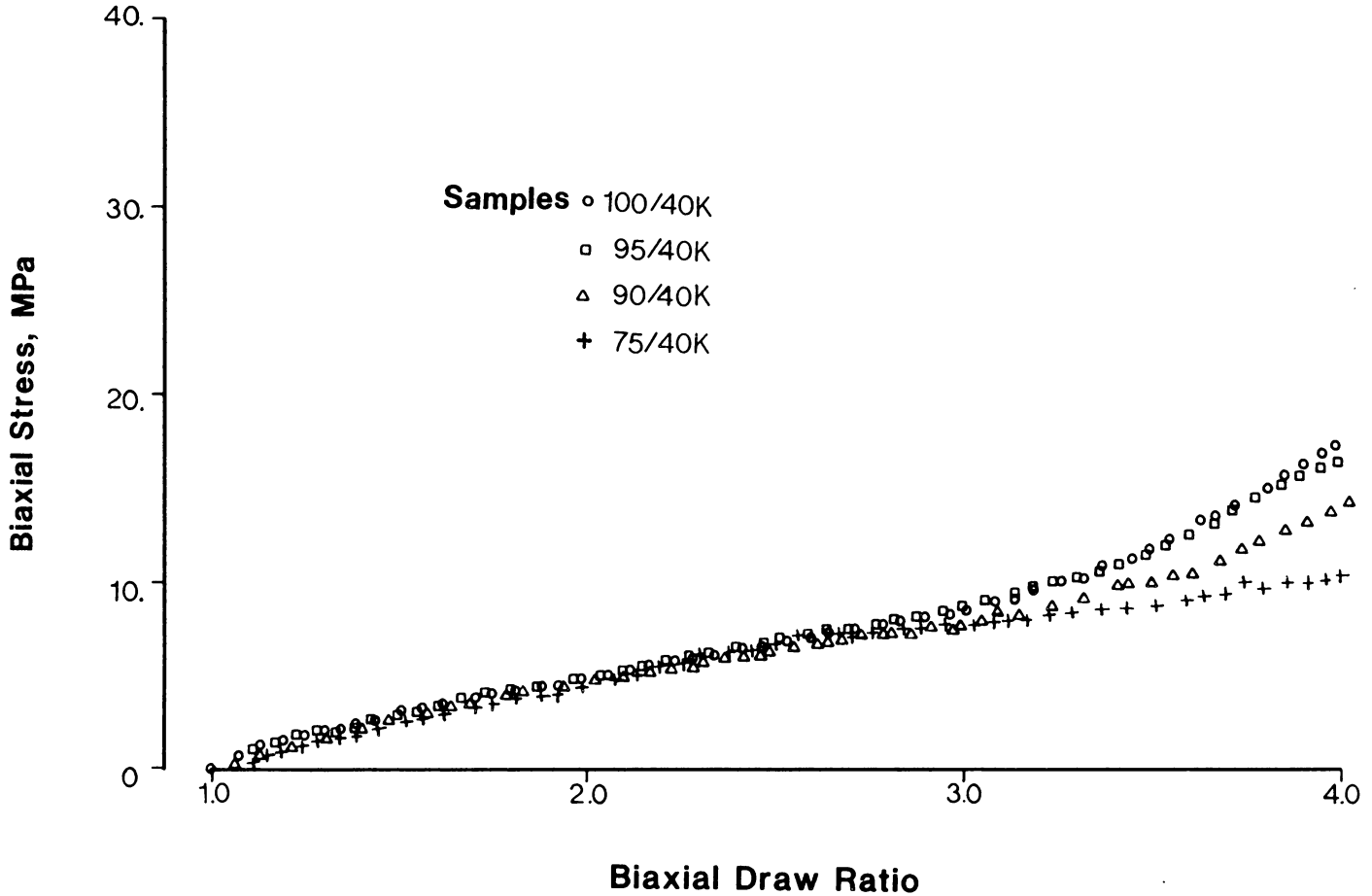

Figure 4.31. Biaxial stress vs. biaxial draw ratio for 40,000 molecular weight poly(lactic acid) blends.
Temperature: 80 C
Crosshead Speed: 25.4 cm./sec.
Final Biaxial Draw Ratio: 4 x 4

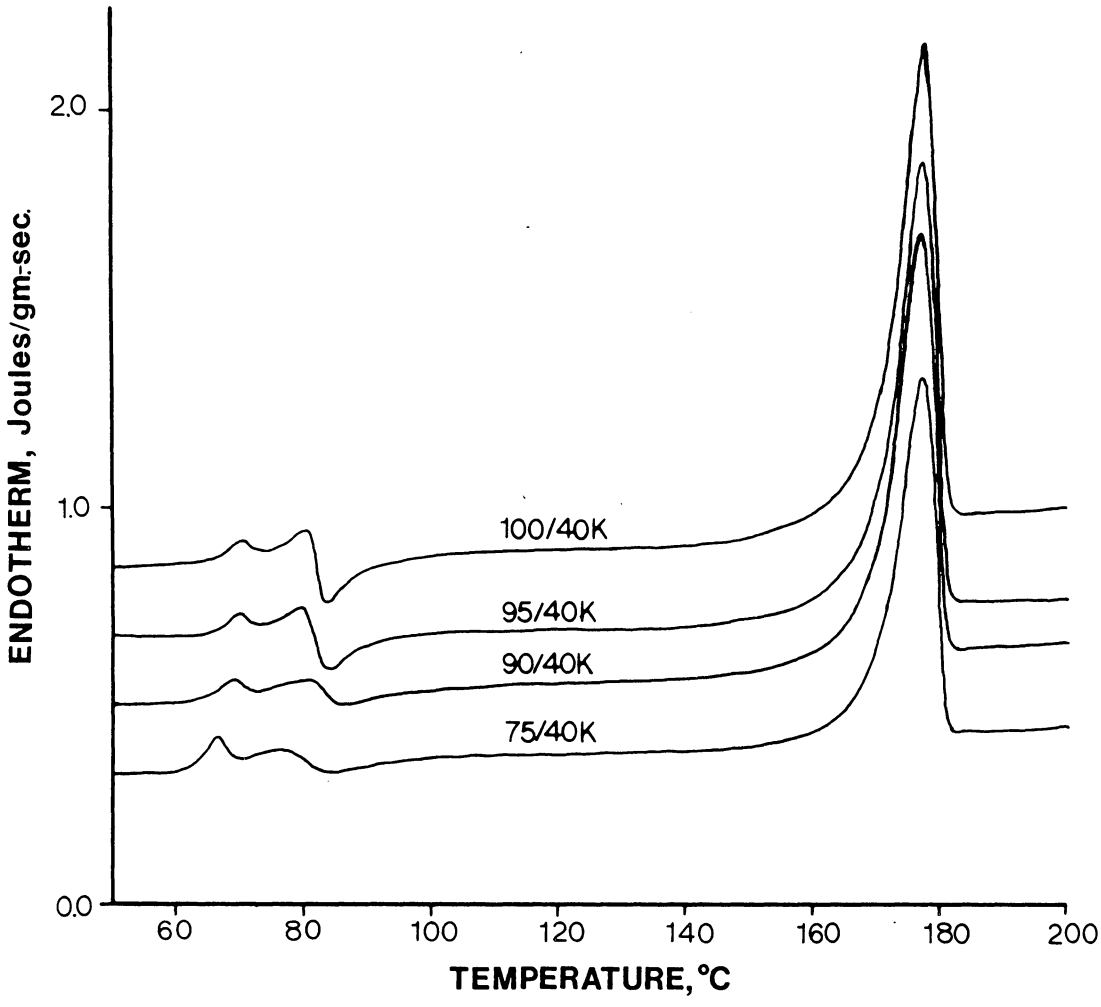

Figure 4.32. DSC thermograms of poly(lactic acid) 40,000 molecular weight blends biaxially stretched at 80 C and 25.4 cm./sec. to a final biaxial draw ratio of 4 x 4.

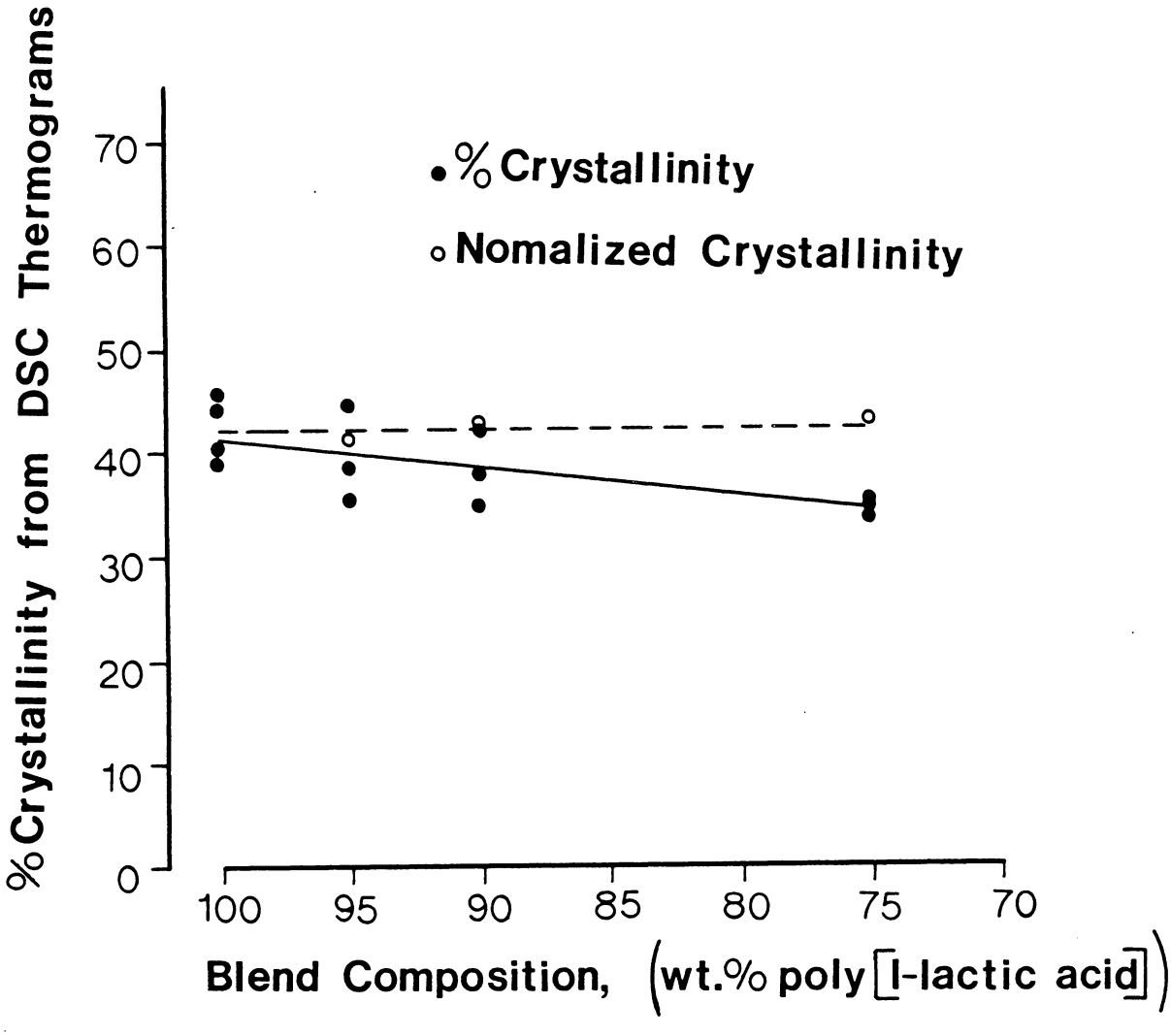

Figure 4.33. % crystallinity vs. blend composition for 40,000 molecular weight biaxial films stretched at 80 C and 25.4 cm./sec. to a final biaxial draw ratio of 4 x 4.

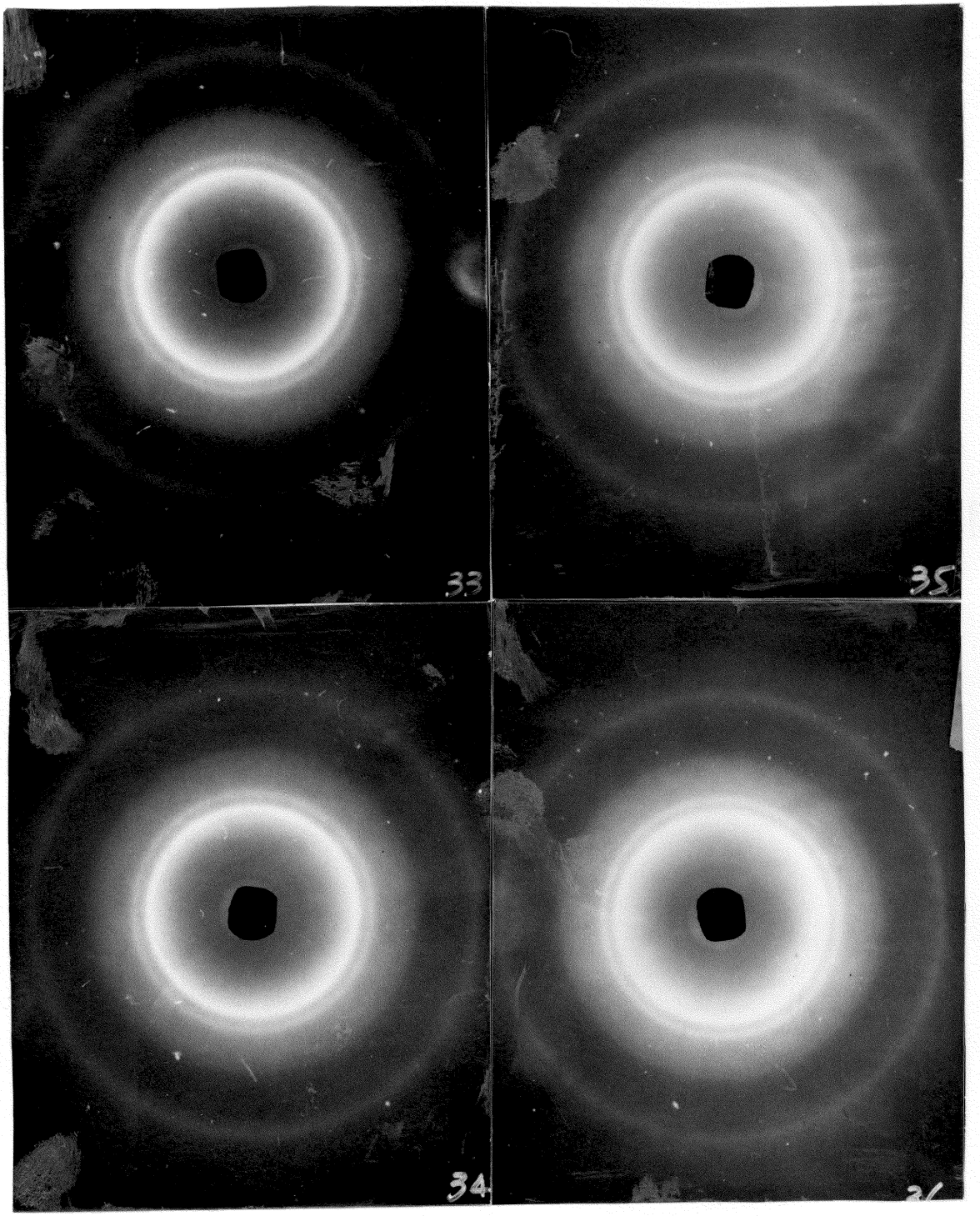

Figure 4.34. WAXS patterns for 40,000 molecular weight biaxial films stretched at 80 C and 25.4 cm./sec. to a final biaxial draw ratio of 4 x 4, X-ray beam oriented normal to film surface.
A) 100/40k B) 95/40k C) 90/40k D) 75/40k

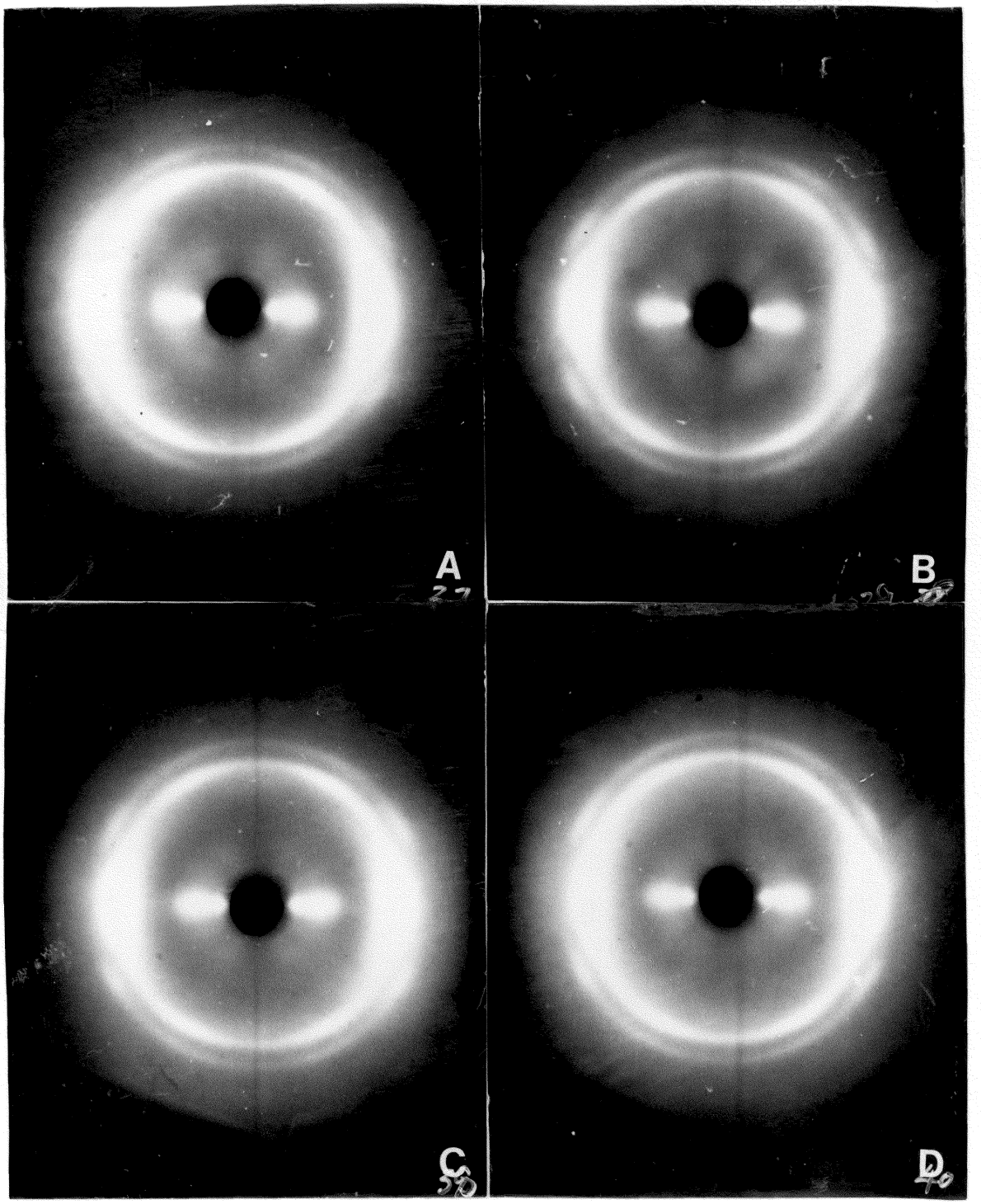

Figure 4.35. WAXS patterns for 40,000 molecular weight biaxial films stretched at 80 C and 25.4 cm./sec. to a final biaxial draw ratio of 4 x 4, X-ray beam oriented parallel to film surface.
A) 100/40k B) 95/40k C) 90/40k D) 75/40k

deformation. As a consequence, only limited amorphous orientation and strain hardening are realized.

At this juncture, a second rationale is offered in order to explain the reduced strain hardening in biaxial deformation at increasing deformation rates. A number of authors (95,96) have postulated that in the uniaxial deformation of amorphous poly(ethylene terephthalate) above its glass transition temperature, the initial temperatures of the samples are increased due to the viscous dissipation of mechanical energy into heat. This phenomenon becomes especially acute at higher rates of deformation (96). If this mechanism is operative on the poly(lactic acid) blends stretched at 25.4 cm./sec., then the reduced strain hardening may well be attributed to an increase in sample temperature beyond the 80 C set point. As demonstrated in section 4.3.3, this will lead to increased mobility of amorphous chain entanglements and less strain hardening.

Figure 4.32 is a composite of four DSC thermograms for each of the four blend compositions stretched at 80 C and 25.4 cm./sec. The general characteristics of the traces are very similar to the DSC traces taken of films stretched at the other two rates, see Figs. 4.6 and 4.27. Note, in particular, the small entropy peaks in Fig. 4.32 which reflect the low deformation of the network structure and amorphous chain segments suggested by the low levels of strain hardening in Fig. 4.31.

The slightly increased crystallinities reported in Fig. 4.33 for 25.4 cm./sec., as compared to the crystallinities at 1.27 cm./sec. and 5.72 cm./sec. reported in Figs. 4.7 and 4.28, may indicate a propensity for the material to crystallize throughout the biaxial deformation unarrested by the onset of a strain hardening. This, in fact, may be accelerated by the viscous heating of the material at this highest rate. The mobility of the amorphous chains suggested by the low levels of strain hardening may allow crystallizations in the 25.4 cm./sec. samples at draw ratios approaching 4 X 4 whereas, in previous samples, the more highly oriented network structures restricted crystallization.

Figures 4.34 presents the WAXS diffraction patterns for these films stretched at 25.4 cm./sec. with the incident X-ray beam normal to the film surface. The slightly improved diffraction ring resolution over those from films stretched at 5.72 cm./sec., see Fig. 4.29, may confirm the crystallization mechanism proposed to explain the DSC data. The enhanced endotherms of fusion in the DSC data for the 25.4 cm./sec. films may just be due to crystallite perfection under low stresses during the final stages of stretching.

At these very highest rates of biaxial deformation, the WAXS diffraction patterns in Fig. 4.35 indicate an enhanced level of orientation not as yet seen in these poly(lactic acid) biaxial films. The azimuthal intensity functionality

in the (110)/(200) and (113)/203) reflections seems to indicate a transition from a planar orientation to a uniplanar orientation. This latter type of film orientation features a more distinct crystallite orientation. Not only does the orientation require the C axis to be parallel to the film plane, but it is suggested that the (010) plane of the unit cell is parallel to the plane of the film as well. Note that this type of orientation has also been seen in biaxial films of poly(ethylene terephthalate) (11,95). It seems appropriate to point out that this improved crystal orientation is obtained with very little strain hardening at 25.4 cm./sec. This suggests that the crystallinity and orientation are developed to a significant extent in the low stress regions of the stress trajectory prior to strain hardening and that subsequent strain hardening is primarily due to amorphous chain segment orientations in elastic networks. The network structures are composed of crosslinks made up of both strain induced crystal nuclei and amorphous chain entanglements.

For the sake of completeness, the tensile modulus data for the films stretched at 5.72 cm./sec. and 25.4 cm./sec. are presented in Figs. 4.36 and 4.37. If the stress relaxation after biaxial stretch could have been prevented with a more adequate film quench, it is supposed that the modulus data in Figs. 4.12, 4.36 and 4.37. would possibly show more variation with blend composition and strain rate.

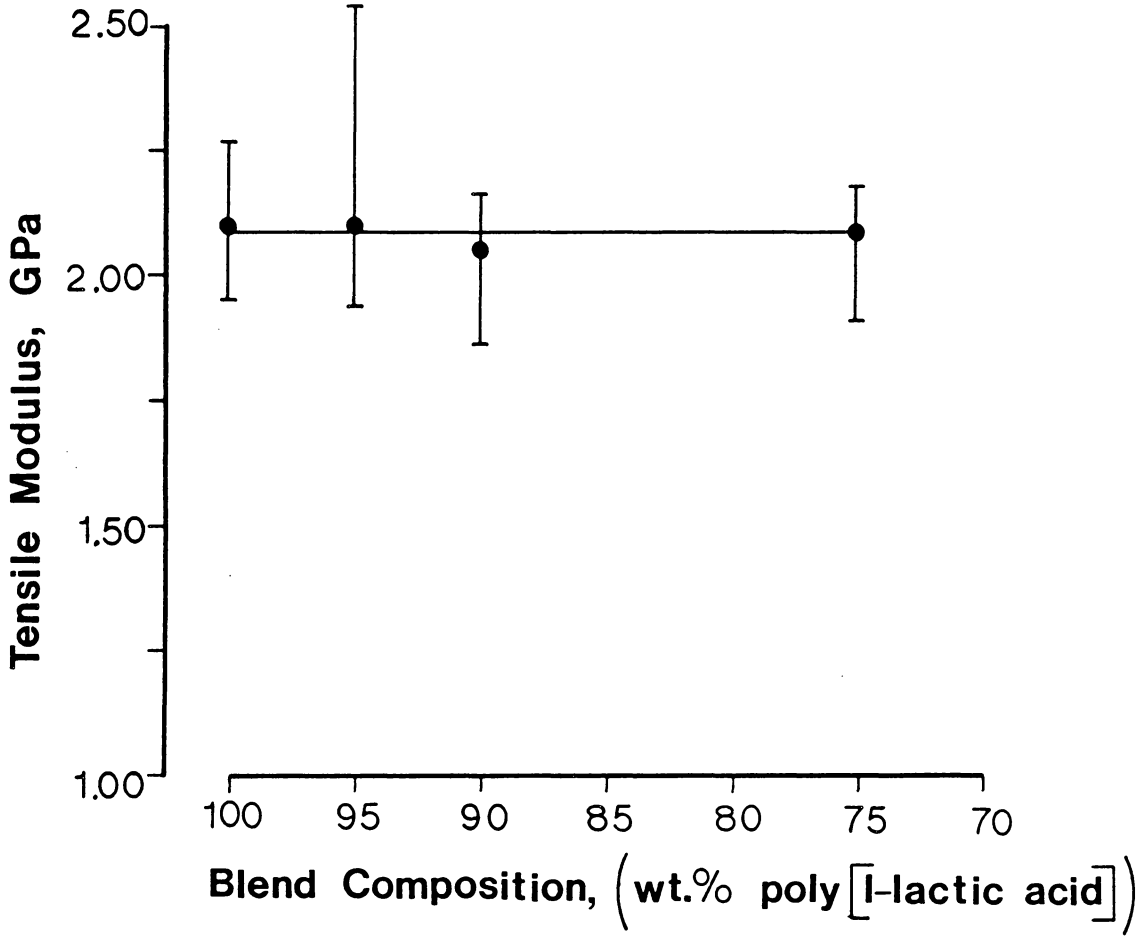

Figure 4.36. Tensile modulus vs. blend composition for 40,000 molecular weight biaxial films stretched at 80 C and 5.72 cm./sec. to a final biaxial draw ratio of 4 x 4.

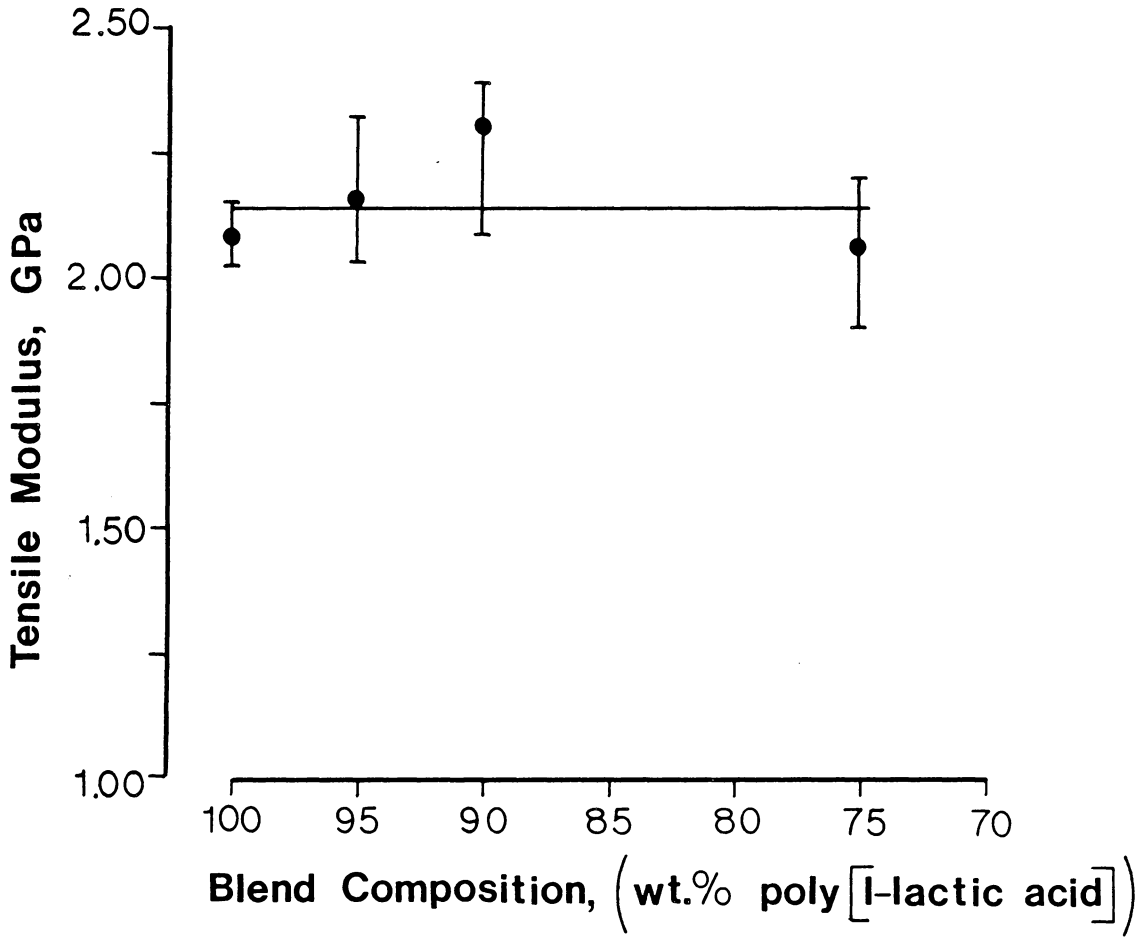

Figure 4.37. Tensile modulus vs. blend composition for 40,000 molecular weight biaxial films stretched at 80 C and 25.4 cm./sec. to a final biaxial draw ratio of 4 x 4.

The anticipated result would suggest that the tensile moduli should follow directly with strain hardening in all the films. However, the stress relaxation during quench probably results in a diminishment of the amorphous phase orientation shown to be responsible for a large part of the mechanical strength in biaxial films (13).

The overall effect of increasing the strain rate of biaxial deformation has been to increase the rate of strain induced crystallization. In effect, the strain induced nuclei augment the amorphous chain entanglements with additional physical crosslinks and convert the originally amorphous thermoplastic to a rubberlike network material above Tg. Strain hardening has been postulated to be a consequence of the deformation of this network structure. Due to the fact that this crystallization rate does not increase in proportion to the strain rate, the strain hardening of the films at higher strain rates is postponed to higher biaxial draw ratios. Under the experimental constraints imposed by a constant biaxial draw ratio of 4 X 4, the strain hardening in films stretched at higher strain rates is diminished. In addition, it is postulated that at the very highest biaxial strain rates, a significant amount of viscous heating of the sample may cause a reduced tenacity of the entanglement structure and, thus, prevent strain hardening.

4.3.5 THE EFFECT OF MOLECULAR WEIGHT ON THE STRAIN HARDENING OF ISOMER BLENDS OF POLY(LACTIC ACIDS) IN BIAXIAL DEFORMATION

The molecular weight of an amorphous material is known to affect the mechanical response in biaxial flow at temperatures just above the glass transition (13). As the molecular weight is increased, the number of chain ends per unit volume of material decreases proportionately. In turn, this is thought to diminish the ability of the material to dissipate strain energy through entanglement slippage and, therefore, lead to enhanced strain hardening. Again, this effect is due to an increased number of chain entanglements per molecule and a concomitant increase in molecular relaxation times. This section presents results aimed at determining the effects of molecular weight upon the strain hardening behavior of poly(lactic acid) blends. As pointed out in section 4.3.1, the isomers of poly(lactic acid) are no longer miscible at a molecular weight of 120,000. However, the results of biaxially orienting these higher molecular weight blended materials was nevertheless perused. To this end, the same experimental methodology discussed in sections 4.3.2, 4.3.3, and 4.3.4 was applied to the samples 100/120k, 95/120k, 90/120k, and 75/120k biaxially stretched at 90 C and 25.4 cm./sec. In order to test some of the hypotheses presented in the last several sections, the biaxial films were taken to two final draw ratios, 3 X 3 and 4 X 4, in two

distinct sets of experiments. The new variable of draw ratio is isolated in order to determine the correspondence between the strain induced crystallization profile and the onset of strain hardening in the biaxial deformation. The discussion begins with a presentation of additional 40,000 molecular weight blend series films also biaxially stretched at 90 C and 25.4 cm./sec. The 40,000 molecular weight data will serve as a basis for comparison in the analysis of the 120,000 molecular weight results.

Figure 4.38 illustrates the strain hardening behavior of the miscible 40,000 molecular weight blend series at 90 C and 25.4 cm./sec. Although the series does show some strain hardening which is enhanced by the increased content of poly(L-lactic acid) in the blend, it would seem that at this temperature the energy dissipation by entanglement slippage dominates. Again, this effect may be accentuated by viscous heating of the material which is a strong possibility at this high rate of deformation. Overall, very little strain hardening is in evidence suggesting that there is also very little amorphous phase orientation. In comparison to the 90 C results presented in Fig. 4.20 of section 4.3.3 for a strain rate of 1.27 cm./sec., only a slight improvement in strain hardening is realized by increasing the rate to 25.4 cm./sec.

Differential scanning calorimetry thermograms on the 40,000 molecular weight series shown in Fig. 4.39 indicates

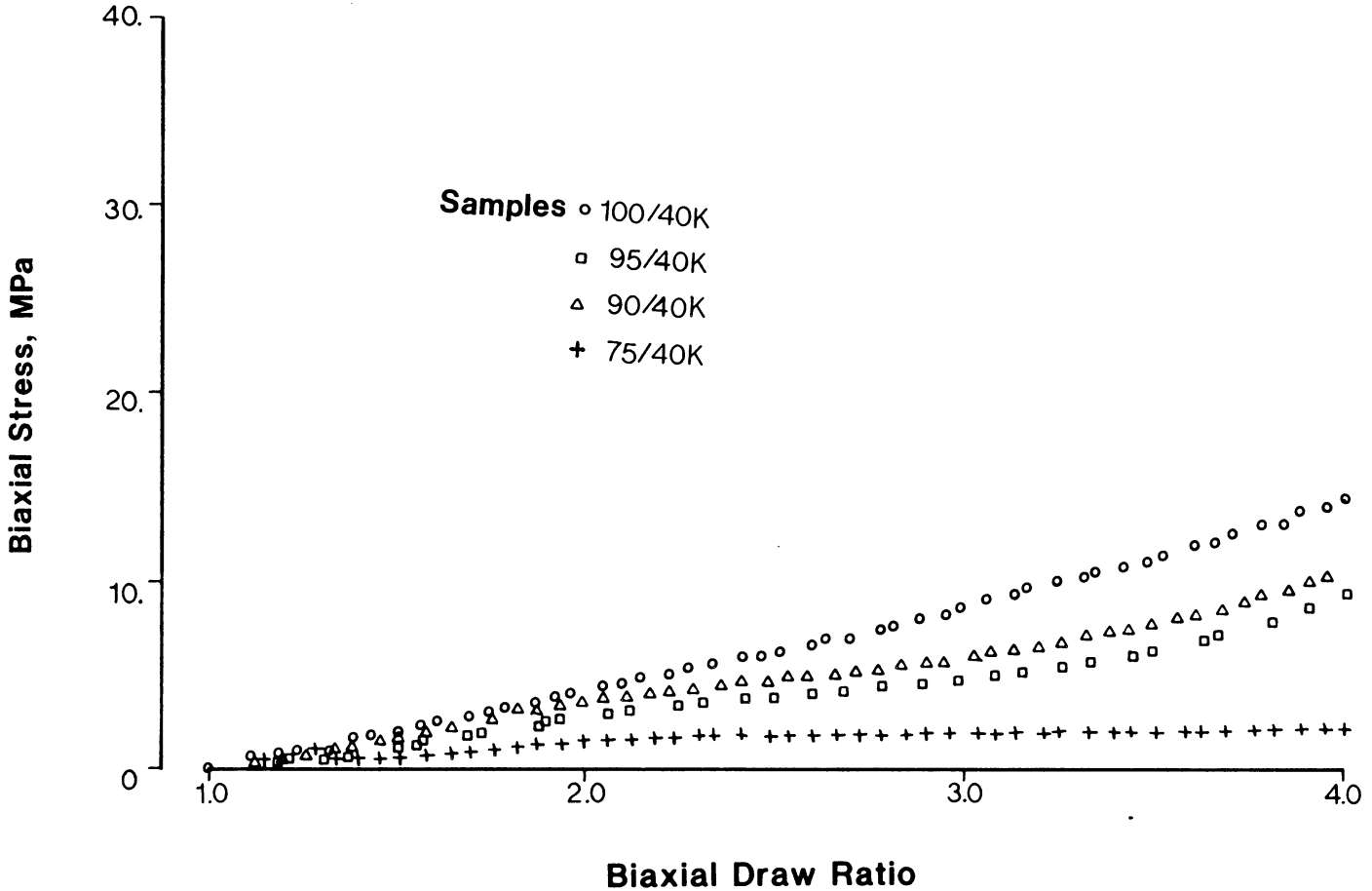

Figure 4.38. Biaxial stress vs. biaxial draw ratio for 40,000 molecular weight poly(lactic acid) blends.
Temperature: 90 C
Crosshead Speed: 25.4 cm./sec.
Final Biaxial Draw Ratio: 4 x 4

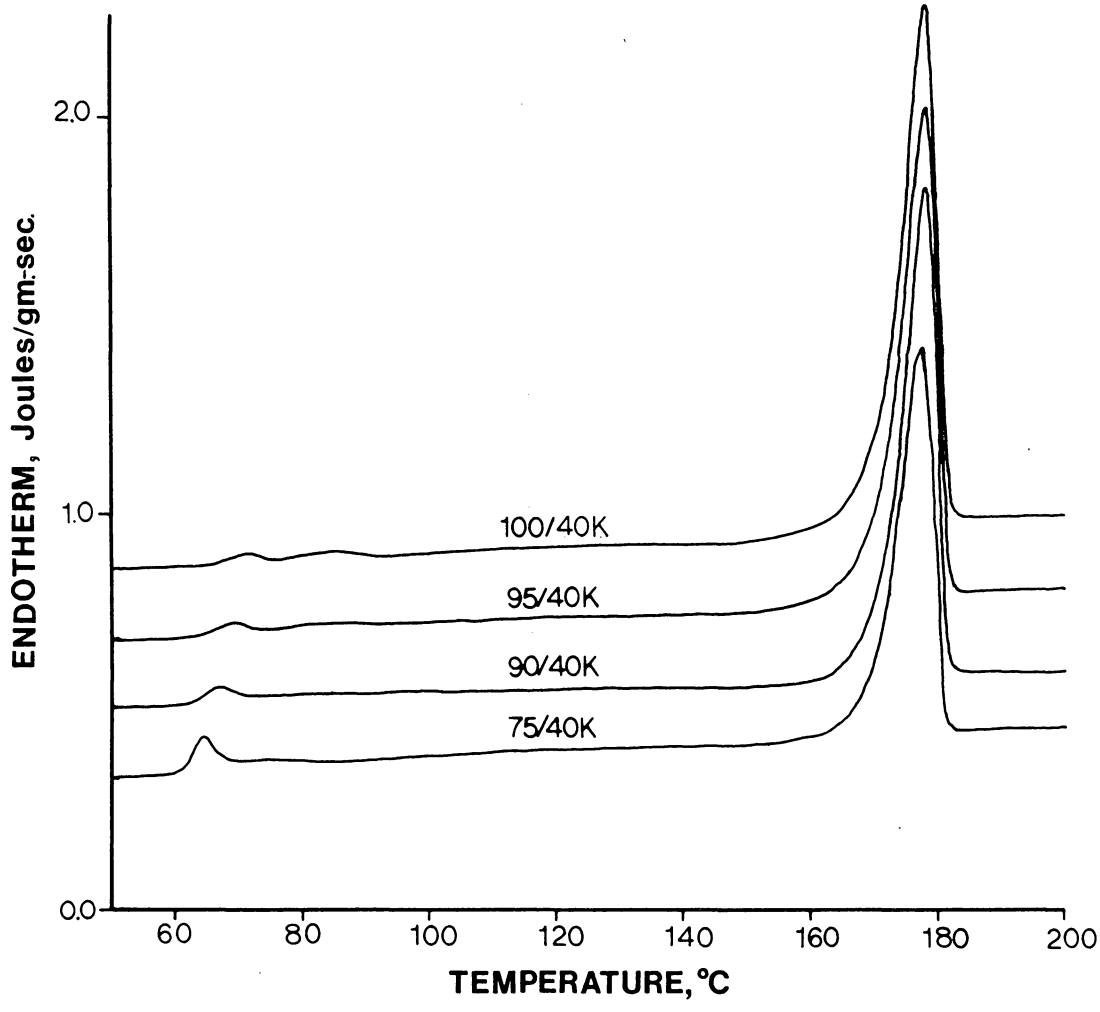

Figure 4.39. DSC thermograms of poly(lactic acid) 40,000 molecular weight blends biaxially stretched at 90 C and 25.4 cm./sec. to a final biaxial draw ratio of 4 x 4.

very little amorphous orientation as evidenced by the lack of any entropy peak. In addition, low exothermic crystallization peaks during the heating scan suggest high levels of crystallinity in the as stretched films. In fact, Fig. 4.40 reports the highest crystallinities yet reported for 40,000 molecular weight biaxial films. Once normalized on the basis of poly(L-lactic acid) content, all films show approximately 57 percent crystallinity. Even this high level of crystallinity would not reinforce the network structure to the point where it would support significant strain hardening.

The WAXS patterns in Fig. 4.41 confirm the high levels of crystallinity by exhibiting relatively intense diffraction peaks. Crystal phase orientation, as characterized by the WAXS diffraction patterns in Fig. 4.42, is significantly higher than that induced in the biaxial stretch of the same material at 90 C and 1.27 cm./sec., see Fig. 4.24. This could suggest that the enhanced biaxial strain rates, even at this elevated temperature, triggered the formation of significant amounts of chain extended crystallites. Recall, it was postulated that the precipitous drop off in crystallinity with increasing racemic content for the biaxial films stretched at 90 C and 1.27 cm./sec. was attributed to a preferred chain folding crystallization mechanism. Due to the relatively high number of chain ends per unit volume and the higher molecular mobility expected at 90 C, the

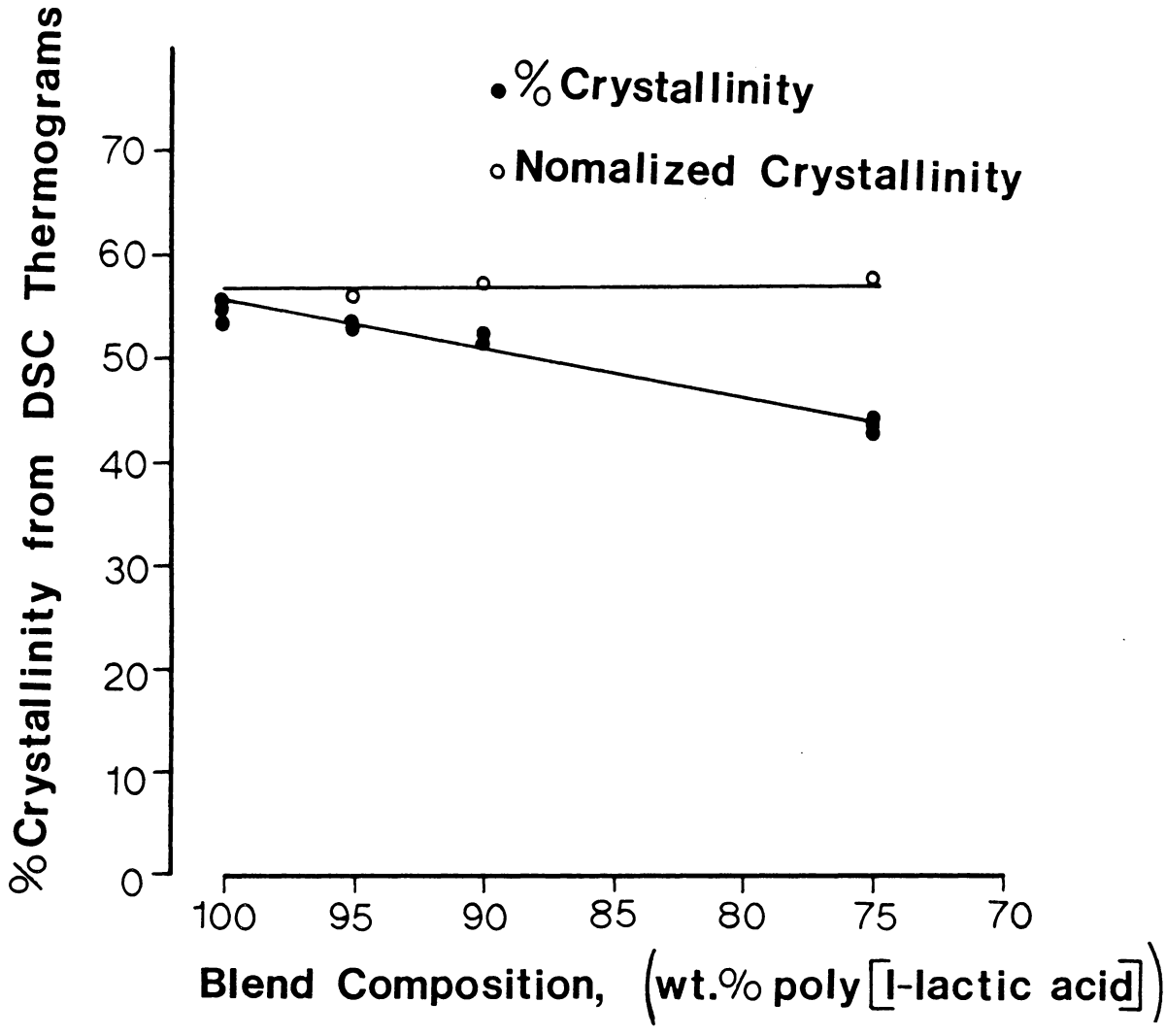

Figure 4.40. % crystallinity vs. blend composition for 40,000 molecular weight biaxial films stretched at 90 C and 25.4 cm./sec. to a final biaxial draw ratio of 4 x 4.

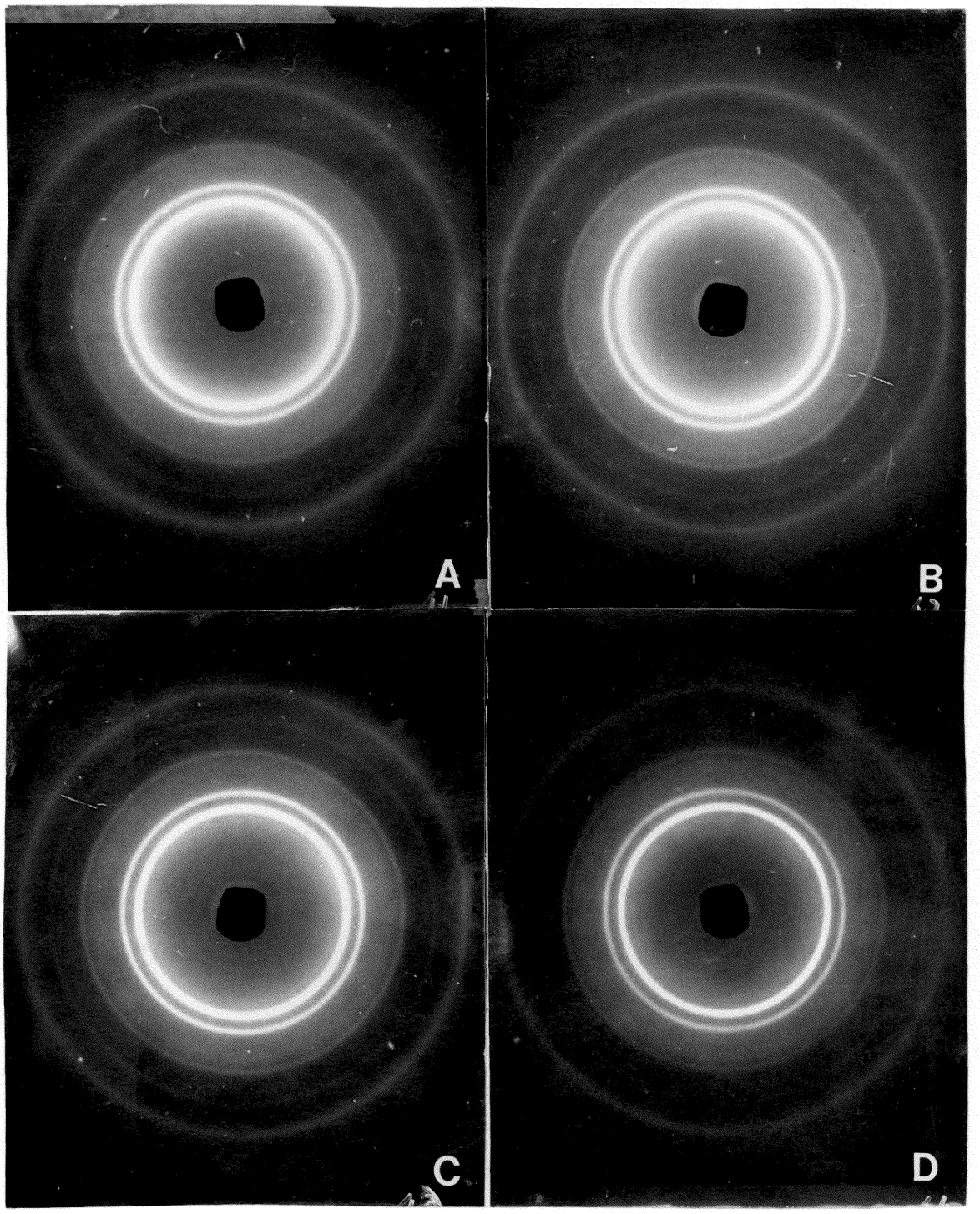

Figure 4.41. WAXS patterns for 40,000 molecular weight biaxial films stretched at 90 C and 25.4 cm./sec. to a final biaxial draw ratio of 4 x 4, X-ray beam oriented normal to film surface.
A) 100/40k B) 95/40k C) 90/40k D) 75/40k

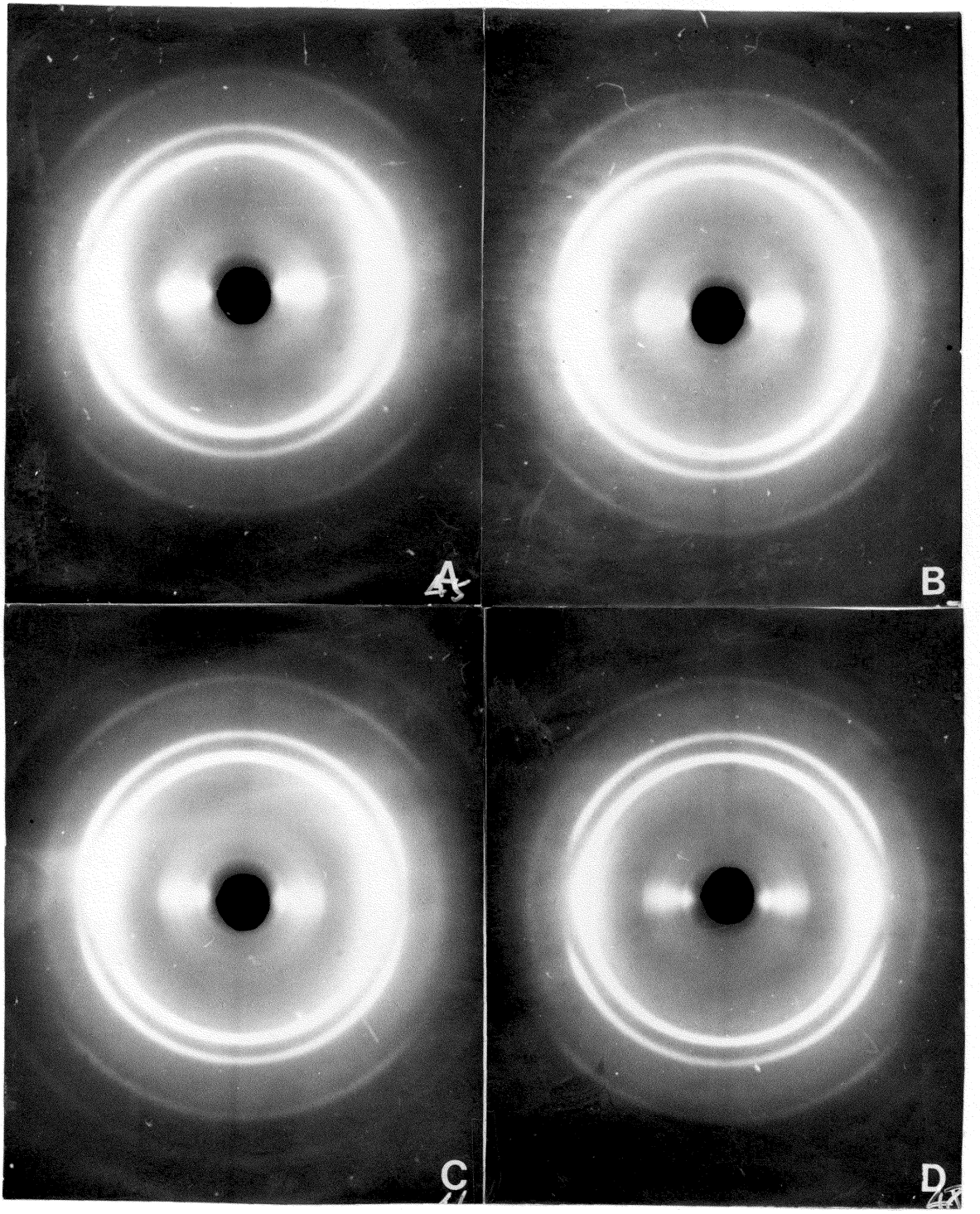

Figure 4.42. WAXS patterns for 40,000 molecular weight biaxial films stretched at 90 C and 25.4 cm./sec. to a final biaxial draw ratio of 4 x 4, X-ray beam oriented parallel to film surface.
A) 100/40k B) 95/40k C) 90/40k D) 75/40k

entanglement slippage is fast enough so as not to allow any significant storage of elastic strain energy at either 1.27 cm./sec. or 25.4 cm./sec. Even with the extended chain crystallization at 25.4 cm./sec., no strain hardening is anticipated if entanglement structure will not support a stress. Thus, for the 40,000 molecular weight series stretched at 90 C, very little strain hardening could be achieved at any strain rate investigated within the experimental program.

The tensile moduli of the four blend films stretched at 90 C and 25.4 cm./sec. are reported in Fig. 4.43. Compared to the moduli reported in Fig. 4.25 for films stretched at 90 C and 1.27 cm./sec., there is an improvement in mechanical response attributed to the slight improvement in strain hardening seen in Fig. 4.38. Although higher crystallinities and higher crystal orientation will contribute to the improved moduli, it is generally considered that the large share of improvement in tensile modulus is attributable to the amorphous phase orientation associated with the slight increase in strain hardening at the highest strain rates.

Figure 4.44 presents the strain hardening characteristics of the 120,000 molecular weight series stretched to a final biaxial draw ratio of 4 X 4. In comparison with the results described above for the similar biaxial deformation of the 40,000 molecular weight blend series, significantly improved strain hardening is clearly

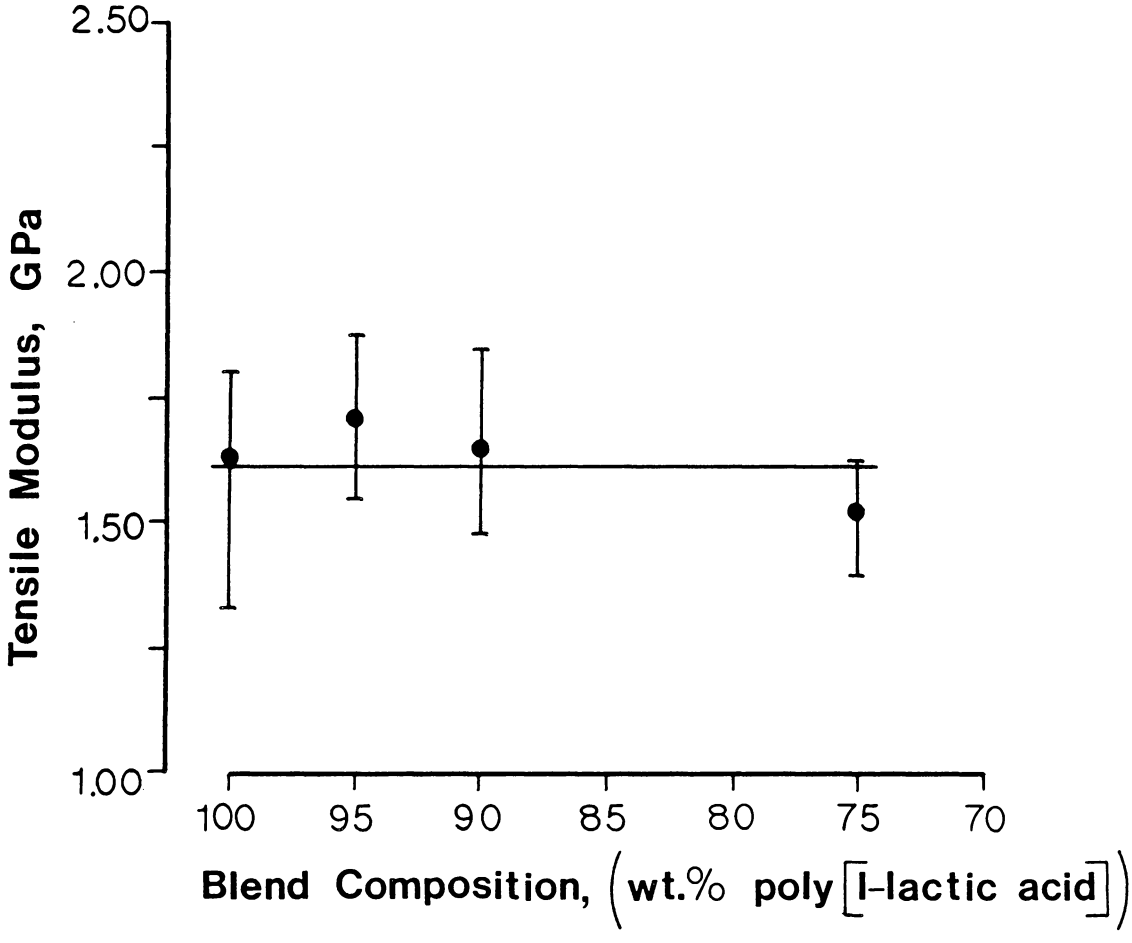

Figure 4.43. Tensile modulus vs. blend composition for 40,000 molecular weight biaxial films stretched at 90 C and 25.4 cm./sec. to a final biaxial draw ratio of 4 x 4.

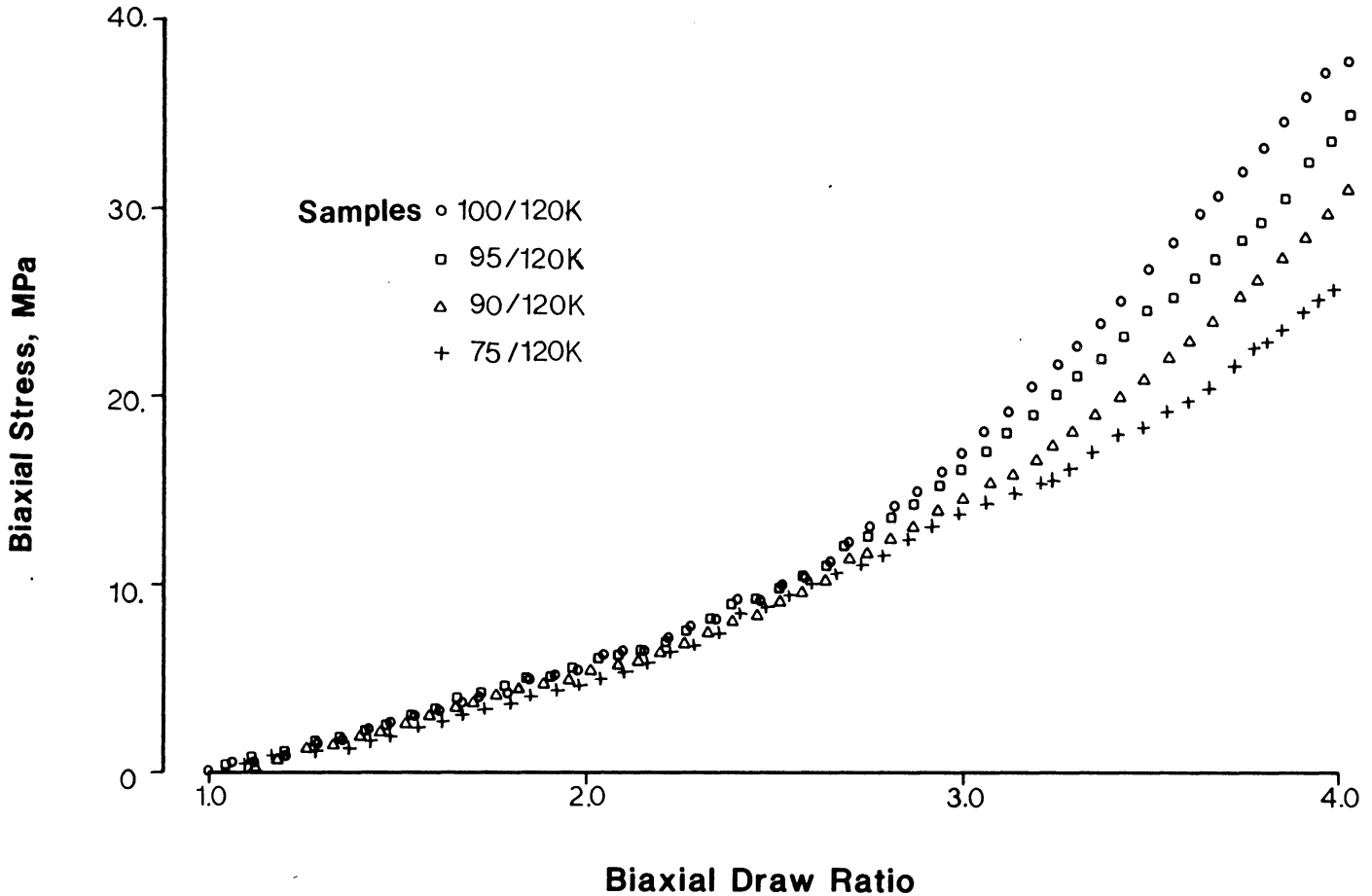

Figure 4.44. Biaxial stress vs. biaxial draw ratio for 120,000 molecular weight poly(lactic acid) blends.
Temperature: 90 C
Crosshead Speed: 25.4 cm./sec.
Final Biaxial Draw Ratio: 4 x 4

demonstrated at the higher molecular weights. Despite the fact that the blend series at 120,000 molecular weight is not a miscible mixture, the influence of poly(L-lactic acid) content on strain hardening is, in general, quite similar to previous results. Increased content of the crystallizable optically active component increases the strain hardening in the biaxial stretch, ostensibly, due to the previously outlined strain induced crystallization mechanism. Note, also, that the drop off in strain hardening with decreasing poly(L-lactic acid) content is not as precipitous in this higher molecular weight series. At this point it is difficult to say whether the relatively lower dependence of final biaxial stress upon composition is due to immiscibility auguments or to molecular weight effects.

Again, it should be pointed out that both amorphous chain entanglements and strain induced nuclei contribute, in tandem, to the network structure necessary for strain hardening. As previously demonstrated for the 40,000 molecular weight blend series, and as will be demonstrated for the 120,000 molecular weight blend series, strain induced crystallization is quite substantial for biaxial stretching at 90 C and 25.4 cm./sec. Increased molecular weight diminishes the dissipation of mechanical energy through entanglement slippage, thus, enhancing the contribution of chain entanglements to the network structure and allowing for strain hardening in the 120,000 molecular weight blend

series.

Figure 4.45 is a composite of the thermograms from the DSC scans of the four 120,000 molecular weight blends stretched at 90 C and 25.4 cm./sec. The increased amorphous chain segment orientation associated with strain hardening is clearly evidenced by the entropy peaks now present after Tg. Note that the Tg behavior is now a bit more complex. The low temperature portion of the thermograms has been expanded in Fig. 4.45 to bring out the dual glass transition behavior exhibited by the immiscible 120,000 molecular weight blends.

Figure 4.46 shows the biaxial film crystallinities calculated from the net endotherms from the DSC traces. The crystallinity is also proportional to the poly(L-lactic acid) content in the higher molecular weight immiscible blends. Thus, the normalized crystallinities, approximately 47%, remain invariant with composition in much the same manner as was observed for the lower molecular weight miscible blends.

WAXS diffraction patterns for this higher molecular weight series are presented in Figs. 4.47 and 4.48. The diffraction patterns for incident X-ray beam normal to the film surface indicate relatively high levels of crystallinity supporting the DSC results. Diffraction patterns for the film samples positioned with the plane of the film parallel to the film surface indicate a uniplanar orientation for the (110)/(200) and (113)/(203) reflections. The increased crystal phase order can also rationalized from a molecular

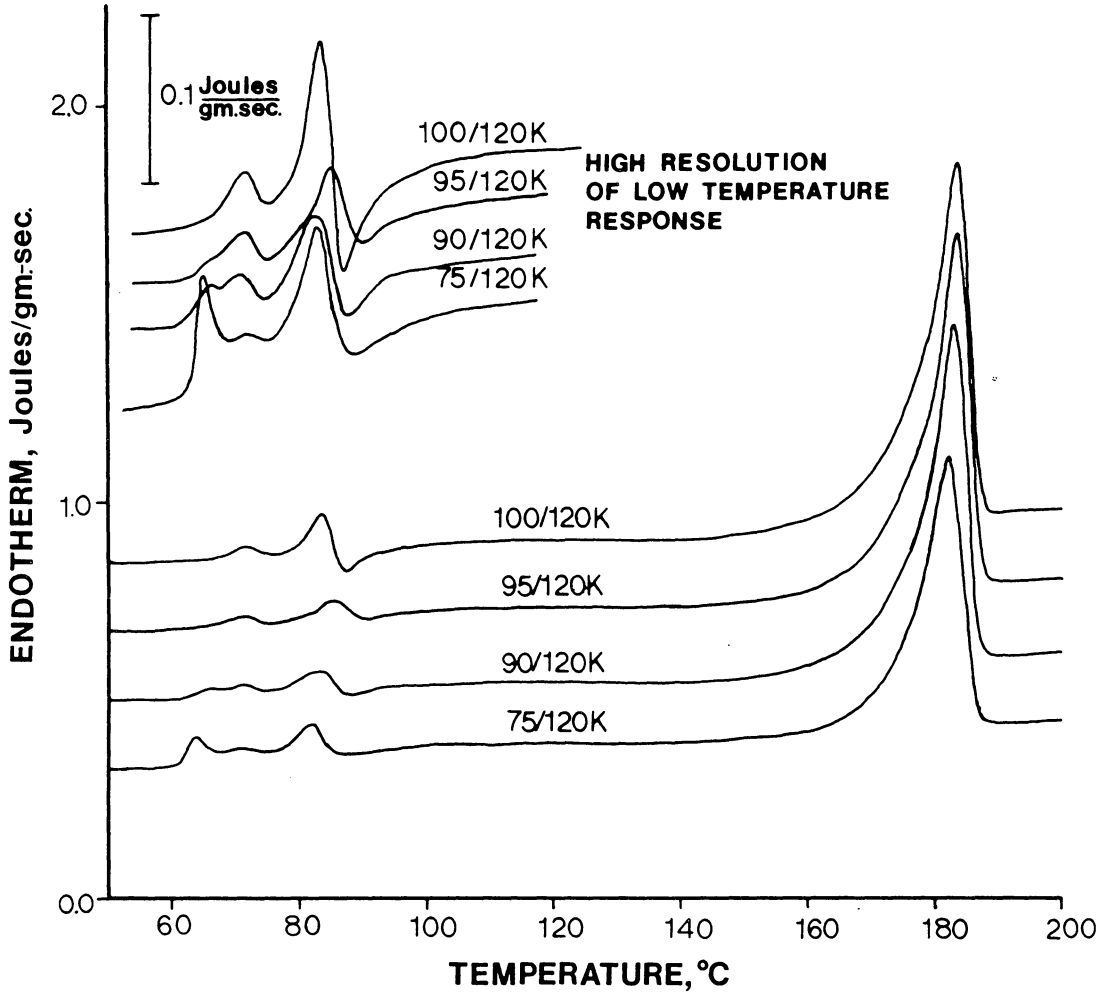

Figure 4.45. DSC thermograms of poly(lactic acid) 120,000 molecular weight blends biaxially stretched at 90 C and 25.4 cm./sec. to a final biaxial draw ratio of 4 x 4.

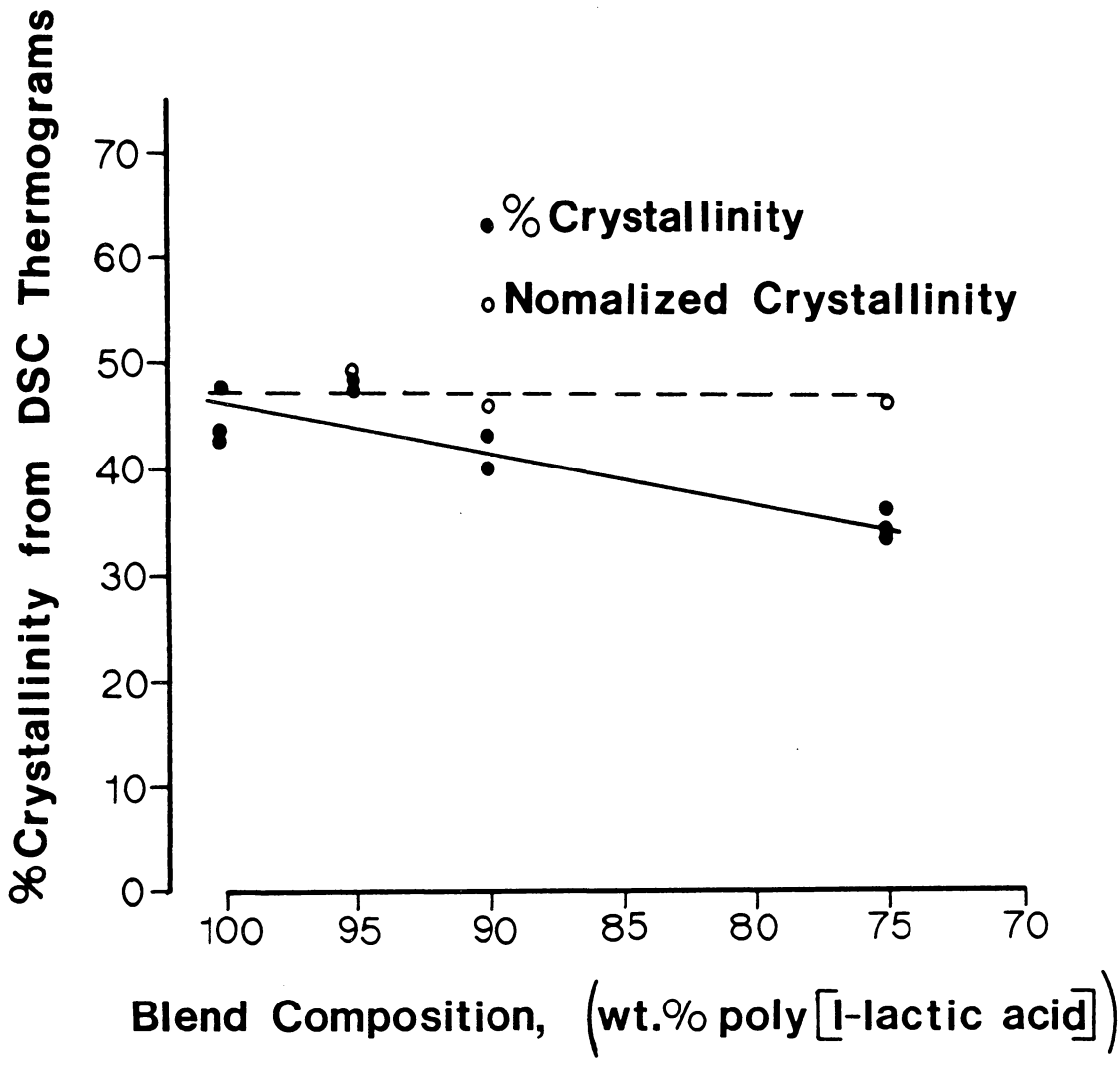

Figure 4.46. % crystallinity vs. blend composition for 120,000 molecular weight biaxial films stretched at 90 C and 25.4 cm./sec. to a final biaxial draw ratio of 4 x 4.

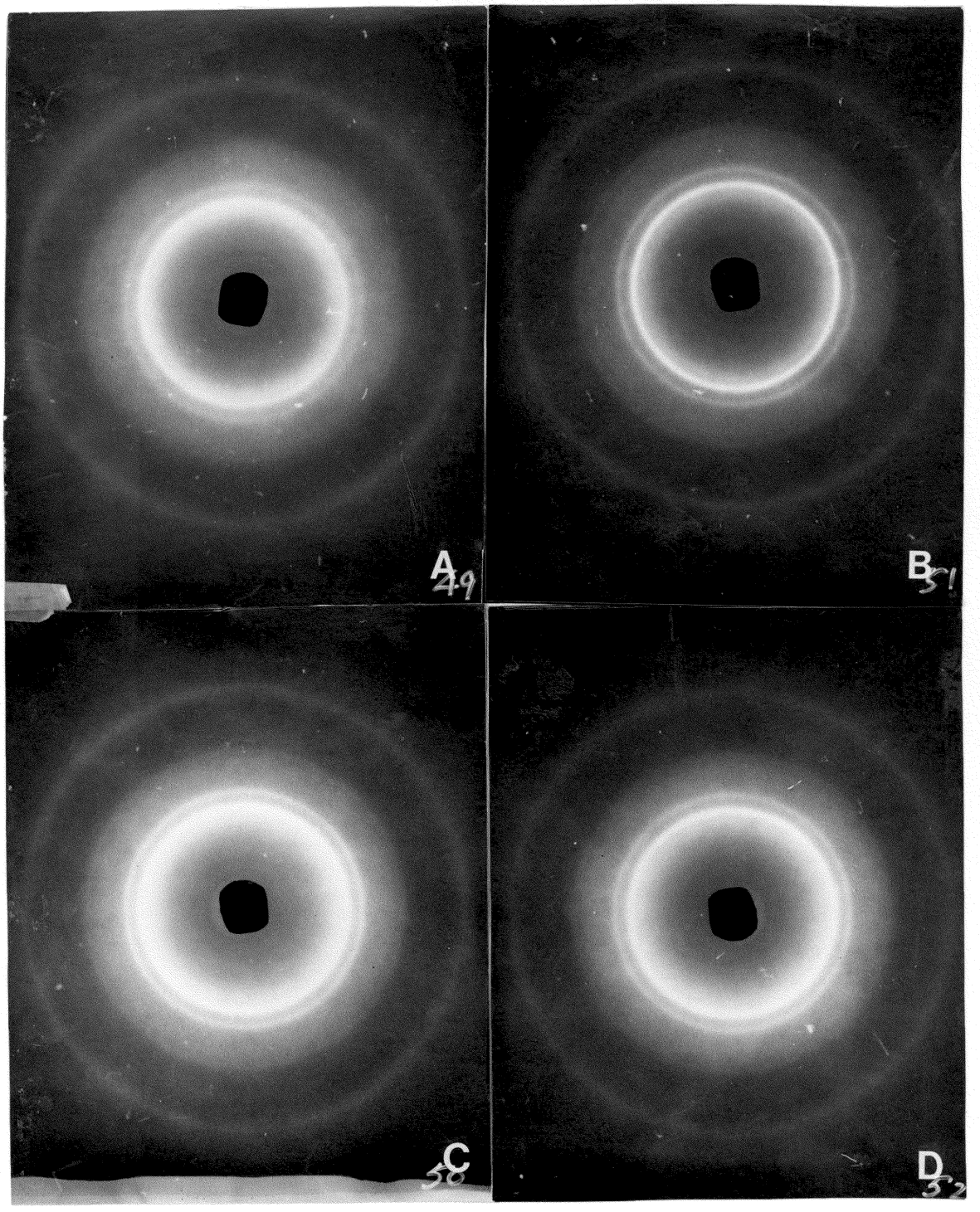

Figure 4.47. WAXS patterns for 120,000 molecular weight biaxial films stretched at 90 C and 25.4 cm./sec. to a final biaxial draw ratio of 4 x 4, X-ray beam oriented normal to film surface.
A) 100/40k B) 95/40k C) 90/40k D) 75/40k

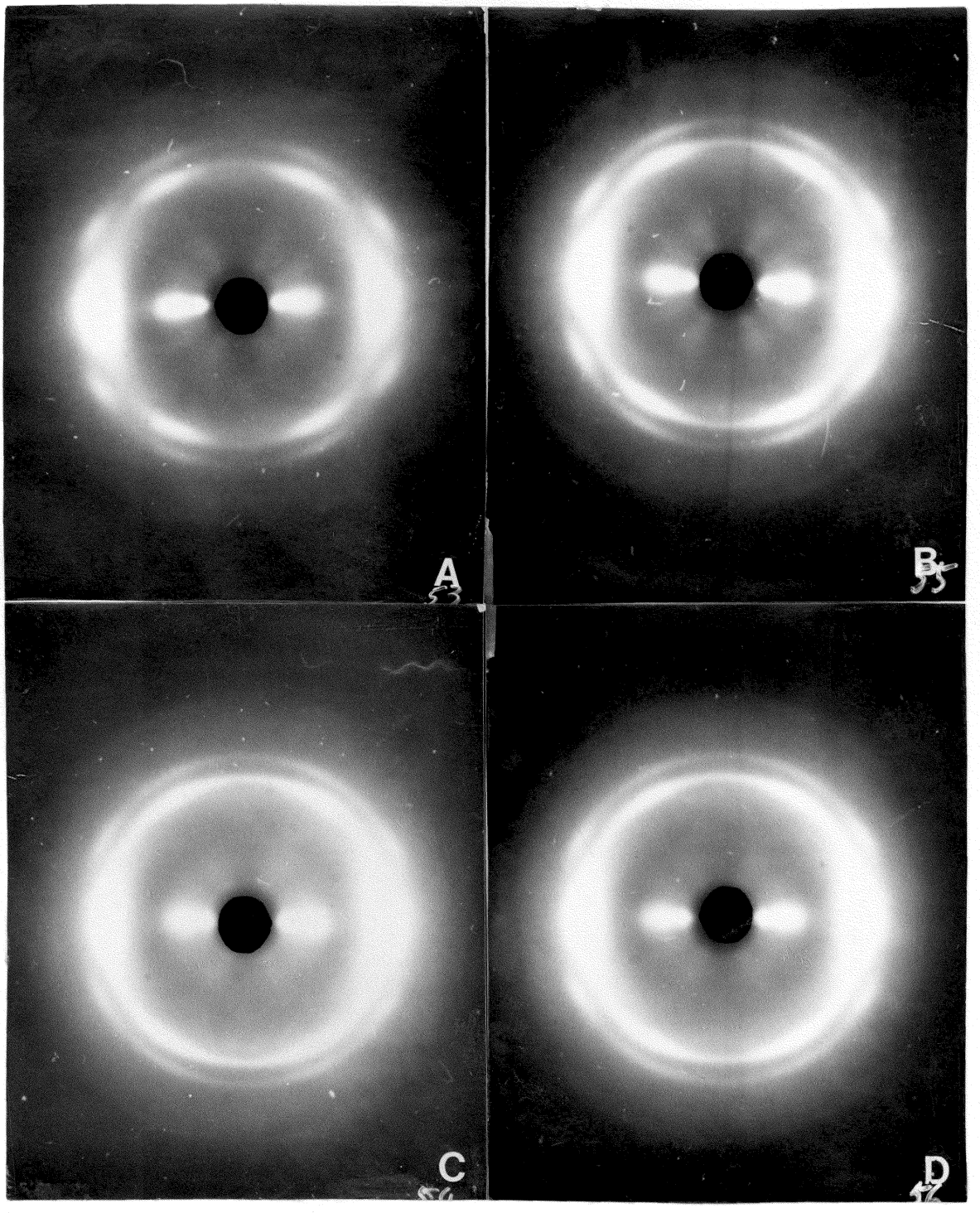

Figure 4.48. WAXS patterns for 120,000 molecular weight biaxial films stretched at 90 C and 25.4 cm./sec. to a final biaxial draw ratio of 4 x 4, X-ray beam oriented parallel to film surface.
A) 100/40k B) 95/40k C) 90/40k D) 75/40k

weight standpoint. It has been postulated that the majority of the strain induced crystallization is established at relatively low draw ratios, i.e. prior to strain hardening. In fact, the formation of chain extended crystallites at this point in the biaxial stress trajectory would induce some significant crystal phase orientation. However, it is suspected that the enhancement of this order to the level of orientation shown in Fig. 4.48 is probably due to the orientation of these preestablished crystallites during the strain hardening of the films.

Higher molecular weight constituents inhibit the stress relaxation after the biaxial stretch as shown in Fig. 4.49. The longer molecular relaxation times allow for the orientation to be frozen in by the forced air quench below Tg applied after the biaxial stretch. In this last figure, the stress relaxation is plotted as a function of time for 120,000 molecular weight films biaxially stretched under comparable conditions of temperature and rate to the 40,000 molecular weight stress relaxation results plotted in Fig 11. With less stress relaxation during the quench of the film after the initial biaxial stretch, more of the orientation is maintained which results in the enhanced crystal orientation of Fig. 4.48.

Figure 4.50 is a plot of the tensile moduli obtained from the four high molecular weight blend compositions stretched to biaxial films at 90 C and 25.4 cm./sec. This

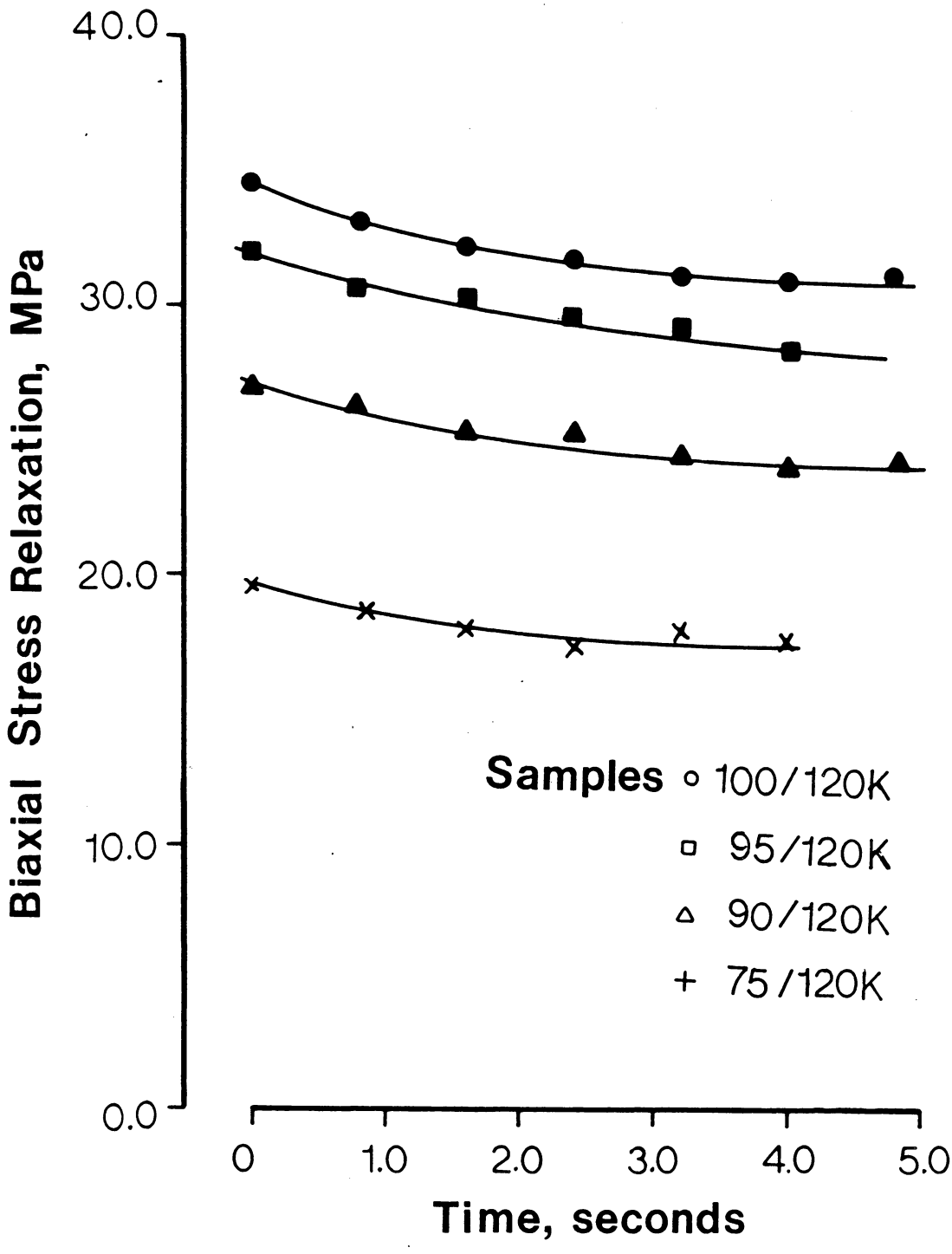

Figure 4.49. Biaxial stress relaxation at termination of biaxial stretch.
Temperature: 90 C
Crosshead Speed: 25.4 cm./sec.
Final Biaxial Draw Ratio: 4 x 4

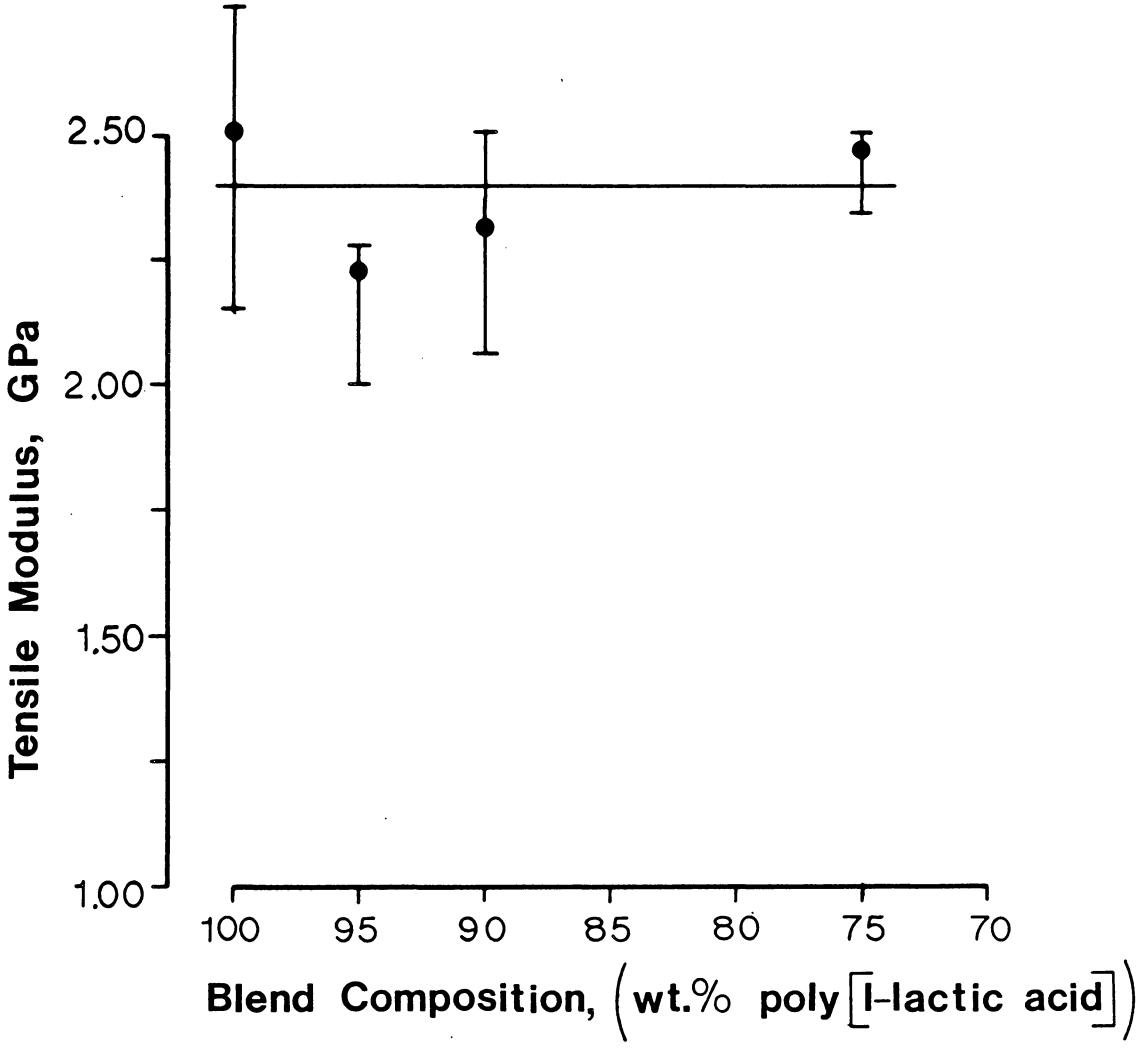

Figure 4.50. Tensile modulus vs. blend composition for 120,000 molecular weight biaxial films stretched at 90 C and 25.4 cm./sec. to a final biaxial draw ratio of 4 x 4.

was the highest mechanical strength measured in a poly(lactic acid) biaxial film and was ostensibly due to the high amorphous chain segment orientation accomplished at the high strain hardening. Note, the levels of strain hardening obtained in some of the 40,000 low molecular weight films were quite comparable to those measured in Fig. 4.44. It is suggested that these lower molecular weight films would also exhibit moduli commensurate with those of Fig. 4.50 if a quench of these films could have been achieved in order to prevent the large stress relaxation after biaxial stretch. Thus both the high crystal phase orientation and the high tensile moduli of the 120,000 molecular weight films resulted from the strain hardening of the material as shown in Fig. 4.44 combined with the lower propensity for loss of orientation from stress relaxation. Both of these two effects are tied to the enhanced entanglement tenacity of the high molecular weight material. In order to confirm the hypothesis that most of the strain induced crystallization in the biaxial deformation of poly(lactic acid) blends was occurring early in the deformation trajectory, a series of 120,000 molecular weight films were stretched to a final draw ratio of 3 X 3 at 90 C and 25.4 cm./sec. As testimony to the reproducibility of these biaxial stretches, Fig. 4.51 presents the stress-draw ratio curves from this second stretch at 90 C and 25.4 cm./sec. Clearly, the curves faithfully reproduce the results in Fig. 4.44 up to 3 X 3.

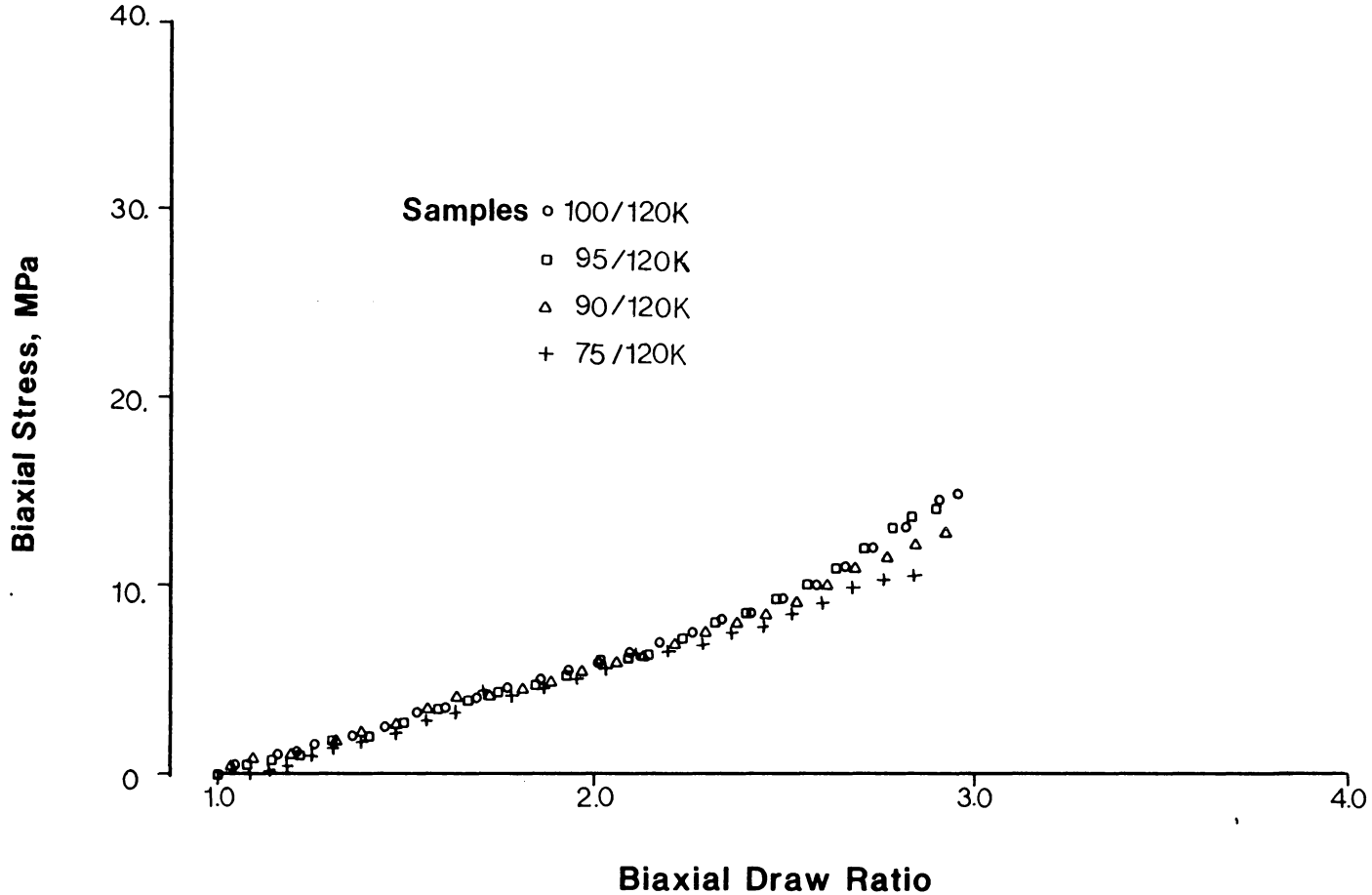

Figure 4.51. Biaxial stress vs. biaxial draw ratio for 120,000 molecular weight poly(lactic acid) blends.
Temperature: 90 C
Crosshead Speed: 25.4 cm./sec.
Final Biaxial Draw Ratio: 3 x 3

Although the final level of strain hardening in the 3 X 3 and 4 X 4 experiments was significantly different, the DSC results presented in Fig. 4.52 and summarized in Fig. 4.53 indicate that the level of crystallinity in every film of the composition series is almost independent of the level of draw ratio. See, for comparison, Figs. 4.45 and 4.46. Note that while the films stretched to a final draw ratio of 4 X 4 are beyond the onset of strain hardening, the films stretched to a final draw ratio of 3 X 3 are terminated very close to the onset of strain hardening, see Figs. 4.44 and 4.51. In comparing the DSC results of the films stretched to the different draw ratios, the one outstanding difference can be seen in the relative intensities of the entropy peaks. As expected, the higher draw ratio of 4 X 4 leads to higher amorphous orientation and larger entropy peaks.

The WAXS patterns from the 3 X 3 stretch are shown on Figs. 4.54 and 4.55. Clearly, in comparing the diffraction patterns of Figs. 4.47 and 4.54, the conclusion obtained from the DSC results suggesting that the crystallinities were the same in both the 3 X 3 and 4 X 4 biaxial stretched films seems quite reasonable. The orientation suggested in Fig. 4.55 is not quite as pronounced as that of Fig. 4.48. This, again, suggests that the strain hardening phenomenon tends to align the preestablished strain induced crystallites through the stretching of the interposing amorphous chain segments in a network structure.

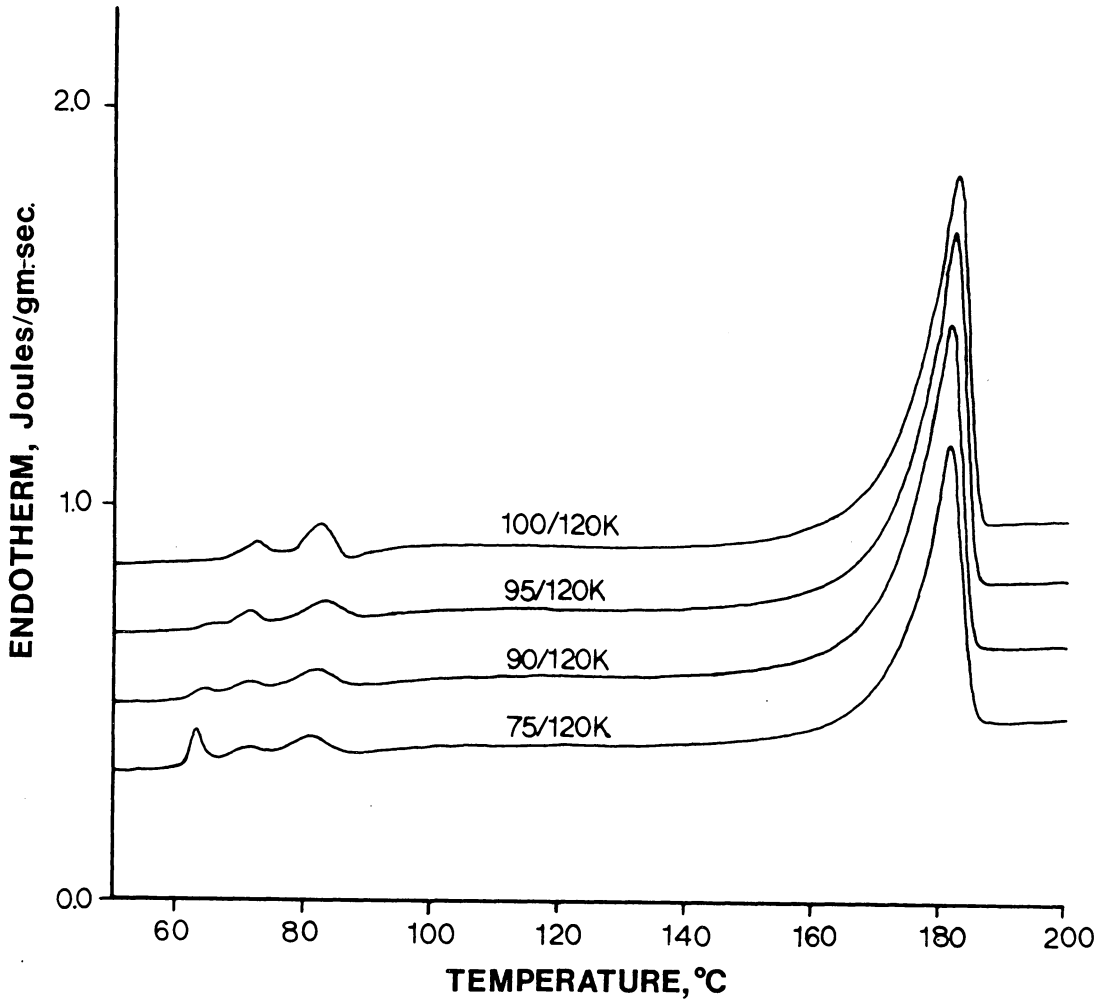

Figure 4.52. DSC thermograms of poly(lactic acid) 120,000 molecular weight blends biaxially stretched at 90 C and 25.4 cm./sec. to a final biaxial draw ratio of 3 x 3.

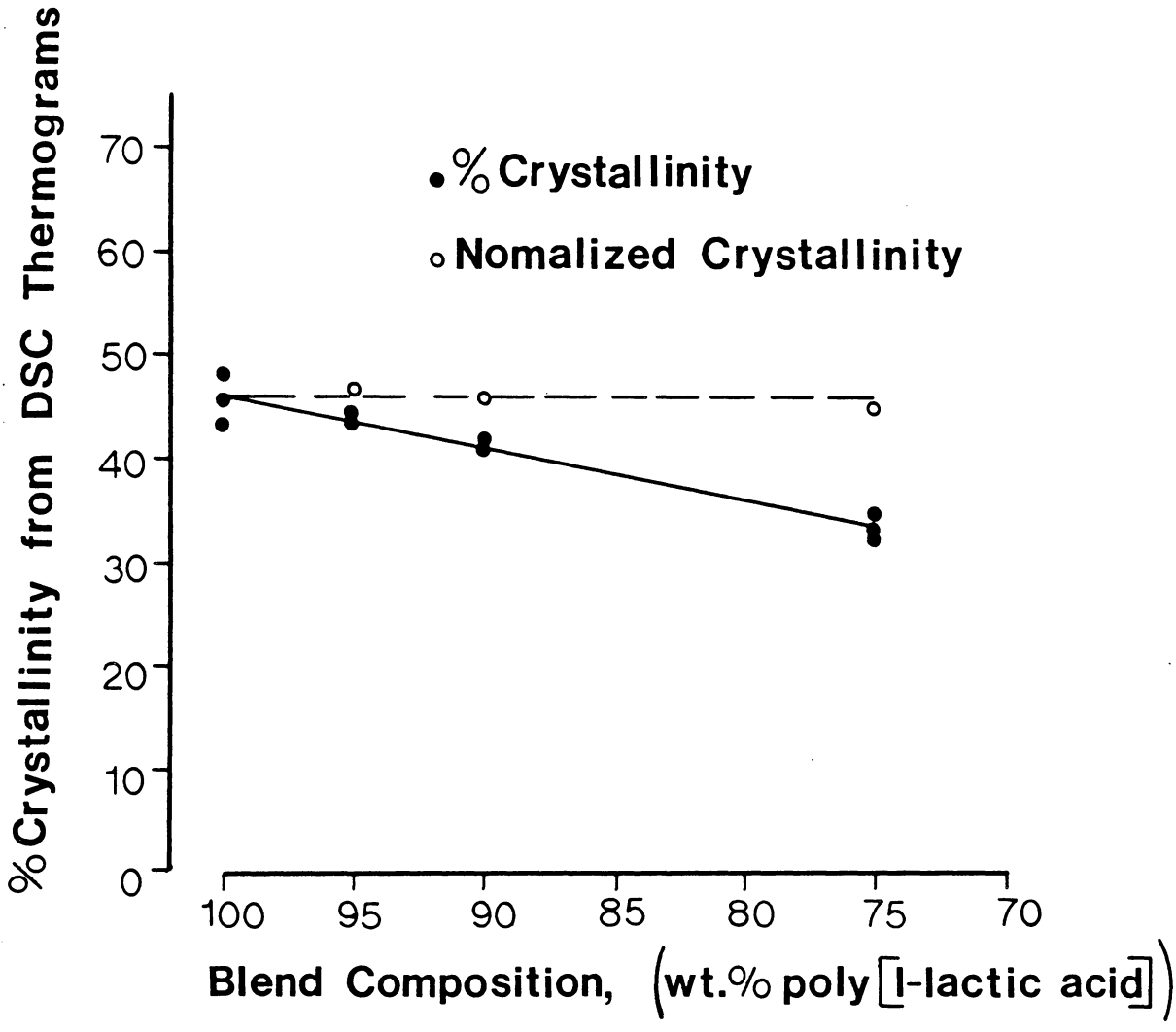

Figure 4.53. % crystallinity vs. blend composition for 120,000 molecular weight biaxial films stretched at 90 C and 25.4 cm./sec. to a final biaxial draw ratio of 3 x 3.

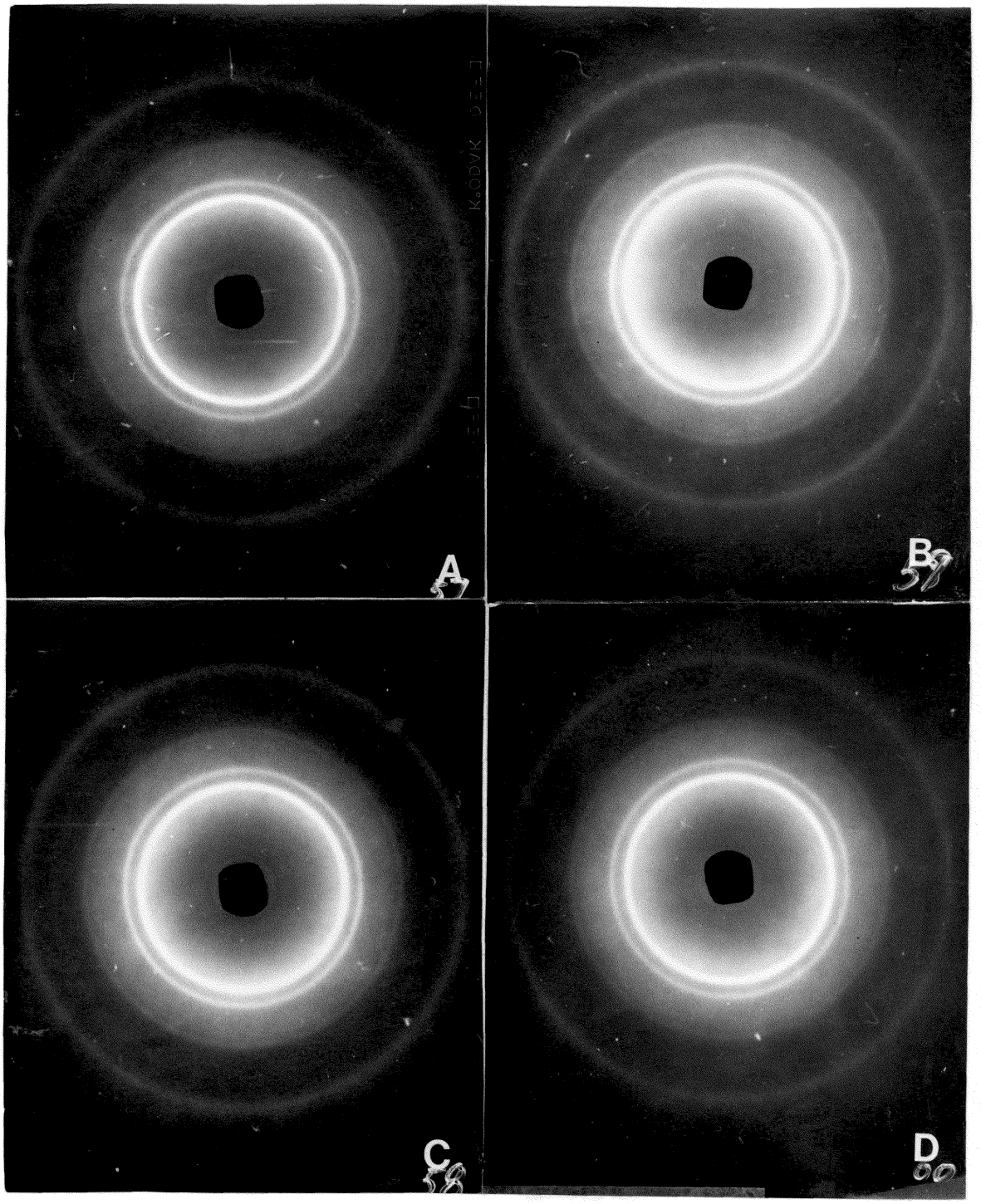

Figure 4.54. WAXS patterns for 120,000 molecular weight biaxial films stretched at 90 C and 25.4 cm./sec. to a final biaxial draw ratio of 3 x 3, X-ray beam oriented normal to film surface.
A) 100/40k B) 95/40k C) 90/40k D) 75/40k

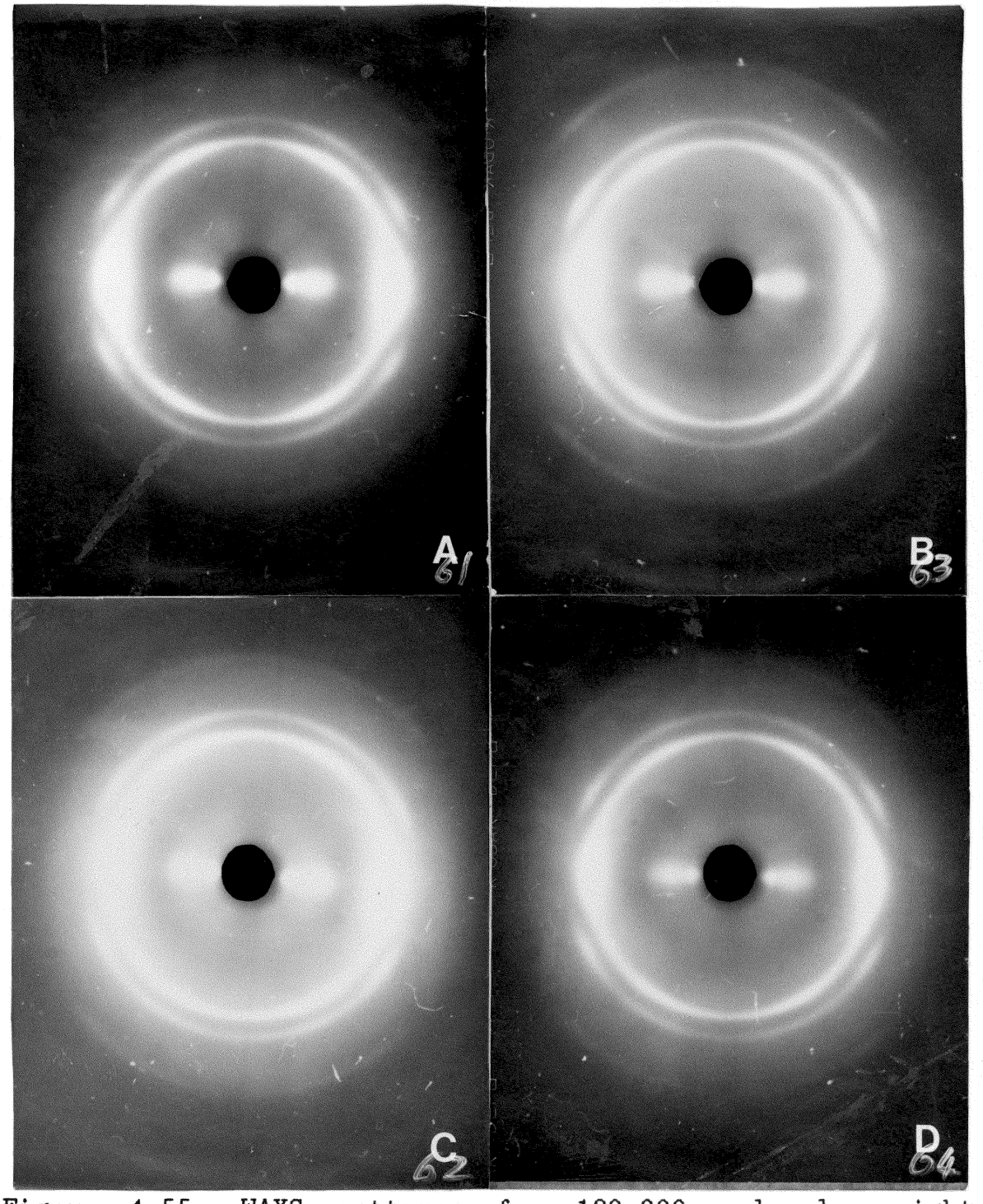

Figure 4.55. WAXS patterns for 120,000 molecular weight biaxial films stretched at 90 C and 25.4 cm./sec. to a final biaxial draw ratio of 3 x 3, X-ray beam oriented parallel to film surface.
A) 100/40k B) 95/40k C) 90/40k D) 75/40k

The tensile data for the 3 X 3 stretch in Fig. 4.56 depicts expectantly lower modulus data as compared to the 4 X 4 data of Fig. 4.50. Since the level of crystallinity at the two draw ratios is approximately the same, it would seem reasonable to assume that the amorphous orientation of the network chains associated with the strain hardening is responsible for the increase in modulus at increased strains.

Several points in the mechanism of strain hardening in biaxial deformation were established from the data presented in this last section and are summarized as follows. First, the enhancement in strain hardening by the crystallizable component in the isomer blends of poly(lactic acid) was not affected by the level of miscibility in the blends. It seems the strain induced crystallization of poly(L-lactic acid) appears to augment the strain hardening as well from miscible or immiscible blends with racemic poly(lactic acid) up to 25 % by weight of the racemic component. Secondly, it was confirmed that increasing molecular weight of the poly(lactic acid) blends increases the tenacity of the entanglement structure and leads to more strain hardening as compared with lower molecular weight materials stretched at similar temperatures and strain rates. And finally, data was presented which confirms that the majority of the strain induced crystallization is established relatively early in the stress-draw ratio deformation history prior to the onset of the film strain hardening phenomenon.

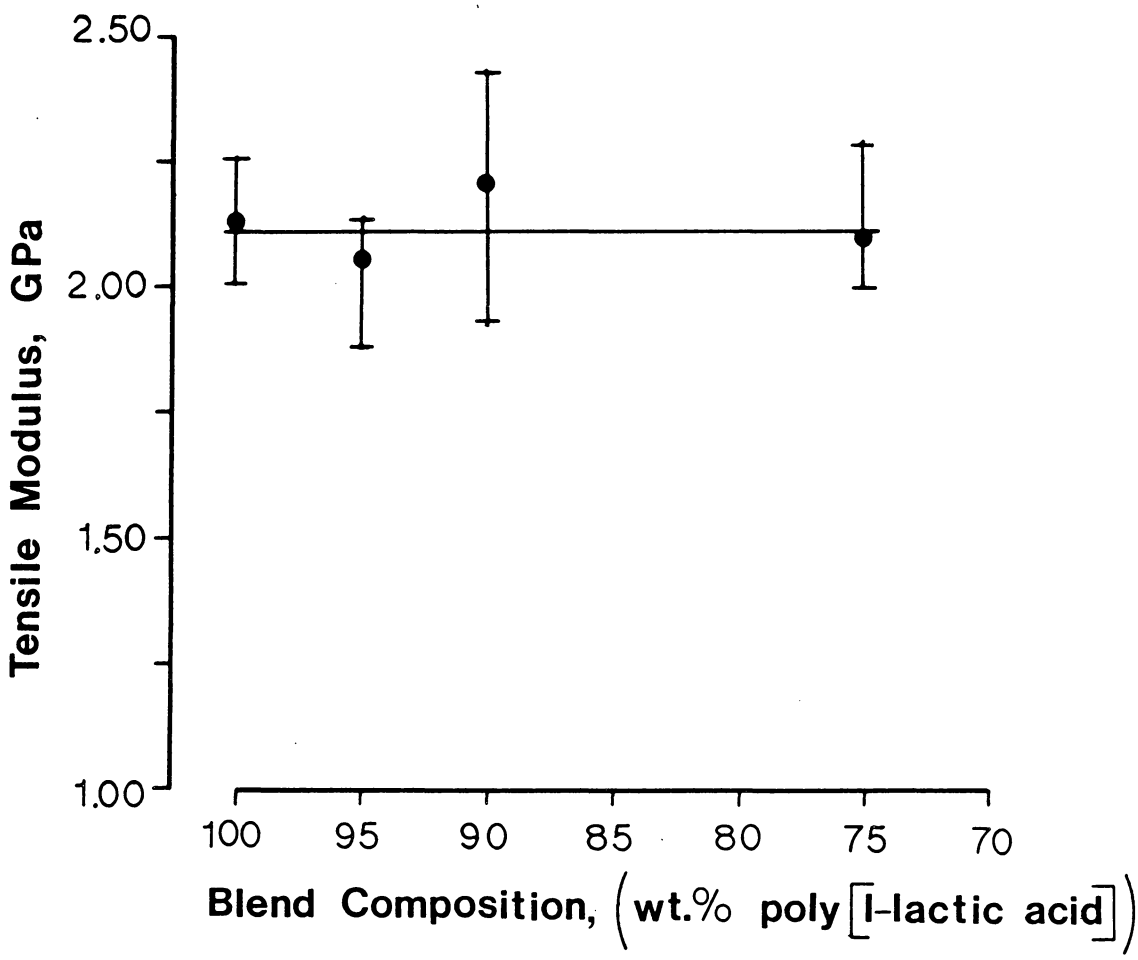

Figure 4.56. Tensile modulus vs. blend composition for 120,000 molecular weight biaxial films stretched at 90 C and 25.4 cm./sec. to a final biaxial draw ratio of 3 x 3.

4.4.0 CONCLUSIONS

4.4.1 BINARY POLYMER BLENDS COMPOSED OF THE OPTICALLY ACTIVE AND RACEMIC ISOMERS OF POLY(LACTIC ACID) WERE FOUND TO BE MISCIBLE AT MOLECULAR WEIGHTS OF 40,000 AND IMMISCIBLE AT MOLECULAR WEIGHTS OF 120,000.

Although the glass transition temperatures of poly(L-lactic acid) and racemic poly(lactic acid) are separated by less than 8 C as determined by DSC, the miscibility of these two blend constituents could be evaluated by investigating the glass transition behavior of the mixtures. Binary blends demonstrated one Tg at all compositions when the blend constituents molecular weights were 40,000. Alternately, the binary blends of poly(lactic acid) isomers with molecular weights of 120,000 demonstrated a dual Tg at all composition ratios investigated. The transition from miscibility to immiscibility on increasing the molecular weight of the blend constituents suggested that the excess enthalpy of mixing for this system was small and positive.

4.4.2 THE MISCIBLE BLENDS OF POLY(LACTIC ACID) ISOMERS IS A UNIQUE SYSTEM FOR THE INVESTIGATION OF THE INTERRELATIONSHIP BETWEEN STRAIN INDUCED CRYSTALLIZATION AND STRAIN HARDENING IN BIAXIAL DEFORMATION.

Low molecular weight (Mv=40,000) miscible blends of optically active poly(L-lactic acid) and racemic poly(lactic acid) offer a unique opportunity for investigating strain induced crystallization and its relationship to strain hardening phenomena in biaxial flow. The close proximity of the glass transition temperatures of the two poly(lactic acid) isomer blend constituents maintains the Tg of the blends nearly invariant over the composition range investigated. This, in turn, minimizes the influence of the blend composition on the transport factor in the crystallization rate expression. The apparently small positive excess enthalpy of mixing associated with the 40,000 molecular weight miscible blends of these two components guarantees that there will be no melting point depression of the crystallizable poly(l-lactic acid) in the blends with racemic poly(lactic acid). This minimizes the influence of blend composition upon the nucleation factor in the crystallization rate expresssion. Thus the impact of blend composition upon the fundamental crystallization rate processes, which are known to be governed by both the resistance to segmental motion and the undercooling below the

thermodynamic equilibrium melting point, is minimized in the blends since both T_g and T_m are nearly independent of blend composition. However, the potential influence of increased racemic content upon the diffusional effects associated with the migration of crystallizing molecules to the crystal growth surface remains as a potential telling effect on the crystallization habits of poly(l-lactic acid) from the blends.

4.4.3 A MECHANISM PROPOSED TO DESCRIBE THE STRAIN HARDENING PHENOMENON DURING THE BIAXIAL DEFORMATION OF BINARY BLENDS OF POLY(LACTIC ACID) ISOMERS IS BASED ON THE ESTABLISHMENT OF A NETWORK STRUCTURE COMPOSED OF BOTH AMORPHOUS CHAIN ENTANGLEMENTS AND STRAIN INDUCED SHISH CRYSTALLITES.

A mechanism formulated to describe the strain hardening behavior observed in the biaxial deformation of binary blends of poly(L-lactic acid) and racemic poly(lactic acid) is presented here as a forerunner to the supporting data outlined in subsequent conclusions. Strain induced nuclei are established early in the stress elongation trajectory of the biaxial stretch. The rate of formation of these nuclei is a strong function of the efficiency of the applied deformation field in reducing the entropy of the amorphous poly(L-lactic acid) chains. The reduction of amorphous chain entropy is correlated with the stress level supported in the low slope portion of the stress elongation response prior to stain hardening. The established strain induced crystal nuclei act in conjunction with amorphous chain entanglements to set up a network of physical crosslinks. The determination of the exact topology is beyond the scope of this work. However, the efficiency of the network structure in storing elastic energy and, thus, supporting stress hardening was found to be dependent upon blend composition, the temperature and strain rate of deformation, as well as

the molecular weight. Strain energy dissipation is considered to be controlled by chain entanglement slippage. If strain energy storage is greater than dissipation, then strain hardening occurs with the concomitant orientation of the amorphous chains between crosslinks. Thus, the strain hardening behavior is thought to be reminiscent of the mechanical response of a rubber to biaxial deformation with both strain induced nuclei and amorphous chain entanglements contributing, in tandem, to the effective crosslink structure. It is the entropic forces in the amorphous molecular segments between crosslinks that supply the elastic forces in strain hardening.

4.4.4 STRAIN HARDENING IN THE BIAXIAL DEFORMATION OF POLY(LACTIC ACID) ISOMER BLENDS IS ENHANCED BY INCREASED CONCENTRATION OF THE CRYSTALLIZABLE COMPONENT, POLY(L-LACTIC ACID).

Ignoring, for the moment, the propensity for isomer blend crystallization, it is proposed that, for a given biaxial deformation rate and temperature of stretch, the molecular dynamics of poly(lactic acid) chains remain unchanged by composition in the miscible blend series. This is a reasonable approximation due to the fact that the glass transition of the miscible isomer blends compositions considered in this work differ by less than 2 C and that the temperatures of stretch vary from approximately 15 to 30 centigrade degrees above Tg. In addition, the molecular weight of each isomer blend constituent was intentionally synthesized as closely as possible. Thus, the stress response to an applied biaxial strain is anticipated to be approximately the same for every blend composition since neither molecular weight nor Tg vary appreciably with relative isomer content. Experimentally, an increase in strain hardening is generally observed for the blends with higher contents of the crystallizable blend constituent, poly(L-lactic acid). Therefore, these pronounced differences in strain hardening are attributed to strain induced crystallization in the blends during biaxial stretch. This

was explicitly demonstrated in section 4.3.2 for the 40,000 molecular weight blend series stretched at 80 C and 1.27 cm./sec. and seen for a number of other biaxial experiments described in section 4.3.0. Strain induced nucleation is thought to increase the number of effective physical crosslinks above the number associated with just amorphous molecular entanglements. The improved strain hardening is, therefore, a consequence of higher amorphous orientation brought about by the enhancement of the network crosslinks by strain induced crystallization.

4.4.5 HIGHER DEGREES OF STRAIN HARDENING AND MOLECULAR ORIENTATION ARE REALIZED IN POLY(LACTIC ACID) FILMS FOR LOWER BIAXIAL DRAW TEMPERATURES

The effect of draw temperature upon strain hardening of poly(lactic acid) isomer blends in biaxial deformation was determined to affect primarily the amorphous chain entanglement contribution to crosslink density. At elevated temperatures, the molecular relaxation times become shorter and, therefore, commensurate with the time scale of the biaxial deformations. Under these conditions, molecular disentanglement and the dissipation of strain energy lead to significantly lower strain hardening despite some relatively high levels of crystallinities induced in the biaxial films. Conversely, lower draw temperatures lead to higher levels of strain hardening. The longer molecular relaxation times characteristic of low temperatures allow for entanglements to become stabilized on the time scale of the biaxial stretch. This increases the contribution of chain entanglements to the network structure. As a result, there is significant strain hardening at the lowest stretch temperatures despite some relatively low levels of strain induced crystallinity. Interestingly, the influence of poly(L-lactic acid) concentration on strain hardening is the greatest at the lowest temperature suggesting that added crosslinks associated with the strain induced nuclei are more efficient

in reinforcing the network at lower temperatures.

4.4.6 INCREASED STRAIN RATES ACCELERATE STRAIN INDUCED CRYSTALLIZATION DURING THE BIAXIAL DEFORMATION OF POLY(LACTIC ACID) ISOMER BLENDS

The results described in section 4.3.4 outline the effects of strain rate on the strain induced crystallization kinetics and strain hardening. Generally, it was determined that increased strain rates accelerated the rate of strain induced crystallization. The higher strain rates promoted a higher stress in the low strain and low slope portion of the stress-elongation trajectory. These higher stresses reflected a decrease in amorphous chain entropy which, in turn, raised the thermodynamic driving force for crystallization. However, the resulting enhancement of crystallization rates was disproportionately lower than the strain rate increase. Thus, higher strains were required to achieve approximately equivalent levels of crystallinity as the biaxial deformation rates were increased. The onset of strain hardening, as promoted by strain induced crystallization, was, therefore, also deferred to higher strains at the elevated strain rates. Note, the higher strains required for strain hardening onset at the elevated strain rates actually convert to shorter times. At the very highest strain rates, the limited strains adopted in the experimental methodology (i.e. a constant 4 X 4 stretch) prohibited the onset of any significant strain hardening. A

mechanism of viscous heating of the poly(lactic acid) materials at the highest deformation rates may also contribute to the reduction in strain-hardening. The conversion of mechanical energy into heat may raise the temperature of the biaxial film to the point where entanglement slippage would prevent the strain-hardening.

4.4.7 INCREASING THE MOLECULAR WEIGHT OF THE POLY(LACTIC ACID) ISOMER BLENDS INCREASES THE PROPENSITY FOR STRAIN HARDENING IN BIAXIAL ORIENTATION

Increasing the molecular weight of the poly(lactic acid) isomer blends increases the tenacity of the entanglement structure. In turn, this leads to significantly added strain hardening as compared to lower molecular weight materials stretched at similar temperatures and strain rates. As molecular weight is increased, the number of molecular entanglements per molecule is concomitantly increased. As a consequence, the mobility of the individual entanglements is diminished along with the ability of the material to dissipate strain energy through entanglement slippage. At lower levels of entanglement slippage, a larger proportion of the entanglement structure will participate in the network structure supporting stress and promoting strain hardening. Although the higher molecular weight series has been demonstrated to be an immiscible mixture, the same general characteristics of increased strain hardening are realized at for increased poly(L-lactic acid) contents. This, again, reinforces the concept that strain hardening is fostered by the combined mechanisms of amorphous chain entanglements and strain induced crystallization.

4.4.8 THE MOLECULAR ORIENTATION IN BIAXIAL FILMS OF POLY(LACTIC ACID) ISOMER BLENDS IS A FUNCTION OF THE LEVEL OF STRAIN HARDENING REALIZED DURING BIAXIAL DEFORMATION

Generally, molecular orientation, as characterized by the tensile modulus of the finished film, followed directly with the amount of strain hardening. As postulated in the discussion of the proposed biaxial strain-hardening mechanism, the overall molecular orientation in the biaxial films is thought to be drastically influenced by the level of stress realized in the biaxial deformation. The strain-hardening is the direct result of a buildup of molecular entropic stresses during the deformation of the rubberlike molecular network. Although the precise network topology is unknown, it is postulated that the network junctions are made up of molecular entanglements and extended chain crystallites. Certainly, the orientation of the amorphous chain segments between the physical crosslinks of the proposed network structure is enhanced in deformations fostering high strain hardening. In addition, the extended chain crystals established prior to strain hardening and which link together the amorphous chain segments, are further enticed into a preferred in plane orientation due to the applied stress transmitted throughout the network structure. At a molecular weight of 40,000, there was not as strong a dependence of modulus on strain hardening as might have been

expected. Ostensibly, this was due to the measured stress relaxation and associated reduction of molecular orientation just after biaxial stretch and before the film quench was complete. For the higher molecular weight series, in which molecular relaxation was significantly slowed, the orientations could be frozen in by the applied forced air quench scheme. Thus, the higher tensile moduli measured in the 120,000 molecular weight series were a much stronger indication of the molecular orientations induced through strain hardening. This was reflected in an increased dependence of modulus upon blend composition in the 120,000 molecular weight series since strain hardening has been clearly demonstrated to be a function of blend composition.

4.4.9 THE ABILITY OF THE POLY(L-LACTIC ACID) TO STRAIN CRYSTALLIZE FROM A BLEND WITH RACEMIC POLY(LACTIC ACID) IN BIAXIAL FLOW WAS UNAFFECTED BY BLEND COMPOSITION.

Under a given set of experimental conditions defined by stretch temperature, biaxial strain rate, and molecular weight of the poly(lactic acid) blend, the crystallinity of the finished films was directly proportional to the poly(L-lactic acid) content. Thus, once normalized on the basis of optically active concentration, all blended films exhibited the same crystallinity. Apparently, the ability of this polymer to strain crystallize from a blend with its uncrystallizable isomer is unaffected by composition, at least for the range of compositions studied. There is some evidence to support previous work (83) suggesting that the diameter of the shish crystals decreases with increasing concentrations of a noncrystallizable polymeric diluent. The one exception to these generalized observations is found in the 40,000 molecular weight film series stretched at 90 C and 1.27 cm./sec. It is postulated that, for these conditions of stretch, the mode of crystallization was closer to that expected under quiescent conditions, i.e. chain folding lamellar crystallization. The strong dependence of crystallinity upon blend composition in this latter series is consistent with previous quiescent crystallization kinetic studies from other polymeric isomer pair blend systems (94).

4.4.10 STRAIN INDUCED CRYSTALLIZATION OF POLY(LACTIC ACID) ISOMER BLENDS UNDER BIAXIAL DEFORMATION OCCURS PRIOR TO STRAIN HARDENING

In presenting the overall mechanism of strain hardening in the biaxial deformation of the binary blends of poly(lactic acid) isomers, it has been proposed that the majority of the strain induced crystallization occurs prior to strain hardening. The rate of crystallization under strain has been correlated with the level of stress developed in the deformation at relatively low stresses. Once the extent of crystallization has reinforced the network structure to the point where strain energy can be stored and strain hardening is promoted, further crystallization is arrested. The relatively high amorphous biaxial orientation experienced during strain hardening may prevent the cooperative alignment of two adjacent crystallizable chain segments. Whereas, in uniaxial deformation, increased elongation may promote the packing of aligned molecules, biaxial deformation fosters alignment of chain segments along divergent directions. In the limit, two adjacent oriented amorphous chains may be orthogonal to one another and, thus, unable to collapse into an order crystal lattice. Equilibrium degree of crystallinity has been previously reported to decrease with increasing biaxial extension ratio in isothermal studies on natural rubber (5). The early

establishment of the crystal structure in the biaxial deformation of the poly(lactic acid) materials was confirmed in the results reported in section 4.3.5. Note that the level of crystallinity in biaxial films determined by DSC and WAXS was unchanged on increasing the extension ratio from 3 X 3 to 4 X 4 under identical conditions of stretch. Under these particular experimental conditions, the onset of strain hardening occurred just prior to a 3 X 3 strain. Clearly, the level of crystallinity had not changed after the development of very significant strain hardening at a 4 X 4 strain.

4.5.0 RECOMMENDATIONS FOR FUTURE WORK

4.5.1 IN ORDER TO MORE ADEQUATELY LOCK IN THE MOLECULAR ORIENTATION APPLIED IN THE BIAXIAL DEFORMATION, IMPROVED QUENCH TECHNIQUES NEED TO BE DEVELOPED FOR COOLING THE FILM SAMPLE ON REMOVAL FROM THE LES.

It was suggested that for the 40,000 molecular weight series, significant molecular relaxation was occurring during the quench after biaxial deformation. In order to preserve the molecular orientation implemented through stretching, an improved quench technique is recommended. A stronger correlation between finished film tensile modulus and strain hardening is anticipated if a better quench could be supplied. Alternately, higher molecular weights could be studied in order to slow the molecular relaxations. However, as demonstrated in the text, increasing molecular weight to 120,000, diminishes the miscibility between the poly(lactic acid) isomers. It may be possible to choose an intermediate molecular weight in order to diminish the effects of relaxation and yet preserve miscibility.

4.5.2 THE EXPERIMENTAL PROGRAM SHOULD BE EXPANDED TO INCLUDE THE DETAILED EFFECTS OF VARIOUS FINAL STRAINS ON BIAXIAL FILM PROPERTIES

It was proposed that the development of biaxial film crystallinity occurred prior to strain hardening and that amorphous molecular orientation was primarily developed after the onset of strain hardening. In order to more adequately confirm these postulates, it is proposed to study the crystallinity and molecular orientation of biaxial films at intermediate elongations. In this way, it is hoped to map the development of crystallinity and orientation in a more systematic fashion. This program is dependent on the development of a more adequate quench as described above so that crystallinity and orientations representative of each elongation can be quickly frozen-in.

4.5.3 THIS INVESTIGATION INTO BIAXIAL DEFORMATION OF POLY(LACTIC ACID) ISOMER BLENDS SHOULD BE EXTENDED TO INCLUDE SAMPLES OF HIGHER RACEMIC POLYMER CONTENTS

The range of poly(lactic acid) blend compositions should be extended to include higher racemic polymer contents. It is expected that by further diluting the crystallizable poly(L-lactic acid) constituent, that diffusional effects should eventually preclude the crystallization processes even under the severe thermodynamic driving forces supplied by molecular orientation. It would be of interest to document the experimental conditions of biaxial stretch at which strain induced crystallization is prohibited by the dilution effects. Note that for the majority of stretch conditions employed in this work, the crystallinity of the optically active components in each biaxial film blend was not affected by composition.

4.5.4 IT IS RECOMMENDED TO INVESTIGATE THE MOLECULAR ENTROPIC EFFECTS OF AMORPHOUS ORIENTATION VIA SHRINKAGE STRESS MEASUREMENTS

The frozen-in elastic potential energy associated with the reduced entropy of the oriented amorphous chains will generally be dissipated as soon as the sample is heated above the glass transition in an unrestrained condition. This was, in fact, documented in this investigation by the appearance of an entropy peak after the Tg on the DSC thermograms and the shrinkage of the samples in the DSC pans. It is proposed to restrain the samples from shrinkage be maintaining the length and width of the samples during a heating process above the glass transition. The measured retraction force required to maintain the dimensional stability can be correlated to molecular orientation through the theories of rubber elasticity (89). Previous investigators have already reported this type of result for purely amorphous biaxial films and correlated retraction forces with molecular entropy and local chain deformation (83). It is proposed that this same methodology be adapted in order to study the amorphous chain elongation in the poly(lactic acid) biaxial films and correlate retraction forces with the observed strain hardening effects. Clearly, this proposed study requires a more effective quench of the biaxial film in order to guarantee the preservation of the amorphous orientation

imparted by the strain hardening deformation.

4.5.5 IT IS PROPOSED TO INVESTIGATE THE BIAXIAL FILM PROPERTIES IN THE POLY(LACTIC ACID) BLEND SERIES AFTER HEAT SETTING

Many industrial processes for producing films involve the heat setting of the biaxial materials above the glass transition at temperatures which promote additional crystallization. Naturally, the films are crystallized on heating from a restrained state in order to minimize the loss of orientation. Among the property improvements realized by the restrained crystallization are reduced film shrinkage, enhanced mechanical properties, and improved barrier properties. It is proposed to investigate the film property improvements on heat setting the biaxial films produced from the poly(lactic acid) isomer blends.

4.5.6 DIRECT OBSERVATION OF ORIENTED CRYSTALLINE MORPHOLOGY VIA SCANNING ELECTRON MICROSCOPY IS RECOMMENDED FOR THE POLY(LACTIC ACID) BIAXIAL FILMS

The technique developed in chapter 2.0 for the observation of crystalline morphology in glycolic and lactic acid copolymers by scanning electron microscopy may be directly applicable to the elucidation of crystalline textures in the poly(lactic acid) biaxial films. Certainly the base hydrolysis etch for preferentially removing the amorphous phase in the semicrystalline copolyesters would be very likely to give the same enhancement of crystalline textures in poly(lactic acid) homopolymers. Although some modification of the etch recipe would be necessary due to the anticipated gross differences in the nature of the crystalline morphology, the direct observation of the proposed extended chain crystalline morphology by scanning electron microscopy would add another interesting dimension to this investigation of biaxial film morphology. The results of a first attempt at adapting the etch technique for the elucidation of crystallaline morphology in these poly(lactic acid) films is reported breifly in the Appendix to this chapter, see section 4.6.0.

4.5.7 BIAXIAL DEFORMATION OF ADDITIONAL MISCIBLE BINARY BLENDS WITH ONE CRYSTALLIZABLE CONSTITUENT SHOULD BE INVESTIGATED WITH A VIEW TO CHARACTERIZING THE EFFECTS OF FINITE NEGATIVE EXCESS ENTHALPIES OF MIXING AND VARIATION OF T_G WITH COMPOSITION.

A blend system was purposefully chosen for the present investigation such that the effects of blend composition upon equilibrium thermodynamic melting point and glass transition temperature were minimized. The influences of strain induced crystallization upon strain hardening could thus be isolated. It is proposed to continue the investigation of polymer blending on biaxial strain hardening and strain induced crystallization by investigating the nonisomeric blends wherein a finite negative excess enthalpy of mixing and an associated shift in equilibrium melting point are anticipated. In addition, shifts in glass transition temperature with blend composition should also be expected. By tailoring the crystallization rate processes as governed by the temperature gap (T_m-T_g) with judicious choice of blend composition, control of strain induced crystallization, strain hardening, and molecular orientation may be obtained. Using this blending methodology, novel biaxial film properties will be sought.

4.5.8 THE BARRIER PROPERTIES AND PHYSIOLOGICAL ABSORBABILITY OF THE BIAXIAL FILMS PRODUCED FROM POLY(LACTIC ACID) ISOMER BLENDS SHOULD BE CHARACTERIZED WITH A VIEW TO POTENTIAL BIOMEDICAL APPLICATIONS

A number of previous applications of poly(lactic acids) in the biomedical field were reviewed in the introduction of chapter 3. The ability to process poly(L-lactic acid) and its blend with the racemic poly(lactic acid) isomer into a biaxial film, clearly demonstrated in this investigation, may add new opportunities for the application of this polymer system as a biomaterial. It is expected that by varying both the blend composition and biaxial processing conditions, the physiological absorbability and barrier properties of the film may be tailored to a number of new biomedical applications. The heat shrinkability of the films may also be an advantage. For example, a shrink to fit wound covering which could be subsequently absorbed into the body may offer an application in burn treatment or surgery. In order to more adequately judge the potential for poly(lactic acid) biaxial films to this important application area, a program targeted at characterizing physiological absorbability, barrier properties, heat shrinkability, and mechanical strength is recommended.

4.6.0 APPENDIX: PRELIMINARY RESULTS ON THE CHEMICAL ETCH OF BIAXIALLY STRETCHED POLY(LACTIC ACIDS) FOR THE ELUCIDATION OF ORIENTED CRYSTALLINE MORPHOLOGY

A 40,000 molecular weight poly(L-lactic acid) amorphous film was biaxially stretched to a final balanced strain of 3 X 3 with a crosshead speed of 25.4 cm/sec. at 90 C. The resulting oriented crystalline structure was investigated by both optical microscopy (OM) and scanning electron microscopy (SEM). For the purposes of the SEM investigation, the film surface texture was enhanced by the chemical etch technique developed in chapter 2.0 of this dissertation. Prior to the etch treatment, optical micrographs were taken at a magnification of 80x with and without crossed polarizers. These two optical micrographs are presented in Fig. 4.57. Figure 4.57 A clearly demonstrates a fibrous texture to the film, while the optical micrograph taken in the same region with crossed polarizers (see Fig. 4.57 B) clearly verifies the biaxial nature of the film orientation. Figure 4.58 is an SEM micrograph of the film surface taken after the chemical etch. The same fiber-like crystalline morphology can be seen in both Figs. 4.57 B and 4.58 supporting the utility of the chemical etch for revealing crystalline textures for direct SEM observation.

Clearly, the level of structure described in this brief example is fairly coarse and certainly larger than might be

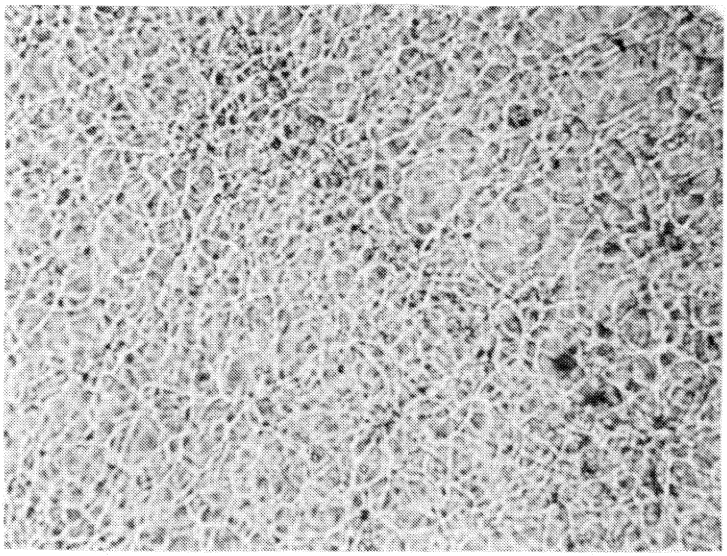

A

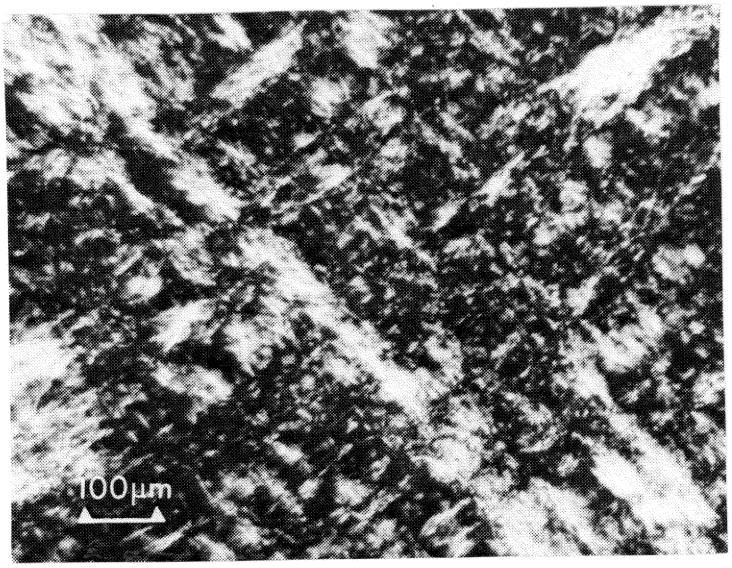

B

Figure 4.57. Optical micrographs of poly(L-lactic acid) biaxial film stretched at 90 C and 25.4 cm./sec. to a final biaxial draw ratio of 4 x 4.
A) Magnification 80x without crossed polarizers.
B) Magnification 80x with crossed polarizers.

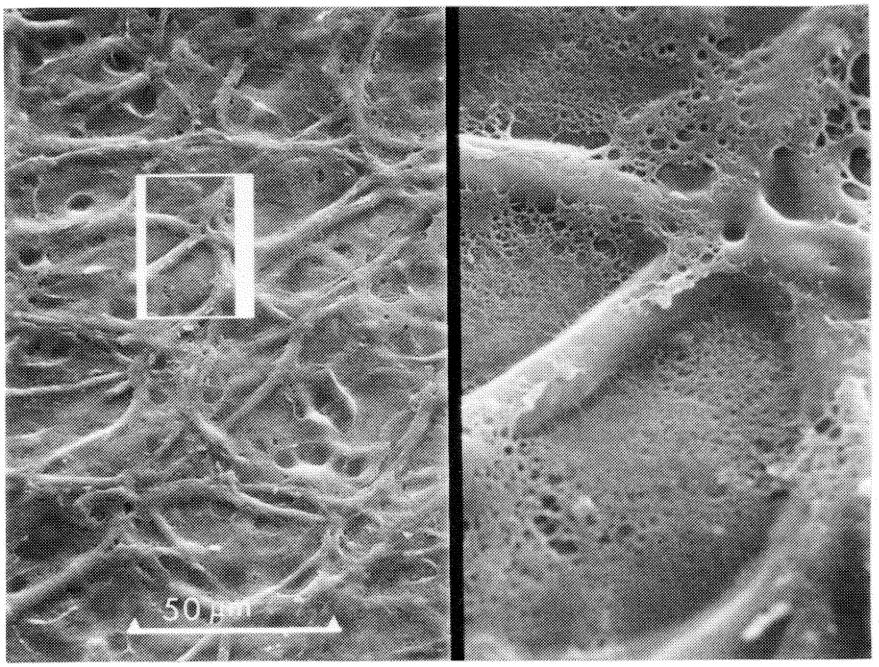

Figure 4.58. Scanning electron micrograph of poly(L-lactic acid) biaxial film stretched at 90 C and 25.4 cm./sec. to a final biaxial draw ratio of 4 x 4. Film surface was chemically etched to reveal crystalline texture. Magnification 500x, insert magnification 2500x.

anticipated for other poly(lactic acid) films stretched at different deformation rates and temperatures. However, this preliminary data is presented as particial proof of the fact that the chemical etch can discriminate between amorphous and crystalline material in these materials as well as the copolyesters descibed in chapter 2.0. These differences in chemical etching rates between crystalline and amorphous areas in the biaxial film is the mechanism whereby texture is introduced on the film surface. It is these chemically induced surface textures which facilitate direct SEM observation of bulk crystalline morphologies. Thus, the chemical etch developed in chapter 2.0 has proven to be a viable technique for the uncovering of strain induced crystalline morphologies in biaxially stretched poly(lactic acids) which then can be observed directly by SEM techniques.

REFERENCES

1) W.R.R. Park, Plastics Film Technology, Reinhold, New York, 1969.

2) W.R.R. Park and J. Conrad, "Biaxial Orientation," Encyclopedia of Polymer Science and Technology, Vol. 2, Interscience, New York, 1965.

3) G. Schuur and A.K. Van Der Vegt, Chapt. 12 in Structure and Properties of Oriented Polymers, John Wiley and Sons, New York, 1975.

4) O. Sweeting, The Science and Technology of Polymer Films, Interscience, New York, 1968.

5) R. Oono, K. Miyasaka, and K. Ishikawa, J. Polym. Sci., Polym. Phys. Ed., **11**, 1477 (1973).

6) P.H. Lindenmeyer and S. Lustig, J. Appl. Polym. Sci., **9**, 227 (1965).

7) T. Nagasawa, T. Matsumura, and S. Hoshino, Appl. Polym. Symp., **20**, 275 (1973).

8) C.A. Garber and E.S. Clark, J. Macromol. Sci., **B4**, 499 (1970).

9) A.T. Widiger and R.L. Butler, Chapt. 6 in O. Sweeting (Ed.), Science and Technology of Polymer Films, Vol. 2, John Wiley and Sons, New York, 1971.

10) T. Alfrey, Jr., SPE Trans., April, 1965.

11) C.J. Heffelfinger and J.L. Knox, Chapt. 14 in O. Sweeting (Ed.), Science and Technology of Polymer Films, Vol. 2, John Wiley and Sons, New York, 1971.

12) S.A. Jabarin, Polym Eng. and Sci., **24**, 376 (1984).

13) A.J. De Vries, C. Bonnebut, and J. Beautemps, J. Polym. Sci., Polym. Symp., **58**, 109 (1977).

14) L.S. Thomas and K.J. Cleereman, SPE J., **28**, 61 (1972).

15) R.S. Stein, M. Hashiyama, and M.K. Parpart, in Flow-Induced Crystallization, R.L. Miller (Ed.), Gordon and Beach Science Publishers Ltd., Great Britain, 1979.

16) A.B. Thompson, J. Polym. Sci., **34**, 741 (1959).

17) G.S.Y. Yeh and P.H. Geil, J. Macromol. Sci., Part B, **1**, 251 (1967).

18) H.D. Keith and F.J. Padden, J. Appl. Phys., **35**, 1270 and 1286 (1964).

19) G.S.Y. Yeh and S.L. Lambert, J. Polym. Sci., Part A-2, **10**, 1183 (1972).

20) F.P. Warner, W.J. MacKnight, and R.S. Stein, J. Polym. Sci., Polym. Phys. Ed., **15**, 2113 (1977).

21) R.S. Stein, F.P. Warner, A. Escala, E. Balizer, T. Russell, and J. Koberstein, ACS Organic Coatings and Plastics Chemistry Preprints, **37**, 7, (1977).

22) J.M. Maerker and W.R. Schowalter, Rheol. Acta, **13**, 627 (1974).

23) L.J. Hart-Smith and J.D. Crisp, Int. J. Eng. Sci., **5**, 1 (1967).

24) M.O. Lai and D.L. Holt, J. Appl. Polym. Sci., **19**, 1805 (1975).

25) A.J. De Vries and C. Bonnebat, Polym. Eng. Sci., **16**, 93 (1976).

26) D. Turnbull and J.E. Fisher, J. Chem. Phys., **17**, 71 (1949).

27) H.D. Keith and F.J. Padden, J. Appl. Phys., **35**, 1270 and 1286 (1969).

28) J.D. Hoffman and T.I. Lauritzen, J. Res. Natl. Bur. Stds., **65A**, 297 (1961).

29) R.L. Cormia, F.L. Price, and T. Turnbull, J. Chem. Phys., **37**, 1333 (1962).

30) L. Mandelkern, F.A. Quinn, and P.J. Flory, J. Appl. Phys., **25**, 830 (1954).

31) B. Wunderlich and A. Mehta, J. Polym. Sci., Phys. Ed., **12**, 255 (1974).

32) D.T. Grubb and A. Keller, Colloid Polym. Sci., **256**, 218 (1978).

33) K. Kobayashi and T. Nagasawa, J. Macromol. Sci., **B4**, 331 (1970).

34) I.L. Hay, M. Jaffe, and K.F. Wissburn, J. Macromol. Sci., **B12**, 423 (1976).

35) D. Acierno, F.P. LaMantia, and G. Marucci, Polym. Eng. Sci., **18**, 817 (1978).

36) G.S.Y. Yeh and D.L. Krueger, Polym. Eng. Sci., **19**, 401 (1979).

37) A. Peterlin, in Flow Induced Crystallization in Polymer Systems, R.L. Miller (Ed.), Gordon and Beach Science Publishers Ltd., Great Britain, 1979.

38) C.A. Silebi and A.J. McHugh, J. Polym. Sci., Polym. Phys. Ed., **17**, 1469 (1979).

39) H.G. Kim and L. Mandelkern, J. Polym. Sci., Part A-2, **6**, 181 (1968).

40) G. Kraus and J.T. Gruver, J. Polym. Sci., Phys. Ed., **10**, 2009 (1972).

41) U.R. Evans, Trans. Fara. Soc., **41**, 365 (1945).

42) R. Becker and W. Doring, Ann. Phys., **24**, 719 (1935).

43) M.L. Williams, R.F. Lundel, and J.D. Ferry, J. Am. Chem. Soc., 77, 3701 (1955).

44) L. Mandelkern, Crystallization of Polymers, McGraw-Hill, New York, 1964.

45) J. Frenkel, Kinetic Theory of Liquids, Oxford Univ. Press, London, 1946.

46) J.D. Hoffman, T.I. Lauritzen, E. Pasagliu, G.S. Ross, and L.J.J. Weeks, Kolloid Z.Z. Poly., **231**, 567 (1969).

47) J.D. Hoffman, SPE Trans., **4**, 315 (1969).

48) J.N. Hay, in Flow-Induced Crystallization, R.L. Miller (Ed.), Gordon and Beach Science Publishers Ltd., Great Britain, 1979.

49) P.G. de Gennes, J. Chem. Phys., **55**, 572 (1971).

50) A.J. Pennings, J.M.A.A. van der Mark, and A.M. Kiel, Kolloid Z.Z. Polym., **237**, 336 (1970).

51) J. Petermann, M. Miles, and H. Gleiter, J. Polym. Sci., Polym. Phys. Ed., **17**, 55 (1979).

52) A.J. Pennings, Macromol Chem. Suppl., **2**, 99 (1979).

53) J.D. Hoffman, Polymer, **20**, 1071 (1979).

54) W.A. Tiller and J. M. Schultz, J. Polym. Sci., Polym. Phys. Ed., **22**, 143 (1984).

55) A.J. Pennings, J. Polym. Sci., Polym. Symp., **59**, 55 (1977).

56) G.S.Y. Yeh, K.G. Hong, and D.L. Krueger, Polym. Eng. Sci., **19**, 401 (1979).

57) P.J. Flory, J. Chem. Phys., **15**, 397 (1947).

58) W.R. Krigbaum and R.J. Roe, J. Polym. Sci., A, **2**, 4391 (1964).

59) H.G. Kim and L. Mandelkern, J. Polym. Sci., **6**, 181, (1968).

60) M. Yamamoto and J.L. White, J. Polym. Sci., A2, **9**, 1399 (1971).

61) G. Marrucci, Trans. Soc. Rheol., **16(2)**, 321 (1972).

62) A.J. McHugh, J. Appl. Polym. Sci., **19**, 125 (1975).

63) T.W. Haas and B. Maxwell, Polym. Eng. Sci., **4**, 225 (1969).

64) L. Jarecki and Z. Ziabicki, Polymer, **18**, 1015 (1977).

65) D. Acierno, F.P. LaMantia, G. Marrucci, and Titomanlio, J. Non-Newt. Fluid Mech., **1**, 125 (1976).

66) L. Jarecki, Colloid and Poly. Sci., **257**, 711 (1979).

67) D.R. Paul and S. Newman (Eds.), Polymer Blends, Vols. 1 and 2, Academic Press, New York, 1978.

68) D.R. Paul and J.W. Barlow, J. Macromol. Sci., Rev. Macromol. Chem., **C18(i)**, 109 (1980).

69) P.J. Flory, Principles of Polymer Chemistry, Cornell University Press, Ithaca, New York, 1962.

70) R.L. Scott, J. Chem. Phys., **17**, 279 (1949).

71) W. J. MacKnight, F. E. Karasz, and J. R. Fried, in Polymer Blends, Vol. 1, D. R. Paul and S Newman (Eds.), Academic Press, New York, 1978.

72) D.S. Kaplan, J. Appl. Polym. Sci., **20**, 2615 (1976).

73) W.A. Krause, R.G. Kriste, J. Haas, B.J. Schmitt, and D.J. Stein, Makromol. Chem., **177**, 1145 (1976).

74) T.K. Kwei, T. Nishi, and R.F. Roberts, Macromolecules, **7**, 607 (1974).

75) C.W. Frank and M.A. Gashgari, Macromolecules, **12**, 163 (1979).

76) D.R. Paul, J.W. Barlow, R.E. Bernstein, and D.C. Wahrmund, Polym. Eng. Sci., **16**, 593 (1976).

77) R. Koningsveld, L.A. Kleintjen, and H.M. Schoffeleers, Pure Appl. Chem., **39**, 1 (1974).

78) S. Krause, J. Macromol. Sci. - Rev. Macromol. Chem., **C7(2)**, 251 (1972).

79) R.E. Robertson and D.R. Paul, J. Appl. Polym. Sci., **17**, 2579 (1973).

80) P. R. Swan, J. Polym. Sci., **56**, 439 (1962).

81) E. Roerdink and G. Challa, Polymer, **19**, 173 (1978).

82) D.R. Paul and J.W. Barlow, Crystallization from Polymer Blends, unpublished manuscript.

83) K. Feit, A. Karbach, and J. Petermann, J. Polym. Sci., Polym. Phys. Ed., **22**, 993 (1984).

84) J. Boon and J.M. Azeue, J. Polym. Sci., Part A-2, **6**, 885 (1968).

85) J. Rau, R. M. Gohil, J. Petermann, and J. M. Schultz, Colloid Poly. Sci., **253**, 241 (1981).

86) J. Petermann, and R. M. Gohil, J. Polym. Sci. Polym. Lett. Ed., **18**, 781 (1980).

87) A. Petermann, Polym. Eng. Sci., **14**, 627 (1974).

88) P. G. de Gennes, Scaling Concepts in Polymer Physics, Cornell University Press, Ithaca, 1979.

89) L. R. G. Treloar, The Physics of Rubber Elasticity, Oxford University Press, London, 1958.

90) R. Vasanthakumari and A. J. Pennings, Polymer, **24**, 175 (1983).

91) P. De Santis and A. J. Kovacs, Biopolymers, **6**, 299 (1968).

92) B. Kalb and A. J. Pennings, Polymer, **21**, 607 (1980).

93) M. R. Tant and G. L. Wilkes, Polym. Eng. Sci., **21**, 874 (1981).

94) H. D. Keith and F. J. Padden, J. Appl. Phys., **35**, 1270 and 1286 (1964).

95) J. W. Song, A. S. Abhiraman, and A. P. Richards, J. Appl. Polym. Sci., **27**, 2369 (1982).

96) G. LeBourvellec, L. Monnerie, and J. P. Jarry, Polymer, **27**, 856 (1986).

97) A. E. Tonelli and P. J. Flory, Macromolecules, **2(3)**, 225 (1969).

98) D. A. Brant, A. E. Tonelli, and P. J. Flory, Macromolecules, **2(3)**, 228 (1969).

99) A. Schindler and D. Harper, J. Polym. Sci.: Polym. Chem. Ed., **17**, 2593 (1979).

The vita has been removed from the scanned document